

**Electron Transfer in Rigid and Semi-Rigid
Iridium d^8 - d^8 Donor-Spacer-Acceptor Complexes**

Thesis by
Ramy Samir Farid

In Partial Fulfillment of the Requirements
for the Degree of
Doctor of Philosophy

California Institute of Technology
Pasadena, California
1991
(Submitted January 15, 1991)

Humanity's deepest desire for knowledge is justification enough for our continuing quest. And our goal is nothing less than a complete description of the universe we live in.

—Stephen Hawking,
A Brief History of Time

Acknowledgments

I want to thank everyone who has been a part of my life in the past 4 years (and longer). The written words to follow cannot fully express the level of indebtedness I feel towards my friends and family who have made this thesis possible, but maybe it's a start.

To fully thank my advisor Harry Gray would take a thesis in itself. He never fails to awe me with his compassion for people and passion for science. His guidance (thankfully on request only), support, and inspiration have left a deep impression on me, that I will carry with me forever. There is, however, a problem with being associated with greatness; it's hard to give up. I'll miss you, Harry.

Members of the Gray Group, past and present, have been sources of help, friendship, and much needed distraction. Miriam (easily a 9 at Caltech), was solely responsible for the personality of the Gray Group while she was here (and it was good). She encouraged me to stand up to Tad and Dave, and explained to me that it was good to be upset about things because it meant you were really alive. For your words of wisdom and friendship, I thank you, Miriam. John Brewer has been a great friend, always ready with answers concerning matters of chemistry and life. John, your words will always be with me. Erica may not know this, but I admire her deeply and I am thankful for her enlightening discussions and arguments. I am thankful for having been friends with Holden, although I wasn't sure for a short period in the middle. I would also like to thank Julia for misunderstanding me (I do like you, really), Wayne for his late night visits while I was writing (a truly awesome, mysterious person), Mark for just being who he is, and David for speaking English every once in a while.

I would like to thank members of the biogroup: Tom Meade and Mike Therien, for demonstrating the virtues of good hair care; Mike and Amanda, for having Charlie; Jeff, for leading the Dim Sum Crew (Brad, Lila, Luet, and ARF, hey where's Michelle) and for marrying Michelle; and Debbie, for always being happy and smiling. Special thanks go to Brad who, although politically wrong, has been a great friend (see ya in Philly).

I would like to thank some non-Gray Group friends: Tom Povsic has been a great friend from early on, his enthusiasm and drive are an inspiration to me and to everyone who knows him; I would like to thank Bryan "FIAT" Balazs, who can fix anything, and I mean *anything*, for listening to me gab and gab over frequent lunches; Diane and I hit it off the first day we played tennis together, and since then we have had many fun conversations concerning marriage, commitment, and other such goodies. Thanks for your wisdom and kindness.

Of course, the support staff at Caltech is the vital link that keeps things running smoothly. I would like to thank Dave "Dude" Malerba for tolerating my *occasional* stupidity, Larry Henling, for help on solving the X-ray structure of my compound and late night math quizzes, Tom Dunn, for knowing everything there is to know about electrical thing-a-ma-jobbers, and of course, Lou and Bill, for the most enlightening conversations I have had here (I'm still not sure that everyone should carry around guns and stop paying taxes, but I'll give it some thought). I would also like to thank Catherine, Fran, Virginia, Pat, and Beth for their answers to every one of my stupid questions.

I was fortunate to have the opportunity to visit BNL for several weeks, where Jay Winkler and I-Jy Chang took time from their own research to help me collect data for this thesis. I am very grateful to them for their help and wisdom. I would also like to thank Dave Beratan, for many informative discussions, and whose brilliance and kindness have made him a true pleasure to be around.

Many people outside of Caltech have had an influence on me before and during my graduate career. My early exposure to science was positive due to Mr. Crane and Rich Eisenberg, who deserve special thanks for sparking my interest in chemistry at an early stage.

Skip, my family away from home, there are no words to explain how important you have been to me, except to say that although mine may be bigger, I *am* the "King." Roger, the best friend an Arab can have, is not even close to Kinghood, but I love him anyway.

I could not have survived my childhood and older years without my parents' undying love and support. My brother has put up with more than his share of grief from me, but I'm going to make it up to him one of these days.

Thanks to Adrienne, my best friend and SBP, for her love. How did I get so lucky?

Finally, I would like to thank the Department of Education for a fellowship during my last two years.

*to my sources of love,
Mom, Dad,
Adrienne,
Hany, Linda, Skip, and Roger*

Abstract

A series of rigid and semi-rigid donor-spacer-acceptor complexes, $[\text{Ir}(\mu\text{-pz}^*)(\text{CO})(\text{Ph}_2\text{P-O-C}_6\text{H}_4\text{-(CH}_2)_n\text{-py}^+\text{-R})_2]$ (pz^* = 3,5-dimethylpyrazolyl; C_6H_4 = phenylene; py^+ = pyridinium; R = H, 4-*tert*-butyl, and 4-amide; and n = 0, 1, 2, and 3), has been synthesized for the purpose of studying photoinduced electron-transfer (ET) reactions. The spacers separating the iridium center (electron donor, Ir_2) and pyridinium cation (electron acceptor, py^+) are based on terminal phosphinite ligands, consisting of a phenylene group and a number of methylene groups ranging from 0 to 3. Three distinct ET reactions can be studied in each complex: singlet excited-state electron transfer (^1ET), triplet excited-state electron transfer (^3ET), and thermal back electron transfer (ET^b).

Atomic positions, obtained from the X-ray crystal structure of $[\text{Ir}(\mu\text{-pz}^*)(\text{CO})(\text{Ph}_2\text{P-O-C}_6\text{H}_4\text{-CH}_3)_2]$, were used as a basis for molecular mechanics calculations, furnishing solution structures for the series of $\text{Ir}_2\text{-py}^+$ donor-acceptor complexes. These results revealed that the spacers in complexes where $n = 0$ and $n = 1$ are rigid, and that in complexes where $n = 2$ and $n = 3$, the spacers are semi-rigid, taking on either *folded* or *stretched* conformations in fluid solution.

Steady-state and time-resolved emission and absorption experiments were employed to determine ^1ET , ^3ET , and ET^b rates in these complexes. The ^1ET and ^3ET rates for the $n = 2$ and $n = 3$ complexes exhibit Gaussian free-energy dependence, in excellent agreement with classical ET theory ($n = 2$: $\lambda = 1.10$ eV, $H_{\text{DA}} = 26$ cm^{-1} ; $n = 3$: $\lambda = 1.05$ eV and $H_{\text{DA}} = 7$ cm^{-1}). However, the ^1ET and ^3ET rates in $n = 0$ and $n = 1$ complexes exhibit dramatically different behavior: the ^3ET rates in these rigid complexes are on the order of 10,000 times slower than the corresponding ^1ET rates. H_{DA} s for the ET^b reactions ($n = 1, 2$) are similar to those of the corresponding ^1ET reactions. These results are discussed in terms of the solution structure parameters obtained for the series of donor-acceptor complexes. Evidence that through-bond and through-space couplings play different roles in singlet and triplet electron transfer is presented for the first time.

Table of Contents

Acknowledgments	iii	
Dedication	vi	
Abstract	vii	
List of Figures	ix	
List of Tables	xii	
List of Abbreviations	xiv	
Chapter 1	Introduction and Background	<i>1</i>
Chapter 2	Synthesis of Donor-Spacer-Acceptor Complexes	<i>18</i>
Chapter 3	X-ray Crystal Structure and Molecular Mechanics Calculations	<i>56</i>
Chapter 4	Steady-State Spectroscopy and Electrochemistry	<i>97</i>
Chapter 5	Time-Resolved Experiments	<i>133</i>
Appendix	Supplementary material for the X-ray crystal structure determination of [Ir(μ-pz*)(CO)(Ph ₂ P-O-C ₆ H ₄ -CH ₃)] ₂	<i>184</i>

List of Figures

Chapter 1

Figure 1.1	Plot of product and reactant potential energy surfaces	4
Figure 1.2	Diagram of avoided crossing at the transition state region	7
Figure 1.3	The driving force dependence data of Marshall et al.	10
Figure 1.4	The driving force dependence data of Fox et al.	13

Chapter 2

Figure 2.1	Structures of model rigid donor-spacer-acceptor complexes	19
Figure 2.2	Structure of donor-spacer-acceptor complexes, [Ir(μ -pz*)(CO)(Ph ₂ PO-C ₆ H ₄ -(CH ₂) _n -py ⁺ -R)] ₂	21
Figure 2.3	Apparatus employed in the synthesis of HO-C ₆ H ₄ -py ⁺	25
Figure 2.4	Structures of the phosphinite ligands	31
Figure 2.5	Scheme for three step synthesis of donor-acceptor complexes	33
Figure 2.6	Synthesis of complex with $n = 0$	35
Figure 2.7	Syntheses of complexes with $n = 1$	37
Figure 2.8	Syntheses of complexes with $n = 2$ and $n = 3$	39
Figure 2.9	Numbering scheme for ¹ H NMR spectra of phenols	42
Figure 2.10	Numbering scheme for ¹ H NMR spectra of iridium complexes	46
Figure 2.11	¹ H NMR spectrum of [Ir(μ -pz*)(CO)(Ph ₂ P-O-C ₆ H ₄ -CH ₃)] ₂	49
Figure 2.12	IR spectrum of Ir(μ -pz*)(CO)(Ph ₂ P-O-C ₆ H ₄ -CH ₃)] ₂	51

Chapter 3

Figure 3.1	ORTEP diagrams of [Ir(μ -pz*)(CO)(Ph ₂ P-O-C ₆ H ₄ -CH ₃)] ₂	61
Figure 3.2	Numbering scheme for [Ir(μ -pz*)(CO)(Ph ₂ P-O-C ₆ H ₄ -CH ₃)] ₂	64
Figure 3.3	ORTEP diagrams of [Ir(μ -pz*)(CO)(Ph ₂ P-O-C ₆ H ₄ -CH ₃)] ₂ , showing approximate C ₂ -axis	71

Figure 3.4	Diagram defining r , θ , and γ	77
Figure 3.5	Solution structure of $[\text{Ir}_2]\text{-py}^+$ ($n = 0$)	78
Figure 3.6	Solution structure of $[\text{Ir}_2]\text{-CH}_2\text{-py}^+$ ($n = 1$)	80
Figure 3.7	Solution structure of stretched $[\text{Ir}_2]\text{-(CH}_2)_2\text{-py}^+$ ($n = 2$)	83
Figure 3.8	Solution structure of folded $[\text{Ir}_2]\text{-(CH}_2)_2\text{-py}^+$ ($n = 2$)	86
Figure 3.9	Solution structure of stretched $[\text{Ir}_2]\text{-(CH}_2)_3\text{-py}^+$ ($n = 3$)	89
Figure 3.10	Solution structure of folded $[\text{Ir}_2]\text{-(CH}_2)_3\text{-py}^+$ ($n = 3$)	92

Chapter 4

Figure 4.1	Molecular orbital diagram for the interaction of two square planar d^8 metal ions	100
Figure 4.2	Absorption spectra of $[\text{Ir}(\mu\text{-pz}^*)(\text{CO})(\text{Ph}_2\text{P-O-C}_6\text{H}_4\text{-CH}_3)]_2$	105
Figure 4.3	Excitation spectra of $[\text{Ir}(\mu\text{-pz}^*)(\text{CO})(\text{Ph}_2\text{P-O-C}_6\text{H}_4\text{-CH}_3)]_2$	108
Figure 4.4	Emission spectrum of $[\text{Ir}(\mu\text{-pz}^*)(\text{CO})(\text{Ph}_2\text{P-O-C}_6\text{H}_4\text{-CH}_3)]_2$	112
Figure 4.5	Absorption/emission spectra of $[\text{Ir}(\mu\text{-pz}^*)(\text{CO})(\text{Ph}_2\text{P-O-C}_6\text{H}_4\text{-CH}_3)]_2$	114
Figure 4.6	Emission spectrum of $[\text{Ir}(\mu\text{-pz}^*)(\text{CO})(\text{Ph}_2\text{P-O-C}_6\text{H}_4\text{-(CH}_2)_3\text{-py}^+)]_2$	116
Figure 4.7	Cyclic voltammogram of $\text{HO-C}_6\text{H}_4\text{-(CH}_2)_2\text{-py}^+$	119
Figure 4.8	Cyclic voltammogram of $\text{HO-C}_6\text{H}_4\text{-CH}_2\text{-py}^+\text{-Am}$	123
Figure 4.9	Cyclic voltammograms of $[\text{Ir}(\text{pz}^*)(\text{CO})(\text{Ph}_2\text{P-O-C}_6\text{H}_4\text{-CH}_3)]_2$	125
Figure 4.10	Cyclic voltammogram of $[\text{Ir}(\text{pz}^*)(\text{CO})(\text{Ph}_2\text{P-O-C}_6\text{H}_4\text{-CH}_2\text{-py}^+)]_2$	127
Figure 4.11	State diagram for donor-acceptor system	130

Chapter 5

Figure 5.1	State diagram of metal localized and charge-transfer excited states	135
------------	---	-----

Figure 5.2	Schematic diagram of Nd:YAG laser source	138
Figure 5.3	Layout of transient absorption experiment	140
Figure 5.4	Transient difference spectra of [Ir(μ -pz*)(CO)(Ph ₂ P-O-C ₆ H ₄ -(CH ₂) ₂ -py ⁺)] ₂	144
Figure 5.5	Bleach kinetics of [Ir(μ -pz*)(CO)(Ph ₂ P-O-C ₆ H ₄ -(CH ₂) ₂ -py ⁺)] ₂	146
Figure 5.6	Kinetics of absorption feature of [Ir(pz*)(CO)(Ph ₂ P-O-C ₆ H ₄ -(CH ₂) ₂ -py ⁺)] ₂	148
Figure 5.7	Streak Camera data of [Ir(pz*)(CO)(Ph ₂ P-O-C ₆ H ₄ -(CH ₂) ₃ -py ⁺)] ₂	152
Figure 5.8	Fluorescence kinetics of [Ir(pz*)(CO)(Ph ₂ P-O-C ₆ H ₄ -(CH ₂) ₃ -py ⁺)] ₂	154
Figure 5.9	Phosphorescence kinetics of [Ir(pz*)(CO)(Ph ₂ P-O-C ₆ H ₄ -CH ₂ -Quin ⁺)] ₂	156
Figure 5.10	Fit of ET rates to Marcus theory for $n = 0, 1, 2$, and 3 complexes	161
Figure 5.11	Edge-view of porphyrin-quinone complexes	165
Figure 5.12	Structure of molecules modeling $n = 2$ donor-acceptor complexes	166
Figure 5.13	Structure of molecule that models p-orbital interactions	167
Figure 5.14	Diagrams defining r , θ , γ , C4 and N	171
Figure 5.15	Newman projections of $n = 2$ donor-acceptor complexes	172
Figure 5.16	Schematic of initial and final states for singlet and triplet electron transfer	180

List of Tables

Chapter 2

Table 2.1	^1H NMR Resonances for Phenols	44
Table 2.2	^{31}P NMR Resonances for Phosphinite Ligands and Iridium Complexes	44
Table 2.3	^1H NMR Resonances for Iridium Complexes	48

Chapter 3

Table 3.1	Crystallographic Data for $[\text{Ir}(\mu\text{-pz}^*)(\text{CO})(\text{Ph}_2\text{P-O-C}_6\text{H}_4\text{-CH}_3)]_2$	60
Table 3.2	Selected Bond Lengths and Angles for $[\text{Ir}(\mu\text{-pz}^*)(\text{CO})(\text{Ph}_2\text{P-O-C}_6\text{H}_4\text{-CH}_3)]_2$	66
Table 3.3	M...M Separations in Pyrazolyl -Bridged Iridium(I) and Rhodium(I) Dimers	74
Table 3.4	Comparison of Bond Lengths and Angles Between $[\text{Ir}_2]\text{-CH}_3$ and $[\text{Ir}(\text{pz}^*)(\text{CO})(\text{Ph}_2\text{POC}_2\text{H}_4\text{-py}^+)]_2$	75
Table 3.5	Structural Parameters Obtained from Molecular Mechanics Calculations for Stretched and Folded Conformations	77

Chapter 4

Table 4.1	Absorption Data for the Iridium Donor-Acceptor Complexes	104
Table 4.2	Singlet Excitation Data	107
Table 4.3	Triplet Excitation Data	107
Table 4.4	Emission Data for the Iridium Donor-Acceptor Complexes	111
Table 4.5	Quantum Yields for Fluorescence and Phosphorescence in $\text{Ir}_2\text{-py}^+$ Complexes	111
Table 4.6	Cathodic Peak Potentials for Phenol-Pyridinium Complexes	118
Table 4.7	Driving Forces for ^1ET , ^3ET , and ET^b Reactions	129

Chapter 5

Table 5.1	Fluorescence, Phosphorescence, and Charge-Transfer State Lifetimes of Model and Donor-Acceptor Complexes	150
Table 5.2	Singlet and Triplet Excited-State Electron-Transfer Rates for Donor-Acceptor Complexes	159
Table 5.3	Thermal Back Electron-Transfer Rates for Two Donor-Acceptor Complexes	159
Table 5.4	Electronic Coupling Matrix Elements for ^1ET , ^3ET and ET^b in the Donor-Acceptor Complexes	160
Table 5.5	Triplet Electron-Transfer Rates in a series of Benzophenone-Quinone Complexes	169
Table 5.6	Structural and Electronic Parameters for Donor-Acceptor Complexes	173
Table 5.7	Calculated Orbital Overlaps and Experimental Matrix Elements	174
Table 5.8	Calculated σ and π Orbital Overlaps and Experimental Matrix Elements	175
Table 5.9	Singlet and Triplet Excited-State Electron-Transfer Rates for Selected Donor-Acceptor Complexes	177

Appendix

Table A.1	Crystal and Intensity Collection Data	185
Table A.2	Final Non-Hydrogen Coordinates and Displacement Parameters	186
Table A.3	Anisotropic Displacement Parameters	190
Table A.4	Assigned Hydrogen Parameters	192
Table A.5	Complete Distances and Angles	194
Table A.6	Observed and Calculated Structure Factors	199

List of Abbreviations

NMR

br	broad
d	doublet
m	multiplet
s	singlet
t	triplet

Electrochemistry

$E_{1/2}$	half-wave potential
E_{pc}	cathodic peak potential
E_{pa}	anodic peak potential
E_j	junction potential
F	the Faraday; charge on one mole of electrons
SSCE	saturated sodium chloride electrode
TBAH	tetra- <i>n</i> -butylammonium hexafluorophosphate

Spectroscopy

ϵ	molar absorptivity
Φ_p^o	intrinsic phosphorescence quantum yield
Φ_f^o	intrinsic fluorescence quantum yield
Φ_p	phosphorescence quantum yield
Φ_f	fluorescence quantum yield
k_r	radiative decay rate constant
k_{nr}	non-radiative decay rate constant
τ_p	triplet excited state lifetime
τ_f	singlet excited-state lifetime
τ_p^o	intrinsic triplet excited-state lifetime
τ_f^o	intrinsic singlet excited-state lifetime
S_0	singlet ground state
S_1	lowest singlet excited-state
T_1	lowest triplet excited-state

Electron Transfer

k_{ET}	electron-transfer rate constant
^1ET	singlet excited-state electron transfer
^3ET	triplet excited-state electron transfer
ET^{b}	thermal back electron transfer
$^1\text{H}_{\text{DA}}$	electronic coupling matrix element for ^1ET
$^3\text{H}_{\text{DA}}$	electronic coupling matrix element for ^3ET
$^{\text{b}}\text{H}_{\text{DA}}$	electronic coupling matrix element for ET^{b}

General

Ph	phenyl
C_6H_4	phenylene
py	pyridine
py^{\bullet}	pyridinium radical
py^+	pyridinium cation
$\text{py}^+ - \text{Am}$	4-amidopyridinium
$\text{py}^+ - \text{tB}$	4- <i>tert</i> -butylpyridinium
pzH	pyrazole
pz	pyrazolyl
pz^*	3,5-dimethylpyrazolyl
Quin^+	Quinuclidinium
Q	quinone
UQ	ubiquinone

Chapter 1

Introduction and Background

Electron-transfer (ET) reactions play a central role in many chemical and biological processes.¹⁻³ For example, energy production in both plants and animals is a direct consequence of ET occurring in cells.⁴ The most extensively studied *biological* electron-transport process is photosynthesis occurring in purple bacteria⁵⁻⁸ (two species of which have been structurally characterized⁹⁻¹¹). These organisms capture the energy of sunlight and through a series of efficient electron-transfer steps, convert it to chemical energy in the form of long-lived oxidative and reductive species. These remarkable reactions occur between several distinct redox components contained within the so-called reaction center (RC). Following light absorption, a bacteriochlorophyll dimer in its singlet excited state transfers an electron, on a picosecond time-scale, to a monomeric bacteriochlorophyll which in turn reduces a quinone, again on a subnanosecond time-scale. The competing back ET reaction to the ground state is ~4,000 times slower than the forward charge-separating reaction. Clearly, an understanding of the precise role the medium plays in determining ET rates, the nature of the high quantum yields, and the origin of the diminished back ET rates is important in the effort to mimic these reactions that lead to efficient conversion of light into chemical energy. However, there are fundamental limitations at present in the ability to manipulate such a complicated natural system. Model compounds that actually mimic important features of the RC thus have a valuable role to play in unraveling the mysteries of RC function.¹²⁻²⁰

Many model systems have been prepared in an effort to understand the effects of (1) electronic parameters such as donor-acceptor distance and relative orientation^{12,16,17,21,22} and the chemical nature of the medium,²³⁻²⁶ and (2) nuclear parameters^{13,27-29} such as solvent and internal reorganization energies, and thermodynamic driving forces.

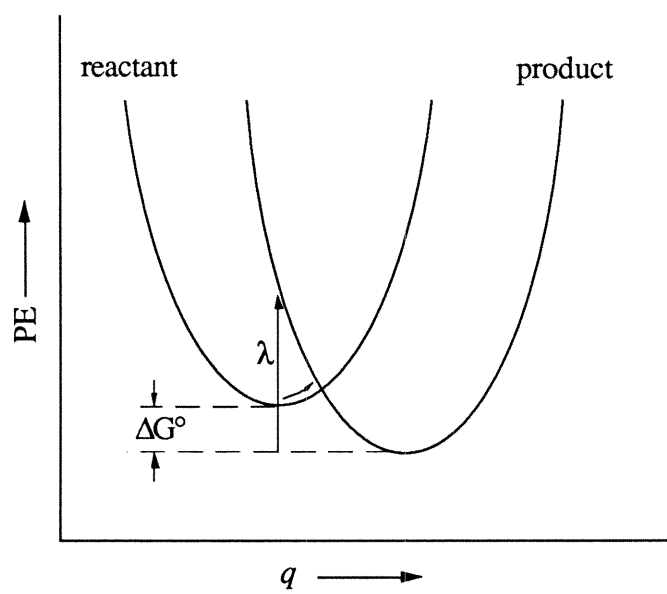
This thesis deals with the mechanistic aspects of photoinduced intramolecular electron transfer in iridium d⁸-d⁸ complexes. Many of the questions posed above will be addressed in the following chapters with the ultimate goal of coupling photoinduced charge transfer to bond-forming chemical reactions (as occurs in photosynthesis) in mind. Our studies have

focused on d^8 - d^8 complexes because they are powerful excited state reductants and their corresponding d^8 - d^7 complexes are reactive toward C-X and C-H bond activation. This chapter reviews theoretical models associated with electron-transfer reactions, introducing relevant concepts and terminology, and presents a summary of the systems that inspired this research.

Electron Transfer Theory: An in-depth description of all existing electron-transfer theories (for some examples see refs. 2,30-37) is beyond the scope of this thesis (and the author), however, a brief review of classical ET theory³¹⁻³³ (where nuclear tunneling effects are neglected) will be provided.

All theoretical expressions for the rate of electron transfer between two redox sites consist of two important components; an electronic factor and a nuclear factor. The nuclear factor can be discussed by considering the potential-energy curves in Figure 1.1. In this figure, the reactant and product potential curves (representations of multi-dimensional potential surfaces) are drawn along a reaction coordinate q which represents the positions of all the nuclei in the system (including solvent). For electron transfer to occur, the system must attain a geometry that is intermediate between that of the reactants and products (a statement of the Franck-Condon principle), corresponding to the intersection of the potential surfaces. The horizontal displacement of the two wells gives an indication of the extent of nuclear motion involved in the electron-transfer event. The energy involved in moving all the nuclei to their appropriate positions is referred to by Marcus as the reorganization energy, λ , from inner sphere effects (λ_{in}) and from outer sphere effects (λ_{out}).³⁸ λ_{in} includes changes in bond angles and bond lengths in the molecule itself while λ_{out} includes changes in solvent configuration, and is largely due to the repolarization energy of the solvent associated with the charge transfer reaction.

Figure 1.1. Product and reactant potential energy surfaces plotted as a function of nuclear coordinates (q), showing free energy change for the reaction (ΔG°), and solvent and internal reorganization energy (λ).

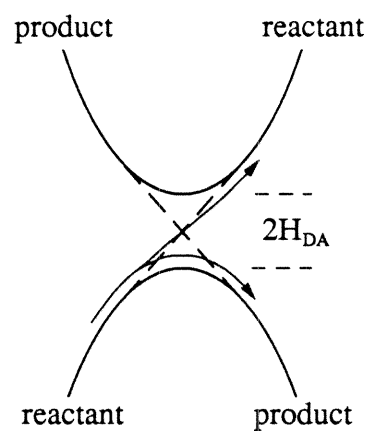


Once a suitable nuclear configuration has been reached, the fate of the transferring electron lies in the electronic factors. If there is no electronic interaction between the wave functions representing the donor and acceptor sites, the surfaces will intersect, and the reaction cannot occur. If, however, there is an electronic interaction, the intersection of the two curves results in an *avoided crossing*, a consequence of overlap between the reactant and product electronic wavefunctions. This situation is represented in Figure 1.2. The overlap causes a splitting of the two surfaces by an amount $2H_{DA}$ (electronic coupling matrix element). The magnitude of this *interaction energy*, which is the main concern of this thesis, depends on structural parameters such as donor-acceptor distance and orientation. If H_{DA} is large enough ($H_{DA} > \sim 100 \text{ cm}^{-1}$), the system remains on the lower surface when passing through the intersection region, with unit probability. This situation is termed the *adiabatic* limit and is represented by an electronic transmission coefficient, κ_E , equal to one. However, when H_{DA} is small ($H_{DA} < \sim 10 \text{ cm}^{-1}$), the splitting between surfaces is also small, and the system can sometimes *jump* to the upper surface, retaining an electronic configuration indicative of the reactants. It may therefore pass through the transition state many times without proceeding on to products. Such a system is said to be *nonadiabatic*, and is characterized by a value of κ_E less than unity.

Electron-transfer rates can be expressed in terms of these electronic and nuclear factors by eq 1.1, where ν_N is the effective frequency for nuclear motion ($\kappa_E \nu_N$ represents the activationless reaction rate constant), and FC is the Frank-Condon factor for electron transfer. Electron-transfer rates in the *nonadiabatic* limit have been treated classically by Marcus,³¹⁻³³ and can be expressed by eqs 1.2 and 1.3, where ΔG° is the free energy change for the reaction.

One of the most remarkable predictions of Marcus theory is that for very exergonic reactions the rate constant should *decrease with increasing* driving force. The range in which such behavior is predicted to occur ($-\Delta G^\circ > \lambda$) is termed the *inverted region*. Naturally, the region ($-\Delta G^\circ < \lambda$) where reaction rates behave normally (increasing with

Figure 1.2. Representation of the avoided crossing at the transition state region, showing the interaction energy, H_{DA} . If electron transfer is adiabatic ($\kappa = 1$), the reactants pass with unit probability to the lower product surface. If, however, the reaction is nonadiabatic ($\kappa < 1$), the system can be excited to the higher energy surface and may have to pass through the transition state many times before being converted into products.



$$k_{\text{ET}} = \kappa_{\text{E}} \nu_{\text{N}}(\text{FC}) \quad (1.1)$$

$$k_{\text{ET}} = \left(\pi / \hbar^2 \lambda k_{\text{B}} T \right)^{1/2} (H_{\text{ab}})^2 \exp \left(\frac{-\left(\Delta G^\circ + \lambda \right)^2}{4 \lambda k_{\text{B}} T} \right) \quad (1.2)$$

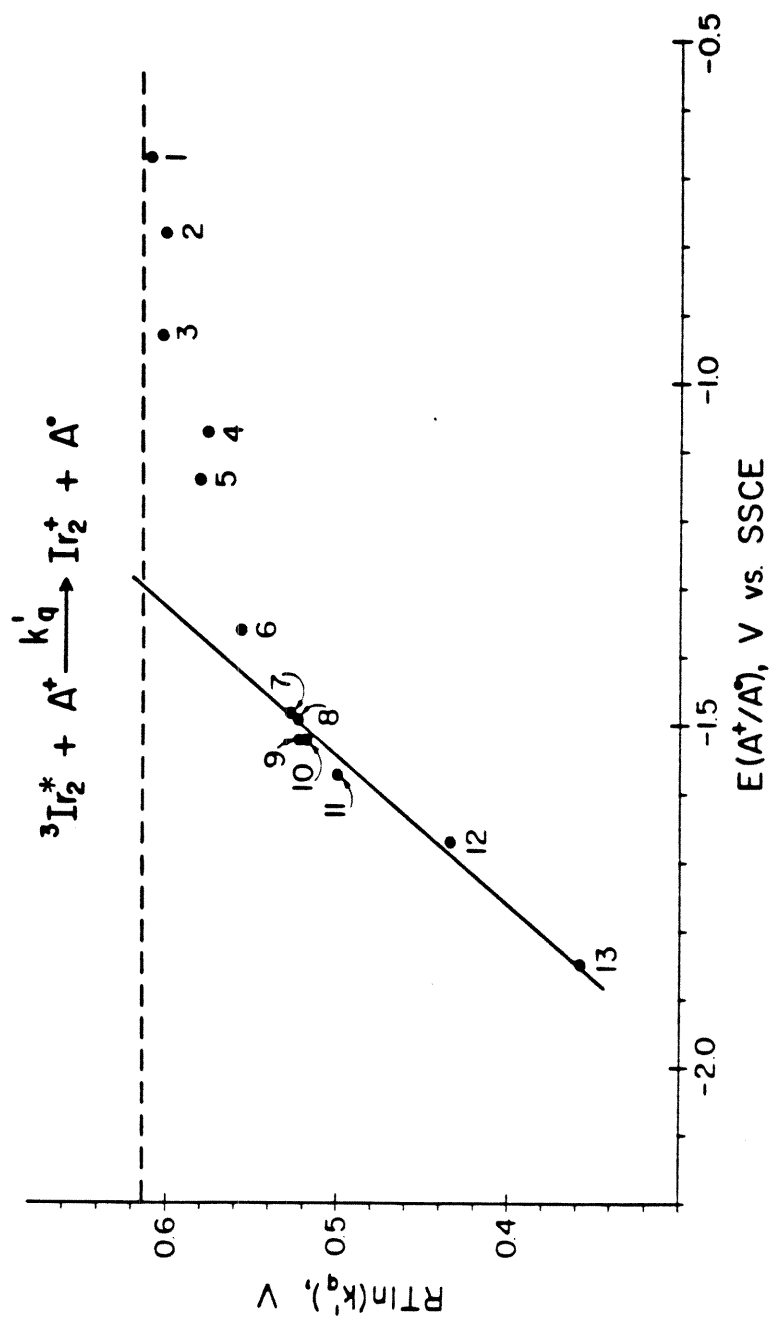
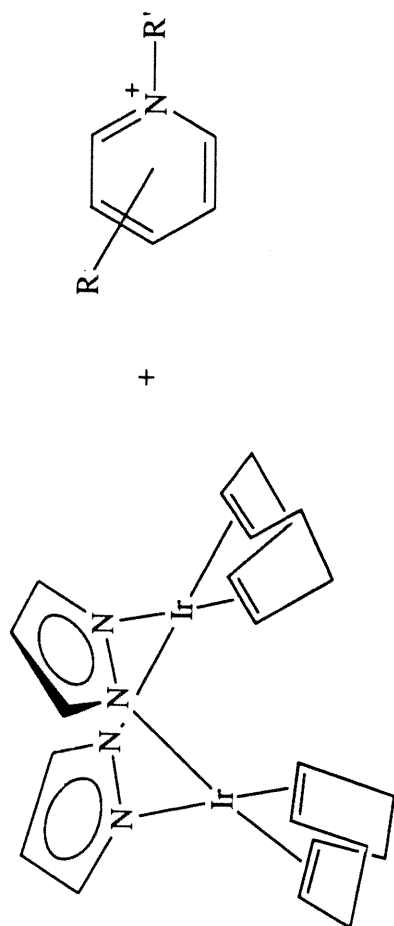
$$\lambda = \lambda_{\text{in}} + \lambda_{\text{out}} \quad (1.3)$$

increasing driving force) is termed the *normal region*.

The inverted region has attracted a great deal of attention. Its experimental confirmation has only recently become available,^{13,22,27,39-42} lending strong support to the validity of Marcus theory for electron transfer. With an adequate knowledge of electron transfer theory in hand, we proceed with an outline of the studies that motivated the research presented in this thesis.

Our research regarding photoinduced electron transfer in d⁸-d⁸ compounds began several years ago with a driving force study of excited-state electron transfer between a pyrazolyl-bridged iridium dimer and a series of substituted pyridiniums dissolved in fluid solution.^{43,44} The results from these bimolecular reactions, summarized in Figure 1.3, demonstrated the reactivity of the metal localized triplet excited state (³Ir₂^{*}) with respect to electron transfer. The expected increase in ET rates at low driving forces was observed; however, the inverted region predicted by Marcus theory was elusive due to diffusion limited reactions at high driving force. The reactivity of the higher lying singlet excited state (¹Ir₂^{*}) also remained a mystery, presumably due to the subnanosecond intrinsic lifetime of the iridium dimer, (COD)Ir(μ-pz)₂Ir(COD). The limitations inherent in this study led to the synthesis of a redox system that eliminated bimolecular diffusion as a rate limiting process. This was accomplished in a series of complexes, [Ir(μ-pz*)(CO)(Ph₂PO-CH₂CH₂-py⁺-R)]₂ (R = -H, -2,4,6-(CH₃)₃, -4-CH₃, -4-Ph), where the pyridinium cation (acceptor) was covalently linked to the iridium dimer chromophore (donor) via a phosphinite ligand.^{27,45,46} With the elimination of bimolecular

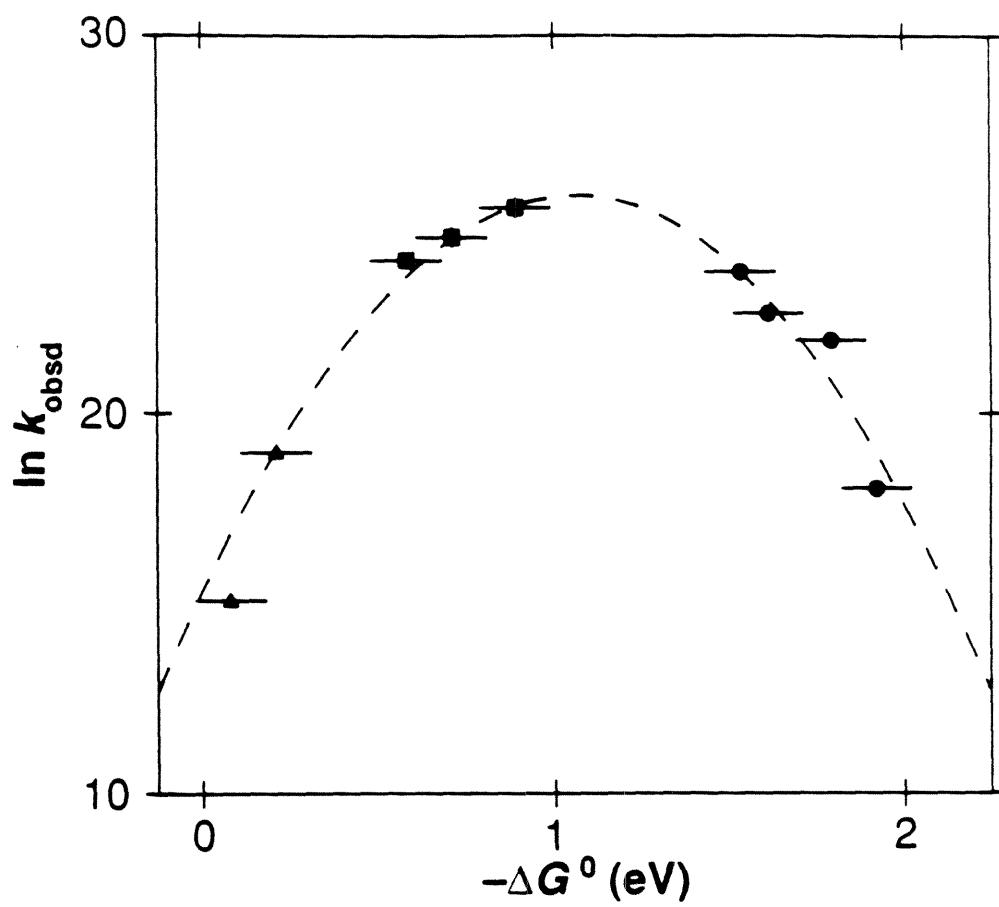
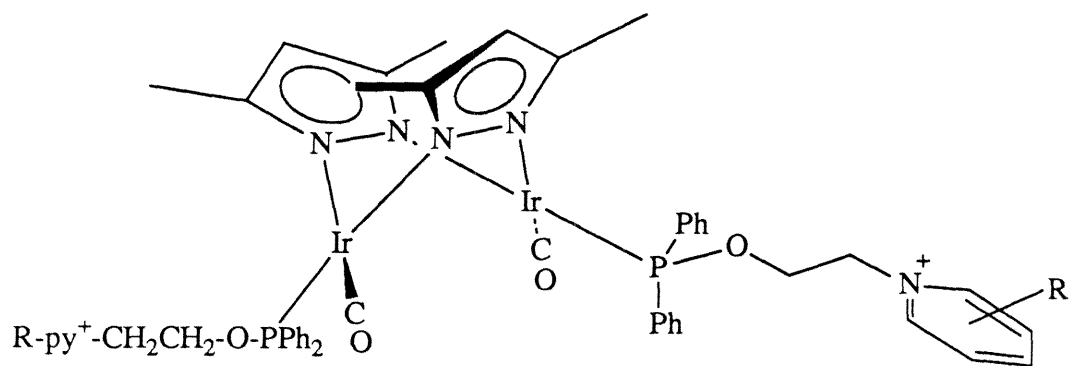
Figure 1.3. The driving force dependence data of Marshall et al., displaying diffusion limited electron-transfer rates at high driving forces.



diffusion, this system revealed the reactivity of $^1\text{Ir}_2^*$ toward electron transfer and the elusive inverted region. Figure 1.4 summarizes the data obtained from the linked donor-acceptor complexes. The singlet, triplet, and recombination ET rates were fit to classical Marcus theory with the same set of nuclear and electronic parameters ($H_{\text{DA}} = 24 \text{ cm}^{-1}$, $\lambda = 1.05 \text{ eV}$). The origin of this surprising result was difficult to ascertain due to the flexible nature of the bridge ($-\text{P}-\text{O}-\text{CH}_2-\text{CH}_2-$) separating the donor and acceptor groups. The effect of the intervening medium on H_{DA} was therefore not possible to determine. Thus, we set out to design a donor-spacer-acceptor system that would facilitate the study of medium effects on intramolecular electron transfer. This was accomplished by incorporating a structurally rigid group into the bridge separating the iridium donor and pyridinium acceptor sites. The goals of this research were (1) to explore the effects of the intervening medium on electron transfer with respect to donor-acceptor distance and orientation, and (2) to determine if differences between singlet and triplet electronic couplings would arise in a system that effectively eliminated direct donor-acceptor interaction.

In this chapter, concepts concerning electron-transfer reactions and the importance of understanding the factors that control them have been presented. Chapter 2 outlines the preparation and characterization of a series of iridium d^8 - d^8 donor-acceptor complexes. In Chapter 3, a discussion of their solution structures, obtained from the X-ray crystal structure of $[\text{Ir}(\mu\text{-pz}^*)(\text{CO})(\text{Ph}_2\text{P}-\text{O}-\text{C}_6\text{H}_4-\text{CH}_3)]_2$, and molecular mechanics calculations, is presented. Chapter 4 is concerned with spectroscopic (steady-state absorption, emission, and excitation) and electrochemical properties of the complexes. These data were used to construct a state diagram of the metal localized and charge-transfer excited states, from which electron-transfer driving forces were extracted. Finally, in Chapter 5, photoinduced (*forward*) and thermal (*back*) electron-transfer rates were measured from time-resolved absorption and emission experiments. These results are discussed in terms of through-bond and through-space mechanisms.

Figure 1.4. The driving force dependence data of Fox et al. ^1ET (■); ^3ET (▲); and ET^{b} (●). The dashed line is the best fit of these data to classical Marcus theory ($H_{\text{DA}} = 24 \text{ cm}^{-1}$, $\lambda = 1.06 \text{ eV}$).



REFERENCES

1. Bowler, B. E.; Raphael, A. L.; Gray, H. B. *Prog. Inorg. Chem.* **1990**, *38*, 259-322.
2. Marcus, R. A.; Sutin, N. *Biochim. Biophys. Acta* **1985**, *811*, 265-322.
3. Guarr, T.; McLendon, G. *Coord. Chem. Rev.* **1985**, *68*, 1-52.
4. Lehninger, A. L. *Biochemistry*; Worth Publishers Inc.: New York, 1975.
5. Okamura, M. Y.; Feher, G.; Nelson, N. In *Photosynthesis: Energy Conversion in Plants and Bacteria*; Govindjee, Ed.; Academic Press: New York, 1982; pp 197-237.
6. Gunner, M. R.; Dutton, P. L. *J. Am. Chem. Soc.* **1988**, *111*, 3400-3412.
7. Giangiacomo, K. M.; Dutton, P. L. *Proc. Natl. Acad. Sci. USA* **1988**, *86*, 2658-2662.
8. Norris, J. R.; Schiffer, M., Photosynthetic reaction centers in bacteria, *Chemical & Engineering News*, July 30, 1990, *68(31)*, 22-37.
9. Dissenhofer, J.; Epp, O.; Miki, K.; Huber, R.; Michel, H. *Nature* **1985**, *318*, 618-624.
10. Chang, C. H.; Tiede, D.; Tang, J.; Smith, U.; Norris, J.; Schiffer, M. *FEBS Lett.* **1986**, *205*, 82-86.
11. Allen, J. P.; Feher, G.; Yeates, T. O.; Komiya, H.; Rees, D. C. *Proc. Natl. Acad. Sci. USA* **1987**, *84*, 5730-5734.
12. Penfield, K. W.; Miller, J. R.; Paddon-Row, M. N.; Cotsaris, E.; Oliver, A. M.; Hush, N. S. *J. Am. Chem. Soc.* **1987**, *109*, 5061-5065.
13. Miller, J. R.; Beitz, J. V.; Huddleston, R. K. *J. Am. Chem. Soc.* **1984**, *106*, 5057-5068.
14. Pasman, P.; Rob, F.; Verhoeven, J. W. *J. Am. Chem. Soc.* **1982**, *104*, 5127-5133.
15. Warman, J. M.; de-Haas, M. P.; Paddon-Row, M. N.; Cotsaris, E.; Hush, N. S.; Oevering, H.; Verhoeven, J. W. *Nature* **1986**, *320*, 615-616.

16. Joran, A. D.; Leland, B. A.; Geller, G. G.; Hopfield, J. J.; Dervan, P. B. *J. Am. Chem. Soc.* **1984**, *106*, 6090-6092.
17. Wasielewski, M. R.; Niemczyk, M. P.; Svec, W. A.; Pewitt, E. B. *J. Am. Chem. Soc.* **1985**, *107*, 1080-1082.
18. Sakata, Y.; Nakashima, S.; Goto, Y.; Tatemitsu, H.; Misumi, S. *J. Am. Chem. Soc.* **1989**, *111*, 8979-8981.
19. Schmidt, J. A.; McIntosh, A. R.; Weedon, A. C.; Bolton, J. R.; Connolly, J. S.; Hurley, J. K.; Wasielewski, M. R. *J. Am. Chem. Soc.* **1988**, *110*, 1733-1740.
20. Schmidt, J. A.; Siemiarczuk, A.; Weedon, A. C.; Bolton, J. R. *J. Am. Chem. Soc.* **1985**, *107*, 6112-6114.
21. Oevering, H.; Paddon-Row, M. N.; Heppener, M.; Oliver, A. M.; Cotsaris, E.; Verhoeven, J. W.; Hush, N. S. *J. Am. Chem. Soc.* **1987**, *109*, 3258-3269.
22. Closs, G. L.; Calcaterra, L. T.; Green, N. J.; Penfield, K. W.; Miller, J. R. *J. Phys. Chem.* **1986**, *90*, 3673-3683.
23. Kemnitz, K. *Chem. Phys. Letters* **1988**, *152*, 305-310.
24. Heitele, H.; Michel-Beyerle, M. E.; Finckh, P. *Chem. Phys. Letters* **1987**, *134*, 273-278.
25. Heitele, H.; Michel-Beyerle, M. E. *J. Am. Chem. Soc.* **1985**, *107*, 8286-8288.
26. Finckh, P.; Heitele, H.; Folk, M.; Michel-Beyerle, M. E. *J. Phys. Chem.* **1988**, *92*, 6584-6590.
27. Fox, L. S.; Kozik, M.; Winkler, J. R.; Gray, H. B. *Science* **1990**, *247*, 1069-1071.
28. Joran, A. D.; Leland, B. A.; Felker, P. M.; Zewail, A. H.; Hopfield, J. J.; Dervan, P. B. *Nature (London)* **1987**, *327*, 508-511.
29. Wasielewski, M. R.; Niemczyk, M. P.; Svec, W. A.; Pewitt, E. B. *J. Am. Chem. Soc.* **1985**, *107*, 1080-1082.

30. Larsson, S. *J. Am. Chem. Soc.* **1981**, *103*, 4034-4040.
31. Marcus, R. A. *J. Chem. Phys.* **1956**, *24*, 966-978.
32. Marcus, R. A. *J. Chem. Phys.* **1957**, *26*, 867-871.
33. Marcus, R. A. *J. Chem. Phys.* **1957**, *26*, 872-877.
34. Beratan, D. N.; Hopfield, J. J. *J. Am. Chem. Soc.* **1984**, *106*, 1584-1594.
35. Beratan, D. N. *J. Am. Chem. Soc.* **1986**, *108*, 4321-4326.
36. Jortner, J. *J. Am. Chem. Soc.* **1980**, *102*, 6676-6686.
37. Sutin, N. *Acc. Chem. Res.* **1982**, *15*, 275-282.
38. Marcus, R. A. *Discuss. Faraday Soc.* **1960**, *29*, 21-30.
39. Gould, I. R.; Ege, D.; Mattes, S. L.; Farid, S. *J. Am. Chem. Soc.* **1987**, *109*, 3794-3796.
40. Gould, I. R.; Moody, R.; Farid, S. *J. Am. Chem. Soc.* **1988**, *110*, 7242-7244.
41. Gould, I. R.; Moser, J. E.; Ege, D.; Farid, S. *J. Am. Chem. Soc.* **1988**, *110*, 1991-1993.
42. Gould, I. R.; Moser, J. E.; Armitage, B.; Farid, S.; Goodman, J.; Herman, M. *J. Am. Chem. Soc.* **1989**, *111*, 1917-1919.
43. Marshall, J. L.; Stobart, S. R.; Gray, H. B. *J. Am. Chem. Soc.* **1984**, *106*, 3027-3029.
44. Marshall, J. L., Ph.D. Dissertation, California Institute of Technology, Pasadena, CA, 1987.
45. Fox, L. S., Ph.D. Dissertation, California Institute of Technology, Pasadena, CA, 1989.
46. Fox, L. S.; Marshall, J. L.; Gray, H. B.; Winkler, J. R. *J. Am. Chem. Soc.* **1987**, *109*, 6901-6902.

Chapter 2

Synthesis of Donor-Spacer-Acceptor Complexes

INTRODUCTION

Electron-transfer (ET) reactions between donor and acceptor groups are governed by parameters that express the nature of the intervening medium, the free energy change for the reaction, and relative donor-acceptor distance and orientation. A majority of studies until the last decade had been conducted on systems where the donor and acceptor were dissolved in fluid solution.¹⁻⁴ In these systems, electron transfer occurs only when diffusion brings the donor and acceptor groups within a contact distance necessary for reaction. However, more recently, numerous *linked* donor-acceptor complexes have been synthesized and studied.⁵⁻²⁵ Two major classes of bridges have been used to link donors and acceptors: (1) flexible bridges such as hydrocarbon chains^{5, 6, 25-27} and (2) rigid or semi-rigid bridges such as ring systems^{7-9, 14-19, 21, 23, 28} or peptide bonds.^{24, 29, 30}

If the bridge is flexible and not too long, it serves to bring the donor and acceptor together, much the way donor and acceptor groups interact in bimolecular reactions, but at a much higher frequency. This type of bridge nearly eliminates the troublesome complication of diffusion limited electron-transfer rates.²⁵

Alternatively, if the bridge is semi-rigid or completely rigid it can serve to orient the donor and acceptor in a specific geometry. Depending on the nature of the bridge it can also provide multiple electron-transfer pathways. For example, in the hypothetical donor-

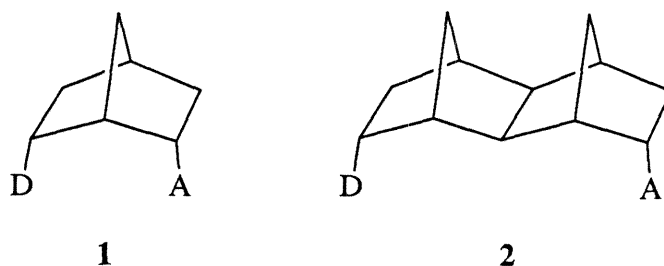
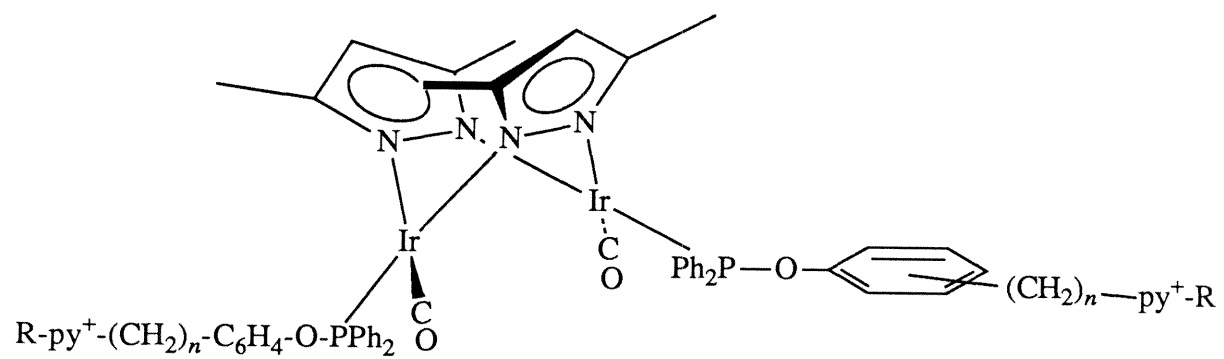


Figure 2.1. Structures of model rigid donor-spacer-acceptor complexes, demonstrating the concept of through-bond versus through-space electron-transfer mechanisms.

acceptor complex **1** (Figure 2.1), bridged by a rigid spacer, electron transfer from the donor to the acceptor can occur via the hydrocarbon chain (through-bond mechanism) and/or via a direct interaction between the donor and acceptor (through-space mechanism). On the other hand, the through-space mechanism in **2** is unlikely to be a contributing factor in the transfer of electrons from the donor to the acceptor due to the large through-space separation. Therefore, only through-bond mechanisms will be important in determining the electron-transfer rate in **2**. From a study of the ET rates in these complexes, a distinction between through-space and through-bond mechanisms can be established. If the ET rates turn out to scale with the number of carbon atoms between the donor and acceptor, we would deduce that the through-bond mechanism in **1** is the only mechanism operable (the dependence of electron-transfer rates on the number of intervening carbon atoms can be determined by extending the series further to include complexes with more than two intervening norbornane groups). However, if the ET rates did not scale with the number of carbon atoms in the bridge, and the electron-transfer rate in **1** was unexpectedly fast, then we would deduce that through-space interactions in **1** are the primary contribution to the overall coupling of the donor and the acceptor. This example demonstrates some of the advantages of linking donors and acceptors with rigid spacers in studies aimed at elucidating orientation, distance, and through-space vs. through-bond effects on electron-transfer rates.

The donor-acceptor complexes used in the present study utilize rigid and semi-rigid bridges to link donor and acceptor groups. These complexes, shown in Figure 2.2, are represented as $[\text{Ir}(\mu\text{-pz}^*)(\text{CO})(\text{Ph}_2\text{PO-C}_6\text{H}_4\text{-(CH}_2\text{)}_n\text{-py}^+\text{-R})]_2(\text{PF}_6^-)_2$, where pz^* = 3,5-dimethylpyrazolyl, Ph = phenyl, $\text{-C}_6\text{H}_4\text{-}$ = phenylene, py^+ = pyridinium, and $n = 0, 1, 2, 3$. They are similar to $\text{d}^8\text{-d}^8$ compounds of previous bimolecular and unimolecular ET studies conducted in our laboratory in which pyrazolyl-bridged iridium dimer chromophores were used as electron donors and pyridinium groups (in solution or covalently attached to the donor) were employed as one-electron acceptors. In the present

Figure 2.2. Structure of donor-spacer-acceptor complexes, $[\text{Ir}(\mu\text{-pz}^*)(\text{CO})(\text{Ph}_2\text{PO-C}_6\text{H}_4\text{-(CH}_2)_n\text{-py}^+\text{-R})]_2$, where the iridium center (Ir_2) and pyridinium group (py^+) act as electron donor and electron acceptor. Ph = phenyl, $n = 0, 1, 2$, or 3 , and R = H, 4-*t*-butyl, or 4-amide.



study the pyridinium acceptor was covalently attached via a phosphinite ligand to the metal center. A phenylene bridge was incorporated into the bridge separating Ir₂ (donor) and py⁺ (acceptor). In all but one molecule the phenylene bridge was 1,4-disubstituted (in one molecule the phenylene group was 1,3-disubstituted). The number of methylene groups, *n*, bridging the pyridinium acceptor to the phenylene group, was varied from *n* = 0 to 3. In addition, the pyridinium R group was varied in *n* = 1 complexes.

As will be demonstrated in Chapter 4, intramolecular electron-transfer studies also require that *model* complexes, in which only the donor is incorporated into the complex, be prepared. Therefore, complexes of the type, [Ir(μ -pz*)(CO)(Ph₂PO-C₆H₄-Y)]₂, where Y is a poor electron acceptor (CH₃ or CH₂-Quin⁺PF₆⁻) have been synthesized.

In this chapter the syntheses of the series of donor-acceptor complexes and two model complexes are presented. The characterization of all the molecules by ¹H, ³¹P NMR and IR spectroscopies is described. The complexes will, from here on, be denoted as [Ir₂]-R. [Ir₂] represents the iridium dimer core including the pyrazolyl bridge and carbonyl ligands, the diphenyl phosphine group, and the oxygen atom and phenylene group of the bridge, *i.e.*, [Ir₂] = (-C₆H₄-O-Ph₂P)(CO)Ir(μ -pz*)₂Ir(CO)(Ph₂P-O-C₆H₄-). R denotes the remainder of the bridge and in all but the two model complexes, the pyridinium acceptor.

EXPERIMENTAL

Materials:

Tetrahydrofuran was distilled from sodium/benzophenone. The color of the solvent/drying agent prior to distillation was dark blue or purple. A yellow color indicated the presence of H₂O or O₂ at unacceptable levels. Methylene chloride was distilled from calcium hydride under argon. Acetone and ethanol were spectral grade in quality and used as received. Acetonitrile was either dried over activated 3Å Linde sieves for 24 hrs and

distilled onto freshly activated 3Å sieves for storage in the dry box (VAC Atmospheres) or the acetonitrile (Burdick & Jackson) was used directly from freshly opened bottles and stored over Linde 3Å molecular sieves for at least three days. Synthesis of *N,N*-dimethyl-*P,P*-diphenylphosphine is described elsewhere.³¹ Tetracarbonyl-bis(μ -3,5-dimethylpyrazolyl)diiridium(I), $[\text{Ir}(\mu\text{-pz}^*)(\text{CO})_2]_2$, was prepared according to previously established procedures.³² All other chemicals were of reagent grade or better and were used as received.

Physical Measurements:

¹H spectra were recorded on either a JEOL FX-90Q or JEOL GX-400 FT spectrometer. ¹H chemical shifts are reported in ppm (δ) using the solvent (CH_2Cl_2 δ 5.32, CH_2CN δ 1.93, CD_3COCH_2 δ 2.04, or HOD δ 4.63) as an internal standard. Proton decoupled ³¹P NMR spectra were recorded on a JEOL FX-90Q spectrometer and referenced to external 85% aqueous phosphoric acid. IR spectra were recorded as Nujol or fluorolube mulls, KBr pressure pellets, or in dichloromethane solutions on a Beckman Instruments IR-4240 spectrometer or on a Perkin-Elmer 1600 FTIR. Elemental analyses were obtained at the Caltech analytical facility.

Synthesis of Phenols:

N-(4-hydroxyphenyl)pyridinium, $\text{HO-C}_6\text{H}_4\text{-py}^+$ ($n = 0$): disodium 4-nitrophenyl phosphate hexahydrate (0.31 g, 1.4 mmol), pyridine (4 mL) and H₂O (25 mL) were added to a Schlenk flask. The flask was immersed in an H₂O filled, jacketed dewar fitted with a Pyrex window (Figure 2.3). A refrigerated cold unit was attached to the dewar and water was circulated at 4°C. While compressed air was directed at the window, to prevent condensation, the sample was broad-band irradiated with excitation from a 1000 W lamp for 24 hrs, upon which the solution turned from pale yellow to bright yellow. The reaction mixture was then evaporated to dryness, leaving a dark yellow residue. The solid was dissolved in 3 mL H₂O followed by the addition of 20 mL of ethanol which forced the

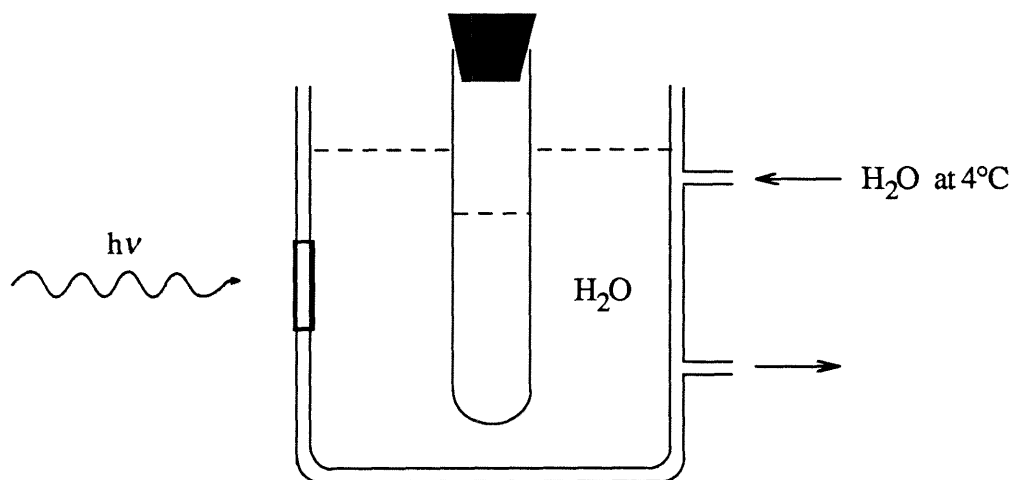


Figure 2.3. Apparatus employed in the synthesis of $\text{HO-C}_6\text{H}_4\text{-py}^+$.

precipitation of the pyridinium salt. The solid was collected by filtration and dissolved in concentrated hydrochloric acid (25 mL) in a round bottom flask fitted with a Kontes Teflon needle valve. The solution was stirred for 24 hrs at 100°C in the *closed* system which resulted in the hydrolyzes of the phosphate group. The solvent was again removed in vacuo. Ethanol was added to the solid (dissolving the desired product), and the solution was filtered and evaporated in vacuo yielding the crude product as a red oily residue. 1 mL of H_2O was added followed by 5 mL of a saturated H_2O solution of ammonium hexafluorophosphate which caused the precipitation of the hexafluorophosphate salt of the desired product, $\text{HO-C}_6\text{H}_4\text{-py}^+$.

N-(4-hydroxyphenylmethyl)pyridinium, $\text{HO-C}_6\text{H}_4\text{-CH}_2\text{-py}^+$ ($n = 1$): *p*-cresol (21.13 g, 0.195 moles) was dissolved in dry THF (30 mL) and triethylamine (27.2 mL, 0.195 moles) was added to the solution. Acetylchloride (13.9 mL, 0.195 moles) was added slowly to the reaction mixture which caused the immediate precipitation of a white

solid. The solution was stirred for ~30 min to ensure complete consumption of the starting material. The product, which is soluble in THF, was separated from the insoluble byproducts by filtration, the solvent was evaporated in vacuo, and the crude product was fractionally distilled yielding $\text{AcO-C}_6\text{H}_4\text{-CH}_3$ as a colorless liquid (24.4 g).

$\text{AcO-C}_6\text{H}_4\text{-CH}_3$ (24.4 g, 0.163 moles) was dissolved in carbon tetrachloride (50 mL) and freshly recrystallized *N*-bromosuccinimide (28.9 g, 0.162 moles) was added as well as *tert*-butyl hydroperoxide (0.1 mL) which acts to catalyze the reaction. The reaction vessel was fitted with a condenser and under constant supervision the mixture was stirred vigorously and heated to reflux. Several minutes after reflux temperature was reached a dark orange gas formed above the solution (presumably Br_2 gas) and the solution itself turned red. After ~15 min the solution cleared and the Br_2 gas was consumed. The solvent was removed in vacuo leaving $\text{AcO-C}_6\text{H}_4\text{-CH}_2\text{Br}$ as yellow oily residue.

$\text{AcO-C}_6\text{H}_4\text{-CH}_2\text{Br}$ (2 g) without further purification was then dissolved in neat pyridine (20 mL) and stirred for 24 hrs. The reaction mixture was filtered and the solid was dried at 40°C yielding $\text{AcO-C}_6\text{H}_4\text{-CH}_2\text{-py}^+\text{Br}^-$. A pyridine molecule of solvation still remained (as evidenced by ^1H NMR) after rigorous drying. No further attempts were made to remove the pyridine and the next reaction was conducted with the unpurified compound.

$\text{AcO-C}_6\text{H}_4\text{-CH}_2\text{-py}^+\text{Br}^- \cdot \text{pyridine}$ was dissolved in 30 mL H_2O and 0.5 mL of 48% HBr was added. The solution was stirred vigorously for 24 hrs. followed by the addition of a large excess of a saturated water solution of ammonium hexafluorophosphate. The hexafluorophosphate salt of $\text{HO-C}_6\text{H}_4\text{-CH}_2\text{-py}^+$ was separated from the solution by filtration and washed extensively with H_2O until the washings were of neutral pH.

N-(4-hydroxyphenylmethyl)quinuclidinium, $\text{HO-C}_6\text{H}_4\text{-CH}_2\text{-Quin}^+$ ($n = 1$): The synthesis of this complex was conducted by the same procedure as described for $\text{HO-C}_6\text{H}_4\text{-CH}_2\text{-py}^+$ except quinuclidine was used instead of pyridine. The reaction of 1 eq of quinuclidine with $\text{AcO-C}_6\text{H}_4\text{-CH}_2\text{Br}$ was conducted in THF.

4-*tert*-butyl-*N*-(4-hydroxyphenylmethyl)pyridinium, HO-C₆H₄-CH₂-py⁺-tB

(*n* = 1): The synthesis of this complex was conducted by the same procedure as described for HO-C₆H₄-CH₂-py⁺ except 4-*t*-butylpyridine was used instead of pyridine. The reaction of 1 eq of 4-*t*-butylpyridine with AcO-C₆H₄-CH₂Br was conducted in THF.

4-amido-*N*-(4-hydroxyphenylmethyl)pyridinium, HO-C₆H₄-CH₂-py⁺-Am

(*n* = 1): The synthesis of this complex was conducted by the same procedure as described for HO-C₆H₄-CH₂-py⁺ except isonicotinamide was used instead of pyridine. The reaction of 1 eq of isonicotinamide with AcO-C₆H₄-CH₂Br was conducted in THF. Analysis Calculated for C₁₃H₁₃F₆N₂O₂P: C, 41.73%; H, 3.50%; N, 7.49%. Found: C, 41.71%; H, 3.50%; N, 7.06%.

***N*-(4-hydroxyphenethyl)pyridinium, HO-C₆H₄-(CH₂)₂-py⁺ (*n* = 2):**

4-hydroxyphenethyl alcohol (2.56 g, 18.53 mmoles) was dissolved in 48% HBr (35 mL) and stirred for 3 hrs. at 90°C upon which dark red-brown droplets separated from the solution. The reaction mixture was then poured onto ice, initiating the precipitation of a white solid. The crude product was extracted with three portions of 30 mL diethylether. The ether solution was then washed with water until the washings were at neutral pH (6 times), dried with anhydrous magnesium sulfate, filtered, and evaporated leaving a white solid. The crude product was collected and recrystallized from hot cyclohexane yielding 1.47 g of white needles. β-(*p*-hydroxyphenyl)ethyl bromide (0.40 g) from the previous step was dissolved in neat pyridine (3 mL) and stirred for 5 hrs. at 40-50°C at which time a white precipitate formed. The mixture was filtered, washed with hexane, metathesized to the hexafluorophosphate salt and washed three times with H₂O, yielding 100 mg of the desired pyridinium salt, HO-C₆H₄-(CH₂)₂-py⁺.

***N*-(3-hydroxyphenethyl)pyridinium, HO-C₆H₄-3-(CH₂)₂-py⁺ (*n* = 2):** The synthesis of this complex was conducted by the same procedure as described for HO-C₆H₄-(CH₂)₂-py⁺ except that 3-hydroxyphenethyl alcohol was used instead of 4-hydroxyphenethyl alcohol.

N-(4-hydroxyphenylpropyl)pyridinium, $\text{HO-C}_6\text{H}_4\text{-(CH}_2\text{)}_3\text{-py}^+$ ($n = 3$): The synthesis of this complex was conducted by the same procedure as described for $\text{HO-C}_6\text{H}_4\text{-(CH}_2\text{)}_2\text{-py}^+$ except that 4-hydroxyphenylpropyl alcohol was used instead of 4-hydroxyphenethyl alcohol.

Synthesis of Phosphinite Ligands:

$\text{Ph}_2\text{P-O-C}_6\text{H}_4\text{-CH}_3$: *p*-cresol (1.83 g, 7.0 mmoles) was dissolved in dry THF (100 mL) in a 50 mL Schlenk flask with a side arm. The solution was pump-flushed three times while being stirred. Triethylamine (2.59 mL, 18.6 mmoles) was added via syringe. After ~1 min of stirring, chlorodiphenylphosphine (3.43 mL) was added slowly via syringe. The total volume was added over 5 min. Upon contact with the solution, the insoluble triethylamine hydrochloride precipitated from solution. The reaction mixture was stirred for 15 min to ensure complete consumption of the starting materials. The solution was separated from the white powder by cannula filtration. The solution at this point could be exposed to ambient atmosphere. The flask containing crude product, solvent, and small amounts of triethylamine hydrochloride was fitted with a short-path distillation apparatus. The solvent was removed at room temperature in vacuo leaving an oily, cloudy residue. The crude product was then fractionally distilled, collecting the product between 145° and 180°C at $\sim 10^{-2}$ torr in a cow receiver. The purified phosphinite product at room temperature solidified in the cow receiver after ~1 hr.

$\text{Ph}_2\text{P-O-C}_6\text{H}_4\text{-py}^+$, $\text{Ph}_2\text{P-O-C}_6\text{H}_4\text{-CH}_2\text{-py}^+$, $\text{Ph}_2\text{P-O-C}_6\text{H}_4\text{-CH}_2\text{-Quin}^+$, $\text{Ph}_2\text{P-O-C}_6\text{H}_4\text{-CH}_2\text{-py}^+\text{-tB}$, $\text{Ph}_2\text{P-O-C}_6\text{H}_4\text{-CH}_2\text{-py}^+\text{-Am}$, $\text{Ph}_2\text{P-O-C}_6\text{H}_4\text{-(CH}_2\text{)}_2\text{-py}^+$, $\text{Ph}_2\text{P-O-C}_6\text{H}_4\text{-3-(CH}_2\text{)}_2\text{-py}^+$, and $\text{Ph}_2\text{P-O-C}_6\text{H}_4\text{-(CH}_2\text{)}_3\text{-py}^+$: In all cases, the syntheses of these phosphinite ligands were accomplished by the following procedure: 0.5 g of the appropriate phenol (syntheses described above) was dissolved in CH_3CN (~2 mL) in the dry box, followed by the addition of an CH_3CN solution of *N,N*-dimethyl-*P,P*-diphenylphosphine, Ph_2PNMe_2

(1 eq). The reaction was stirred for 1 hr, then transferred to a Schlenk flask. The solvent was removed in vacuo outside the box, leaving an oily residue which was not further purified owing to the extreme air-sensitivity of the phosphinite ligands.

Synthesis of Iridium(I) Complexes:

$[\text{Ir}_2]\text{-CH}_3$, $[\text{Ir}_2]\text{-py}^+$, $[\text{Ir}_2]\text{-CH}_2\text{-py}^+$, $[\text{Ir}_2]\text{-CH}_2\text{-Quin}^+$, $[\text{Ir}_2]\text{-CH}_2\text{-py}^+\text{-tB}$, $[\text{Ir}_2]\text{-CH}_2\text{-py}^+\text{-Am}$, $[\text{Ir}_2]\text{-(CH}_2)_2\text{-py}^+$, $[\text{Ir}_2]\text{-3-(CH}_2)_2\text{-py}^+$, and $[\text{Ir}_2]\text{-(CH}_2)_3\text{-py}^+$: The iridium complexes were all synthesized by a similar procedure. A concentrated acetonitrile solution of the phosphinite (2.1 eq) was added to an acetonitrile solution of $[\text{Ir}(\mu\text{-pz}^*)(\text{CO})_2]_2$ (1 eq) in the dry box (the scale of this reaction was typically 100-200 mg of $[\text{Ir}(\mu\text{-pz}^*)(\text{CO})_2]_2$). An immediate liberation of carbon monoxide gas was observed with a corresponding change in solution color from orange to orange/red. The reaction mixture was stirred for ~2 hrs to ensure complete consumption of the starting materials. CH_3CN was removed in vacuo, leaving in all cases an orange/red residue, which was taken up in a minimum of dichloromethane. Addition of excess ethanol to the saturated, deep red solutions precipitated the iridium(I) products as light orange powders. $[\text{Ir}_2]\text{-CH}_3$ Analysis: Calculated for $\text{Ir}_2\text{C}_{50}\text{H}_{48}\text{N}_4\text{O}_4\text{P}_2$: C, 49.42%; H, 3.98%; N, 4.61%. Found C, 49.19%; H, 3.96%; N, 4.69%. $[\text{Ir}_2]\text{-py}^+$ Analysis: Calculated for $\text{Ir}_2\text{C}_{58}\text{H}_{52}\text{F}_{12}\text{N}_6\text{O}_4\text{P}_4$: C, 42.65%; H, 3.21%; N, 5.15%. Found: C, 42.34%; H, 3.18%; N, 4.96%. $[\text{Ir}_2]\text{-CH}_2\text{-py}^+$ Analysis: Calculated for $\text{Ir}_2\text{C}_{60}\text{H}_{56}\text{F}_{12}\text{N}_6\text{O}_4\text{P}_4$: C, 43.38%; H, 3.40%; N, 5.06%. Found: C, 44.26%; H, 3.38% N, 4.60%.

RESULTS and DISCUSSION

The series of donor-acceptor complexes, $[\text{Ir}(\mu\text{-pz}^*)(\text{CO})(\text{Ph}_2\text{PO-C}_6\text{H}_4\text{-(CH}_2)_n\text{-py}^+\text{-R})]_2(\text{PF}_6^-)_2$ ($n = 0, 1, 2, 3$), and two model complexes, $[\text{Ir}(\mu\text{-pz}^*)(\text{CO})(\text{Ph}_2\text{PO-C}_6\text{H}_4\text{-Y})]_2$ ($\text{Y} = \text{CH}_3$ or $\text{CH}_2\text{-Quin}^+\text{PF}_6^-$) have been synthesized, and are shown in Figure 2.4. The syntheses of these iridium complexes were accomplished in three general steps, outlined in Figure 2.5.

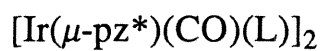
Step 1:

The phenol, **1**, was first synthesized by simple, relatively high yield reactions. Four classes of phenols, categorized by the number of methylene groups in the molecule, have been synthesized ($n = 0$: $\text{HO-C}_6\text{H}_4\text{-py}^+$; $n = 1$: $\text{HO-C}_6\text{H}_4\text{-CH}_2\text{-py}^+$, $\text{HO-C}_6\text{H}_4\text{-CH}_2\text{-Quin}^+$, $\text{HO-C}_6\text{H}_4\text{-CH}_2\text{-py}^+\text{-tB}$, and $\text{HO-C}_6\text{H}_4\text{-CH}_2\text{-py}^+\text{-Am}$; $n = 2$: $\text{HO-C}_6\text{H}_4\text{-(CH}_2)_2\text{-py}^+$, and $\text{HO-C}_6\text{H}_4\text{-3-(CH}_2)_2\text{-py}^+$; $n = 3$: $\text{HO-C}_6\text{H}_4\text{-(CH}_2)_3\text{-py}^+$). The synthetic schemes used to prepare the four classes of compounds are outlined in Figures 2.6 ($n = 0$), 2.7 ($n = 1$), and 2.8 ($n = 2, 3$). The final step in the synthesis of the pyridinium salts was to metathesize them to their corresponding hexafluorophosphate salts, in order to enhance the solubility of their corresponding phosphinite ligands and iridium complexes in organic solvents.

The isolated yield of the $n = 0$ reaction (Figure 2.6) was approximately 40%. Attempts to increase the yield of **2** by increasing reaction times were unsuccessful and served only to produce more byproducts, decreasing the overall yield. This reaction was also found to be specific to pyridine. Attempts to react substituted pyridines with **1** were unsuccessful due to the poor solubility of the pyridine in H_2O at 4°C .

The syntheses of $n = 1$ complexes (Figure 2.7) were complicated by the susceptibility of the intermediate benzyl bromide to attack by base, specifically, the phenol itself; initial attempts at preparing this class of compounds were frustrated by the unavoidable production of polymers. This complication necessitated capping the hydroxy group with a

Figure 2.4. Structures of the phosphinite ligands in the two model complexes and the series of Ir₂-py⁺ donor-acceptor complexes.



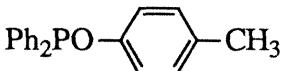
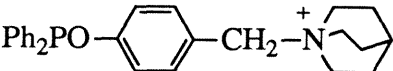

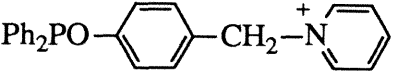
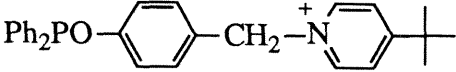
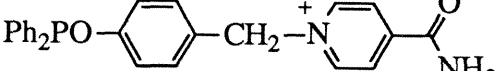
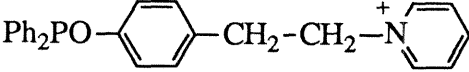
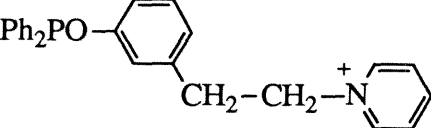
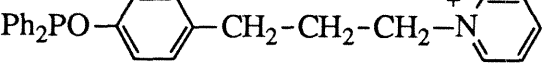
L	Symbol
	$[\text{Ir}_2]\text{-CH}_3$
	$[\text{Ir}_2]\text{-Quin}^+$
	$[\text{Ir}_2]\text{-py}^+$
	$[\text{Ir}_2]\text{-CH}_2\text{-py}^+$
	$[\text{Ir}_2]\text{-CH}_2\text{-py}^+\text{-tB}$
	$[\text{Ir}_2]\text{-CH}_2\text{-py}^+\text{-Am}$
	$[\text{Ir}_2]\text{-(CH}_2)_2\text{-py}^+$
	$[\text{Ir}_2]\text{-3-(CH}_2)_2\text{-py}^+$
	$[\text{Ir}_2]\text{-(CH}_2)_3\text{-py}^+$

Figure 2.5. Three step synthesis of $\text{Ir}_2\text{-py}^+$ donor-acceptor complexes. (1) Synthesis of pyridinium phenols. (2) Synthesis of phosphinite ligands. (3) Synthesis of iridium complexes.

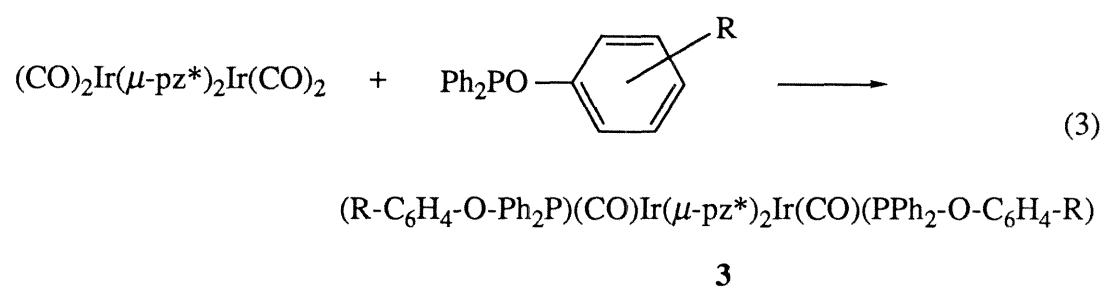
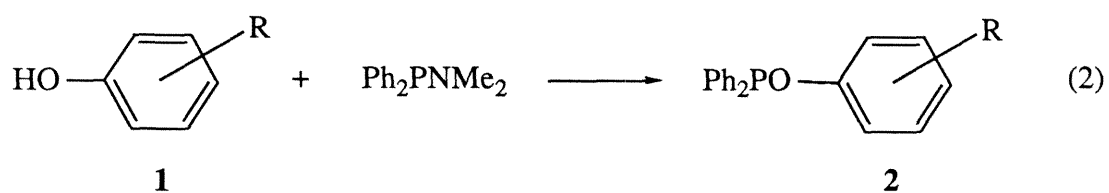
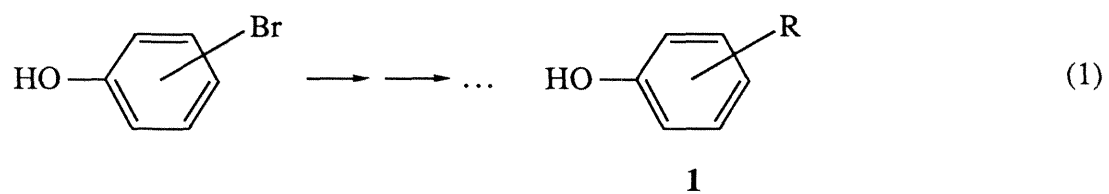


Figure 2.6. Synthesis of complex with $n = 0$.

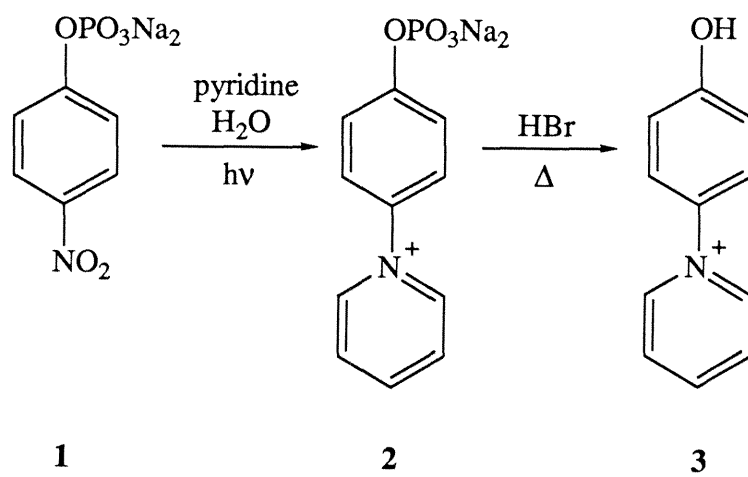


Figure 2.7. Syntheses of complexes with $n = 1$. AcCl = acetyl chloride, Et₃N = triethylamine, NBS = *N*-bromosuccinimide, *t*-BuOOH = *tert*-butyl hydroperoxide.

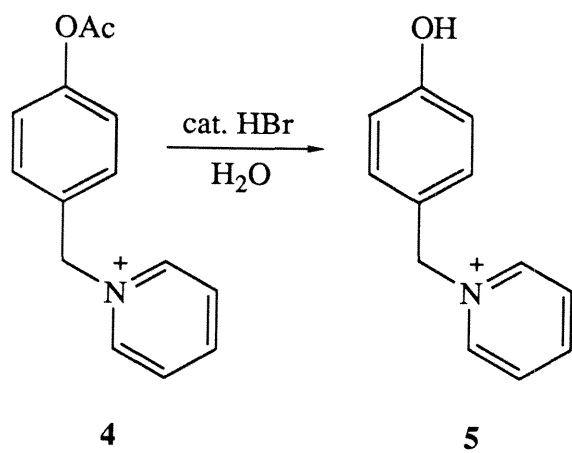
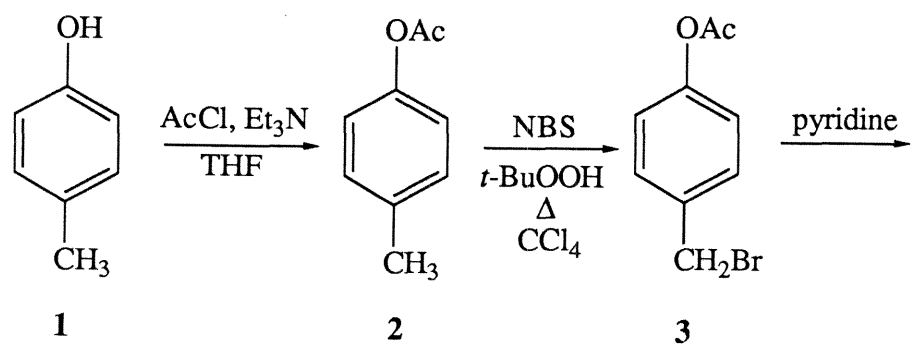
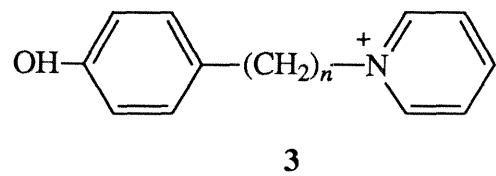
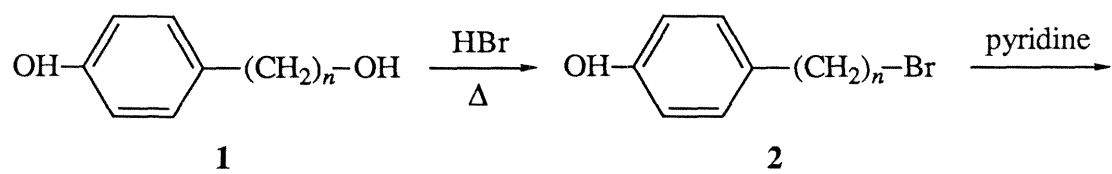


Figure 2.8. Syntheses of complexes with $n = 2$ and $n = 3$.



protecting group until the benzyl bromide was converted into the corresponding pyridinium salt, at which point the protecting group was hydrolyzed off.

The reactions used to synthesize complexes with $n = 2$ and 3 (Figure 2.8) are straightforward and will not be discussed further.

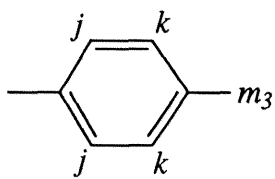
Characterization of Phenols:

Each of the phenols was characterized by ^1H and ^{31}P NMR spectroscopy. These data are summarized in Table 2.1, and the corresponding numbering scheme is shown in Figure 2.9. The 1,4-phenylene groups of all the molecules exhibit the characteristic AA'BB' doublet of doublets between 6.6 and 7.5 ppm, the precise chemical shift of which depends on the nature of the 4-substituent (columns j and k in Table 2.1). The methylene groups in $n = 1$ compounds show up as singlets shifted downfield (~ 5.5 ppm) by the effect of the positive charge on the adjacent pyridinium cation (column m). For $n = 2$ and 3 compounds, the methylene resonance closest to the pyridinium is a triplet at ~ 4.5 ppm, while the remaining resonances are in normal positions (2.2 to 3.2 ppm). The pyridinium resonances are resolved for each unique position (2-position: 8.45-8.81 ppm; 3-position: 7.78-8.23 ppm; 4-position: 8.30-8.59 ppm).

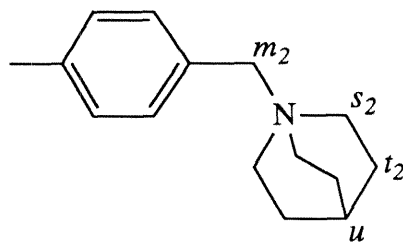
Step 2:

The next step was the alcoholysis of *N,N*-dimethyl-*P,P*-diphenylphosphine by the phenol synthesized in Step 1.³¹ This transformation was carried out in a dry box. The phosphinite product was isolated but not purified for the next step. Characterization by ^{31}P NMR was conducted, showing single peaks between 109.8 and 112.6 ppm for each compound (first column of Table 2.2), identifying the ligands as esters of diphenylphosphinous acid.³³

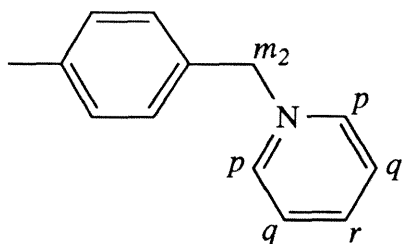
Figure 2.9. Numbering scheme used in assigning ^1H NMR spectra of phenols. *j* and *k* are phenylene protons; *m*, *n*, and *o* are methylene protons; *p*, *q*, and *r* are pyridinium protons; *s*, *t*, and *u* are quinuclidine protons; and *v* are the methyl protons of the *tert*-butyl group.



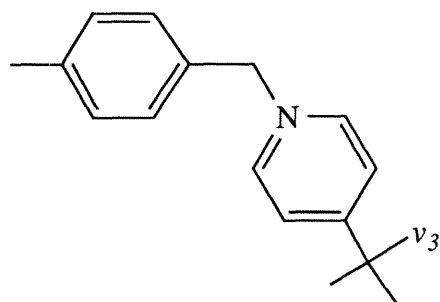
HO-C₆H₄-CH₃



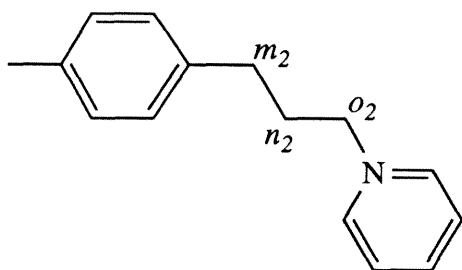
HO-C₆H₄-CH₂-Quin⁺



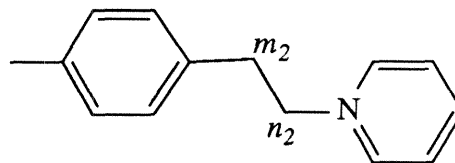
HO-C₆H₄-CH₂-py⁺



HO-C₆H₄-CH₂-py⁺-tB



HO-C₆H₄-(CH₂)₃-py⁺



HO-C₆H₄-(CH₂)₂-py⁺

Table 2.1. ^1H NMR Resonances for Phenols ^e

Compounds	<i>j</i>	<i>k</i>	<i>m</i>	<i>n</i>	<i>o</i>	<i>p(s)</i>	<i>q(t)</i>	<i>r(u)</i>	<i>v</i>
HO-C ₆ H ₄ -CH ₃	7.04	7.10	—	—	—	—	—	—	—
HO-C ₆ H ₄ -CH ₂ -Quin ⁺	6.82	7.10	4.08	—	—	3.31 (t)	— ^b (m)	1.88 (m)	—
HO-C ₆ H ₄ -py ⁺	7.07	7.51	—	—	—	8.81 (d)	8.11 (t)	8.59 (t)	—
HO-C ₆ H ₄ -CH ₂ -py ⁺	6.88	7.32	5.60	—	—	8.68 (d)	7.98 (t)	8.48 (t)	—
HO-C ₆ H ₄ -CH ₂ -py ⁺ -Am	6.89	7.34	5.64	—	—	8.80 (d)	8.23 (d)	—	—
HO-C ₆ H ₄ -CH ₂ -py ⁺ -tB ^a	— ^c	— ^c	5.31	—	—	8.31 (d)	7.81 (d)	—	1.38
HO-C ₆ H ₄ -(CH ₂) ₂ -py ⁺	6.70	6.93	4.69 (t)	3.16 (t)	—	8.43 (d)	7.92 (t)	8.48 (t)	—
HO-C ₆ H ₄ -3-(CH ₂) ₂ -py ⁺	— ^d	— ^d	4.73 (t)	3.18 (t)	—	8.45 (d)	7.93 (t)	8.38 (t)	—
HO-C ₆ H ₄ -(CH ₂) ₃ -py ⁺ ^a	6.58	6.89	4.39 (t)	2.17 (q)	2.48 (t)	8.53 (d)	7.78 (t)	8.30 (t)	—

^a Bromide salt in D₂O.

^b Obscured by phenyl resonances.

^c Obscured by resonances from Ph₄B[−] which are at 6.95 and 7.30 ppm.

^d The phenylene resonances are 7.20 (s), 7.11 (s), 7.02 (s), 6.73 (br,s), and 6.55 (m).

^e The splitting patterns are given in parentheses; a singlet is inferred unless otherwise indicated.

Table 2.2. ^{31}P NMR Resonances for Phosphinite Ligands and Iridium Complexes

R	Ph ₂ PO-C ₆ H ₄ -R	[Ir ₂]-R
-CH ₃ ^a	109.8	100.4
-Quin ⁺	110.4	— ^b
-py ⁺	112.6	103.6
-CH ₂ -py ⁺	111.2	102.5
-CH ₂ -py ⁺ -Am	110.9	102.3
-CH ₂ -py ⁺ -tB	110.4	102.5
-(CH ₂) ₂ -py ⁺	110.3	101.0
-(CH ₂) ₃ -py ⁺	— ^b	100.6

^a In d₆-acetone.

^b These values were not obtained.

Step 3:

The series of iridium(I) donor-acceptor complexes and corresponding model compounds were prepared using procedures similar to those described previously for an analogous series of pyrazolyl-bridged phosphinite iridium dimers.³¹ Two equivalents of the phosphinite ligand were added to a solution of $[\text{Ir}(\mu\text{-pz}^*)(\text{CO})_2]_2$ in acetonitrile at room temperature and the immediate liberation of carbon monoxide gas followed by a darkening of the solution from orange to orange/red indicated the formation of the pyrazolyl-bridged dicarbonylbisphosphinite iridium(I) dimer. As observed previously in phosphine reactions with analogous metal complexes,³⁴ the phosphinite added in a transoid fashion. The *trans* configuration of the terminal ligands has a pronounced effect on the ^1H NMR resonances. There are two separate resonances for the methyl substituents on the pyrazolyl bridge (~ 1.97 and ~ 2.10 ppm). As expected, the NMR spectra also reveal two magnetically inequivalent phenyl groups. These NMR data are summarized in Table 2.3, and the numbering scheme is shown in Figure 2.10. An ^1H NMR spectrum of the model complex, $[\text{Ir}_2]\text{-CH}_3$, is provided in Figure 2.11, showing the inequivalent phenyl and pyrazolyl methyl resonances as well as the AA'BB' doublet of doublets for the phenylene proton resonances (see Table 2.3 for chemical shifts).

^{31}P NMR revealed a singlet for each complex with chemical shifts between 100.4 and 103.6 ppm (second column of Table 2.2), consistent with coordination of the phosphinite ligands to an Ir(I) metal center.³⁵

The solution IR spectrum of $[\text{Ir}_2]\text{-CH}_3$, given in Figure 2.12, reveals a single strong band at 1966 cm^{-1} , corresponding to the carbonyl C-O stretching mode. This is comparable to the value of 1955 cm^{-1} for the analogous compound, $[\text{Ir}(\mu\text{-pz}^*)(\text{CO})(\text{Ph}_2\text{PO-C}_2\text{H}_4\text{-py}^+)]_2(\text{Ph}_4\text{B}^-)_2$.

Figure 2.10. Numbering scheme used in assigning ^1H NMR spectra of iridium complexes. *a* and *b* are the methyl protons on the pyrazolyl bridge; *c* is the proton in the 4-position on the pyrazolyl bridge; *d*, *e*, *f*, *g*, *h*, and *i* are the phenyl protons; *j* and *k* are the phenylene protons; and remaining protons *m-v* are as shown in Figure 2.9.

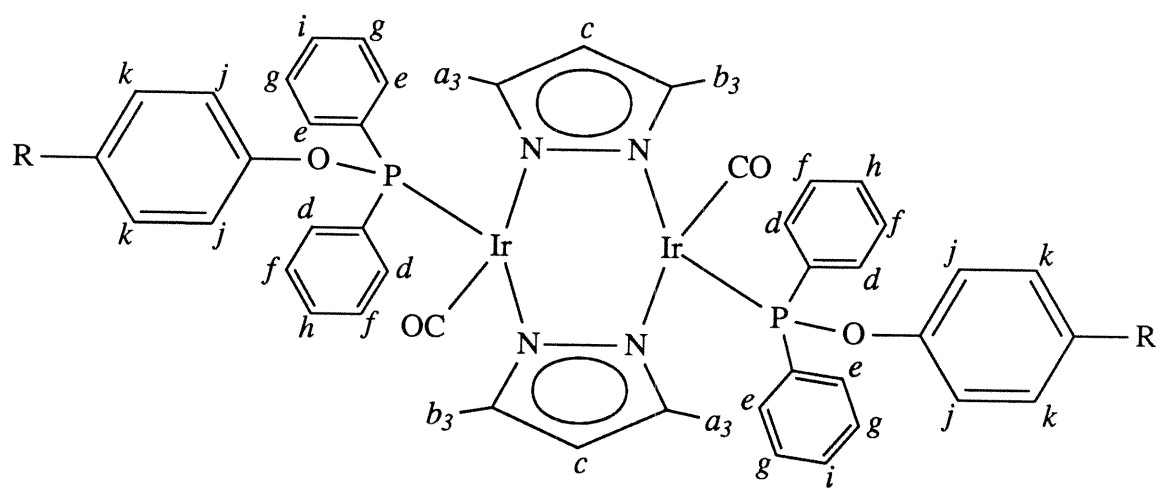


Table 2.3. ^1H NMR Resonances for Iridium Complexes

R	<i>a</i>	<i>b</i>	<i>c</i>	<i>d</i>	<i>e</i>	<i>f, g, h, i</i>	<i>j</i>	<i>k</i>
$[\text{Ir}_2]\text{-CH}_3^a$	1.97	2.14	5.37	7.96	8.28	7.24, 7.48	7.13	7.24
$[\text{Ir}_2]\text{-py}^+$	1.97	2.14	5.46	7.95	8.20	7.50	7.64	7.84
$[\text{Ir}_2]\text{-CH}_2\text{-py}^+$	1.95	2.00	5.38	7.89	8.17	7.43	6.95	— ^b
$[\text{Ir}_2]\text{-CH}_2\text{-py}^+\text{-Am}$	1.95	2.18	5.59	— ^b	— ^b	— ^b	6.91	— ^b
$[\text{Ir}_2]\text{-CH}_2\text{-py}^+\text{-tB}$	1.97	2.00	5.38	7.89	8.18	7.43	6.82	— ^b
$[\text{Ir}_2]\text{-(CH}_2)_2\text{-py}^+$	1.96	2.12	5.43	7.90	8.19	7.24, 7.45	7.08	7.53
$[\text{Ir}_2]\text{-(CH}_2)_3\text{-py}^+$	1.95	2.10	5.39	7.90	8.21	7.42	7.16	7.52

R	<i>m</i>	<i>n</i>	<i>o</i>	<i>p</i>	<i>q</i>	<i>r</i>	<i>s</i>	<i>t</i>	<i>u</i>	<i>v</i>
$[\text{Ir}_2]\text{-CH}_3^a$	2.27	—	—	—	—	—	—	—	—	—
$[\text{Ir}_2]\text{-py}^+$	—	—	—	8.82	8.16	8.66	—	—	—	—
$[\text{Ir}_2]\text{-CH}_2\text{-py}^+$	5.65	—	—	8.67	7.98	8.51	—	—	—	—
$[\text{Ir}_2]\text{-CH}_2\text{-py}^+\text{-Am}$	5.62	—	—	8.75	8.24	—	—	—	—	—
$[\text{Ir}_2]\text{-CH}_2\text{-py}^+\text{-tB}$	5.59	—	—	8.55	7.95	—	—	—	—	1.35
$[\text{Ir}_2]\text{-(CH}_2)_2\text{-py}^+$	4.72	3.23	—	8.46	7.91	8.45	—	—	—	—
	(t)	(t)		(d)	(q)	(t)				
$[\text{Ir}_2]\text{-(CH}_2)_3\text{-py}^+$	4.50	2.30	2.67	8.62	7.99	8.48	—	—	—	—
	(t)	(q)	(t)	(d)	(t)	(t)				

^a In d_6 -acetone.

^b Obscured by phenyl resonances.

Figure 2.11. ^1H NMR (400 MHz) spectrum of $[\text{Ir}(\mu\text{-pz}^*)(\text{CO})(\text{Ph}_2\text{P-O-C}_6\text{H}_4\text{-CH}_3)]_2$ in CD_3CN , showing inequivalent pyrazolyl methyl resonances at 1.97 and 2.14 ppm, and *o*-phenyl resonances at 7.96 and 8.28 ppm, indicating transoid configuration of terminal phosphinite ligands.

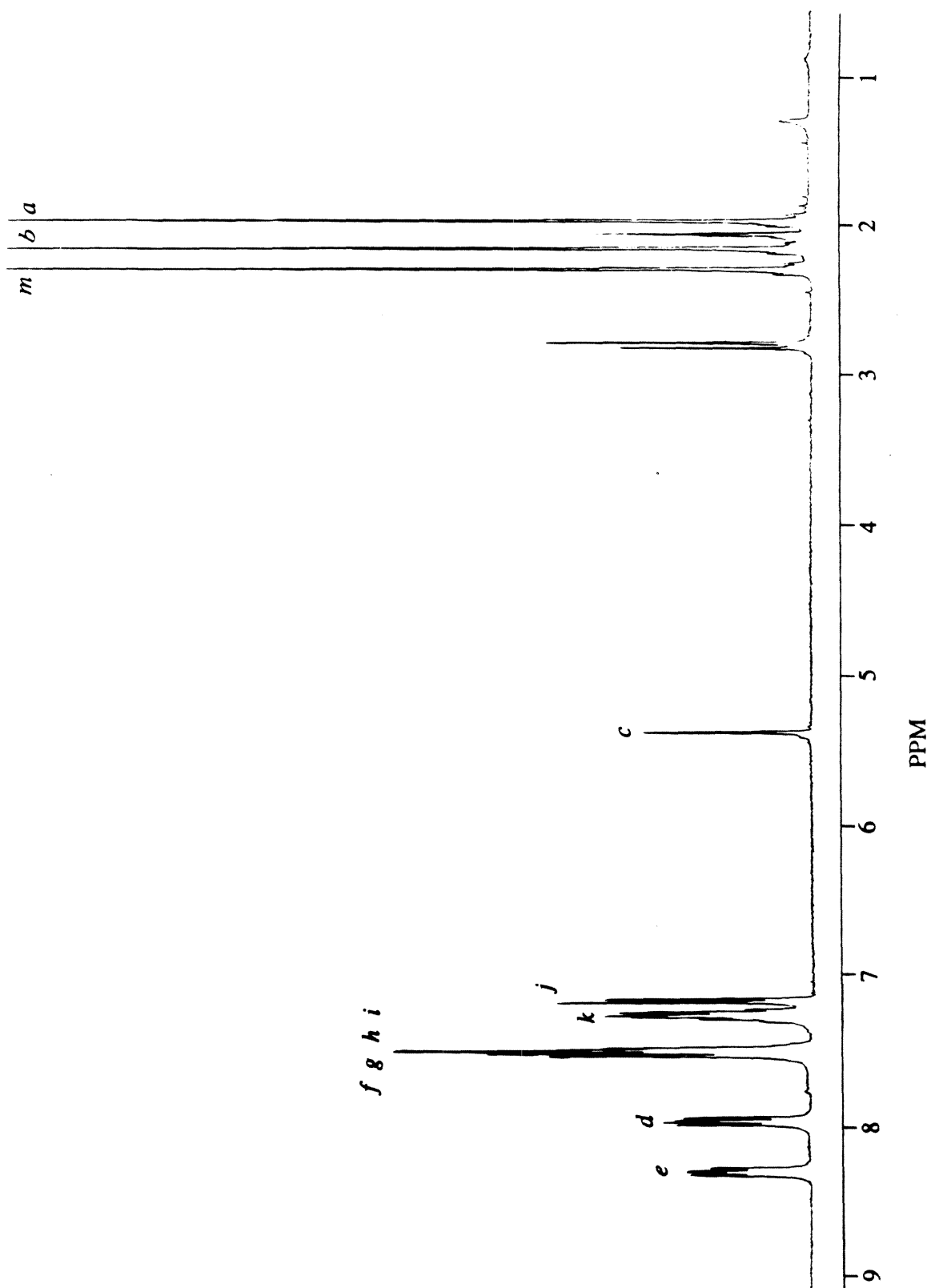
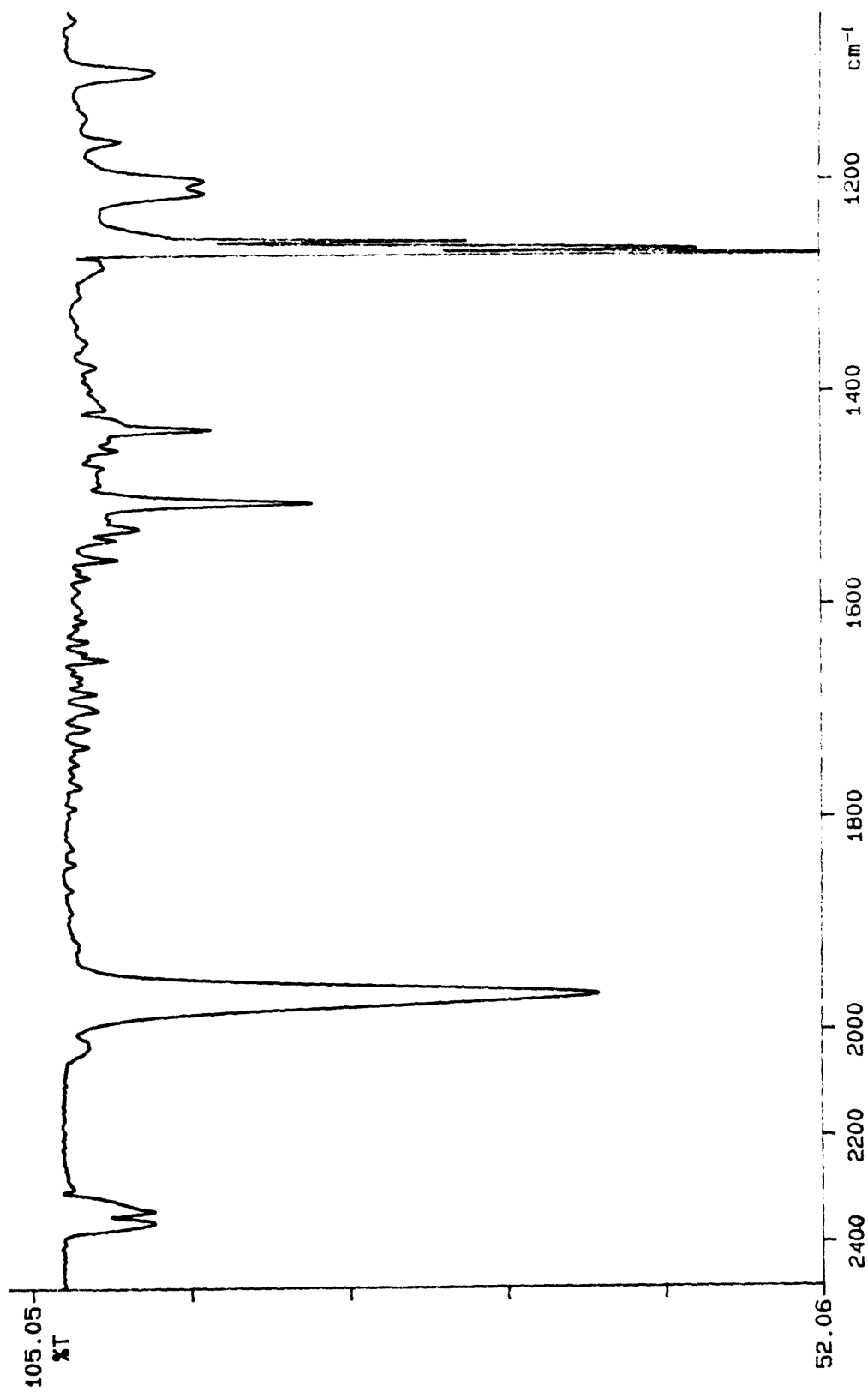


Figure 2.12. Solvent subtracted IR spectrum of $\text{Ir}(\mu\text{-pz}^*)(\text{CO})(\text{Ph}_2\text{P-O-C}_6\text{H}_4\text{-CH}_3)_2$ in CH_2Cl_2 , showing single CO band at 1966 cm^{-1} . Other unassigned bands appear at 2350 (d) , 1506 , 1437 , 1206 (d) , 1166 , and 1102 cm^{-1} . The large feature at $\sim 1270\text{ cm}^{-1}$ corresponds to an intense solvent (CH_2Cl_2) band assigned.



CONCLUDING REMARKS

The synthetic methodology used to prepare the series of donor-acceptor complexes, $[\text{Ir}(\mu\text{-pz}^*)(\text{CO})(\text{Ph}_2\text{PO-C}_6\text{H}_4\text{-(CH}_2)_n\text{-py}^+\text{-R})]_2(\text{PF}_6^-)_2$, can be applied to the preparation of a wider class of donor-acceptor complexes. Three features of these complexes make this an attractive prospect: (1) the phosphinite ligand containing the electron acceptor can be attached to a large variety of chromophores with metal centers that bind phosphines; (2) the nature of the bridge can also be easily varied by either completely replacing the phenylene group or by simple substitution directly on the phenylene group; (3) and the pyridinium acceptor can be replaced with other one-electron acceptors by utilizing similar synthetic methods as described in the previous sections. Research involving the preparation and study of new ligands and complexes is currently being pursued in our laboratory.

REFERENCES

1. Meyer, T. J.; Taube, H. *Inorg. Chem.* **1964**, *7*, 2369-2379.
2. Chou, M.; Creutz, C.; Sutin, N. *J. Am. Chem. Soc.* **1977**, *99*, 5615-5623.
3. Weaver, M. J.; Yee, E. L. *Inorg. Chem.* **1980**, *19*, 1936-1945.
4. Marshall, J. L.; Stobart, S. R.; Gray, H. B. *J. Am. Chem. Soc.* **1984**, *106*, 3027-3029.
5. Masuhara, H.; Maeda, Y.; Mataga, N.; Tomita, K.; Tatemitsu, H.; Sakata, Y.; Misumi, S. *Chem. Phys. Letters* **1980**, *69*, 182-184.
6. Nakatani, K.; Okada, T.; Mataga, N.; De Schryver, F. C.; Van der Auweraer, M. *Chem. Phys. Lett.* **1981**, *145*, 81-84.
7. Pasman, P.; Rob, F.; Verhoeven, J. W. *J. Am. Chem. Soc.* **1982**, *104*, 5127-5133.
8. Stein, C. A.; Lewis, N. A.; Seitz, G. *J. Am. Chem. Soc.* **1982**, *104*, 2596-2599.

9. Richardson, D. E.; Taube, H. *J. Am. Chem. Soc.* **1983**, *105*, 40-51.
10. Joran, A. D.; Leland, B. A.; Geller, G. G.; Hopfield, J. J.; Dervan, P. B. *J. Am. Chem. Soc.* **1984**, *106*, 6090-6092.
11. Miller, J. R.; Beitz, J. V.; Huddleston, R. K. *J. Am. Chem. Soc.* **1984**, *106*, 5057-5068.
12. Wasielewski, M. R.; Niemczyk, M. P.; Svec, W. A.; Pewitt, E. B. *J. Am. Chem. Soc.* **1985**, *107*, 1080-1082.
13. Wasielewski, M. R.; Niemczyk, M. P.; Svec, W. A.; Pewitt, E. B. *J. Am. Chem. Soc.* **1985**, *107*, 1080-1082.
14. Heitele, H.; Michel-Beyerle, M. E. *J. Am. Chem. Soc.* **1985**, *107*, 8286-8288.
15. Heitele, H.; Michel-Beyerle, M. E.; Finckh, P. *Chem. Phys. Letters* **1987**, *134*, 273-278.
16. Closs, G. L.; Calcaterra, L. T.; Green, N. J.; Penfield, K. W.; Miller, J. R. *J. Phys. Chem.* **1986**, *90*, 3673-3683.
17. Warman, J. M.; de-Haas, M. P.; Paddon-Row, M. N.; Cotsaris, E.; Hush, N. S.; Oevering, H.; Verhoeven, J. W. *Nature* **1986**, *320*, 615-616.
18. Geselowitz, D. A. *Inorg. Chem.* **1987**, *26*, 4135-4237.
19. Oevering, H.; Paddon-Row, M. N.; Heppener, M.; Oliver, A. M.; Cotsaris, E.; Verhoeven, J. W.; Hush, N. S. *J. Am. Chem. Soc.* **1987**, *109*, 3258-3269.
20. Joran, A. D.; Leland, B. A.; Felker, P. M.; Zewail, A. H.; Hopfield, J. J.; Dervan, P. B. *Nature (London)* **1987**, *327*, 508-511.
21. Penfield, K. W.; Miller, J. R.; Paddon-Row, M. N.; Cotsaris, E.; Oliver, A. M.; Hush, N. S. *J. Am. Chem. Soc.* **1987**, *109*, 5061-5065.
22. Kemnitz, K. *Chem. Phys. Letters* **1988**, *152*, 305-310.
23. Finckh, P.; Heitele, H.; Folk, M.; Michel-Beyerle, M. E. *J. Phys. Chem.* **1988**, *92*,

6584-6590.

24. Schmidt, J. A.; McIntosh, A. R.; Weedon, A. C.; Bolton, J. R.; Connolly, J. S.; Hurley, J. K.; Wasielewski, M. R. *J. Am. Chem. Soc.* **1988**, *110*, 1733-1740.
25. Fox, L. S.; Kozik, M.; Winkler, J. R.; Gray, H. B. *Science* **1990**, *247*, 1069-1071.
26. Verhoeven, J. W.; Dirkx, I. P.; deBoer, T. J. *Tetrahedron* **1966**, *37*, 4399-4404.
27. Chandross, E. A.; Thomas, H. T. *Chem. Phys. Letters* **1971**, *9*, 393-396.
28. Fisher, H.; Tom, G. M.; Taube, H. *J. Am. Chem. Soc.* **1976**, *98*, 5512-5517.
29. Schanze, K. S.; Sauer, K. *J. Am. Chem. Soc.* **1988**, *110*, 1180-1186.
30. Moore, T. A.; Gust, D.; Hatlevig, S.; Moore, A. L.; Makings, L. R.; Pessike, P. J.; DeSchryver, F. C.; Van der Auweraer, M.; Lexa, D.; Bensasson, R. V.; Rougee, M. *Isr. J. Chem.* **1988**, *28*, 87-95.
31. Fox, L. S., Ph.D. Dissertation, California Institute of Technology, Pasadena, CA, 1989.
32. Marshall, J. L., Ph.D. Dissertation, California Institute of Technology, Pasadena, CA, 1987.
33. Mavel, G. *Ann. Rev. NMR Spect.* **1973**, *58*, 1-89.
34. Atwood, J. L.; Beveridge, K. A.; Bushnell, G. W.; Dixon, K. R.; Eadie, D. T.; Stobart, S. R.; Zaworotko, M. J. *Inorg. Chem.* **1984**, *23*, 4050-4057.
35. Nixon, J. F.; Pidcock, A. *Ann. Rev. NMR Spec.* **1969**, *2*, 346-422.

Chapter 3

X-ray Crystal Structure and Molecular Mechanics Calculations

INTRODUCTION

A main goal of our research is to understand how structural parameters such as distance and orientation affect excited-state and thermal electron-transfer rates in linked donor-acceptor complexes. The series of $\text{Ir}_2\text{-py}^+$ donor-acceptor complexes, described in the previous chapter, were prepared with this goal in mind. A study aimed at correlating donor-acceptor distance and orientation to electron-transfer rates must clearly involve a detailed investigation of their solution structures.^{1,2} We have therefore obtained conceivable solution structures for the series of donor-spacer-acceptor complexes, $[\text{Ir}(\mu\text{-pz}^*)(\text{CO})(\text{Ph}_2\text{PO-C}_6\text{H}_4\text{-(CH}_2)_n\text{-py}^+)]_2$ ($n = 0, 1, 2$, and 3). This was accomplished by using data from an X-ray crystal structure of *one* model complex as a basis for constructing the remaining $\text{Ir}_2\text{-py}^+$ complexes by computer modeling (in most cases two distinct low energy structures were proposed to exist in solution).

In this chapter, the X-ray crystal structure determination of $[\text{Ir}(\mu\text{-pz}^*)(\text{CO})(\text{Ph}_2\text{P-O-C}_6\text{H}_4\text{-CH}_3)]_2$ is presented, followed by a description of the molecular mechanics calculations conducted on the four general classes of $\text{Ir}_2\text{-py}^+$ donor-acceptor complexes ($n = 0, 1, 2$, and 3). The results of these calculations will be discussed in relation to donor-acceptor electronic couplings in Chapter 5.

EXPERIMENTAL

X-Ray Structure Determination:

Slow evaporation of a methylene chloride/acetonitrile solution produced acicular crystals of $[\text{Ir}(\mu\text{-pz}^*)(\text{CO})(\text{Ph}_2\text{P-O-C}_6\text{H}_4\text{-CH}_3)]_2$. A section, cut from a needle, was coated with epoxy to prevent reaction with air and solvent loss. Unit cell parameters and an orientation matrix were obtained on a CAD-4 diffractometer by a least squares calculation from the setting angles of 24 reflections with $30^\circ < 2\theta < 33^\circ$. Two equivalent data sets out

to a 2θ of 45° were collected. The data were corrected for a slight decay in intensity. Since calculated absorption correction increased goodness of fit (GOF) for merging, an absorption coefficient 30% of the calculated value was used (this value was found to minimize GOF for merging). Lorentz and polarization factors were applied and the two data sets were then merged to yield the final data set. Preliminary Weissenberg photographs and systematic absences in the diffractometer data revealed the space group to be $P2_1/c$.

Hydrogen atom positions were determined from difference maps for the methyl groups and by calculation for the remainder. All hydrogen atoms were placed at 0.95 Å from the attached carbon atom and given isotropic B values 20% greater than that of the attached atom. No hydrogen parameters were refined.

Analysis of a Patterson map provided the iridium atom coordinates. The electron density maps indicated the presence of a dichloromethane solvent molecule. The remaining non-hydrogen atoms were located via successive structure factor-Fourier calculations. The complete least squares full matrix, consisting of spatial and anisotropic thermal parameters for the non-hydrogen atoms, a population factor for the solvent molecule, and a scale factor, contained 588 parameters. A final difference Fourier map showed deviations ranging from $-0.64 \text{ e}\text{\AA}^{-3}$ to $+0.78 \text{ e}\text{\AA}^{-3}$. The refinement converged with an R -factor of 0.0316 (0.0235 for $F_o^2 > 3\sigma(F_o^2)$) and a goodness of fit of 1.46 for all 6662 reflections.

Calculations were done with programs of the CRYM Crystallographic Computing System and ORTEP. Scattering factors and corrections for anomalous scattering were taken from a standard reference.³ $R = \Sigma |F_o - |F_c|| / \Sigma F_o$, for only $F_o^2 > 0$, and goodness of fit = $[\Sigma w(F_o^2 - F_c^2)^2 / (n - p)]^{1/2}$, where n is the number of data and p the number of parameters refined. The function minimized in least squares was $\Sigma w(F_o^2 - F_c^2)^2$, where $w = 1/\sigma^2(F_o^2)$. Variances of the individual reflections were assigned based on counting statistics plus an additional term, $(0.014I)^2$. Variances of the merged reflections were determined by standard propagation of error plus another additional term, $(0.014\langle I \rangle)^2$. The

absorption correction was done by Gaussian integration over an $8 \times 8 \times 8$ grid.

Transmission factors varied from 0.39 to 0.54.

Molecular Mechanics Calculations:

Molecular mechanics calculations were carried out on the full series of donor-acceptor complexes using Biograf (the molecular design and analysis program from Biodesign Inc.).⁴ version 2.10 with the Dreiding force field. Atomic positions from the X-ray structure of $[\text{Ir}(\mu\text{-pz}^*)(\text{CO})(\text{Ph}_2\text{P-O-C}_6\text{H}_4\text{-CH}_3)]_2$, $[\text{Ir}_2]\text{-CH}_3$, were used as a base upon which the remaining portion of the bridge and pyridinium group were constructed. Energy minimizations of the computer constructed complexes were carried by holding the iridium core atomic coordinates fixed (both Ir atoms, the entire 3,5-dimethylpyrazolyl bridges, and the phosphorous atoms and attached phenyl groups and oxygens), and allowing the atoms of the phenylene groups, the hydrocarbon chains, and the pyridinium groups to be adjustable.

RESULTS and DISCUSSIONS

X-ray Structure:

The structure of dicarbonylbis(μ -3,5-dimethylpyrazolyl)bis(*O*-4-tolyl-*P,P*-diphenylphosphinite)diiridium(I) ($[\text{Ir}_2]\text{-CH}_3$), $\text{Ir}_2\text{C}_{50}\text{H}_{48}\text{N}_4\text{O}_4\text{P}_2 \cdot \text{CH}_2\text{Cl}_2$, has been determined by X-ray diffraction techniques. The molecule crystallized in the monoclinic system, in the space group $\text{P2}_1/\text{c}$ (#14), with $a = 18.677(2) \text{ \AA}$, $b = 13.817(1) \text{ \AA}$, $c = 20.225(3) \text{ \AA}$, $\beta = 101.37(1)^\circ$, volume = $5116.8(10) \text{ \AA}^3$; $Z = 4$ and density = 1.688 g cm^{-3} . Crystallographic data are summarized in Table 3.1.

ORTEP diagrams showing the iridium coordination sphere and ligand geometry are presented in Figures 3.1a and b. The atomic numbering scheme is given in Figure 3.2. Selected bond lengths and angles are provided in Table 3.2. All other data pertaining to

Table 3.1. Crystallographic Data for $[\text{Ir}(\mu\text{-pz}^*)(\text{CO})(\text{Ph}_2\text{P-O-C}_6\text{H}_4\text{-CH}_3)]_2$

Formula: $\text{Ir}_2\text{C}_{50}\text{H}_{48}\text{N}_4\text{O}_4\text{P}_2\cdot\text{CH}_2\text{Cl}_2$

$a = 18.677(2) \text{ \AA}$

$b = 13.817(1) \text{ \AA}$

$c = 20.225(3) \text{ \AA}$

$\beta = 101.27(1)^\circ$

$V = 5116.8(10) \text{ \AA}^3$

Space Group: $\text{P2}_1/\text{c}$ (#14)

$T = 293^\circ\text{K}$

$\lambda = 0.7107 \text{ \AA}$

$\rho_{\text{calc}} = 1.688 \text{ g cm}^{-3}$

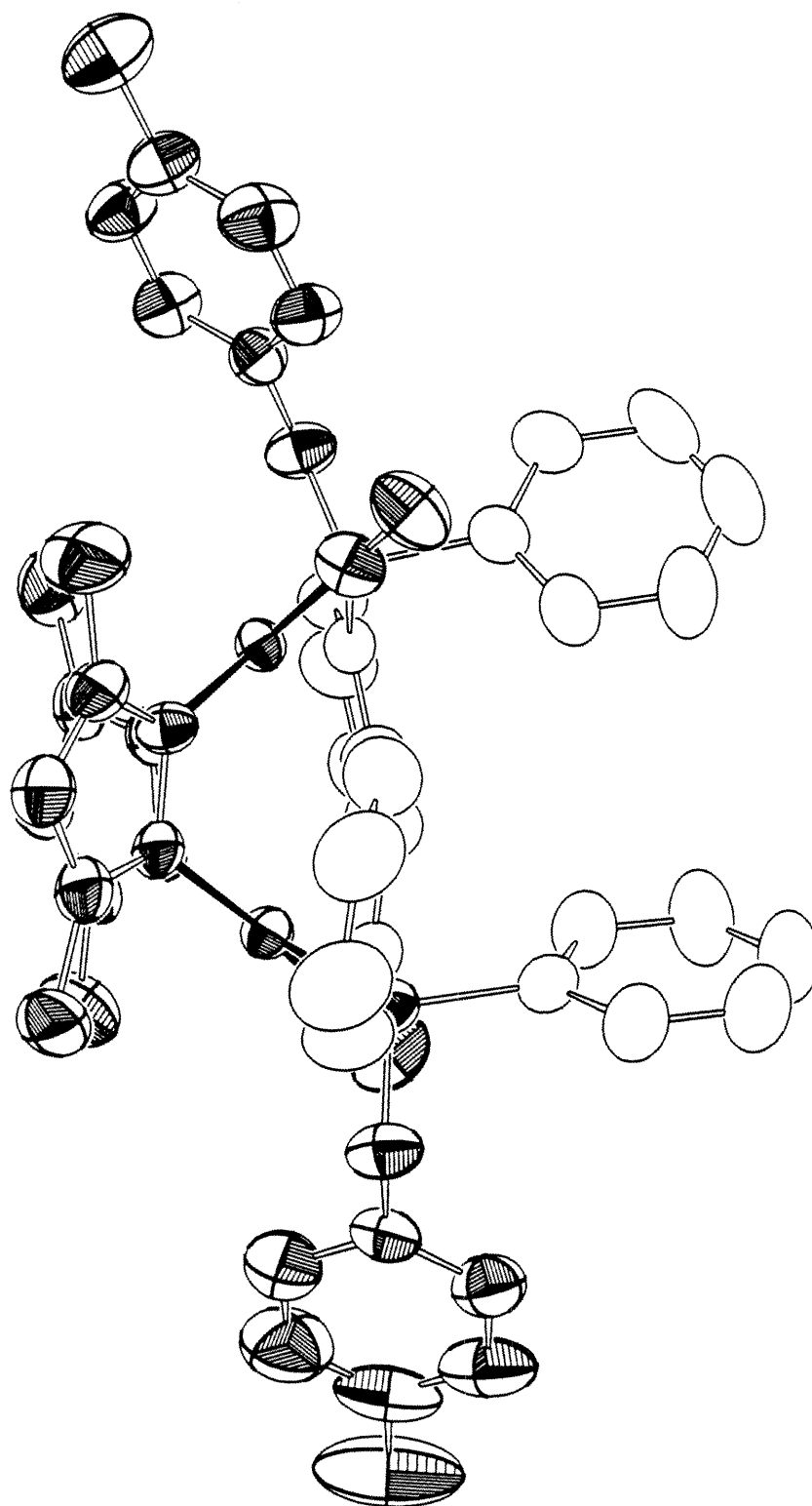
$\mu = 57.28 \text{ cm}^{-1}$

Transmission coeff. = 0.39 – 0.54

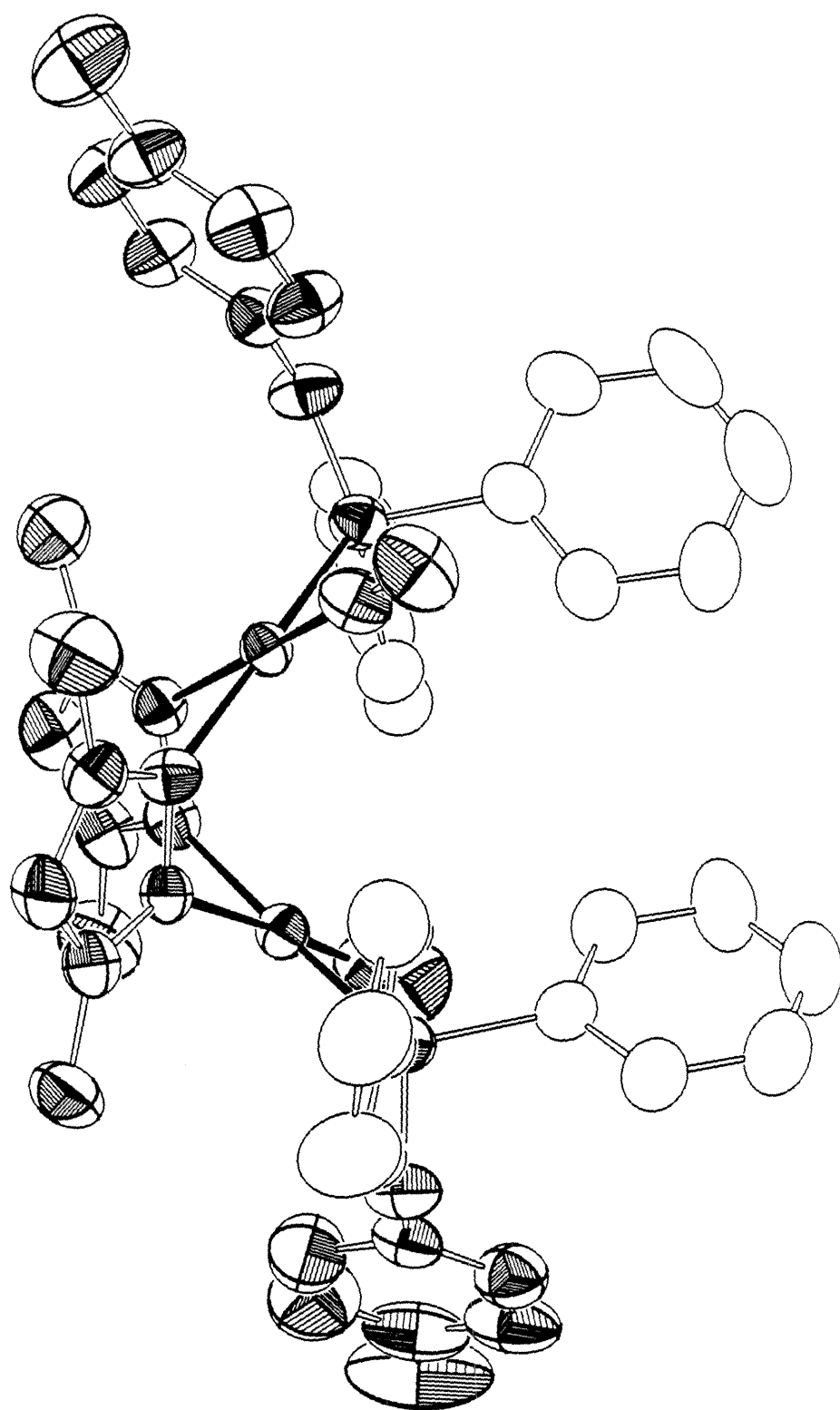
$R(F_o) = 0.316$

GOF = 1.46

Figure 3.1. (a) ORTEP diagram of $[\text{Ir}(\mu\text{-pz}^*)(\text{CO})(\text{Ph}_2\text{P-O-C}_6\text{H}_4\text{-CH}_3)]_2$, showing the nearly eclipsed 3,5-dimethylpyrazolyl groups. (b) A second view of the same complex, showing the square planar coordination of Ir and the *trans* CO and phosphinite ligands. For the sake of clarity, the four phenyl groups have not been shaded.



a



b

Figure 3.2. Atomic number scheme for $[\text{Ir}(\mu\text{-pz}^*)(\text{CO})(\text{Ph}_2\text{P-O-C}_6\text{H}_4\text{-CH}_3)_2]$.

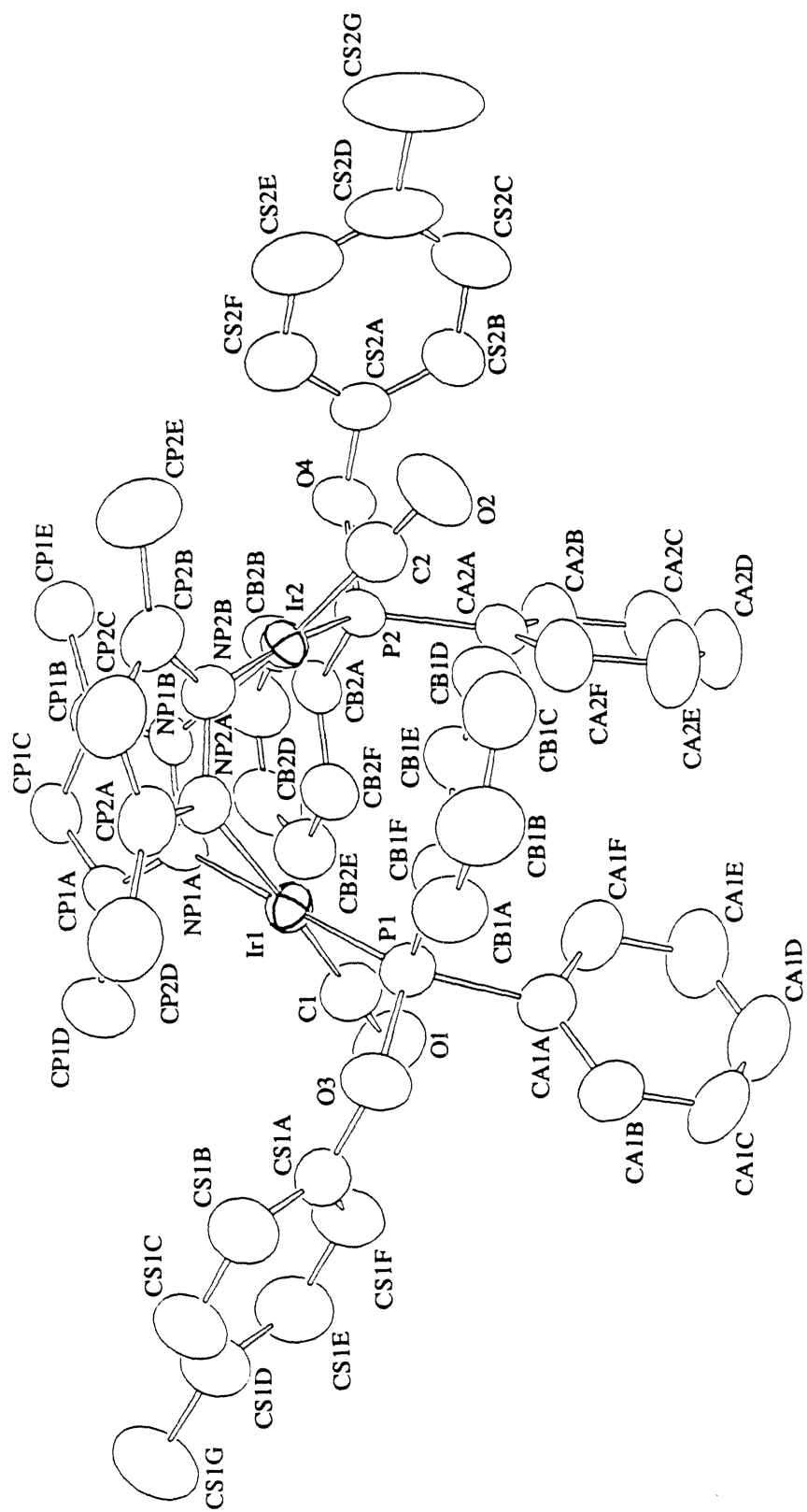
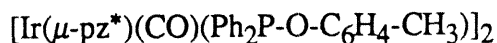


Table 3.2. Selected Bond Lengths and Angles for



Iridium Coordination Sphere

Distance(Å)		Angle(°)	
Ir1 – Ir2	3.307(1)	NP1A – Ir1 – NP2A	85.1(2)
Ir1 – C1	1.797(6)	NP1A – Ir1 – C1	91.6(2)
Ir2 – C2	1.810(6)	P1 – Ir1 – C1	91.0(2)
Ir1 – P1	2.224(1)	P1 – Ir1 – NP2A	92.3(1)
Ir2 – P2	2.224(1)	NP2A – Ir1 – C1	176.3(2)
Ir1 – NP1A	2.075(4)	P1 – Ir1 – NP1A	177.4(1)
Ir2 – NP1B	2.068(4)	NP1B – Ir2 – NP2B	83.1(2)
Ir1 – NP2A	2.091(4)	NP2B – Ir2 – C2	92.9(2)
Ir2 – NP2B	2.073(4)	P2 – Ir2 – C2	91.8(2)
		P2 – Ir2 – NP1B	92.5(1)
		NP1B – Ir2 – C2	174.1(2)
		P2 – Ir2 – NP2B	174.2(1)
		Ir1 – NP1A – NP1B	117.9(3)
		Ir1 – NP2A – NP2B	117.2(3)
		Ir2 – NP1B – NP1A	117.1(3)
		Ir2 – NP2B – NP2A	118.0(3)
		NP1A – Ir1 – Ir2	61.7(1)
		NP2A – Ir1 – Ir2	62.2(1)
		P1 – Ir1 – Ir2	117.0(1)
		C1 – Ir1 – Ir2	117.4(2)
		NP1B – Ir2 – Ir1	62.3(1)
		NP2B – Ir2 – Ir1	62.5(1)
		P2 – Ir2 – Ir1	112.1(1)
		C2 – Ir2 – Ir1	119.6(2)

CO Ligands

Distance(Å)		Angle(°)	
C1 – O1	1.174(7)	O1 – C1 – Ir1	179.3(5)
C2 – O2	1.165(7)	O2 – C2 – Ir2	178.0(5)

Pyrazole Ligands

Distance(Å)		Angle(°)	
NP1A - NP1B	1.370(6)	Ir1 - NP1A - CP1A	135.1(3)
NP1A - CP1A	1.349(7)	CP1A - NP1A - NP1B	106.8(4)
NP1B - CP1B	1.334(7)	CP1B - NP1B - NP1A	109.3(4)
CP1A - CP1C	1.371(8)	Ir2 - NP1B - CP1B	133.0(3)
CP1A - CP1D	1.493(9)	CP1C - CP1A - NP1A	109.2(5)
CP1B - CP1C	1.377(8)	CP1D - CP1A - NP1A	120.8(5)
CP1B - CP1E	1.494(8)	CP1D - CP1A - CP1C	130.0(5)
NP2A - NP2B	1.376(6)	CP1C - CP1B - NP1B	108.2(5)
NP2A - CP2A	1.337(7)	CP1E - CP1B - NP1B	120.8(5)
NP2B - CP2B	1.332(7)	CP1E - CP1B - CP1C	130.9(5)
CP2A - CP2C	1.365(9)	CP1B - CP1C - CP1A	106.5(5)
CP2A - CP2D	1.488(9)	Ir1 - NP2A - CP2A	134.3(4)
CP2B - CP2C	1.377(9)	CP2A - NP2A - NP2B	108.4(4)
CP2B - CP2E	1.493(9)	CP2B - NP2B - NP2A	107.4(4)
		Ir2 - NP2B - CP2B	134.5(4)
		CP2C - CP2A - NP2A	108.6(5)
		CP2D - CP2A - NP2A	121.6(5)
		CP2D - CP2A - CP2C	129.7(6)
		CP2C - CP2B - NP2B	109.1(5)
		CP2E - CP2B - NP2B	121.5(5)
		CP2E - CP2B - CP2C	129.5(6)
		CP2B - CP2C - CP2A	106.5(5)

Phosphinite Ligands

Distance(Å)		Angle(°)	
P1 – O3	1.629(4)	Ir1 – P1 – O3	119.3(1)
P2 – O4	1.633(4)	Ir1 – P1 – CA1A	116.5(2)
P1 – CA1A	1.817(5)	Ir1 – P1 – CB1A	116.4(2)
P1 – CB1A	1.820(5)	CB1A – P1 – CA1A	101.7(2)
P2 – CA2A	1.826(5)	Ir2 – P2 – O4	119.7(1)
P2 – CB2A	1.815(5)	Ir2 – P2 – CA2A	116.2(2)
O3 – CS1A	1.410(6)	Ir2 – P2 – CB2A	117.8(2)
O4 – CS2A	1.404(7)	CB2A – P2 – CA2A	102.1(2)
CS1D – CS1G	1.512(9)	CA1B – CA1A – P1	122.2(4)
CS2D – CS2G	1.524(14)	CA1F – CA1A – P1	119.4(4)
		CB1B – CB1A – P1	117.6(4)
		CB1F – CB1A – P1	124.0(4)
		CA2B – CA2A – P2	119.9(4)
		CA2F – CA2A – P2	122.0(4)
		CB2B – CB2A – P2	117.5(4)
		CB2F – CB2A – P2	123.0(4)
		CA1A – P1 – O3	102.4(2)
		CB1A – P1 – O3	97.5(2)
		CS1A – O3 – P1	125.9(3)
		CA2A – P2 – O4	101.8(2)
		CB2A – P2 – O4	95.8(2)
		CS2A – O4 – P2	121.0(3)
		CS1B – CS1A – O3	116.5(5)
		CS1F – CS1A – O3	122.7(5)
		CS2B – CS2A – O4	119.5(5)
		CS2F – CS2A – O4	119.6(5)
		CS1G – CS1D – CS1C	121.6(6)
		CS1G – CS1D – CS1E	120.9(6)
		CS2G – CS2D – CS2C	121.2(8)
		CS2G – CS2D – CS2E	120.1(8)

Dihedral Angles

	Angle (°)
CP2D – CP2A – NP2A – Ir1	-1.51
CP1D – CP1A – NP1A – Ir1	-6.19
CP2E – CP2B – NP2B – Ir2	-4.76
CP1E – CP1B – NP1B – Ir2	-11.43
Ir1 – NP2A – NP2B – Ir2	4.93
Ir1 – NP1A – NP1B – Ir2	12.15
CP1D – CP1A – CP1C – CP1B	178.97
CP2D – CP2A – CP2C – CP2B	-178.37
CP1E – CP1B – CP1C – CP1A	-177.44
CP2E – CP2B – CP2C – CP2A	179.97

Angles Involving Ir...Ir Connectivity

	Angle (°)
Ir1 – Ir2 – NP1B	62.46
Ir1 – Ir2 – NP2B	62.23
Ir2 – Ir1 – NP1A	62.25
Ir2 – Ir1 – NP2A	61.70
Ir1 – Ir2 – C2	119.61
Ir2 – Ir1 – C1	117.36
Ir1 – Ir2 – P2	112.10
Ir2 – Ir1 – P1	117.01

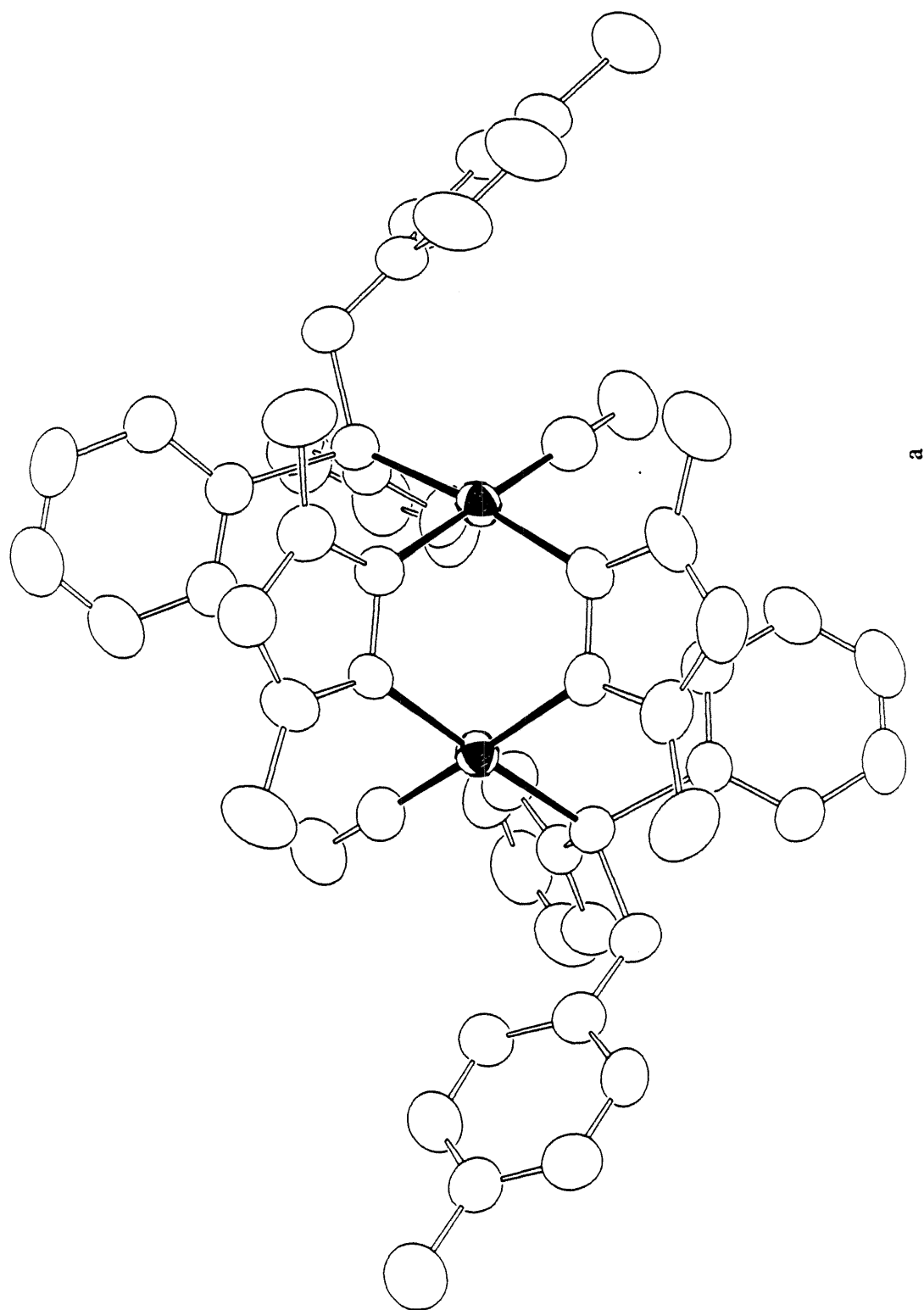
this structure have been collected in Appendix I (Table A.1. Crystal and Intensity Collection Data, Table A.2. Final Non-Hydrogen Coordinates and Displacement Parameters, Table A.3. Anisotropic Displacement Parameters, Table A.4. Assigned Hydrogen Parameters, Table A.5. Complete Distances and Angles, and Table A.6. Observed and Calculated Structure Factors). A brief description of the structure is now presented.

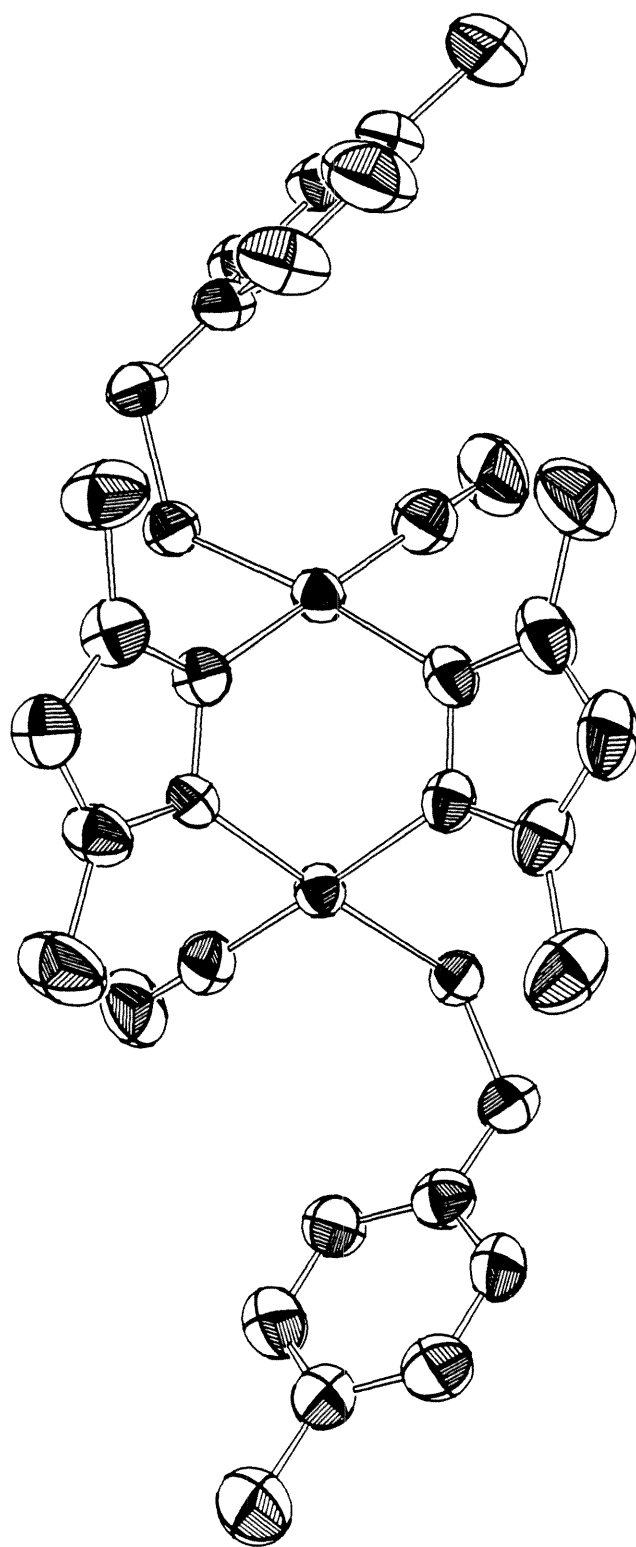
The molecule has approximate C_{2v} symmetry. Figures 3.3a and b show ORTEP diagrams for $[\text{Ir}_2]\text{-CH}_3$ with views down the approximate C_2 -symmetry axis. The largest deviations from perfect C_{2v} symmetry occur between the axial phenyl groups (CA1 and CA2) and between the tolyl groups (CS1 and CS2). An illustration of the former deviation is the difference in relative geometry of the CA1/CB1 axial phenyl groups compared to the equatorial phenyls, CA2/CB2. The CA1 and CB1 phenyl groups are nearly eclipsed (dihedral angle, CA1B-CA1A-CB1A-CB1B = 3.1°), while phenyls CA2 and CB2 are far from eclipsed (analogous dihedral angle, CA2B-CA2A-CB2A-CB2B = 44°). Examination of more than one unit cell reveals the origin of these particular deviations. It appears that the benzene rings of the molecule (four phenyl groups and two tolyl groups) accommodate positions that maximize their overlap. Perfect C_{2v} symmetry is, however, not a necessary condition for this overlap to occur.

The iridium atoms exhibit slightly distorted square planar coordination geometry. The standard deviation from 90° of the angles N-Ir-N, N-Ir-C, N-Ir-P, and P-Ir-C is 3.8° . The average of the two N-Ir-N angles is less than 90° (84°), while the average of the N-Ir-C, P-Ir-C, and P-Ir-N angles is greater than 90° (92°).

The bridging-pyrazolyl groups retain their isolated structure, deviating by no more than 0.8° from perfect planarity. The angle between the planes of the pyrazolyl groups is $78.8(6)^\circ$ which is 5.3° less than the average N-Ir-N angle, implying that the pyrazolyl groups are not perfectly eclipsed (this is indeed apparent in Figure 3.1a).

Figure 3.3. (a) ORTEP diagram of $[\text{Ir}(\mu\text{-pz}^*)(\text{CO})(\text{Ph}_2\text{P-O-C}_6\text{H}_4\text{-CH}_3)]_2$, showing the approximate C_2 -axis. Two of the phenyl groups and the pyrazolyl groups are superimposed by rotation about the C_2 -axis. (b) However, the tolyl groups, as seen in this view of the molecule, deviate from perfect C_2 -symmetry (phenyl groups have been omitted for clarity).





b

The Ir...Ir solid-state non-bonding separation in the present structure is the same as the M...M separations in analogous pyrazolyl-bridged Ir and Rh dimers within the standard deviation of distances (Table 3.3). It appears that the nature of X, Y, R, or M has no consistent effect on the M...M separation. For example, the average M...M separations in Ir and Rh dimers are 3.28 ± 0.12 Å and 3.31 ± 0.18 Å (the same within the standard error), for dimers with R = CH₃ and R = H the average M...M separations are 3.24 ± 0.06 Å and 3.34 ± 0.18 Å, and for dimers with X = Y = CO and X,Y = COD the average M...M separations are 3.34 ± 0.15 Å and 3.21 ± 0.06 Å.

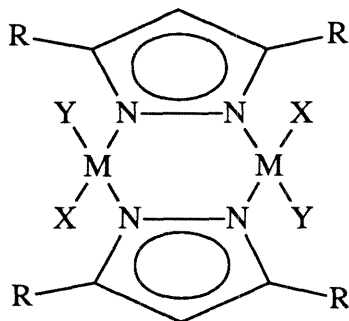


Table 3.3. M...M Separations in Pyrazolyl -Bridged Iridium(I) and Rhodium(I) Dimers

M	R	X	Y	M...M (Å)	Ref.
Ir	CH ₃	CO	CO	3.245	5
Ir	CH ₃	CO	Ph ₂ POC ₂ H ₄ -py ⁺	3.219	6
Ir	CH ₃	CO	Ph ₂ POC ₆ H ₄ -CH ₃	3.307	here
Ir	H	CO	CO	3.506	5
Ir	H	COD		3.216	7, 8
Ir	H	CO	Ph ₃ P	3.162	9
Rh	CH ₃	CO	CO	3.262	10
Rh	CH ₃	COD		3.154	10
Rh	H	COD		3.267	7
Rh	H	CO	(PhO) ₃ P	3.568	11

COD = 1,4-cyclooctadiene; Ph = phenyl; py⁺ = pyridinium; C₆H₄ = phenylene; C₂H₄ = ethylene

Having demonstrated that the Ir...Ir separation in $[\text{Ir}(\mu\text{-pz}^*)(\text{CO})(\text{Ph}_2\text{P-O-C}_6\text{H}_4\text{-CH}_3)]_2$ is typical of analogous $\text{d}^8\text{-d}^8$ dimers, a comparison of other bond lengths and angles to analogous complexes will be made. This was accomplished by considering the structure of $[\text{Ir}(\mu\text{-pz}^*)(\text{CO})(\text{Ph}_2\text{PO-C}_2\text{H}_4\text{-py}^+)]_2(\text{Ph}_4\text{B}^-)_2$ (a donor-acceptor complex previously studied in our laboratory), which also contains a 3,5-dimethylpyrazolyl bridge, and CO and phosphinite ligands.⁶ Table 3.4 summarizes selected bond lengths and angles for this complex (**2**) and for the structure of concern (**1**). The short Ir-C and long C-O bond lengths in **2** have been attributed to systematic errors in correcting the diffraction intensities for iridium absorption effects. Other than this discrepancy, however, deviations were found to be minimal. The iridium coordination spheres show similar structural parameters for both complexes: Ir-P = 2.22 Å, and Ir-N = 2.08(2) Å. The pyrazolyl bridge also exhibits similar structural parameters: N-N = 1.36(2) Å, and Ir-N-N = 117(2)°.

In Chapter 4 it will become apparent that the similarities between these two structures will serve to simplify the analyses of absorption and emission spectra for $[\text{Ir}_2]\text{-CH}_3$, as well as the series of donor-acceptor complexes described in Chapter 2.

Table 3.4. Comparison of Bond Lengths and Angles Between $[\text{Ir}_2]\text{-CH}_3$, **1**, and $[\text{Ir}(\text{pz}^*)(\text{CO})(\text{Ph}_2\text{POC}_2\text{H}_4\text{-py}^+)]_2$, **2**

Bonds and Angles	1	2
Ir1-Ir2	3.31 Å	3.22 Å
Ir1-C1	1.80	1.65±0.01
Ir2-C2	1.81	1.76±0.01
Ir-P (avg)	2.22	2.22
Ir-N (avg)	2.08±0.01	2.07±0.02
C-O (avg)	1.17±0.01	1.23±0.02
P-O (avg)	1.63	1.64±0.01
N-N (avg)	1.37	1.35
Ir-N-N (avg)	117.6±0.5°	116.8±3.0°
N-Ir-P(C) (avg)	175.5	172.9

Molecular Mechanics Calculations:

Possible solution structures for the series of donor-acceptor complexes, $[\text{Ir}(\mu\text{-pz}^*)(\text{CO})(\text{Ph}_2\text{P-O-C}_6\text{H}_4\text{-(CH}_2\text{)}_n\text{-py}^+)]_2$ ($n = 0, 1, 2$, and 3), have been determined by the method described in the Experimental Section of this chapter. The complexes are categorized based on the number of methylene groups, n , in the bridge between Ir_2 (donor) and py^+ (acceptor). The computer generated structures of the $n = 0$ and $n = 1$ complexes are shown in Figures 3.5 and 3.6a. The angles and distances, defined in Figure 3.4 and summarized in Table 3.5, will be used to structurally describe these two complexes. θ is the angle between the planes of the phenylene and pyridinium rings, and γ is the cant angle between the rings. A more detailed view of the Ir-spacer- py^+ ($\text{Ir-P-O-C}_6\text{H}_4\text{-(CH}_2\text{)}_n\text{-py}^+$, $n = 1$) portion of the complex is provided in Figure 3.6b, showing the interaction between the pyridinium and phenylene rings. This depiction of the electron-transfer pathway also serves to demonstrate that the pyridinium acceptor cannot come within van der Waals contact of the iridium donor.

The pyridinium group of the $n = 2$ complex can exist in one of two possible low energy conformations in relation to the phenylene ring (there are many other possible conformations; however, knowledge of the two extreme conformers will be sufficient to understand the dynamics of the spacer and acceptor). The first conformer, shown in Figure 3.7a, and in more detail in 3.7b, is the lowest energy structure (minimum gauche interactions) in which the methylene chain is completely *stretched*. The relevant distances and angles that characterize the relative orientation of the pyridinium and phenylene rings in the stretched conformer are given in Table 3.5. The second conformer, shown in Figure 3.8a and b, is a slightly higher energy structure in which the pyridinium ring is brought as close to the phenylene group as allowed by van der Waals interactions. In this extreme conformation the pyridinium ring is 3.1 Å from the phenylene ring at its closest contact point, and will therefore be termed the *folded* conformation.

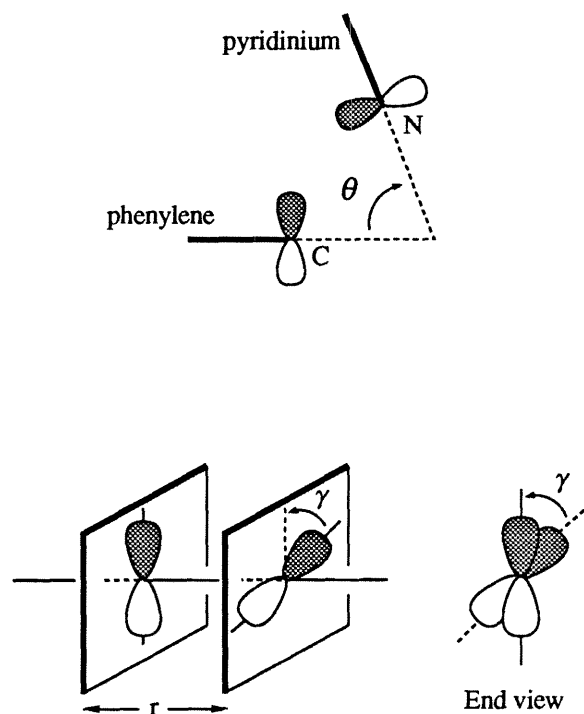


Figure 3.4. Definition of r , θ , and γ between the phenylene and pyridinium rings. These angles and distance are used to characterize the series of Ir₂-py⁺ donor-acceptor complexes.

Table 3.5. Structural Parameters Obtained from Molecular Mechanics Calculations for Stretched and Folded Conformations

compounds	stretched			folded			
	Ir-N ^s	Ir-N ^b	θ (°)	Ir-N ^s	θ (°)	γ (°)	r (Å)
[Ir ₂]-py ⁺	6.5	9.5	180	6.5	180	42	1.4
[Ir ₂]-CH ₂ -py ⁺	7.0	11.0	110	7.0	110	0	2.4
[Ir ₂]- (CH ₂) ₂ -py ⁺	9.4	12.5	180	6.4	50	0	3.1
[Ir ₂]- (CH ₂) ₃ -py ⁺	10.4	14.0	110	6.3	40	0	3.7

^s Edge-to-edge iridium-pyridinium through-*space* distance in Å.

^b Edge-to-edge iridium-pyridinium through-*bond* distance in Å.

Figure 3.5. Computer generated solution structure of $[\text{Ir}_2]\text{-py}^+$ ($n = 0$).

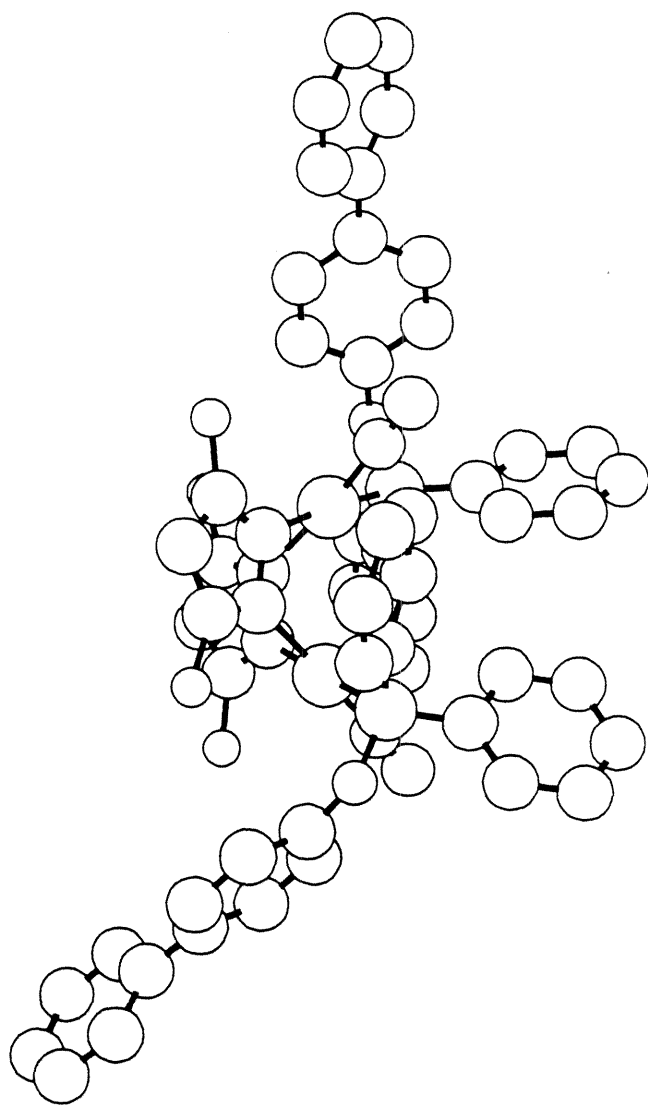
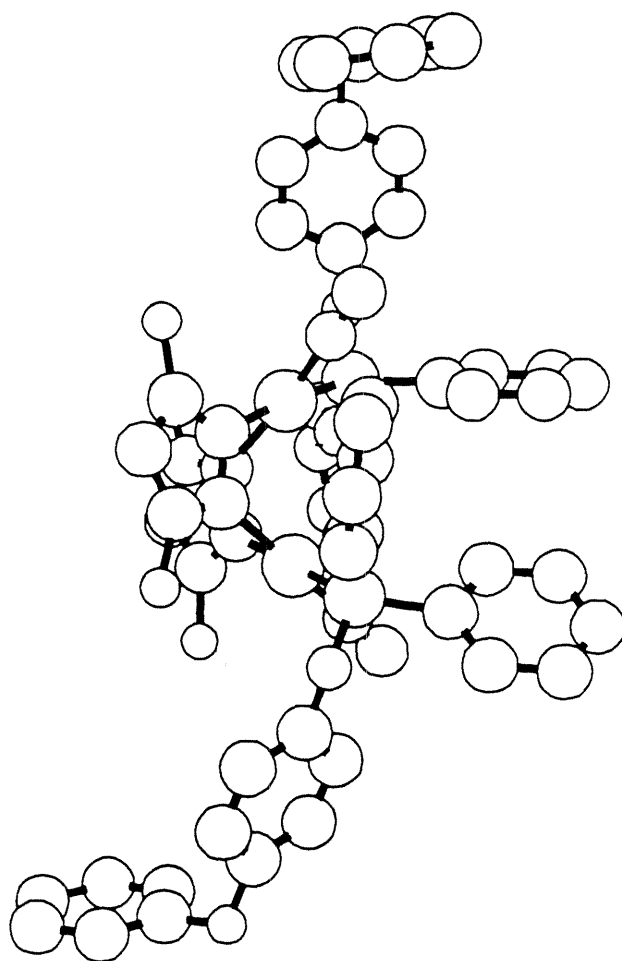
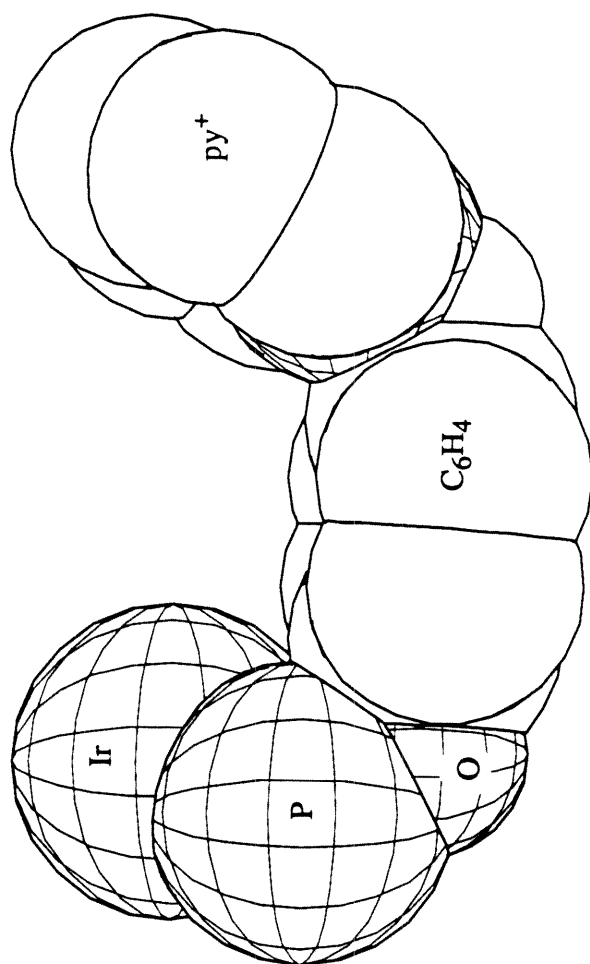


Figure 3.6. (a) Solution structure of $[\text{Ir}_2]\text{-CH}_2\text{-py}^+$ ($n = 1$). (b) Detailed view of electron-transfer pathway.

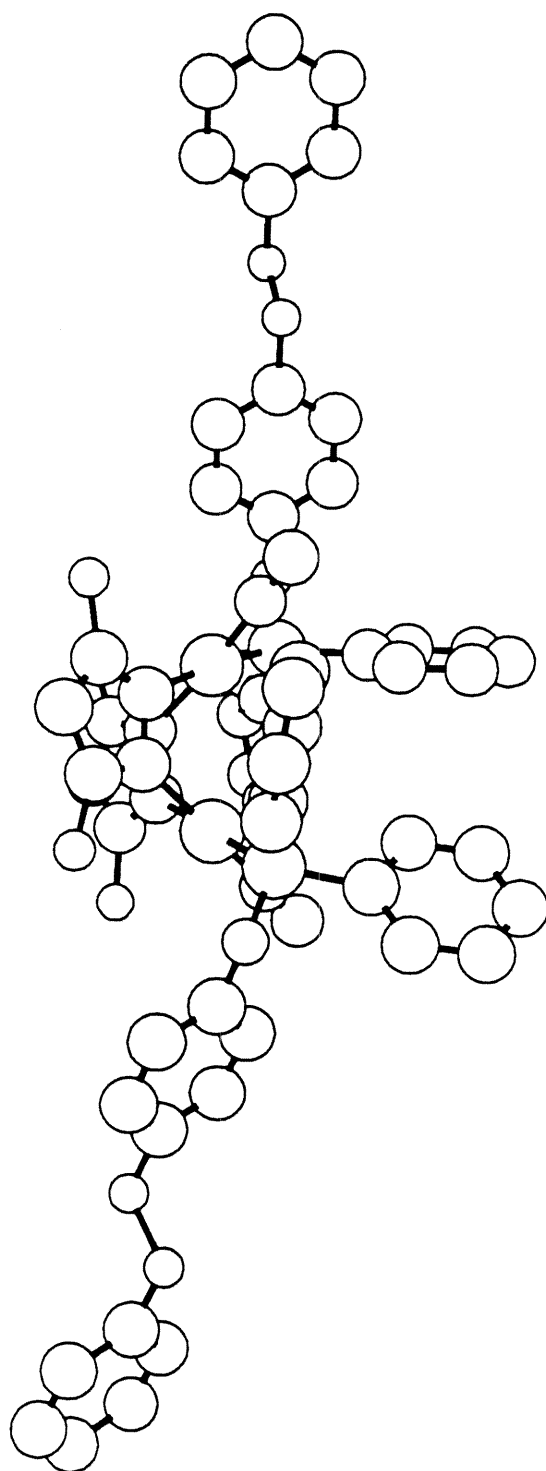


a

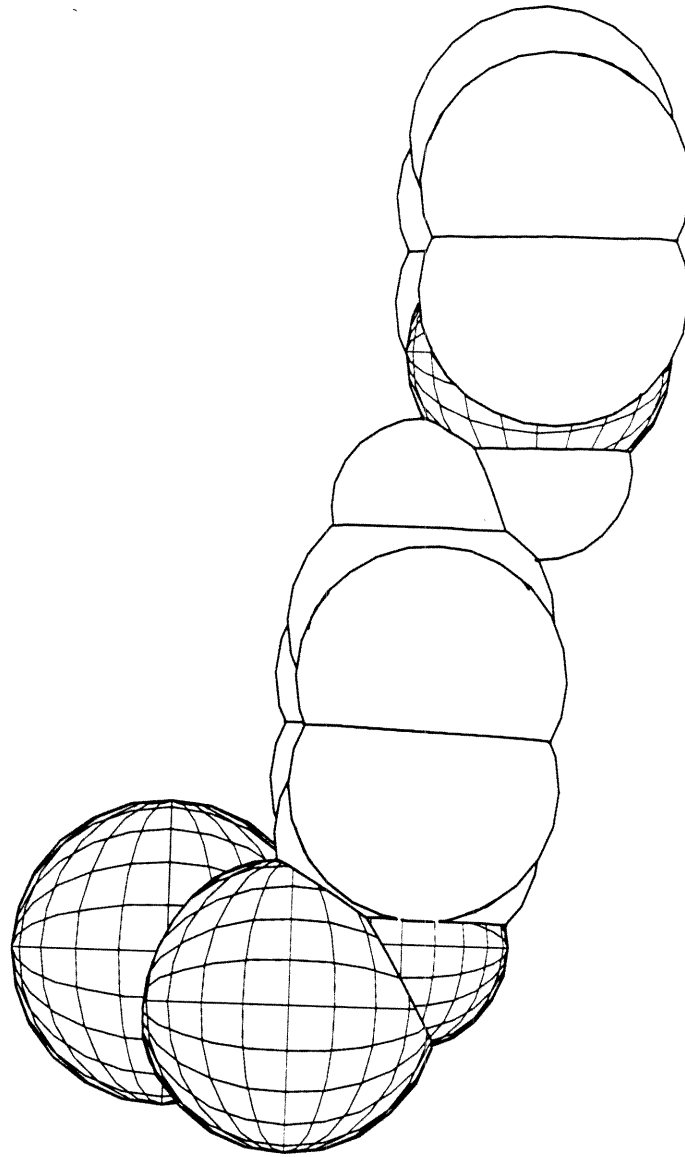


b

Figure 3.7. (a) Solution structure of the stretched conformation of $[\text{Ir}_2]-(\text{CH}_2)_2\text{-py}^+$ ($n = 2$). (b) Detailed view.

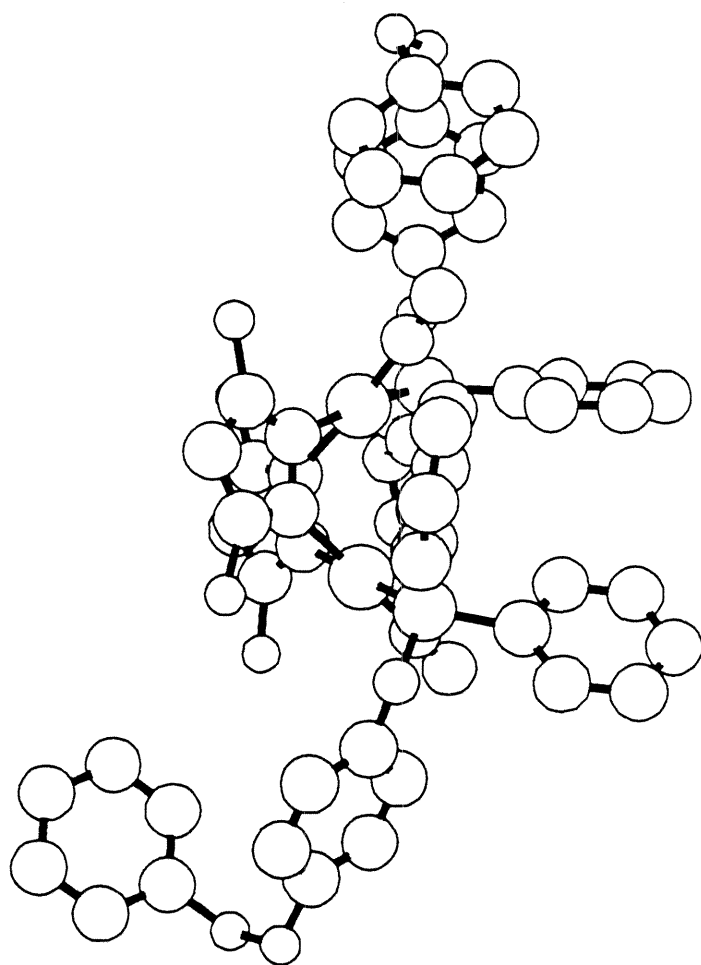


a

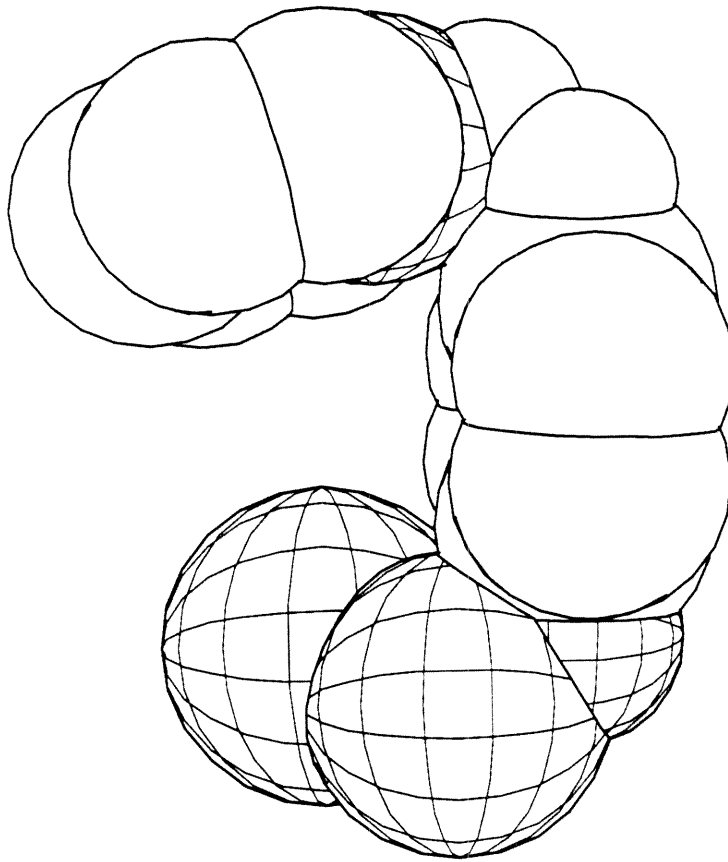


b

Figure 3.8. (a) Solution structure of the folded conformation of $[\text{Ir}_2](\text{CH}_2)_2\text{-py}^+$ ($n = 2$). (b) Detailed view.

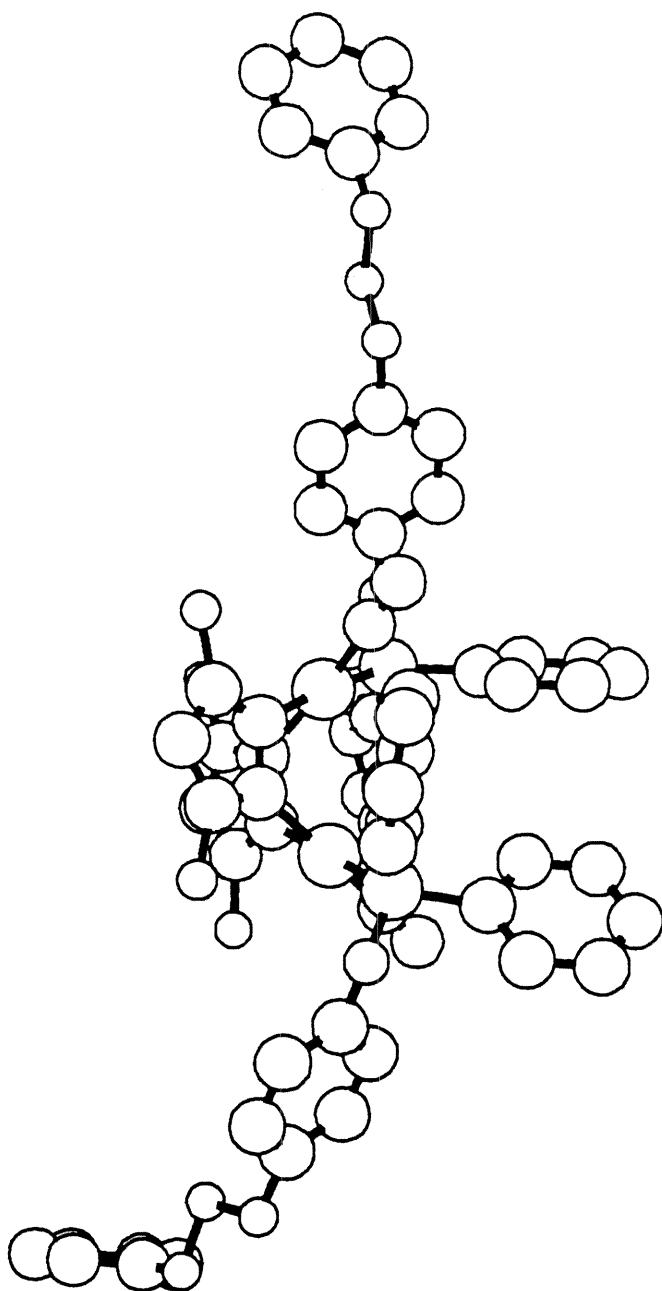


a

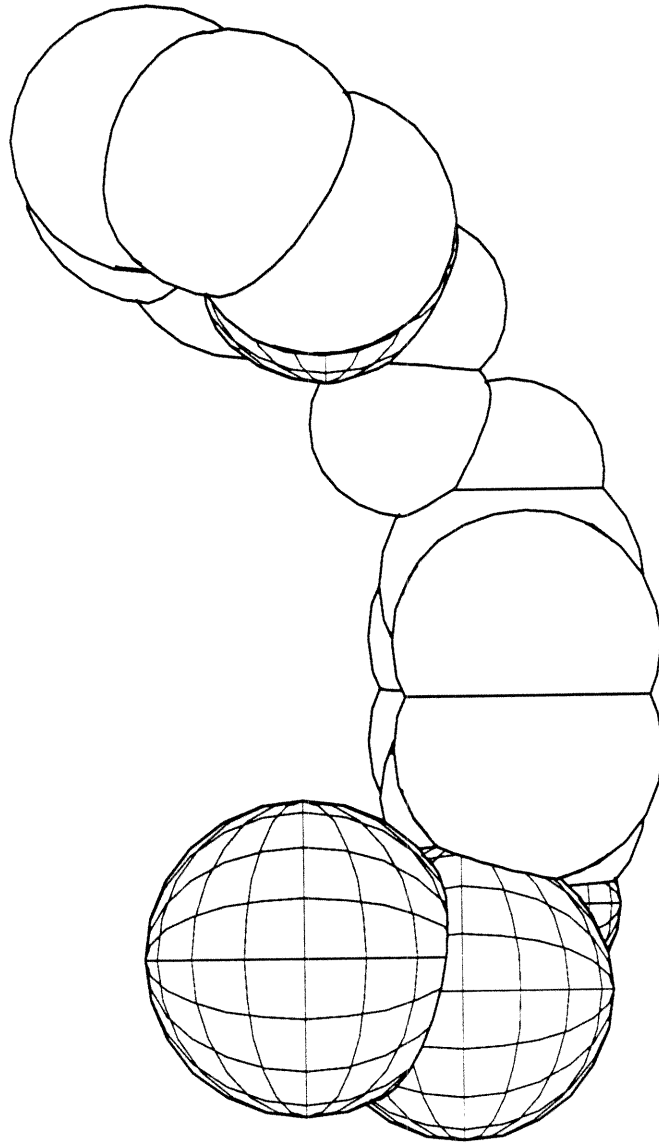


b

Figure 3.9. (a) Stretched conformation of $[\text{Ir}_2]-(\text{CH}_2)_3\text{-py}^+$ ($n = 3$). (b) Detailed view.

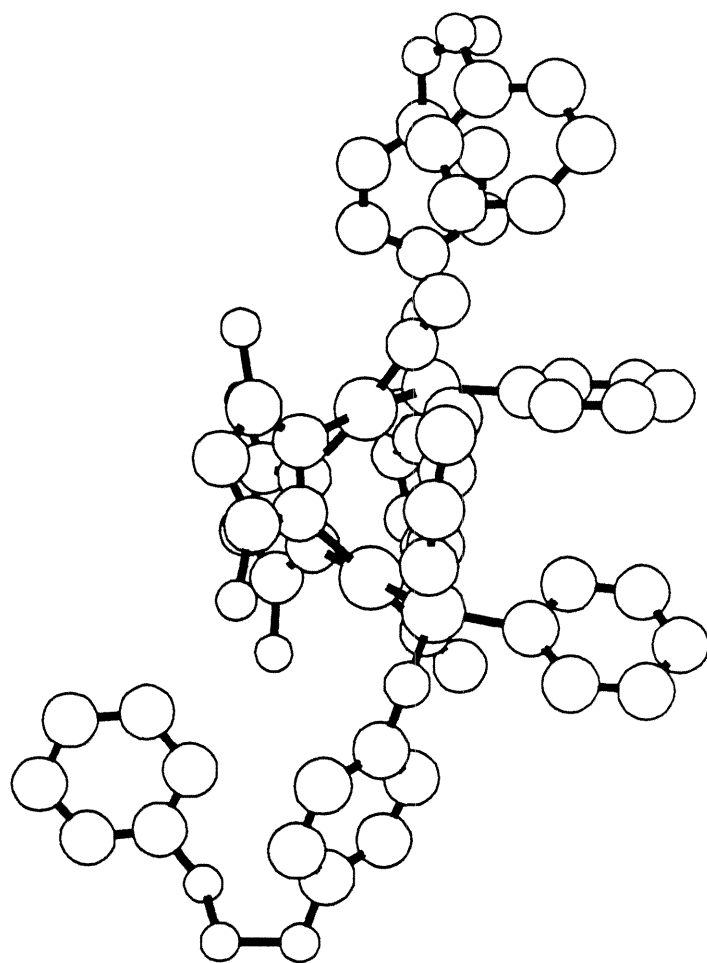


a

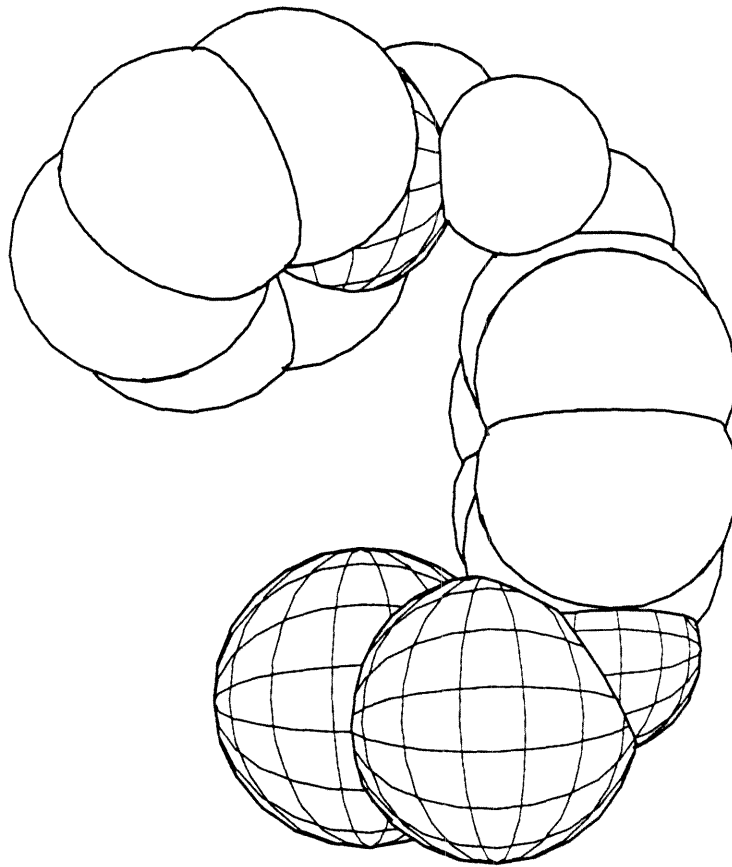


b

Figure 3.10. (a) Folded conformation of $[\text{Ir}_2](\text{CH}_2)_3\text{-py}^+$ ($n = 3$). (b) Detailed view.



a



b

The structures of the two extreme conformations (stretched and folded) for the $n = 3$ complex are shown in Figures 3.9a and b, and 3.10a and b. The difference in values of r (see Table 3.5) between the stretched and folded conformations for this complex are much larger than in the previous three complexes ($n = 0, 1$ and 2).

The pronounced dependence of the calculated pyridinium and methylene chain geometries on n has been demonstrated in Figures 3.5-3.10. The results, shown in Table 3.5, reveal interesting dependencies of angles and distances on the value of n . In the folded conformations of $n = 0$ and 1 complexes, θ values are greater than 90° , while for complexes with $n = 2$ and 3 , θ values are less than 90° . In the folded conformations the value of r increases as n increases while the values of θ decrease. In the stretched conformations θ alternates between 180° and 110° for all complexes: for $n = 0$ and 2 , $\theta = 180^\circ$; and for $n = 1$ and 3 , $\theta = 110^\circ$. An attempt to correlate these structural parameters to observed electron-transfer rates will be described in Chapter 5.

REFERENCES

1. Weiser, J.; Staab, H. A. *Tetrahedron Lett* **1985**, 6059-6063.
2. Sessler, J. L.; Johnson, M. R.; Lin, T. *Tetrahedron* **1989**, *45*, 4767-4784.
3. International Union of Crystallography. In *International Tables for X-ray Crystallography*; Kynoch Press: Birmingham, England, 1974; pp 71, 149.
4. Original program written by S. L. Mayo, B. D. Olafson and W. A. Goddard, California Institute of Technology, Pasadena, CA 91125. Copyright 1988, 1989 by Molecular Simulations Inc.
5. Nussbaum, S.; Rettig, S. J.; Storr, A.; Trotter, J. *Can. J. Chem.* **1985**, *63*, 692-702.
6. Fox, L. S., Ph.D. Dissertation, California Institute of Technology, Pasadena, CA, 1989.

7. Beveridge, K. A.; Bushnell, G. W.; Stobart, S. R. *Organometallics* **1983**, 2, 1447-1451.
8. Coleman, A. W.; Eadie, D. T.; Stobart, S. R.; Zaworotko, M. J.; Atwood, J. L. *J. Am. Chem. Soc.* **1982**, 104, 922.
9. Beveridge, K. A.; Bushnell, G. W.; Dixon, K. R.; Eadie, D. T.; Stobart, S. R.; Atwood, J. L.; Zaworotko, M. J. *J. Am. Chem. Soc.* **1982**, 104, 920-921.
10. Louie, B. M.; Rettig, S. J.; Storr, A.; Trotter, J. *Can. J. Chem.* **1984**, 62, 1057.
11. Uson, R.; Oro, L. A.; Ciriano, M. A.; Pinillos, M. T.; Tiripicchio, A.; Carmellini, M. J. *Organomet. Chem.* **1981**, 205, 247.

Chapter 4

Steady-State Spectroscopy and Electrochemistry

INTRODUCTION

Having chemically and structurally characterized the series of donor-spacer-acceptor complexes, $[\text{Ir}(\mu\text{-pz}^*)(\text{CO})(\text{Ph}_2\text{PO-C}_6\text{H}_4\text{-(CH}_2)_n\text{-py}^+\text{-R})]_2(\text{PF}_6^-)_2$ ($n = 0, 1, 2$ or 3), an investigation of their photophysical properties is now presented. It was demonstrated in the previous chapter that the nature of the spacer has pronounced effects on the orientation of the pyridinium acceptor relative to the Ir_2 donor. The spacer-acceptor unit also plays an important role in determining the photophysical properties of the $\text{Ir}_2\text{-py}^+$ donor-acceptor complexes. For example, the quantum yields of emission from the $\text{d}^8\text{-d}^8$ iridium donor-acceptor complexes are all attenuated relative to an appropriate model complex. The source of this emission quenching is electron transfer, originating from the metal-localized excited states (singlet and triplet) of the iridium chromophore and terminating at the pyridinium cation. The result is the formation of an excited charge-transfer state with an electron deficient metal center and a neutral pyridinium radical. An important goal of the spectroscopic studies described in this chapter is to quantify the effects that each spacer-acceptor group ($n = 0, 1, 2$, and 3) has on the photophysical properties of these $\text{d}^8\text{-d}^8$ excited states.

In this chapter, results from steady-state absorption and emission studies were used to determine Ir_2 singlet and triplet excited-state energies, and results from ground-state electrochemical studies were used to calculate energies of the $\text{Ir}_2^+\text{-py}^\bullet$ charge-transfer states for each donor-acceptor complex. These calculations were combined to yield driving forces for each electron-transfer step. Fluorescence and phosphorescence quantum yield measurements were obtained for the series of $\text{Ir}_2\text{-py}^+$ donor-acceptor complexes, revealing the extent of electron-transfer quenching of the iridium $\text{d}^8\text{-d}^8$ singlet and triplet excited-states.

BACKGROUND

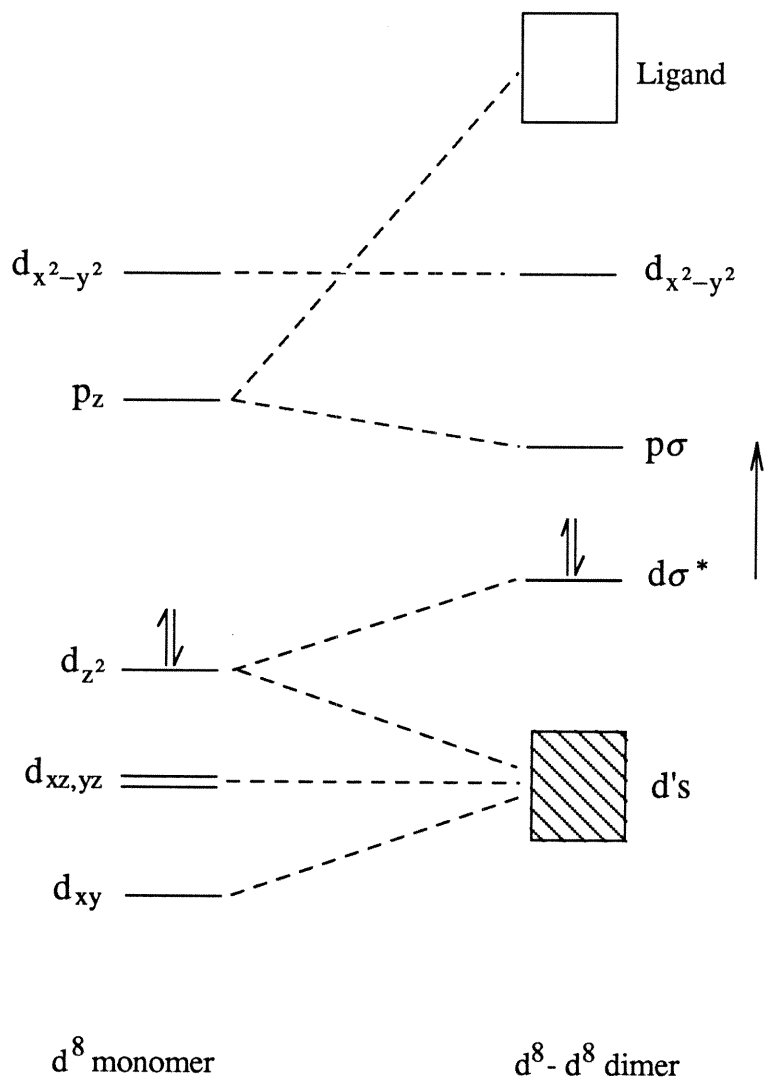
Research in our laboratories have established the rich reactivity of d^8 - d^8 transition metal complexes toward C-X and C-H bond activation,¹⁻³ and outer and inner-sphere electron transfer.⁴⁻⁷ Spectroscopic studies of these complexes have indicated that the electronic structure of these complexes can be represented by the MO diagram shown in Figure 4.1.⁸⁻¹⁰ The interaction between two square planar d^8 fragments in these molecules forces an interaction between the d_{z^2} and p_z orbitals of each monomer fragment forming $d\sigma$ and $p\sigma$ dimer MOs. Filling the molecular orbitals with $16e^-$ for each monomer leaves the $d\sigma^*$ level as the HOMO and the $p\sigma$ level as the LUMO. The lowest electronic excited states in these complexes are generated by promoting a $d\sigma^*$ electron into the vacant $p\sigma$ orbital, which forms a $d\sigma^*p\sigma$ state in either a singlet or triplet spin state. These excited states, $^1(d\sigma^*p\sigma)$ and $^3(d\sigma^*p\sigma)$, can then decay by radiative and nonradiative pathways, at characteristic rates, back to the ground state, $(d\sigma^*)^2$. This model will be used as a basis for understanding the electronic absorption and emission spectra of the iridium donor-acceptor complexes presented here.

EXPERIMENTAL

Materials:

Acetonitrile (Burdick & Jackson) was used as received for UV-vis experiments; for emission measurements this solvent was degassed with three freeze-pump-thaw cycles on a high-vacuum line ($<10^{-5}$ torr), dried, and stored under vacuum over activated 3 Å sieves. Dichloromethane and acetonitrile were freshly distilled from calcium hydride and syringe-degassed before use for electrochemical experiments. Tetra-n-butylammonium hexafluorophosphate (TBAH) was recrystallized 2 times from 95% ethanol.

Figure 4.1. Molecular orbital diagram for the interaction of two square planar d^8 metal ions, showing HOMO and LUMO for d^8 - d^8 metal dimers.



Electronic Absorption Spectroscopy:

Electronic absorption spectra were measured on one of three spectrophotometers: Cary 14, converted to computer operation by On-Line Instruments Systems Inc.; Shimadzu UV-260; or Hewlett Packard 8450A Diode Array. Samples were prepared in high-precision 1 cm quartz cells, fitted with a Kontes needle valve, and either freeze-pump-thawed or bubble deoxygenated with argon.

Electronic Emission Spectroscopy:

Electronic emission spectra were obtained on an emission spectrometer constructed at Caltech, which has been described previously.^{10,11} Measurements were made on freeze-pump-thawed acetonitrile solutions in 1 cm non-precision quartz cells. The samples were excited with the 436 nm line of an Oriel 200 Watt Hg/Xe lamp. This line was selected with a SPEX 1620 monochromator and filtered with an Oriel 436 nm interference filter to remove stray excitation light. The luminescence from the sample was collimated, focused, and then filtered with a Corning 3387 sharp-cut filter to remove stray excitation before being directed into a SPEX 1870 monochromator. Detection of the signal was achieved using a Hamamatsu R955 PMT. The signal from the PMT was amplified with an EG&G PAR 182A lock-in amplifier and plotted on a Soltec 3314 chart recorder. The data was digitized and corrected for PMT response. Room temperature quantum yields were determined by the optically dilute solution method described by Crosby and Demas.¹² Integrated emission intensities were determined by calculating the areas under Gaussian curves that best fit the data. The quantum yield standard was [Ru(bpy)₃]Cl₂ in water ($\Phi = 0.042$, $\lambda_{\text{ex}} = 436 \text{ nm}$).¹³ The absorbance of the samples and reference at 436 nm were adjusted so that they were equivalent within experimental error and less than or equal to 0.2.

Electronic Excitation Spectroscopy:

Electronic excitation spectra of optically dilute solutions (in CH₃CN) were recorded

using an instrument built at Brookhaven National Laboratories. Singlet and triplet spectra were obtained by detection at 560 and 750 nm, respectively. Excitation was controlled by an electronic feed-back circuit that kept the excitation source constant and eliminated the necessity to correct for excitation fluctuations.

Electrochemistry:

Electrochemical measurements were conducted using a Princeton Applied Research (PAR) model 173 potentiostat/galvanostat, a model 175 universal programmer, and a model 179 digital coulometer. Cyclic voltammograms were plotted on a Houston Instruments Omnigraphic 2000 x,y recorder. All electrochemical studies were conducted in acetonitrile (dried over 3Å sieves) using a standard one-compartment cell¹⁴ with a Pt disk electrode as working electrode (surface area approximately 1.3 mm²), coiled Pt wire or mesh as counter electrode, and aqueous saturated sodium calomel electrode (SSCE) as reference electrode. The ferrocene/ferrocenium couple was used as an internal reference redox system. The use of aqueous SSCE as a reference electrode introduces an unknown and irreproducible liquid junction potential, E_j . Therefore, all potentials were referenced to the ferrocene/ferrocenium couple (0.302 vs. SSCE) and reported versus SSCE. Supporting electrolyte in all cases was 0.1 M tetra-n-butyl ammonium hexafluorophosphate (TBAH).

RESULTS and DISCUSSION

Absorption Spectra: Electronic absorption spectra of the model complexes, $[\text{Ir}(\mu\text{-pz}^*)(\text{CO})(\text{Ph}_2\text{PO-C}_6\text{H}_4\text{-Y})_2]$ (Y is poor electron acceptors, CH₃ or CH₂-Quin⁺PF₆⁻), and donor-acceptor complexes, $[\text{Ir}(\mu\text{-pz}^*)(\text{CO})(\text{Ph}_2\text{PO-C}_6\text{H}_4\text{-(CH}_2)_n\text{-py}^+\text{-R})_2](\text{PF}_6^-)_2$, all show identical features at nearly equivalent frequencies, indicating the dominance of the spectra by the photophysical properties of the d⁸-d⁸ iridium core (see Background section

of this chapter). The spectra in acetonitrile solution show two intense bands with maxima at approximately $22,000\text{ cm}^{-1}$ ($\lambda = 460\text{ nm}$, $\epsilon = \sim 10,000\text{ M}^{-1}\text{ cm}^{-1}$) and $28,000\text{ cm}^{-1}$ ($\lambda = 350\text{ nm}$, $\epsilon = \sim 5,000\text{ M}^{-1}\text{ cm}^{-1}$). Table 4.1 summarizes the absorption data for the iridium complexes. Figure 4.2 shows the absorption spectrum of the model complex, $[\text{Ir}_2]\text{-CH}_3$, which was typical of absorption spectra for all the iridium $d^8\text{-}d^8$ complexes. The band at $22,000\text{ cm}^{-1}$ is assigned, by analogy to similar $d^8\text{-}d^8$ metal complexes,¹⁰ to a fully allowed $S_0 \rightarrow S_1(d\sigma^* \rightarrow p\sigma)$ electronic transition. The corresponding absorption into the triplet manifold ($S_0 \rightarrow T_1$) was not observed at room temperature due to its low extinction coefficient.¹⁰ The band at $28,000\text{ cm}^{-1}$ has been tentatively assigned to ($d_{xz}, d_{yz} \rightarrow p_z$) transitions also by analogy to similar $d^8\text{-}d^8$ metal complexes. More research into the precise nature of this and other higher energy bands is still necessary to unequivocally assign them to specific electronic transitions.

Table 4.1. Absorption Data for the Iridium Donor-Acceptor Complexes

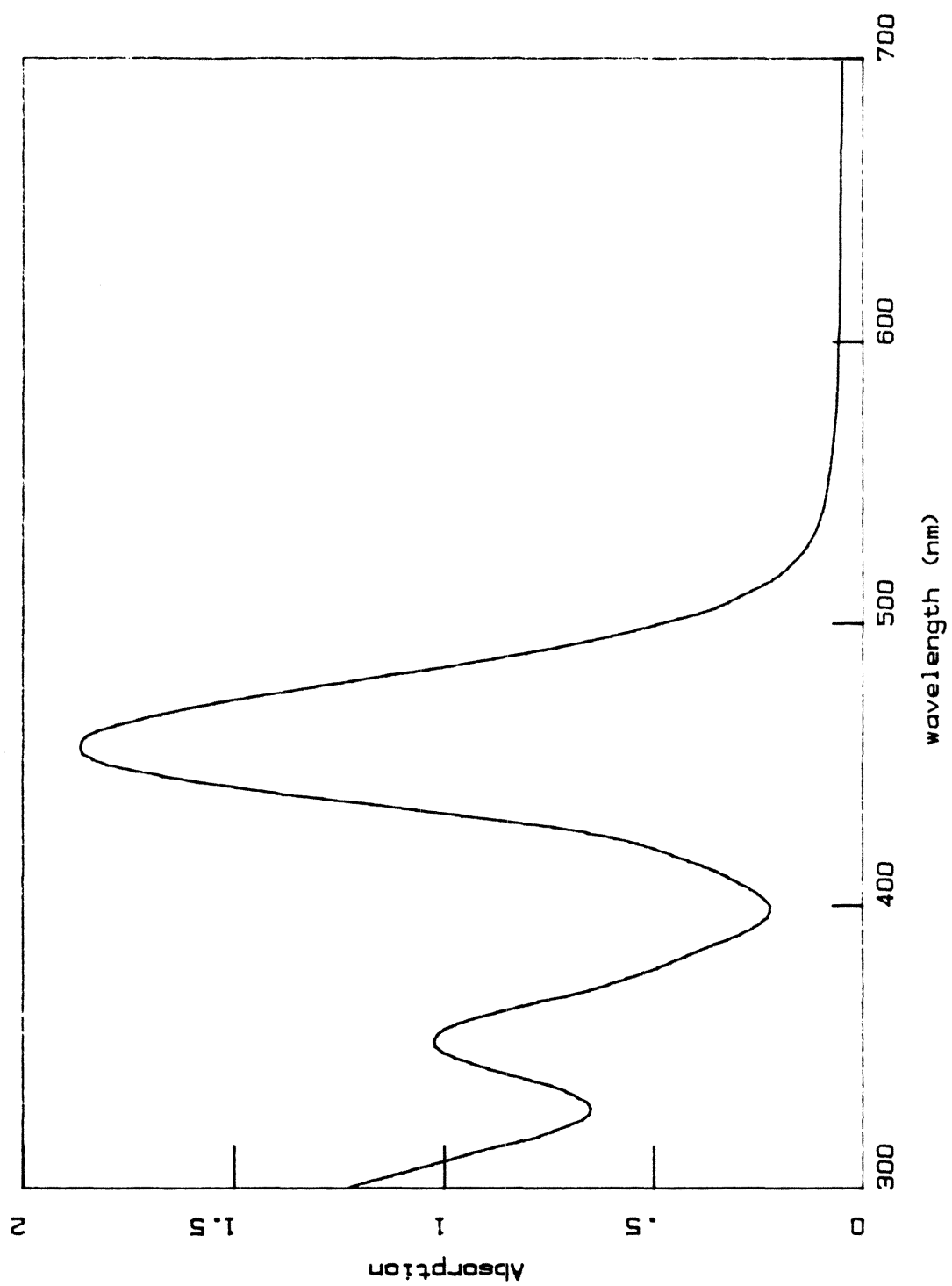
Compounds ^a	$S_0 \rightarrow S_1$		Band II ^c	
	cm^{-1}	nm	cm^{-1}	nm
$[\text{Ir}_2]\text{-CH}_3$	21,800	458	28,400	353
$[\text{Ir}_2]\text{-CH}_2\text{-Quin}^+{}^b$	21,700	460	28,200	355
$[\text{Ir}_2]\text{-py}^+$	21,700	460	28,200	355
$[\text{Ir}_2]\text{-CH}_2\text{-py}^+$	21,700	461	28,300	354
$[\text{Ir}_2]\text{-CH}_2\text{-py}^+\text{-tB}$	21,700	462	28,400	353
$[\text{Ir}_2]\text{-CH}_2\text{-py}^+\text{-Am}^b$	21,700	460	28,200	355
$[\text{Ir}_2]\text{-(CH}_2)_2\text{-py}^+$	21,800	460	28,200	354
$[\text{Ir}_2]\text{-3-(CH}_2)_2\text{-py}^+{}^b$	21,700	460	28,200	355
$[\text{Ir}_2]\text{-(CH}_2)_3\text{-py}^+{}^b$	21,700	460	28,200	355

^a All measurements were conducted in CH_3CN solutions.

^b These data have an error of $\pm 2\text{ nm}$.

^c This band is referred to in the text as the higher energy transition.

Figure 4.2. Absorption spectrum of $[\text{Ir}(\mu\text{-pz}^*)(\text{CO})(\text{Ph}_2\text{P-O-C}_6\text{H}_4\text{-CH}_3)]_2$. The band at 460 nm is assigned to the $\text{S}_0 \rightarrow \text{S}_1(\text{d}\sigma^* \rightarrow \text{p}\sigma)$ electronic transition.



Excitation Spectra: Singlet and triplet excitation spectra were obtained by detection of emission at 560 nm and 750 nm, respectively. These wavelengths correspond to emission maxima for fluorescence and phosphorescence of the iridium complexes. Tables 4.2 and 4.3 summarize excitation data for two model complexes and one donor-acceptor complex. Figures 4.3a and b show singlet and triplet excitation spectra for the model complex, [Ir₂]-CH₃. The features of these spectra are similar to those of the absorption spectra described above. The S₀→S₁ transitions appear in both singlet and triplet excitation spectra at wavelengths comparable to those in the absorption spectra. The high energy band at ~370 nm is weaker in the singlet excitation spectra, presumably due to diminished intersystem crossing to the singlet manifold from these higher lying excited-states (or possibly enhanced intersystem crossing to the triplet manifold). This point was not further investigated and is left for more extensive studies in the future.

Table 4.2. Singlet Excitation Data

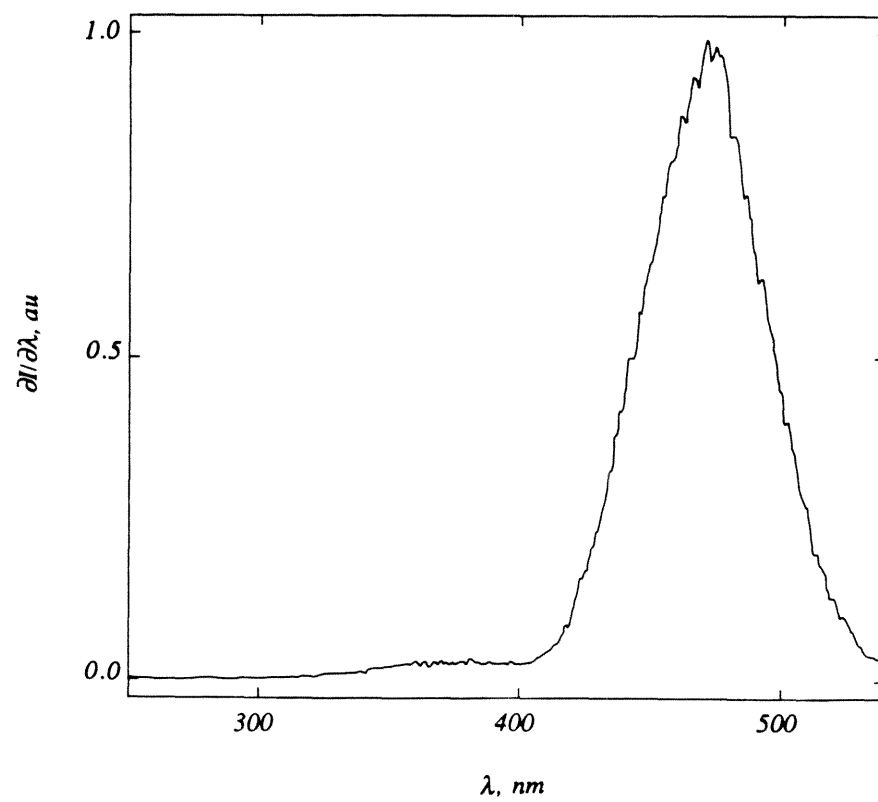
Compounds	S ₀ →S ₁	
	cm ⁻¹	nm
[Ir ₂]-CH ₃	21,300	471
[Ir ₂]-CH ₂ -Quin ⁺	20,900	479
[Ir ₂]-CH ₂ ₃ -py ⁺	21,200	472

Table 4.3. Triplet Excitation Data

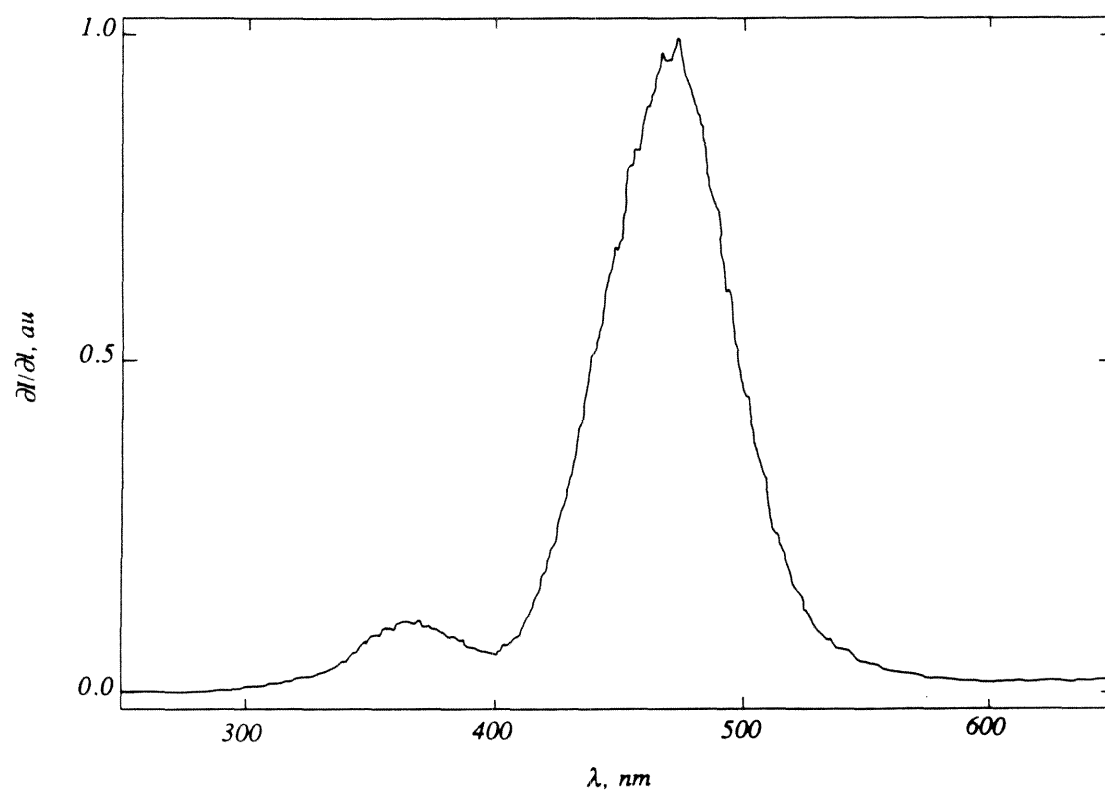
Compounds	S ₀ →S ₁		Band II	
	cm ⁻¹	nm	cm ⁻¹	nm
[Ir ₂]-CH ₃	21,200	471	27,400	365
[Ir ₂]-CH ₂ -Quin ⁺	20,900	478	26,900	372
[Ir ₂]-CH ₂ ₃ -py ⁺	21,200	471	27,400	365

Figure 4.3. (a) Singlet excitation spectrum of $[\text{Ir}(\mu\text{-pz}^*)(\text{CO})(\text{Ph}_2\text{P-O-C}_6\text{H}_4\text{-CH}_3)]_2$, at room temperature in CH_3CN solution, showing band corresponding to $\text{S}_0 \rightarrow \text{S}_1$ transition at 470 nm. (b) Triplet excitation spectrum of $[\text{Ir}(\mu\text{-pz}^*)(\text{CO})(\text{Ph}_2\text{P-O-C}_6\text{H}_4\text{-CH}_3)]_2$, at room temperature in CH_3CN solution, showing band corresponding to $\text{S}_0 \rightarrow \text{S}_1$ transition at 470 nm and a higher energy band at 365 nm.

a



b



Emission Spectra: Electronic emission spectra of the model compounds, $[\text{Ir}(\mu\text{-pz}^*)(\text{CO})(\text{Ph}_2\text{P-O-C}_6\text{H}_4\text{-CH}_3)]_2$ and $[\text{Ir}(\mu\text{-pz}^*)(\text{CO})(\text{Ph}_2\text{P-O-C}_6\text{H}_4\text{-CH}_2\text{-Quin}^+)]_2$, at room temperature in acetonitrile solution show two emission bands in the spectral region between $11,000$ and $22,000\text{ cm}^{-1}$ (450 and 900 nm) with maxima at approximately $17,500\text{ cm}^{-1}$ (570 nm) and $13,500\text{ cm}^{-1}$ (750 nm). The steady-state emission spectrum of $[\text{Ir}_2]\text{-CH}_3$ is given in Figures 4.4. The absorption and emission spectra for $[\text{Ir}_2]\text{-CH}_3$ are combined in Figure 4.5. These bands are assigned to $\text{S}_1 \rightarrow \text{S}_0(\text{p}\sigma \rightarrow \text{d}\sigma^*)$ and $\text{T}_1 \rightarrow \text{S}_0(\text{p}\sigma \rightarrow \text{d}\sigma^*)$ electronic transitions, respectively, by analogy to emission features observed for similar $\text{d}^8\text{-d}^8$ chromophores.¹⁰ The emission spectra of all the donor-acceptor complexes also show two emission bands at nearly the same energies as the model complexes, however, they exhibit diminished emission intensities compared to the model complexes. Table 4.4 summarizes the emission data for the series of $\text{Ir}_2\text{-py}^+$ complexes, and Figure 4.6 shows the emission spectrum of the donor-acceptor complex, $[\text{Ir}_2]\text{-(CH}_2)_3\text{-py}^+$, demonstrating the decrease in emission intensities upon incorporation of the pyridinium acceptor into the molecule. The fluorescence and phosphorescence quenching is attributed to excited-state electron transfer, culminating in formation of an excited charge-transfer state. This deactivation pathway has been thoroughly characterized in similar $\text{d}^8\text{-d}^8$ iridium donor-acceptor complexes, where other possible mechanisms have been ruled out by energy and intensity considerations.¹⁰ Table 4.5 lists the fluorescence and phosphorescence quantum yields. The dramatic effect of the number of methylene groups in the bridge between the donor group ($\text{d}^8\text{-d}^8$ iridium center) and the acceptor group (pyridinium cation) is apparent on inspection of the data in Table 4.5. The fluorescence of the donor-acceptor complex, $[\text{Ir}_2]\text{-py}^+$, is 96% quenched as compared to model complexes ($[\text{Ir}_2]\text{-CH}_3$ and $[\text{Ir}_2]\text{-CH}_2\text{-Quin}^+$), however, only 52% of the fluorescence is quenched in $[\text{Ir}_2]\text{-CH}_2\text{-py}^+$. In the next chapter, these results will be combined with excited-state lifetime data, yielding singlet and triplet electron-transfer rates, and the origin of these differences will also be discussed in Chapter 5.

Table 4.4. Emission Data for the Iridium Donor-Acceptor Complexes

Compounds ^a	$S_1 \rightarrow S_0$		$T_1 \rightarrow S_0$	
	cm ⁻¹	nm	cm ⁻¹	nm
[Ir ₂]-CH ₃	17,200	583	13,300	754
[Ir ₂]-CH ₂ -Quin ⁺	17,200	583	13,200	758
[Ir ₂]-py ⁺	18,300	547	— ^b	— ^b
[Ir ₂]-CH ₂ -py ⁺	17,500	572	13,400	749
[Ir ₂]-CH ₂ -py ⁺ -Am	17,300	577	13,300	750
[Ir ₂]-CH ₂ -py ⁺	17,800	563	13,900	720
[Ir ₂]-3-(CH ₂) ₂ -py ⁺	17,900	558	13,700	729
[Ir ₂]-CH ₂ -py ⁺	17,400	576	13,700	732

^a All measurements were conducted in CH₃CN solution.

^b Signal intensity too low to observe.

Table 4.5. Quantum Yields for Fluorescence and Phosphorescence in Ir₂-py⁺ Complexes

Compounds	Quantum Yields ^a	
	$\Phi_f (\times 10^3)$	$\Phi_{ph} (\times 10^3)$
[Ir ₂]-CH ₃	1.0	12
[Ir ₂]-CH ₂ -Quin ⁺	1.2	17
[Ir ₂]-py ⁺	0.039	— ^b
[Ir ₂]-CH ₂ -py ⁺	0.53	4.3
[Ir ₂]-CH ₂ -py ⁺ -Am	0.69	11
[Ir ₂]-CH ₂ -py ⁺	0.19	0.045
[Ir ₂]-3-(CH ₂) ₂ -py ⁺	0.093	0.021
[Ir ₂]-CH ₂ -py ⁺	0.76	0.25

^a These values are associated with error of $\pm 30\%$.

^b Emission too weak to measure.

Figure 4.4. Emission spectrum of $[\text{Ir}(\mu\text{-pz}^*)(\text{CO})(\text{Ph}_2\text{P-O-C}_6\text{H}_4\text{-CH}_3)_2]$ showing $\text{S}_1 \rightarrow \text{S}_0$ transition at $17,200 \text{ cm}^{-1}$ and $\text{T}_1 \rightarrow \text{S}_0$ transition at $13,300 \text{ cm}^{-1}$.

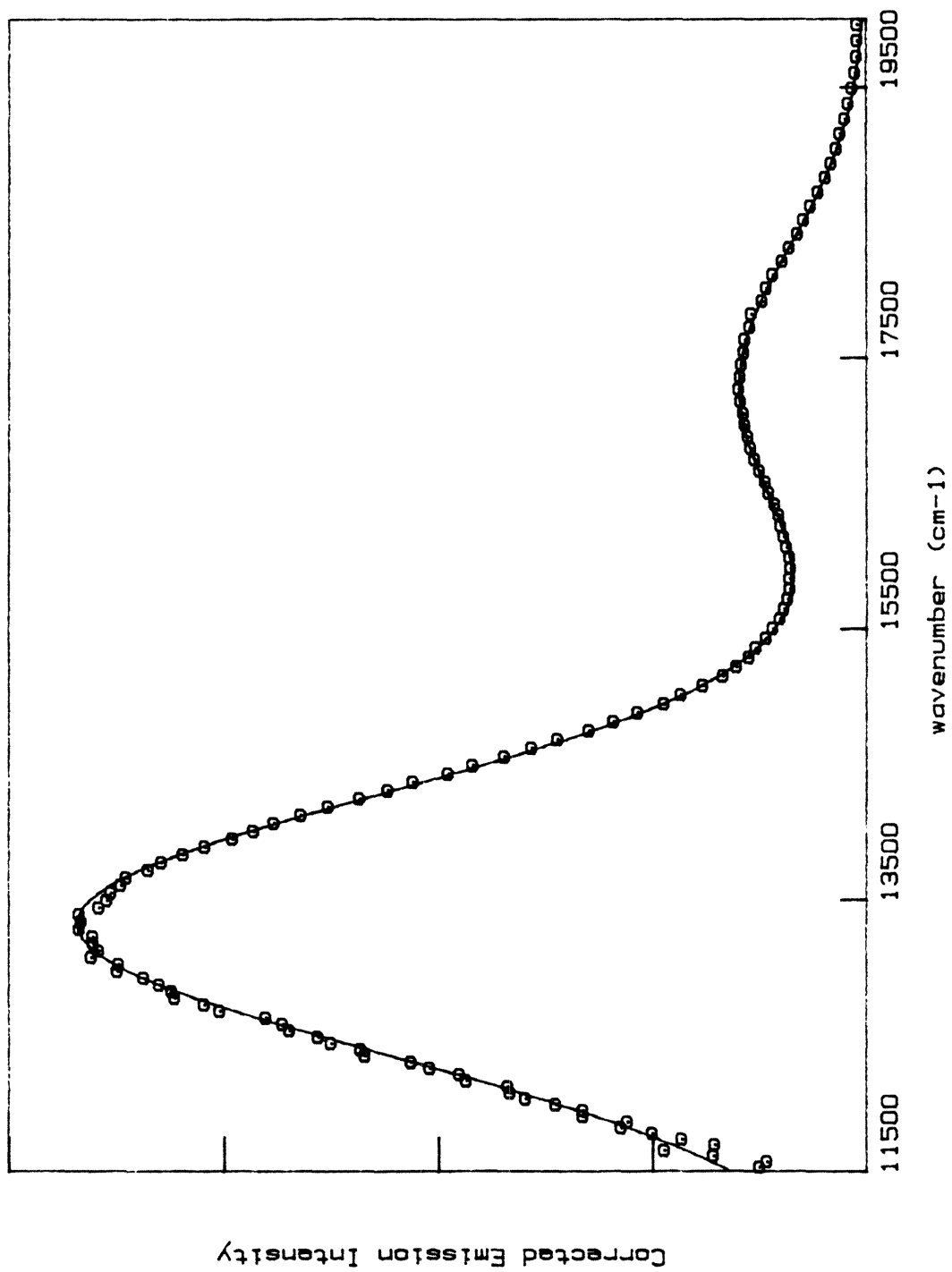


Figure 4.5. Absorption spectrum (— — —) of $[\text{Ir}(\mu\text{-pz}^*)(\text{CO})(\text{Ph}_2\text{P-O-C}_6\text{H}_4\text{-CH}_3)]_2$ and emission spectrum (— · —) generated by excitation into 460 nm band.

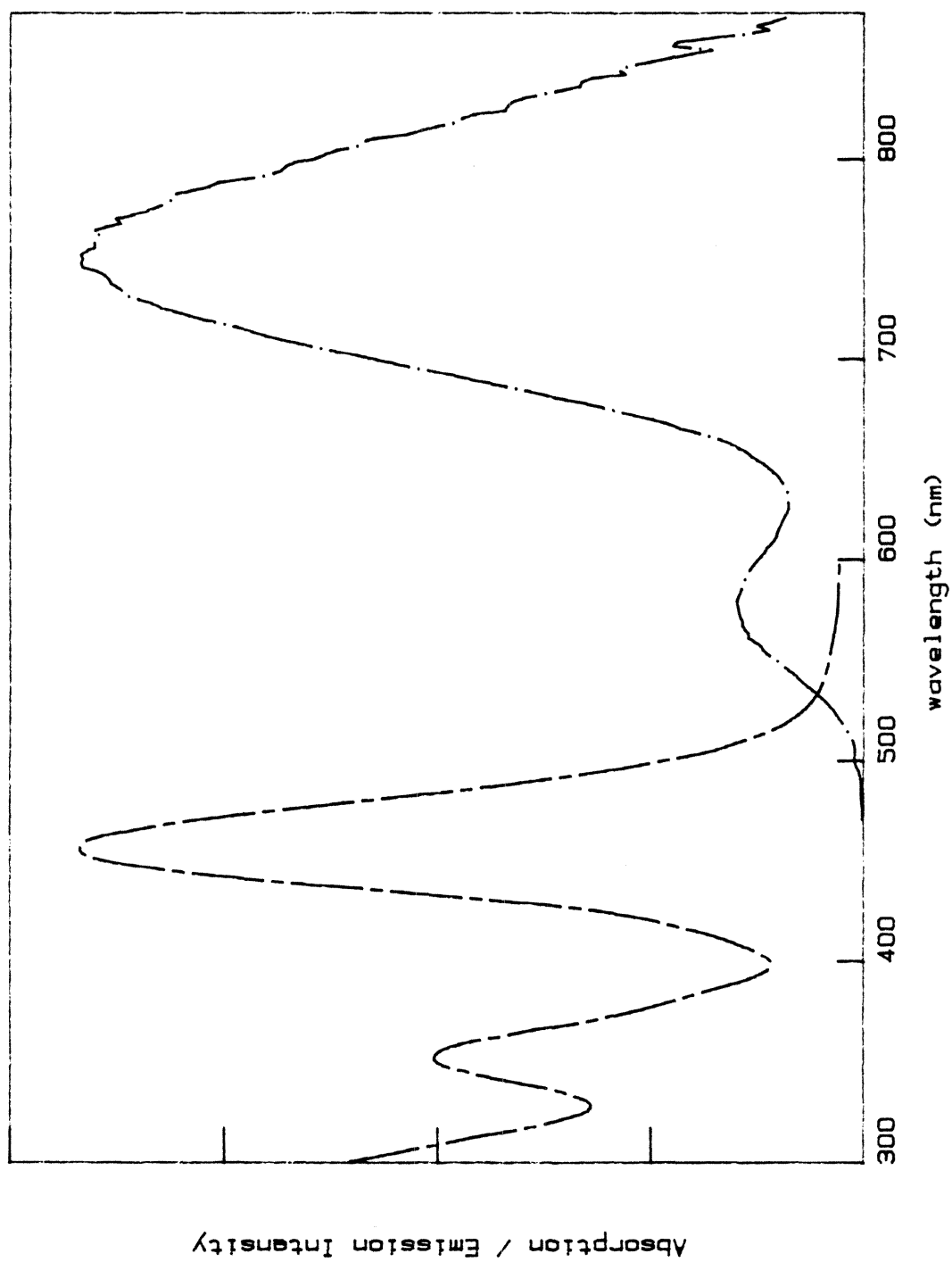
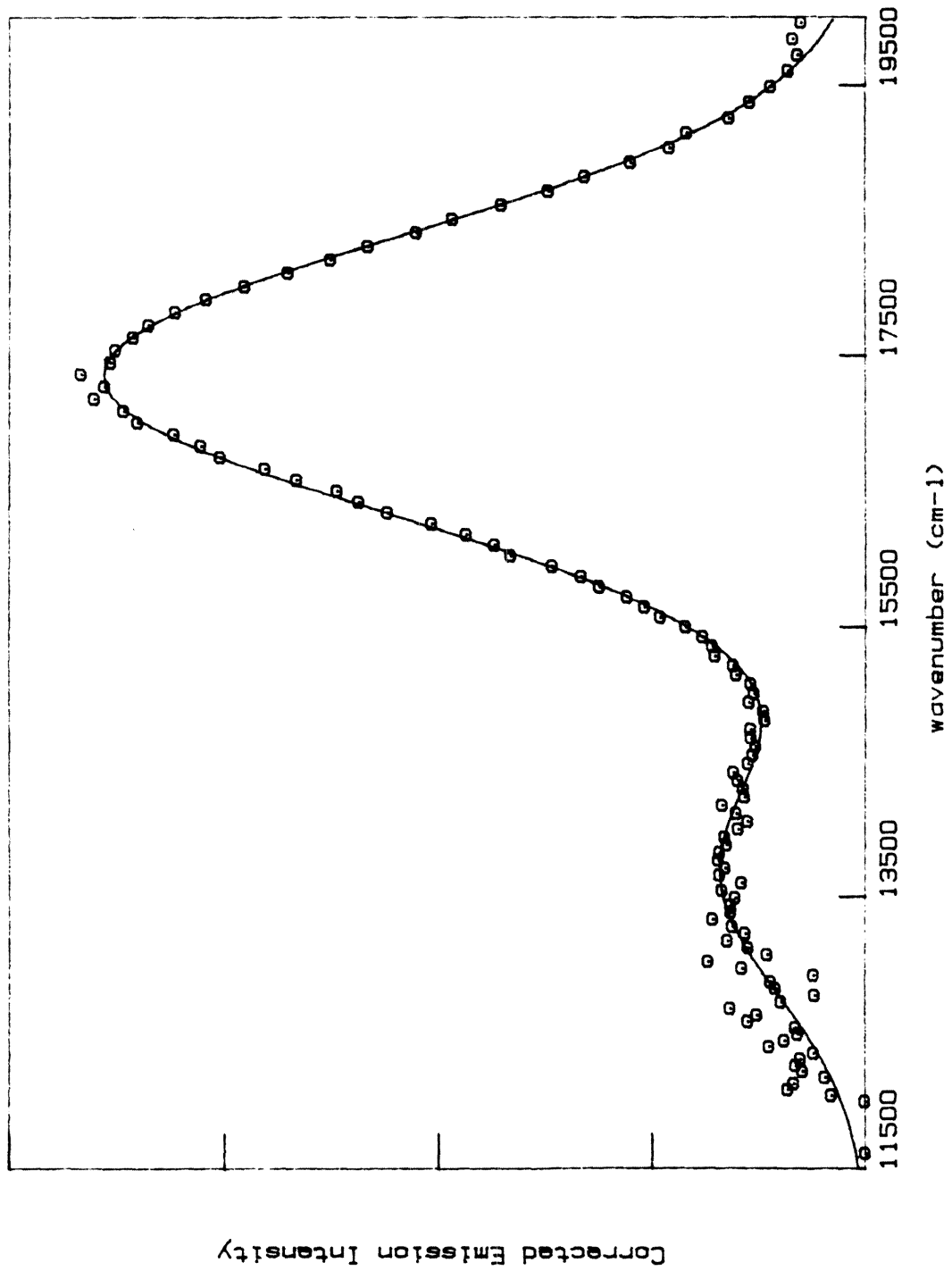


Figure 4.6. Emission spectrum of $[\text{Ir}(\mu\text{-pz}^*)(\text{CO})(\text{Ph}_2\text{P-O-C}_6\text{H}_4\text{-(CH}_2)_3\text{-py}^+)]_2$ showing $\text{S}_1 \rightarrow \text{S}_0$ and $\text{T}_1 \rightarrow \text{S}_0$ transition, at decreased intensity compared to the model complexes. The emission intensity scale is 8 times that of the spectrum in Figure 4.4.



Electrochemistry:

Electrochemical studies were conducted on the series of phenol-pyridinium complexes, $\text{HO-C}_6\text{H}_4\text{-(CH}_2)_n\text{-py}^+\text{-R}$, and $\text{Ir}_2\text{-py}^+$ donor-acceptor complexes. The one-electron reduction of the pyridinium cation in the former complexes was irreversible on the time scale of the cyclic voltammetry experiment (up to 20 V/s scan rate), with the exception of $\text{HO-C}_6\text{H}_4\text{-CH}_2\text{-py}^+\text{-Am}$ ($\text{Am} = 4\text{-C(O)NH}_2$) which showed a reversible ($\text{py}^+/\text{py}^\bullet$) couple. The cathodic peak potentials, E_{pc} , (and half-wave potential for $\text{HO-C}_6\text{H}_4\text{-CH}_2\text{-py}^+\text{-Am}$) are summarized in Table 4.6.

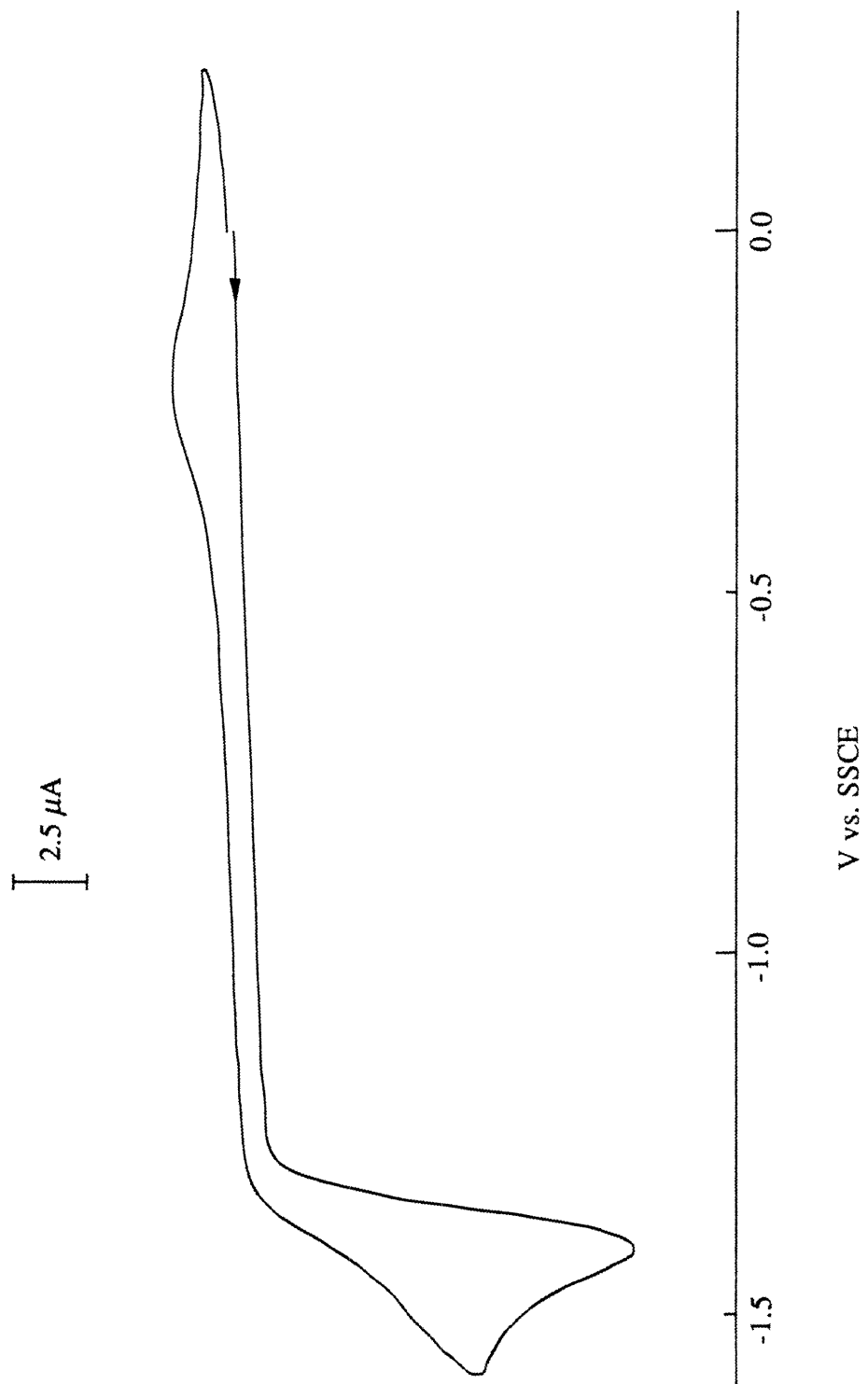
Table 4.6. Cathodic Peak Potentials of $\text{py}^+ + e^- \rightarrow \text{py}^\bullet$ Reaction in Phenol-Pyridinium Complexes

Compounds	E_{pc}
$\text{HO-C}_6\text{H}_4\text{-py}^+$	-1.19
$\text{HO-C}_6\text{H}_4\text{-CH}_2\text{-py}^+$	-1.33
$\text{HO-C}_6\text{H}_4\text{-CH}_2\text{-py}^+\text{-tB}$	-1.56
$\text{HO-C}_6\text{H}_4\text{-CH}_2\text{-py}^+\text{-Am}^a$	-0.93
$\text{HO-C}_6\text{H}_4\text{-(CH}_2)_2\text{-py}^+$	-1.42
$\text{HO-C}_6\text{H}_4\text{-3-(CH}_2)_2\text{-py}^+$	-1.40
$\text{HO-C}_6\text{H}_4\text{-(CH}_2)_3\text{-py}^+$	-1.40

^a This couple was reversible, $E_{1/2}$ is given.

Figure 4.7 shows a cyclic voltammogram (CV) of $\text{HO-C}_6\text{H}_4\text{-(CH}_2)_2\text{-py}^+$, which is representative of the irreversible ($\text{py}^+/\text{py}^\bullet$) couples for the phenol-pyridinium complexes. The wave at -1.4 V vs. SSCE corresponds to the one-electron reduction of py^+ . The wave at ~ -0.2 V has not been definitively assigned, but is only observed after initial negative scans through the reduction wave, indicating the oxidation of a species formed as a consequence of reducing the pyridinium cation to its radical (see below).

Figure 4.7. Cyclic voltammogram of HO-C₆H₄-(CH₂)₂-py⁺, in 0.1 M TBAH CH₃CN solution, showing the irreversible wave at -1.4 V vs. SSCE corresponding to reduction of the pyridinium cation. Scan rate was 200 mV/s.



The irreversible behavior of the pyridinium reduction is due to the rapid dimerization of the pyridinium radical to form bipyridine complexes,¹⁵ represented by the eqs 4.1 and 4.2.



The process in which an electrochemical reduction is followed by a second-order chemical reaction (EC₂ mechanism) has been treated theoretically.^(14,p. 451-461.) The equations that relate the cathodic peak potentials (E_{pc}) to their corresponding half-wave potentials ($E_{1/2}$) are given below:

$$E_{1/2} = E_{pc} + \frac{RT}{nF} 0.902 - \frac{RT}{3nF} \ln(2k_f C_o RT/3nFv) \quad (4.3)$$

$$E_{1/2} = E_{pc} + 0.058 - 0.008563 \ln(k_f C_o/v), \quad (4.4)$$

where k_f is the rate of the following second-order chemical reaction, C_o is the concentration, and v is the CV scan rate. These equations, however, break down at large k_f (more specifically, when $|E_{1/2} - E_p| \geq \sim 60$ mV). Since the rates of dimerization are nearly diffusion limited ($\sim 10^8 \text{ M}^{-1} \text{ s}^{-1}$), eq 4.4 cannot be applied to the present electrochemical experiments. The experimental values for E_{pc} were, therefore, not converted to $E_{1/2}$ values as has previously been done.¹⁰ The errors associated with using E_{pc} values in calculating driving forces will be discussed in the next section of this chapter.

The complex HO-C₆H₄-CH₂-py⁺-Am exhibited reversible electrochemical behavior which has been attributed to the stability of the radical py^{*}-Am in acetonitrile solution. The electron-withdrawing 4-amide group is the origin of this stability (4-cyanopyridiniums also exhibit reversible reduction waves). The CV of HO-C₆H₄-CH₂-py⁺-Am, showing the

reversible pyridinium reduction, is given in Figure 4.8.

The CVs of the $\text{Ir}_2\text{-py}^+$ donor-acceptor complexes exhibit the same irreversible waves between -1.6 and -0.9 V vs. SSCE, corresponding to the familiar one-electron reduction of the pyridinium cation. The E_{pc} values for the iridium complexes were the same as those given in Table 4.6, within experimental error, indicating that there is virtually no effect of the phosphine or iridium dimer on the isolated electrochemical reactions of the pyridinium cation. The one-electron oxidation of the $d^8\text{-}d^8$ dimers to form their corresponding $d^8\text{-}d^7$ species was observed in methylene chloride solution as a reversible wave at $E_{1/2} = 0.31$ V vs. SSCE. An irreversible wave at ~ -0.7 V was also observed (as of yet unassigned). The wave was, however, only observed when the initial scan direction was positive (forming Ir_2^+ species) and was not observed when the initial potential sweep was negative. CVs of the model complex, $[\text{Ir}_2]\text{-CH}_3$, where the initial scans were positive (Figure 4.9a) or negative (Figure 4.9b) demonstrate the behavior of this irreversible cathodic wave.

In acetonitrile solution, however, the $(\text{Ir}_2/\text{Ir}_2^+)$ couple is not reversible, presumably due to coordination of acetonitrile solvent molecule(s) to the oxidized iridium species. In Figure 4.10 a typical CV of the donor-acceptor complex, $[\text{Ir}_2]\text{-CH}_2\text{-py}^+$, in acetonitrile is shown. This CV is simply a combination of the oxidation wave corresponding to the $(\text{Ir}_2/\text{Ir}_2^+)$ couple (seen in the CV of $[\text{Ir}_2]\text{-CH}_3$ in Figure 4.9) and the reduction wave corresponding to the $(\text{py}^+/\text{py}^\bullet)$ couple (seen in the CV of the phenol-pyridinium complexes, $\text{HO-C}_6\text{H}_4\text{-(CH}_2)_n\text{-py}^+\text{-R}$ in Figures 4.7 and 4.8).

These electrochemical data, in combination with spectroscopic data, are now used to calculate driving forces for all three electron-transfer reactions in the series of donor-acceptor complexes: (1) singlet excited-state electron transfer, $^1\text{ET} = {}^1\text{Ir}_2^*\text{-py}^+ \rightarrow \text{Ir}_2^+\text{-py}^\bullet$; (2) triplet excited-state electron transfer, $^3\text{ET} = {}^3\text{Ir}_2^*\text{-py}^+ \rightarrow \text{Ir}_2^+\text{-py}^\bullet$; (3) and thermal back electron transfer, $\text{ET}^b = \text{Ir}_2^+\text{-py}^\bullet \rightarrow \text{Ir}_2\text{-py}^+$.

The approximate energetics of the charge-transfer complexes, $\text{Ir}_2^+\text{-py}^\bullet$, were obtained by summing the half-wave potential for one-electron oxidation of the iridium dimer and the

Figure 4.8. Cyclic voltammogram of HO-C₆H₄-CH₂-py⁺-Am, in 0.1 M TBAH CH₃CN solution, showing the reversible wave at -0.9 V vs. SSCE corresponding to reduction of the pyridinium cation. Scan rate was 200 mV/s.

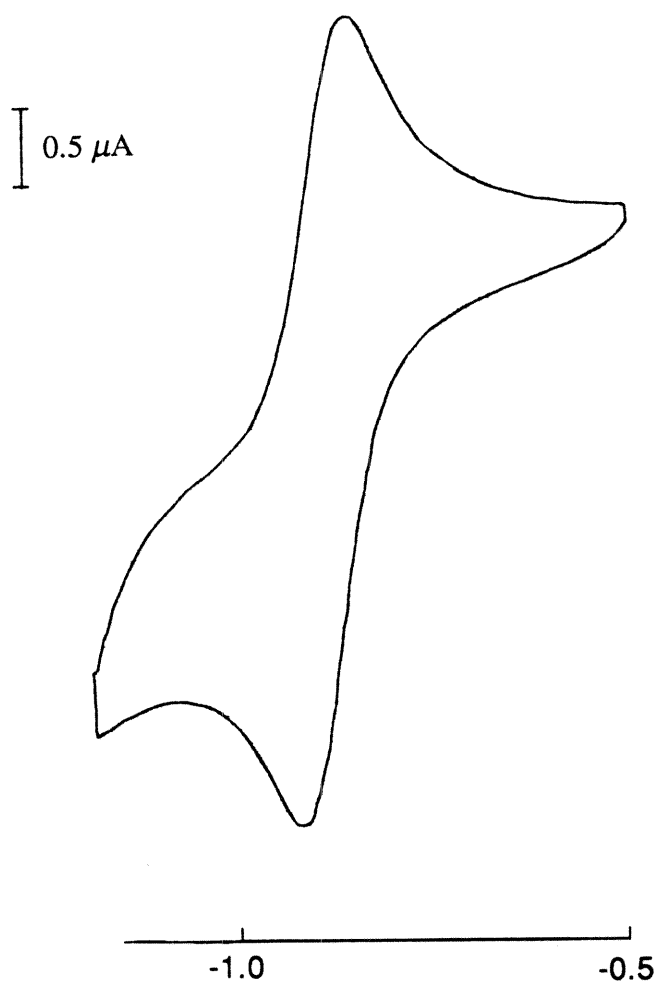


Figure 4.9. (a) Cyclic voltammogram of model complex, $[\text{Ir}(\mu\text{-pz}^*)(\text{CO})(\text{Ph}_2\text{P-O-C}_6\text{H}_4\text{-CH}_3)]_2$, in 0.1 M TBAH CH_2Cl_2 solution, showing the reversible wave at 0.3 V vs. SSCE corresponding to the $(\text{Ir}_2/\text{Ir}_2^+)$ redox couple. The initial scan direction was anodic, and the scan rate was 500 mV/s. (b) Same as Figure a, except initial scan direction was cathodic.

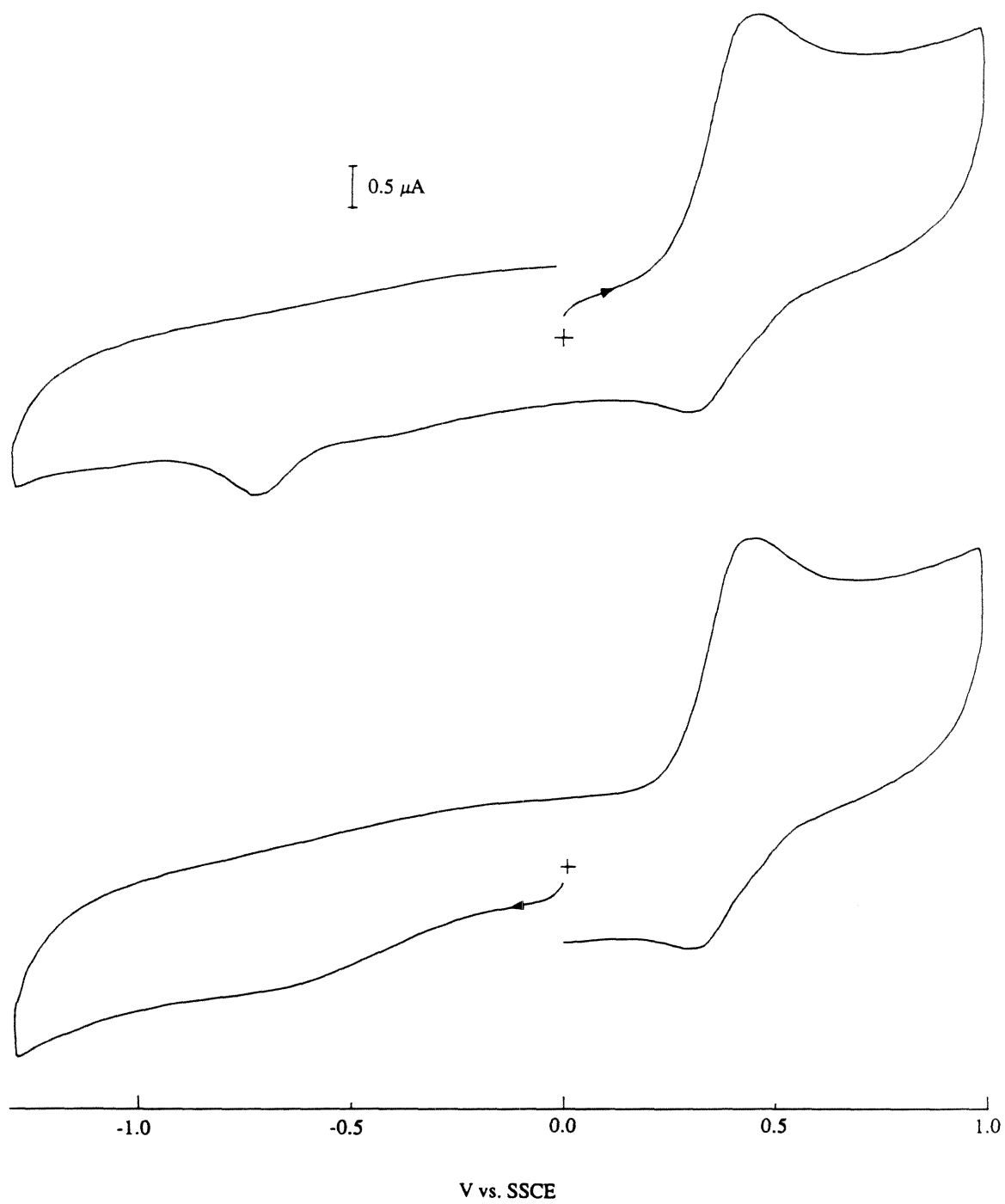
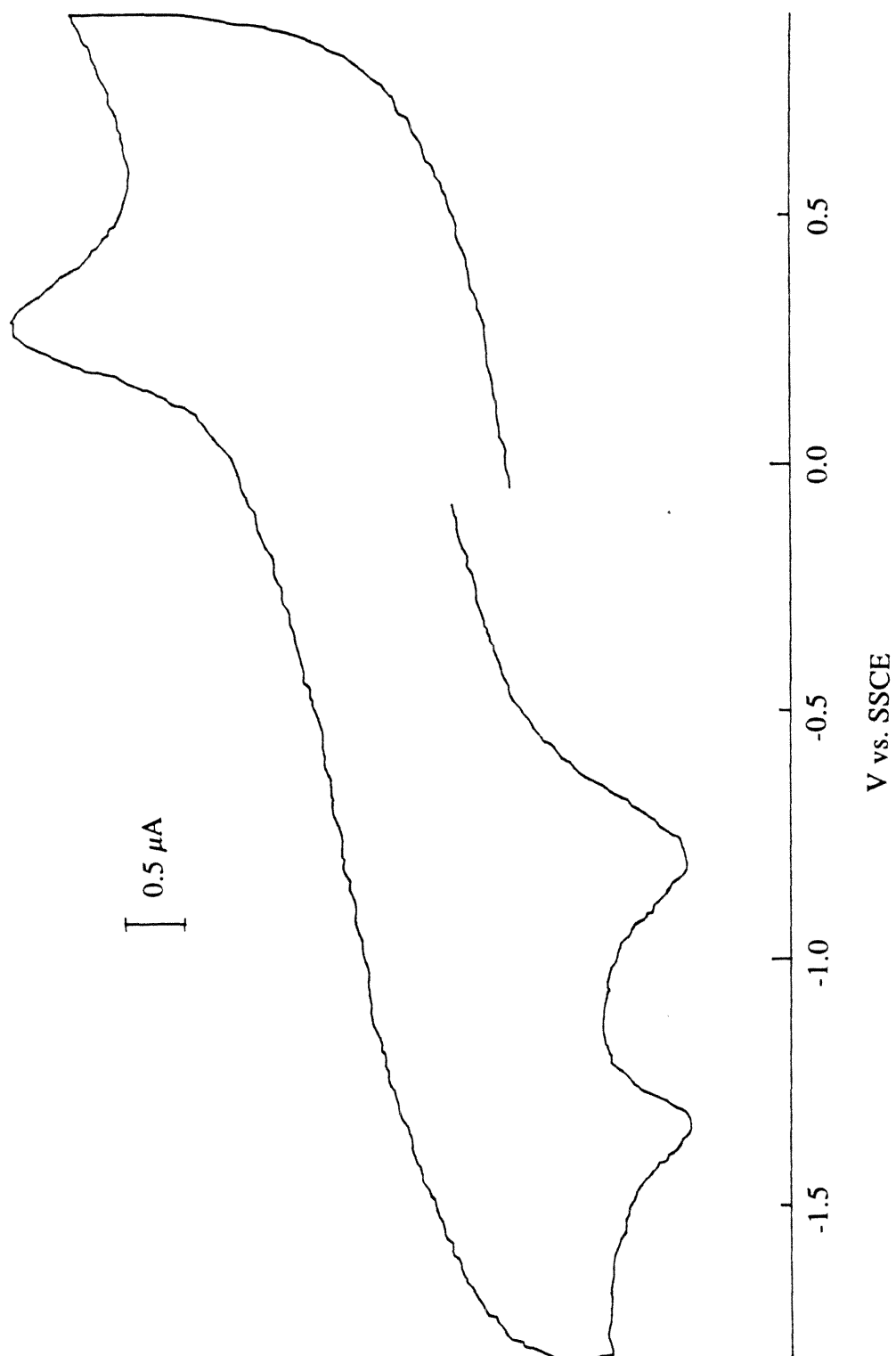


Figure 4.10. Cyclic voltammogram of donor-acceptor complex, $[\text{Ir}(\mu\text{-pz}^*)(\text{CO})(\text{Ph}_2\text{P-O-C}_6\text{H}_4\text{-CH}_2\text{-py}^+)]_2$, in 0.1 M TBAH CH_3CN solution, showing irreversible one-electron oxidation of Ir_2 at 0.3 V vs. SSCE and one-electron reduction of py^+ at -1.3 V. Scan rate was 20 V/s.



peak potentials of the one-electron reductions of the pyridinium acceptor. Thus, the driving forces for ET^b in the donor-acceptor complexes can be given by eq 4.5.¹⁶ The driving forces for the two excited state electron-transfer reactions (¹ET, ³ET) are logically expressed by eqs 4.6 and 4.7.

$$-\Delta G^\circ(\text{ET}^b) = E_{1/2}(\text{Ir}_2/\text{Ir}_2^+) - E_{1/2}(\text{py}^+/\text{py}^\bullet) \quad (4.5)$$

$$-\Delta G^\circ(^1\text{ET}) = E_{00}(\text{S}_1) + \Delta G^\circ(\text{ET}^b) \quad (4.6)$$

$$-\Delta G^\circ(^3\text{ET}) = E_{00}(\text{T}_1) + E_{1/2}(\text{py}^+/\text{py}^\bullet) - E_{1/2}(\text{Ir}_2/\text{Ir}_2^+) \quad (4.7)$$

The results of these calculations are given in Table 4.7, and in Figure 4.11 in the form of a state diagram. In the next chapter, the driving forces presented here will be employed in calculations aimed at elucidating electronic-couplings for the electron-transfer reactions described above.

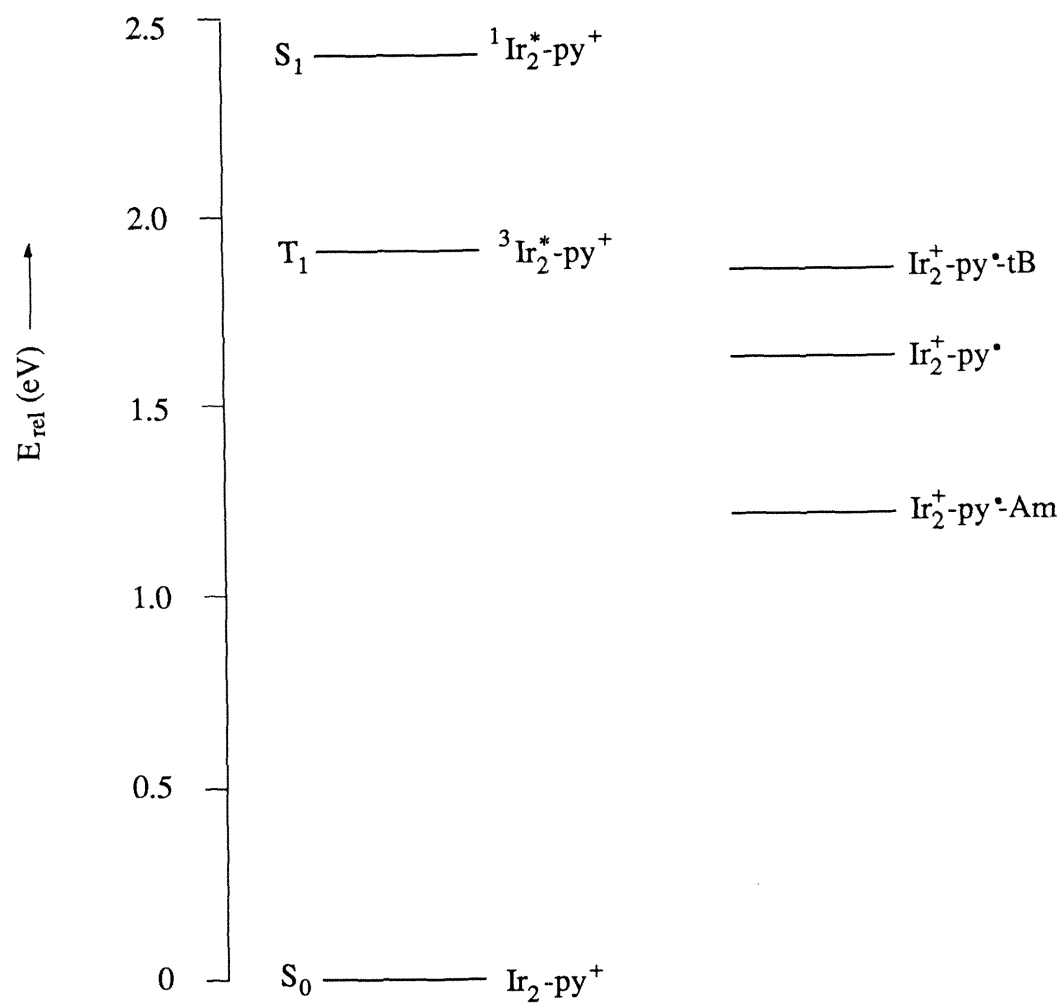
Table 4.7. Driving Forces for ¹ET, ³ET, and ET^b Reactions^a

compounds	$-\Delta G^\circ (^1\text{ET})^b$	$-\Delta G^\circ (^3\text{ET})^b$	$-\Delta G^\circ (\text{ET}^b)^b$
[Ir ₂]-py ⁺	0.90	0.40	1.50
[Ir ₂]-CH ₂ -py ⁺	0.76	0.26	1.64
[Ir ₂]-CH ₂ -py ⁺ -tB	0.53	0.03	1.87
[Ir ₂]-CH ₂ -py ⁺ -Am	1.16	0.66	1.24
[Ir ₂]-CH ₂) ₂ -py ⁺	0.67	0.17	1.73
[Ir ₂]-3-(CH ₂) ₂ -py ⁺	0.69	0.19	1.71
[Ir ₂]-CH ₂) ₃ -py ⁺	0.69	0.19	1.71

^a E₀₀(S₁) = 2.40 ± 0.05 eV, E₀₀(T₁) = 1.90 ± 0.03 eV.

^b Driving forces are associated with an error of 0.1 eV.

Figure 4.11. State diagram for donor-acceptor system, constructed from the spectroscopic and electrochemical data found in Tables 4.1, 4.2, 4.3 and 4.6.



REFERENCES

1. Caspar, J. V.; Gray, H. B. *J. Am. Chem. Soc.* **1984**, *106*, 3029-3030.
2. Vlcek, A.; Gray, H. B. *J. Am. Chem. Soc.* **1987**, *109*, 286-287.
3. Harvey, E. L.; Stiegman, A. E.; Vlcek, A.; Gray, H. B. *J. Am. Chem. Soc.* **1987**, *109*, 5233-523.
4. Marshall, J. L.; Stobart, S. R.; Gray, H. B. *J. Am. Chem. Soc.* **1984**, *106*, 3027-3029.
5. Marshall, J. L.; Stiegman, A. E.; Gray, H. B. *ACS Symposium Series 307*, **1986**, 166-176.
6. Fox, L. S.; Kozik, M.; Winkler, J. R.; Gray, H. B. *Science* **1990**, *247*, 1069-1071.
7. Fox, L. S.; Marshall, J. L.; Gray, H. B.; Winkler, J. R. *J. Am. Chem. Soc.* **1987**, *109*, 6901-6902.
8. Marshall, J. L., Ph.D. Dissertation, California Institute of Technology, Pasadena, CA, 1987.
9. Smith, D. C., Ph.D. Dissertation, California Institute of Technology, Pasadena, CA, 1989.
10. Fox, L. S., Ph.D. Dissertation, California Institute of Technology, Pasadena, CA, 1989.
11. Rice, S. F.; Gray, H. B. *J. Am. Chem. Soc.* **1983**, *105*, 4571-4575.
12. Demas, J. N.; Crosby, G. A. *J. Phys. Chem.* **1971**, *75*, 991-1024.
13. Van Houten, J.; Watts, R. *J. Am. Chem. Soc.* **1976**, *98*, 4853-4858.
14. Bard, A. J.; Faulkner, L. R. *Electrochemical Methods, Fundamentals and Applications*; John Wiley & Sons: New York, 1980.
15. Akiyama, K.; Tero-Kubota, S.; Ikegami, Y.; Ikenone, T. *J. Phys. Chem.* **1985**, *89*, 339-342.
16. The error associated with the calculated driving forces is $\pm 100\text{mV}$ due to the irreversible $\text{py}^+/\text{py}^\bullet$ couple.

Chapter 5

Time-Resolved Experiments

INTRODUCTION

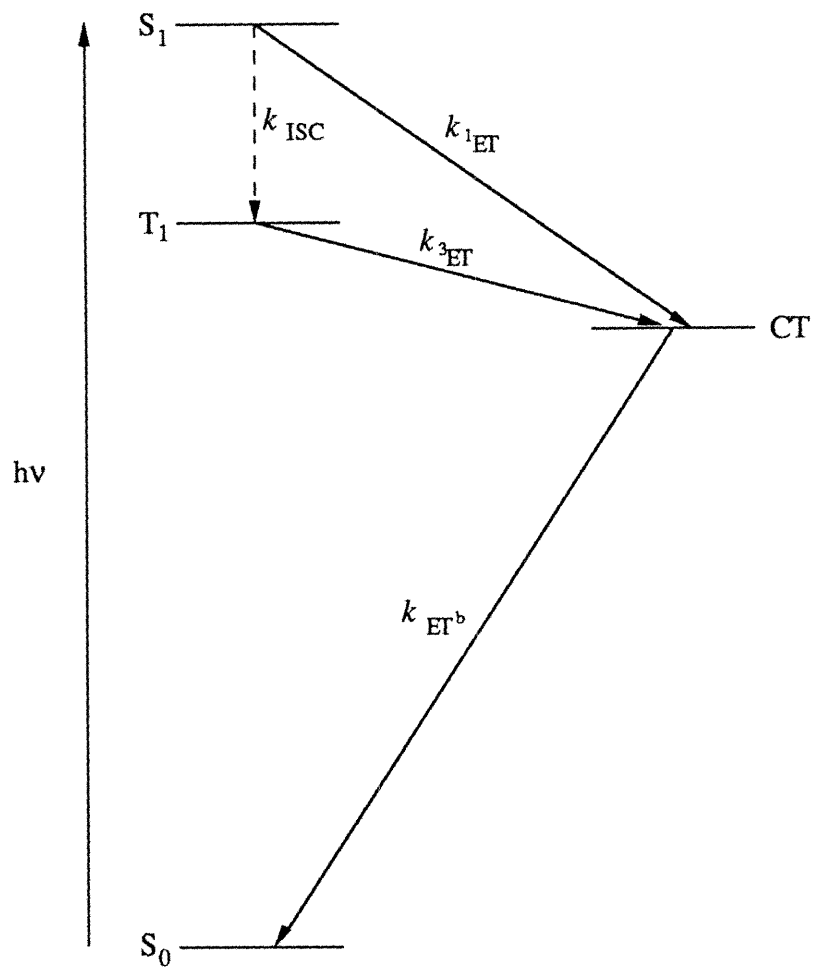
The steady-state spectroscopic results presented in Chapter 4 demonstrated that emission quenching in the series of $\text{Ir}_2\text{-py}^+$ donor-spacer-acceptor complexes was a direct consequence of electron transfer from both the singlet and triplet excited states of the $d^8\text{-d}^8$ iridium donor. It was also established that the extent of quenching depended dramatically on the number of methylene groups in the bridge separating the donor and pyridinium acceptor. In this chapter, excited-state and thermal back electron-transfer rates were measured for the series of complexes by employing time-resolved experiments. Figure 5.1 summarizes the three distinct reactions under investigation: (1) singlet excited-state electron transfer, $^1\text{Ir}_2^* \rightarrow \text{py}^+$ (^1ET); (2) triplet excited-state electron transfer, $^3\text{Ir}_2^* \rightarrow \text{py}^+$ (^3ET); and (3) thermal back electron transfer from $\text{py}^* \rightarrow \text{Ir}_2^+$ (ET^b). An expression that correlates the electron-transfer rates to the number of methylene groups in the bridge is presented in this chapter. The issue of through-space versus through-bond mechanisms of electron transfer is also discussed. The evidence presented in this chapter suggests for the first time that electron transfer in linked donor-acceptor complexes can occur via different mechanisms, depending on the initial spin state of the donor.

EXPERIMENTAL

General Procedures:

Samples of the iridium donor-acceptor complexes were prepared in acetonitrile solution and placed in sealed quartz cells. For picosecond experiments, the samples were flowed at rates rapid enough to ensure that a fresh portion of sample was irradiated with each laser shot. Acetonitrile was dried over activated 3 Å Linde sieves for a minimum of 3 days, and freeze-pumped-thawed 4 times before being vacuum distilled into the quartz cells holding the samples.

Figure 5.1. A state diagram, showing approximate energy levels of the metal localized and charge-transfer excited states, and summarizing photoinduced (^1ET , ^3ET) and thermal back (ET^{b}) electron-transfer reactions.



Picosecond Experiments:

Transient absorption and emission experiments on the picosecond time-scale were conducted using the same laser source.

Laser source: Figure 5.2 shows the layout of the optical table which was common to both transient absorption and emission experiments. A train of 25 ps (FWHM) pulses was generated in an active/passive mode-locked Nd:YAG laser cavity. A saturable absorber was positioned near the back mirror (passive) and an acousto-optic mode-lock was placed near the front mirror (active). A Pockel cell pulse extractor was used to select one peak from the train of picosecond pulses. The beam was then amplified at Amp1, passed through apertures and amplified a second time at Amp2. The beam was then split into two beams: 20% was sent through a third amplifier, Amp3, and the remaining 80% was directed to a second optical table with no further amplification. In both experiments the former beam became the excitation source, and the latter beam became either the trigger pulse in the emission experiment or the probe and reference beams in the transient absorption experiment.

Transient Absorption Experiment: This experiment was conducted by using the pump-probe method for detecting changes in absorption after laser excitation.^{1,2} The schematic in Figure 5.3 shows the setup used in this experiment. The excitation beam was generated by frequency doubling the beam from Amp2 and sending it directly to the sample. The probe beam was generated in the following manner: the beam from Amp3 was frequency doubled and tripled, filtered with a 350 nm sharp cut-off filter, passed through a prism and directed to a double-pass movable track. The beam was then passed through a 10 cm cell containing an 80:20 mixture of D₂O/H₂O which generated continuum light. The beam was then passed through a 1:1 beam splitter. One of the beams, which was used as the probe beam, was sent directly to the sample and the other was allowed to bypass the sample and was used as a reference beam. The probe beam, which was delayed

Figure 5.2. Schematic diagram of Nd:YAG laser source used to generate 25 ps (FWHM) laser pulses.

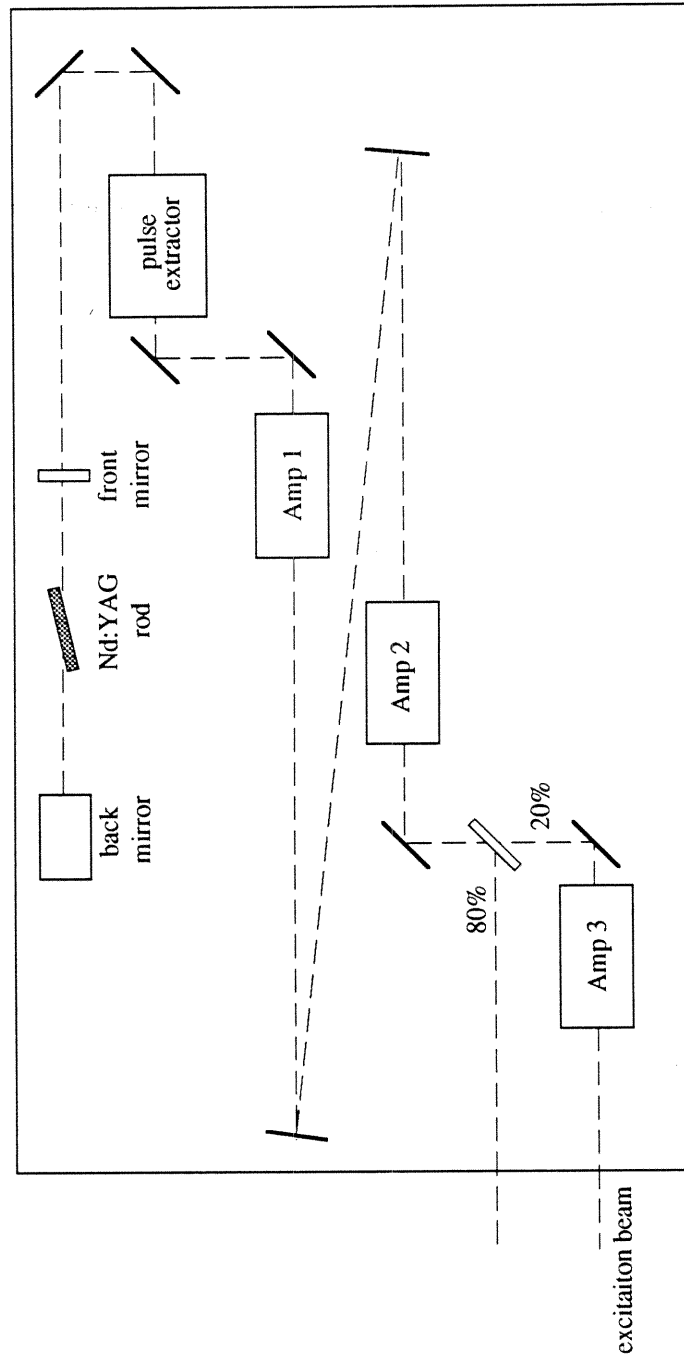
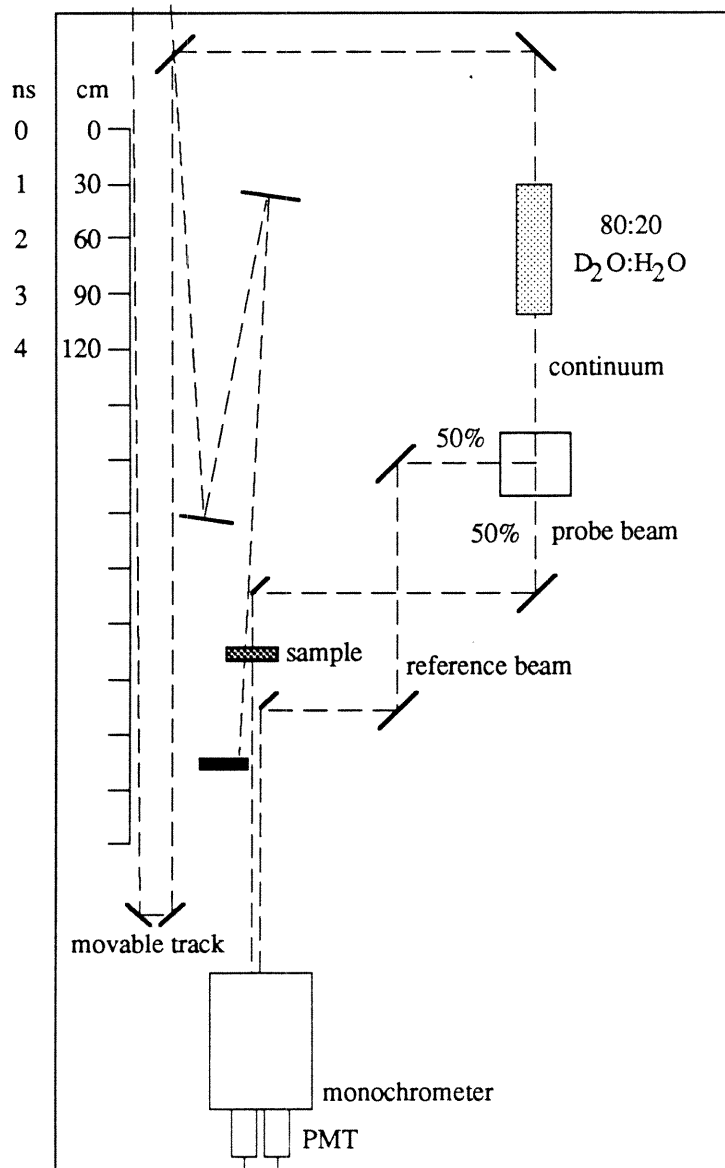
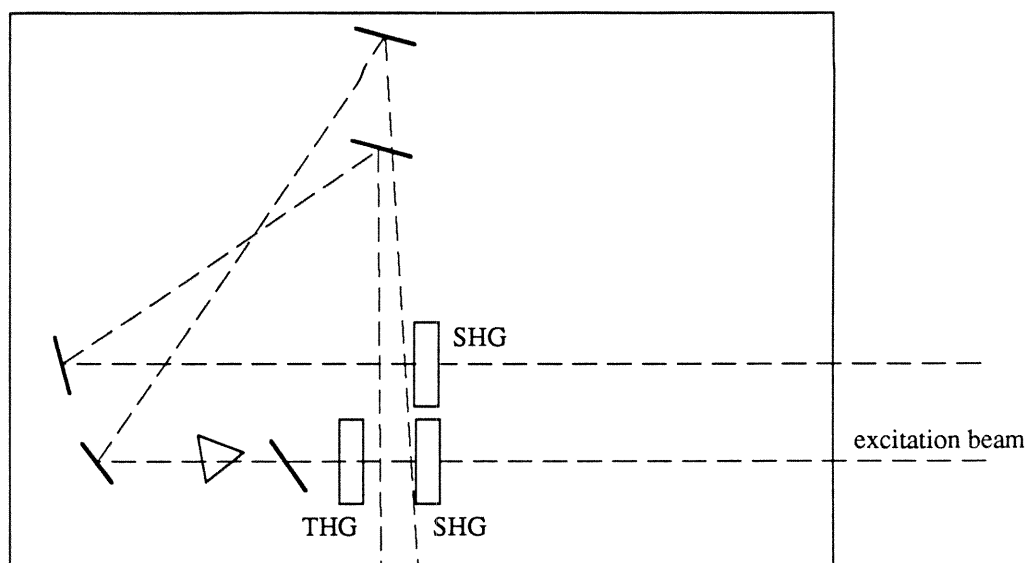


Figure 5.3. Layout of transient absorption experiment showing excitation, probe, and reference beams.



relative to the excitation beam by adjusting the position of the double-pass movable track, was passed through one of two slits of a monochrometer. The reference beam was passed through the other slit and both beams were detected using one photomultiplier tube for each. 200 laser shots were used for each delay time and wavelength. 100 ratios of the probe and reference beams were measured without sample excitation and another 100 ratios were measured with sample excitation. The log of the ratio of these ratios is equal to Δ Absorbance. Data were transferred to a PDP 11/23 computer and analyzed using software developed at Brookhaven National Laboratories.

Emission Experiment: In this experiment, the beam from Amp3 was frequency doubled and tripled, then sent through an IR filter where about 20% of the beam was reflected and used as a timing pulse. The remaining 80% was focused into a 10 cm cell containing methanol which generated raman shifted Stokes and anti-Stokes emission at ~ 630 and ~ 460 nm. The anti-Stokes emission was separated from the Stokes and fundamental emission by passing the beam through a prism. The trigger pulse was generated from filtered leakage of intensity from Amp2. The trigger pulse, timing pulse and picosecond excitation pulse at 460 nm were directed to a third optical table. The excitation beam was made to pass through a 460 nm narrow-band-pass filter, focused, and vertically polarized before exciting the sample. Emission from the sample was directed into a spectrometer at magic angle polarization (57.74°), eliminating artifacts arising from solute rotation. The signal (spectrally confined to 250 nm) was then focused into the $400\ \mu\text{m}$ slit of a Hamamatsu Temporal Disperser C1587. The data was transmitted from a High Speed Streak Unit M1952 to a monitor via a high resolution video camera. Data were transferred to a PDP11/23 computer and analyzed using software developed at BNL.

Nanosecond Experiment:

A laser system built at Caltech that has been previously described,³ was used for determining phosphorescence lifetimes. The excitation source was a Quanta Ray DCR-1

Q-switched Nd:YAG laser, which was frequency doubled and tripled with a Quanta Ray HG-1 harmonic generator (KDP). Doubled (532 nm) and tripled (~355 nm) 8 ns (FWHM) laser pulses were separated from the YAG fundamental (1064 nm) using a Quanta Ray PHS-1 prism harmonic separator. Light emitted from the sample was collimated at 90° from the excitation beam, and focused through a Corning 3483 sharp cut-off filter onto the entrance slit of a MacPherson monochrometer. Luminescence was detected using a Hamamatsu R955 photomultiplier tube, and the signal was amplified with a LeCroy VV101ATM amplifier. Signals were digitized with a Biomation 6500 waveform recorder and transferred to a Digital PDP11/103-L computer. The data were analyzed on a Compaq 386 PC using OLIS software.

RESULTS

Figure 5.4 shows transient difference spectra immediately following (0-20 ps) and 90 ps after 355 nm laser irradiation for the $n = 2$ donor-acceptor complex, $[\text{Ir}(\mu\text{-pz}^*)(\text{CO})(\text{Ph}_2\text{P-O-C}_6\text{H}_4\text{-(CH}_2\text{)}_2\text{-py}^+)]_2$ ($[\text{Ir}_2]\text{-(CH}_2\text{)}_2\text{-py}^+$). Two main features are apparent in the spectra: a bleach centered around 460 nm which corresponds to the position of the ground-state $\text{S}_0 \rightarrow \text{S}_1$ absorption, and a broad positive absorption feature at around 400 nm which was logically assigned to absorption by the singlet and triplet ($\text{d}\sigma^*\text{p}\sigma$) excited states.⁴ The kinetics of these features obtained by detection at 460 nm and 405 nm are given in Figures 5.5 and 5.6. Both show biexponential behavior with lifetimes of 120 ± 20 ps and 2.4 ± 0.2 ns for the positive absorption region, and 190 ± 30 ps and 2.5 ± 0.2 ns for the bleach region. Independent time-resolved emission measurements conducted on $[\text{Ir}_2]\text{-(CH}_2\text{)}_2\text{-py}^+$ (presented in the next section) revealed triplet and singlet lifetimes of 1.7 ns and 36 ps, respectively. The transient species in the absorption experiments are, therefore, assigned to the triplet excited state ($\tau = \sim 2$ ns) and a species ($\tau = \sim 150$ ps) which

Figure 5.4. Transient difference spectra of $[\text{Ir}(\text{pz}^*)(\text{CO})(\text{Ph}_2\text{P}-\text{O}-\text{C}_6\text{H}_4-(\text{CH}_2)_2-\text{py}^+)]_2$ at 0 ps (\circ) and 90 ps (\bullet) after laser excitation. The spectra show the decay of the bleach and absorption regions.

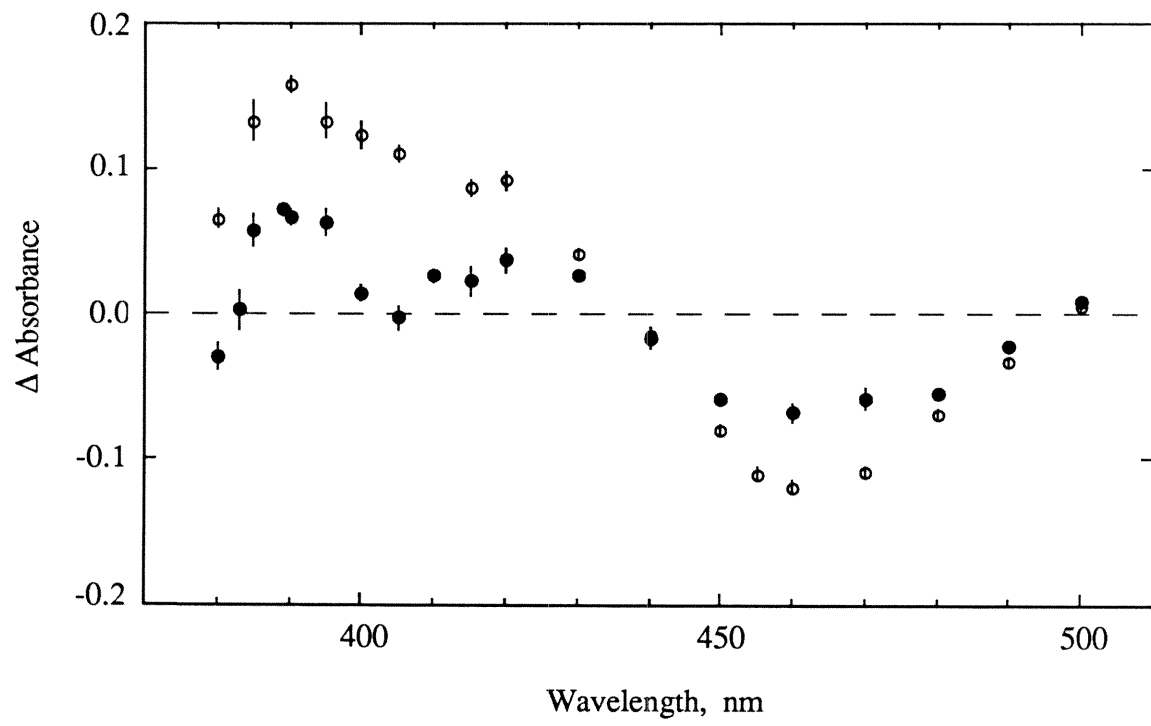


Figure 5.5. Kinetics of bleach obtained by excitation at 355 nm and detection at 460 nm of $[\text{Ir}(\text{pz}^*)(\text{CO})(\text{Ph}_2\text{P}-\text{O}-\text{C}_6\text{H}_4-(\text{CH}_2)_2\text{-py}^+)]_2$ donor-acceptor complex. Biexponential fit to the data yielded $\tau_1 = 2.5$ ns and $\tau_2 = 190$ ps.

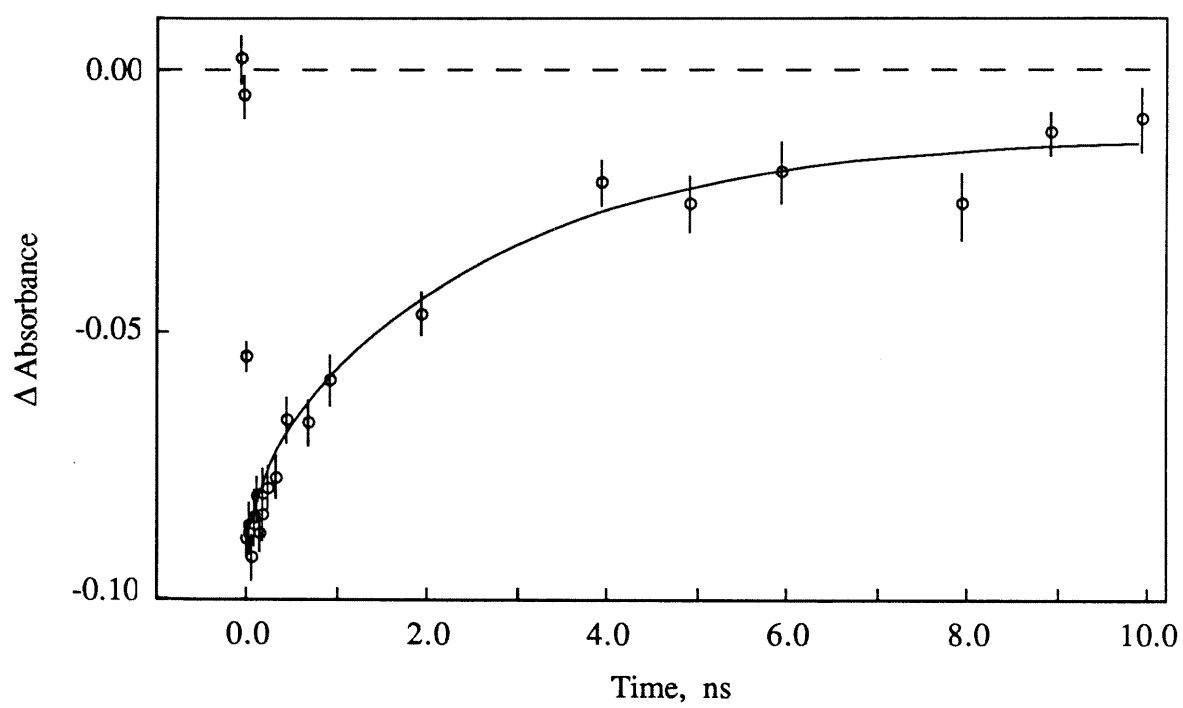
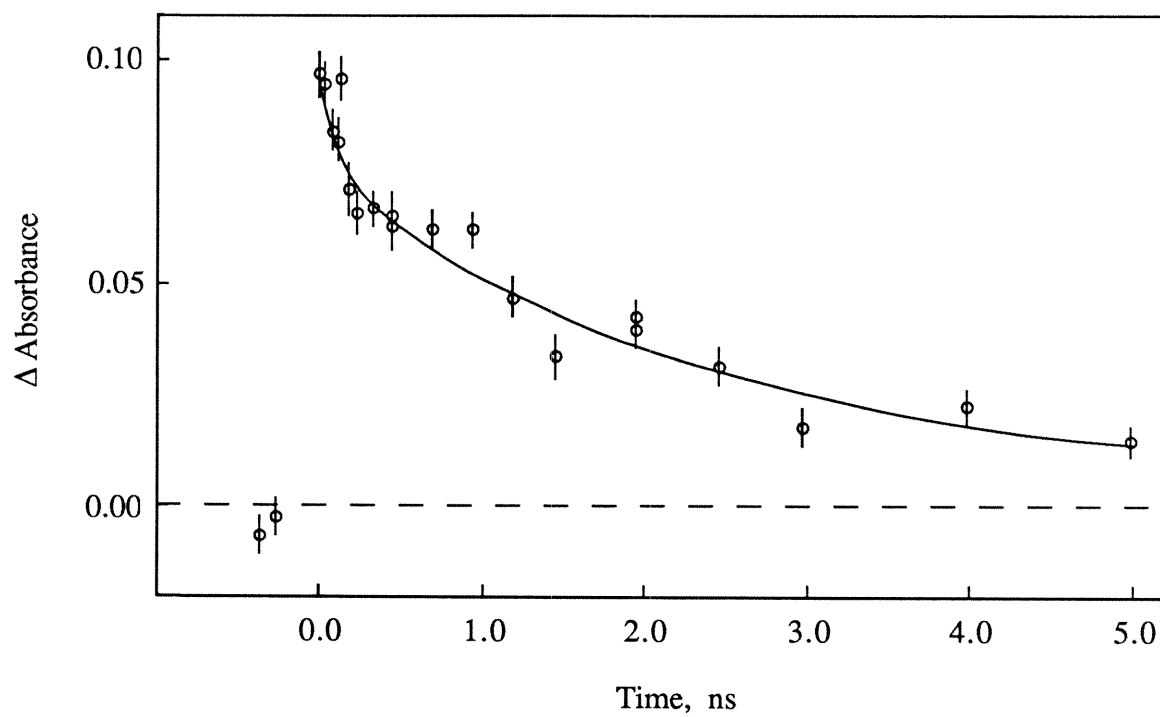


Figure 5.6. Kinetics of absorption feature obtained by excitation at 355 nm and detection at 405 nm of $[\text{Ir}(\text{pz}^*)(\text{CO})(\text{Ph}_2\text{P}-\text{O}-\text{C}_6\text{H}_4-(\text{CH}_2)_2\text{-py}^+)]_2$ donor-acceptor complex. Biexponential fit to the data yielded $\tau_1 = 2.4$ ns and $\tau_2 = 120$ ps.



does *not* correspond to the singlet or triplet excited state. This species has been identified, by analogy to transient absorption experiments conducted on similar donor-acceptor complexes,⁴ as the charge-transfer complex. Similar results were obtained for the $n = 1$ complex, $[\text{Ir}_2]\text{-CH}_2\text{-py}^+$, which revealed a charge transfer state lifetime, τ_{CT} , of about an order of magnitude longer than was found for $[\text{Ir}_2]\text{-(CH}_2)_2\text{-py}^+$. These results are summarized in Table 5.1.

Time-resolved emission experiments, conducted on the series of donor-acceptor complexes, $[\text{Ir}(\mu\text{-pz}^*)(\text{CO})(\text{Ph}_2\text{P-O-C}_6\text{H}_4\text{-(CH}_2)_n\text{-py}^+\text{-R})]_2$, and on two model complexes, $[\text{Ir}(\mu\text{-pz}^*)(\text{CO})(\text{Ph}_2\text{P-O-C}_6\text{H}_4\text{-Y})]_2$ (Y was either CH_3 or $\text{CH}_2\text{-Quin}^+$, both of which are extremely poor electron acceptors), were employed to measure singlet and triplet excited-state lifetimes. Either of two emission experiments was used depending on the lifetime of the complexes. A Streak Camera experiment was utilized in obtaining the

Table 5.1. Fluorescence, Phosphorescence, and Charge-Transfer State Lifetimes of Model and Donor-Acceptor Complexes

Compounds	τ_f (ps)	τ_p (ns)	τ_{CT} (ns)
$[\text{Ir}_2]\text{-CH}_3$	— ^a	640 ± 50 ^{d,e}	— ^a
$[\text{Ir}_2]\text{-CH}_2\text{-Quin}^+$	124 ± 7 ^c	1000 ± 100 ^e	— ^a
$[\text{Ir}_2]\text{-py}^+$	— ^b	360 ± 40 ^d	— ^a
$[\text{Ir}_2]\text{-CH}_2\text{-py}^+$	— ^a	660 ± 50 ^d	1.8 ± 0.2 ^f
$[\text{Ir}_2]\text{-CH}_2\text{-py}^+\text{-tB}$	93 ± 6 ^c	740 ± 110 ^e	— ^a
$[\text{Ir}_2]\text{-CH}_2\text{-py}^+\text{-Am}$	— ^a	680 ± 50 ^d	— ^a
$[\text{Ir}_2]\text{-(CH}_2)_2\text{-py}^+$	36 ± 3 ^c	1.7 ± 0.1 ^c	0.15 ± 0.02 ^f
$[\text{Ir}_2]\text{-3-(CH}_2)_2\text{-py}^+$	19 ± 1 ^c	1.8 ± 0.2 ^c	— ^a
$[\text{Ir}_2]\text{-(CH}_2)_3\text{-py}^+$	74 ± 6 ^c	20 ± 2 ^e	— ^a

^a These lifetimes were not measured.

^b The lifetime of this complex was too short to measure.

^c Obtained from Streak Camera experiment.

^d Obtained from nanosecond emission experiment, Caltech.

^e Obtained from picosecond emission experiment, Brookhaven National Laboratories.

^f Obtained from picosecond transient absorption experiment, Brookhaven National Laboratories.

singlet lifetimes of $[\text{Ir}_2]-(\text{CH}_2)_2\text{-Quin}^+$, $[\text{Ir}_2]-\text{CH}_2\text{-py}^+\text{-tB}$, $[\text{Ir}_2]-(\text{CH}_2)_2\text{-py}^+$, $[\text{Ir}_2]-3-(\text{CH}_2)_2\text{-py}^+$, and $[\text{Ir}_2]-(\text{CH}_2)_3\text{-py}^+$ donor-acceptor complexes, as well as the short triplet lifetimes of $[\text{Ir}_2]-(\text{CH}_2)_2\text{-py}^+$ and $[\text{Ir}_2]-3-(\text{CH}_2)_2\text{-py}^+$. Figure 5.7 shows spectral/kinetic data for the $n = 3$ complex, $[\text{Ir}_2]-(\text{CH}_2)_3\text{-py}^+$. This time-resolved emission spectrum in the range between 440 and 580 nm showed the expected maximum at ~550 nm (refer to Table 4.4. Emission Data) which decayed with a lifetime of 74 ps over the entire emission band (470-570 nm). Figure 5.8 shows the kinetic data accumulated from the most intense spectral window (520-580 nm). The data for this compound and the complexes mentioned above were all fit to monoexponential intensity functions, the results of which are given in Table 5.1.

The triplet lifetimes of the $[\text{Ir}_2]-\text{CH}_3$, $[\text{Ir}_2]-\text{CH}_2\text{-Quin}^+$, $[\text{Ir}_2]-\text{CH}_2\text{-py}^+\text{-tB}$, and $[\text{Ir}_2]-(\text{CH}_2)_3\text{-py}^+$ complexes were obtained using standard emission experiments (laser excitation at 460 or 355 nm, and detection of emission at 750 nm using a PMT). Figure 5.9 shows representative kinetic data for the model complex, $[\text{Ir}_2]-(\text{CH}_2)_2\text{-Quin}^+$, ($\tau = 1.0 \mu\text{s}$). The data for all compounds were fit satisfactorily to monoexponential intensity functions and are summarized in Table 5.1.

The excited-state electron-transfer rates were calculated from the lifetime data by using eq 5.1. The factor of 1/2 in the equation is required by the 2:1 acceptor/donor

$$k_{\text{ET}} = 1/2 \left(\frac{1}{\tau} - \frac{1}{\tau^0} \right) \quad (5.1)$$

stoichiometry in these complexes. τ_0 is the intrinsic singlet or triplet lifetime of the unquenched complexes, *i.e.*, the lifetime of the model complex, and τ is the singlet or triplet lifetimes of the donor-acceptor complex. This equation is valid because the radiative and nonradiative rate constants, intrinsic to the $d^8\text{-}d^8$ chromophore, are unperturbed by the pyridinium cation (this situation was established from the spectroscopic data presented in Chapter 4). In cases where lifetime data were not available, emission quantum yields were

Figure 5.7. Kinetic/spectral data obtained from Streak Camera experiment for $[\text{Ir}(\mu\text{-pz}^*)(\text{CO})(\text{Ph}_2\text{P-O-C}_6\text{H}_4\text{-(CH}_2\text{)}_3\text{-py}^+)]_2$.

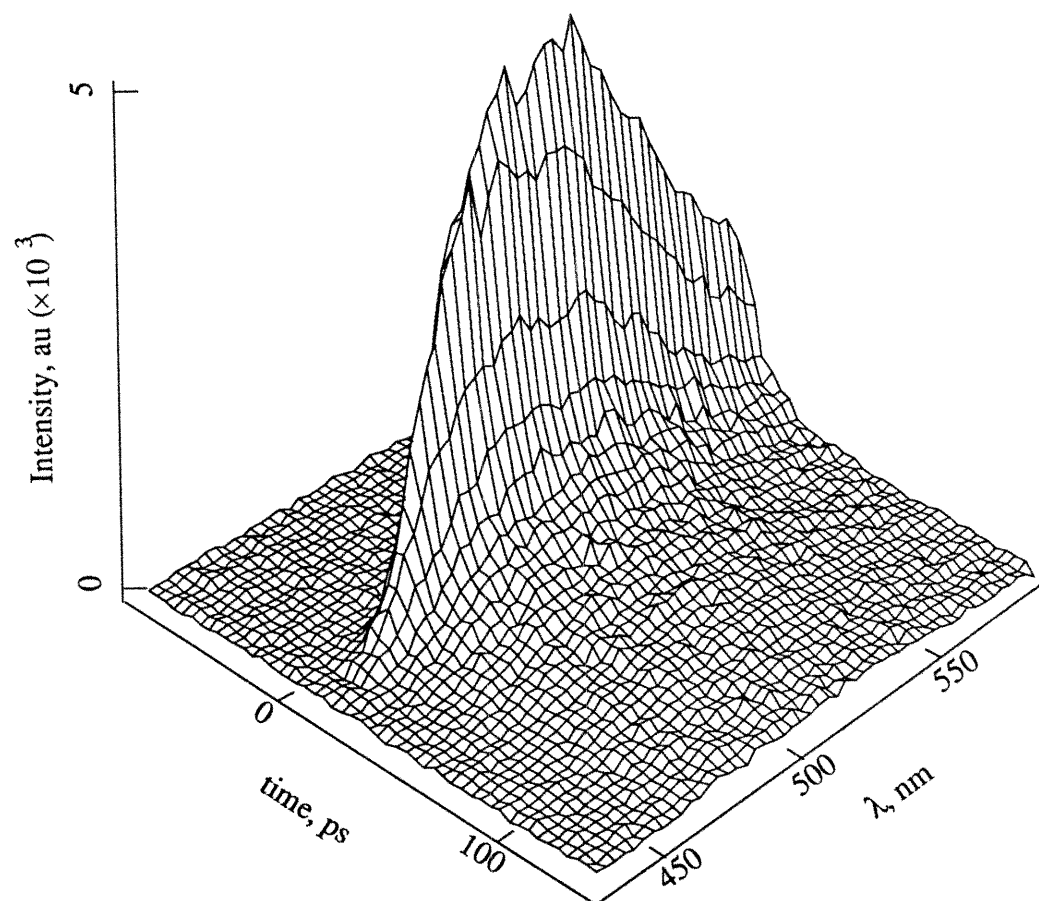


Figure 5.8. Kinetics of $[\text{Ir}(\mu\text{-pz}^*)(\text{CO})(\text{Ph}_2\text{P-O-C}_6\text{H}_4\text{-(CH}_2\text{)}_3\text{-py}^+)]_2$, $\tau_f = 74$ ps, $\lambda_{\text{ex}} = 460$ nm, data collected between 520 and 580 nm. The dashed line is the best fit to the data, and the dotted line is the instrument response function.

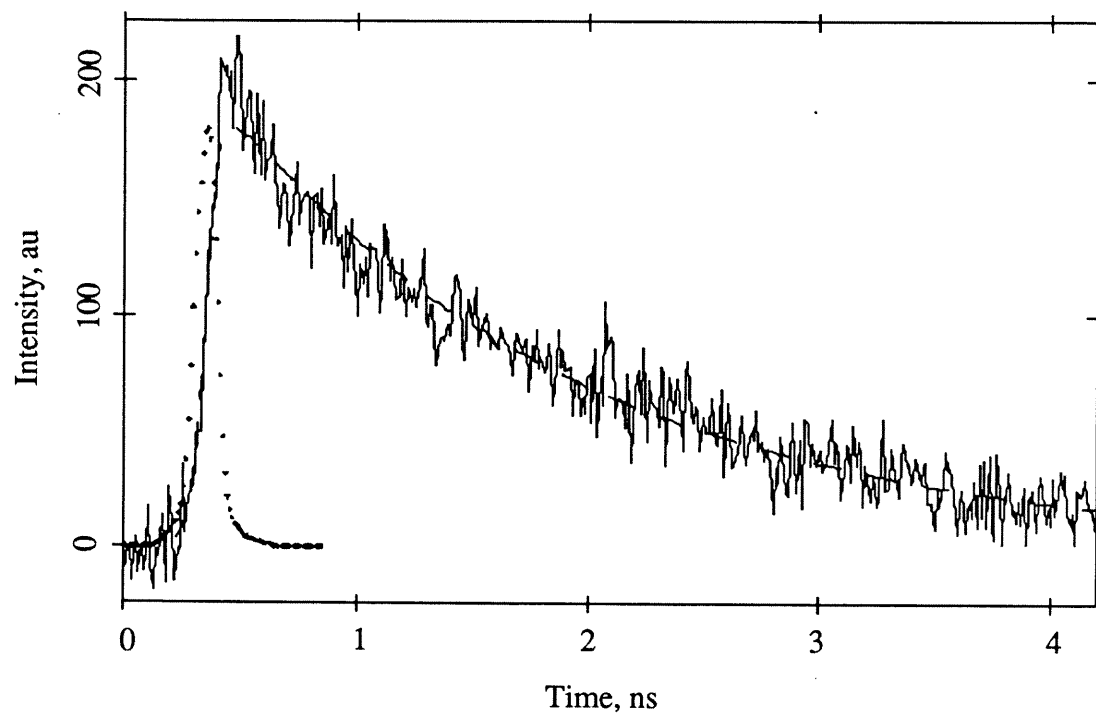
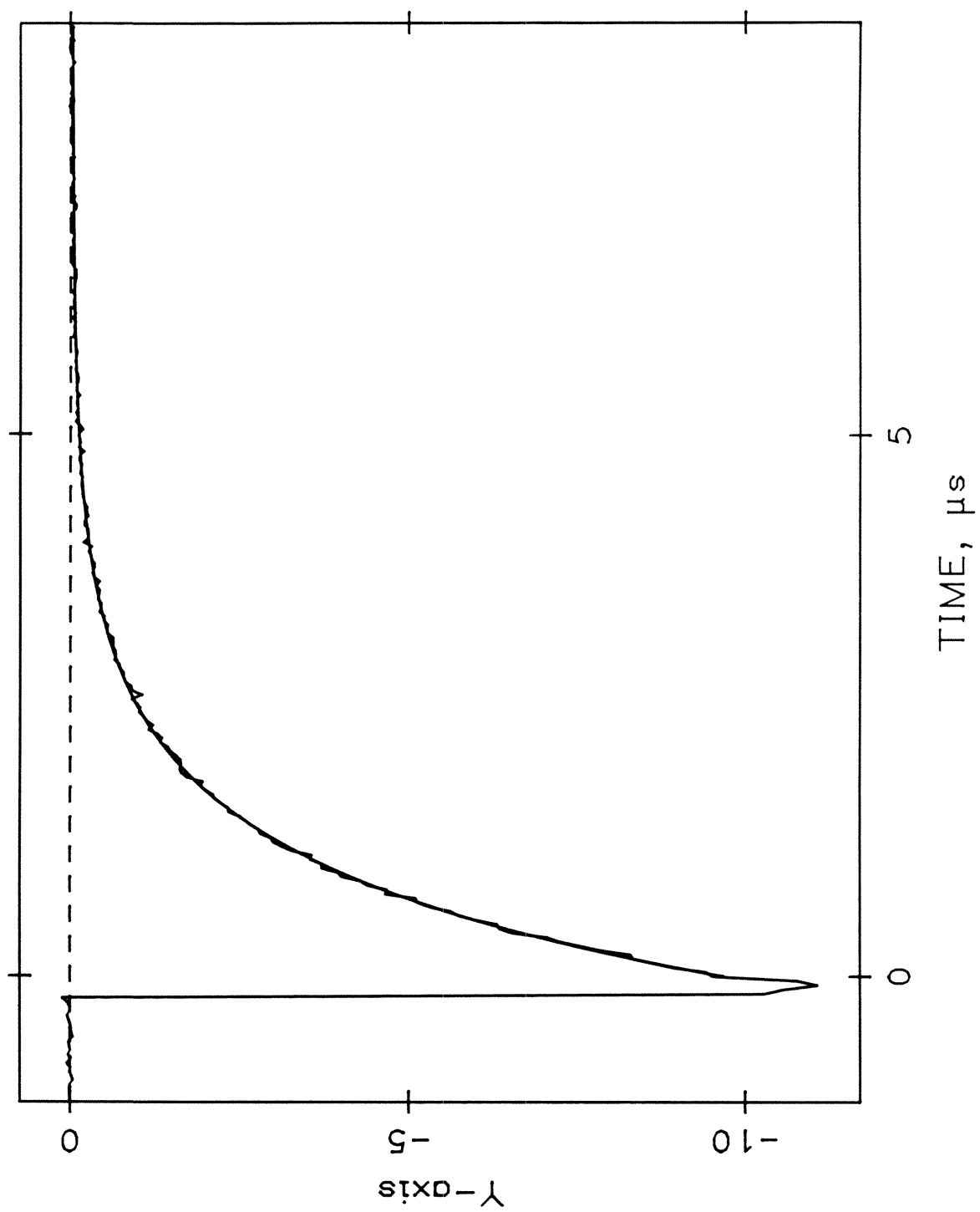


Figure 5.9. Kinetics of $[\text{Ir}(\mu\text{-pz}^*)(\text{CO})(\text{Ph}_2\text{P-O-C}_6\text{H}_4\text{-CH}_2\text{-Quin}^+)]_2$, $\tau_{\text{ph}} = 1.0 \mu\text{s}$, $\lambda_{\text{ex}} = 460 \text{ nm}$, $\lambda_{\text{em}} = 750 \text{ nm}$, obtained from nanosecond emission experiment.



employed to determine singlet and triplet electron-transfer rates using eqs 5.2 and 5.3, respectively. Φ_f^o and Φ_p^o are the fluorescence and phosphorescence quantum yields for the model complex and Φ_f and Φ_p are the corresponding quantum yields for the donor-acceptor complex. Thermal back electron-transfer rates were calculated using eq 5.4, where k_{ET^b} is simply the inverse of the charge-transfer state lifetime, τ_{CT} .

$$\frac{\Phi_f^o}{\Phi_f} = 1 + 2k_{1ET}\tau_f^o \quad (5.2)$$

$$\frac{\left(\frac{\Phi_f^o}{\Phi_f}\right)}{\left(\frac{\Phi_p^o}{\Phi_p}\right)} = 1 + 2k_{3ET}\tau_p^o \quad (5.3)$$

$$k_{ET^b} = 1/\tau_{CT} \quad (5.4)$$

The results of these calculations are summarized in Tables 5.2 and 5.3. The driving forces for each reaction, calculated in Chapter 4, are also given. In the next section these ET rates will be discussed in light of the structural parameters presented in Chapter 3. A discussion of the effects of the initial spin-state of the donor on ET rates will also be given.

DISCUSSION

A previous study conducted in our laboratory on the donor-acceptor complexes, $[\text{Ir}(\text{pz}^*)(\text{CO})(\text{Ph}_2\text{P}-\text{O}-(\text{CH}_2)_2\text{-py}^+-\text{R})]_2$, has demonstrated the effects of driving force on electron-transfer rates.⁵ The ^1ET , ^3ET , and ET^b rates were fit to classical Marcus theory with the same set of parameters: $\lambda = 1.0$ eV and $H_{DA} = 24$ cm⁻¹. These results are applied to the present investigation in an effort to extract electronic coupling matrix elements. This was accomplished by first assuming that the nuclear reorganization energies (mainly due to

Table 5.2. Singlet and Triplet Excited-State Electron-Transfer Rates for Donor-Acceptor Complexes

Compounds	¹ ET		³ ET	
	$-\Delta G^\circ(\text{eV})^a$	$k_{\text{ET}}(\text{s}^{-1})$	$-\Delta G^\circ(\text{eV})^a$	$k_{\text{ET}}(\text{s}^{-1})$
[Ir ₂]-py ⁺	0.90	$1.0 \pm 0.3 \times 10^{11}{}^b$	0.40	$8.9 \pm 1.8 \times 10^5$
[Ir ₂]-CH ₂ -py ⁺	0.76	$3.6 \pm 0.9 \times 10^9{}^b$	0.26	$2.5 \pm 0.5 \times 10^5$
[Ir ₂]-CH ₂ -py ⁺ -tB	0.53	$1.3 \pm 0.1 \times 10^9$	0.03	$1.8 \pm 0.4 \times 10^5$
[Ir ₂]-CH ₂ -py ⁺ -Am	1.16	$1.8 \pm 0.5 \times 10^9{}^b$	0.66	$2.4 \pm 0.5 \times 10^5$
[Ir ₂]-CH ₂ -py ⁺	0.67	$1.4 \pm 0.1 \times 10^{10}$	0.17	$1.6 \pm 1.4 \times 10^8$
[Ir ₂]-3-(CH ₂) ₂ -py ⁺	0.69	$3.1 \pm 0.2 \times 10^{10}$	0.19	$1.6 \pm 1.3 \times 10^8$
[Ir ₂]-CH ₂ -py ⁺	0.69	$2.7 \pm 0.3 \times 10^9$	0.19	$2.1 \pm 0.3 \times 10^7$

^a Driving forces are associated with an error of ± 0.1 eV.

^b Obtained from quantum yield measurements using eq 5.3 since triplet lifetimes were not available.

Table 5.3. Thermal Back Electron-Transfer Rates for Two Donor-Acceptor Complexes ^a

Compounds	$-\Delta G^\circ(\text{eV})$	$k_{\text{ET}}(\text{s}^{-1})$
[Ir ₂]-CH ₂ -py ⁺	1.50	$5.6 \pm 0.6 \times 10^8$
[Ir ₂]-CH ₂ -py ⁺	1.73	$6.7 \pm 1.9 \times 10^9$

^a the back electron-transfer rates for the remaining Ir₂-py⁺ complexes were not measured.

solvent reorganization with little contribution from internal modes⁴) in both systems are similar. This assumption is valid because the same solvent (CH₃CN) was used, and the approximate donor-acceptor separations are comparable. The values of H_{DA} for electron transfer in [Ir(pz*)(CO)(Ph₂P-O-C₆H₄-(CH₂)_n-py⁺)]₂ were then calculated by solving the Marcus expression for electron-transfer rates,⁶ imputing a value for λ of ~ 1.0 eV. These calculations were conducted on the four classes of donor-acceptor complexes ($n = 0, 1, 2$, and 3) for ¹ET, ³ET, and ET^b reactions. We will refer to electronic couplings associated

with singlet and triplet excited-state electron transfer as $^1H_{DA}$ and $^3H_{DA}$, respectively, and the electronic couplings associated with the thermal back electron transfer as $^bH_{DA}$. In Figures 5.10a-d, the results of these calculations are shown in the form of four separate Marcus curves for the $n = 0, 1, 2$, and 3 complexes. The results are also summarized in Table 5.4.

It is apparent from the calculations of H_{DA} for 1ET , 3ET and ET^b in the series of donor-acceptor complexes that: (1) in complexes with $n = 0$ and 1 , $^1H_{DA} \gg ^3H_{DA}$; (2) in complexes with $n = 2$ and 3 , $^1H_{DA} = ^3H_{DA}$; and (3) in the two complexes where k_{ET^b} were measured, $^1H_{DA} = ^bH_{DA}$.

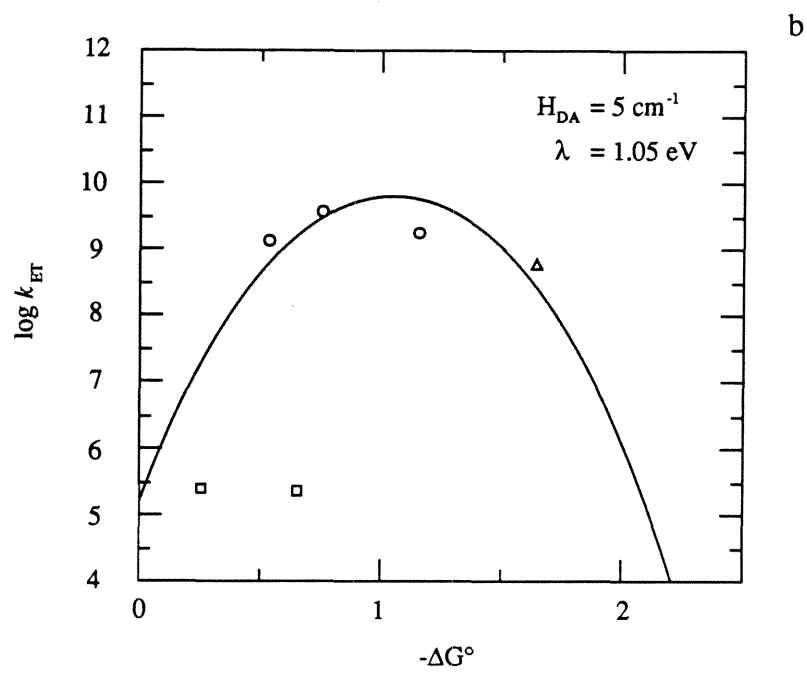
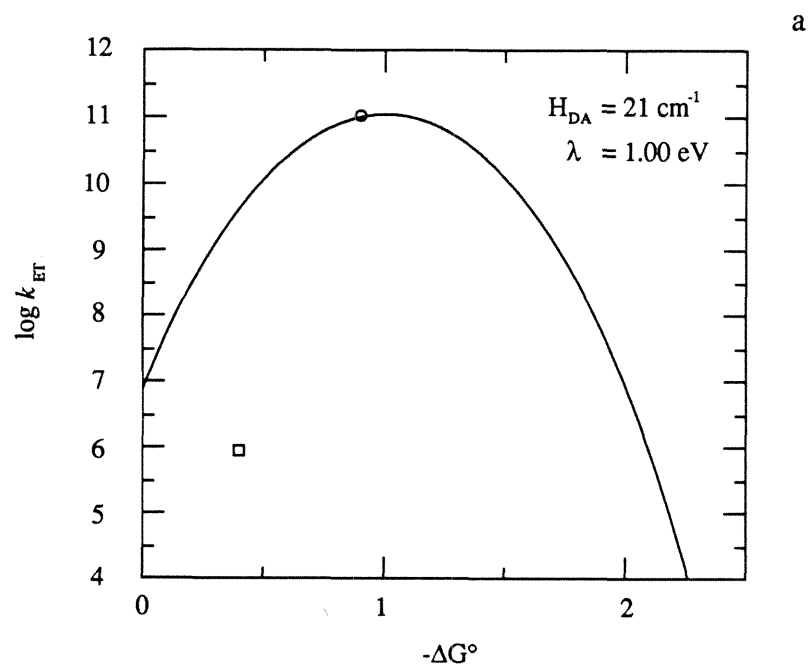
Table 5.4. Electronic Coupling Matrix Elements for 1ET , 3ET and ET^b in the Donor-Acceptor Complexes

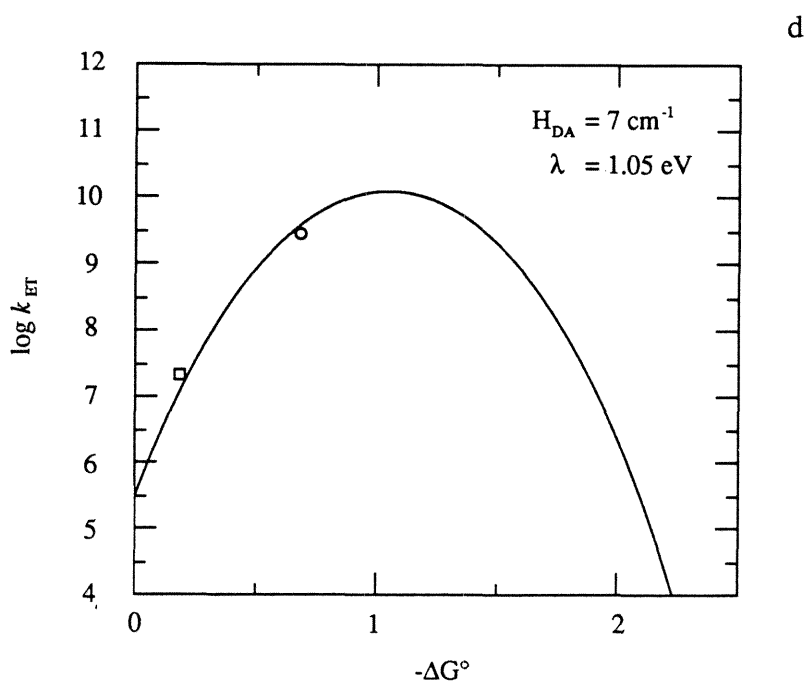
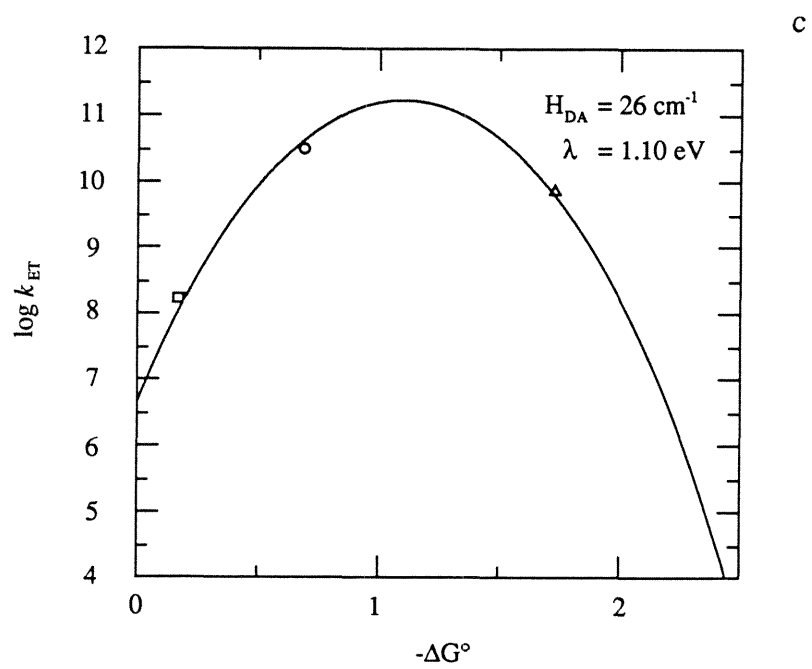
Compounds	n	$^1H_{DA}$ (cm ⁻¹)	$^3H_{DA}$ (cm ⁻¹)	$^bH_{DA}$ (cm ⁻¹)
[Ir ₂]-py ⁺	0	21	0.4	— ^a
[Ir ₂]-CH ₂ -py ⁺ -R	1	5	<0.3	5
[Ir ₂]-[(CH ₂) ₂]-py ⁺	2	26	26	26
[Ir ₂]-[(CH ₂) ₃]-py ⁺	3	7	7	— ^a

^a Back electron-transfer rates were not measured for these complexes.

In an effort to understand these observations, the singlet ET reactions (along with the thermal back ET reactions) will first be discussed followed by a discussion of the triplet ET reactions. Once we have established the possible explanations for the electronic couplings observed for each excited-stated ET reaction, the results from the donor-acceptor complex, [Ir₂]-3-[(CH₂)₂]-py⁺, which has in its bridge a 1,3-disubstituted phenylene group, will be discussed. This complex will serve to further substantiate our theoretical models concerning electron transfer from singlet and triplet excited states.

Figure 5.10. (a) Fit of ^1ET (\circ) rate for $[\text{Ir}_2]\text{-py}^+$ ($n = 0$) to Marcus theory (eq 1.2). (b) Fit of ^1ET (\circ) and ET^{b} (Δ) rates for $[\text{Ir}_2]\text{-CH}_2\text{-py}^+$ ($n = 1$). (c) Fit of ^1ET (\circ), ^3ET (\square), and ET^{b} (Δ) rates for $[\text{Ir}_2]\text{-(CH}_2)_2\text{-py}^+$ ($n = 2$). (d) Fit of ^1ET (\circ) and ^3ET (\square) rates for $[\text{Ir}_2]\text{-(CH}_2)_2\text{-py}^+$ ($n = 3$).





Singlet Electron Transfer:

Even though the through-bond edge-to-edge Ir₂ to py⁺ distance in [Ir₂]-CH₂-py⁺ is ~1.5 Å shorter than that of [Ir₂]--(CH₂)₂-py⁺ (refer to Table 3.5. Structural Parameters), the ¹H_{DA} in the former is about five times smaller. This strongly suggests that the principal pathway for the electron transfer from the singlet excited state of the iridium dimer is through the bonds of the hydrocarbon bridge.⁷ We will therefore discuss the singlet electronic couplings in terms of through-bond mechanisms only. Through-bond (TB) interactions are the result of mutual mixing of orbitals via the intervening σ (or π) framework. Model calculations⁷⁻⁹ and experimental results¹⁰⁻¹⁵ have led to several important generalizations concerning orbital interactions through *n* methylene groups: (1) The extent of orbital interactions through *n* methylene groups (*n* - 1 = *m* bonds), for a given value of *n*, depends on the geometry of the σ relay and is maximized for an all-*trans* arrangement of σ bonds; (2) ET rates, in a series of donor-acceptor complexes with all *trans* bridges (*n* must be even), decay exponentially with an increasing number of intervening σ-bonds. Oliver *et al.*¹⁶ recently observed this behavior in molecules possessing 1,4-dimethoxynaphthalene donors attached via rigid hydrocarbon spacers (norbornyl groups) to 1,1-dicyanoethylene acceptors. Their hydrocarbon spacers had either an all-*trans* arrangement of single bonds or a single σ-*cis* kink in the chain. In each case the all-*trans* isomer gave the faster rate by about a factor of 10. Similar results were also obtained by Wasielewski *et al.*¹⁷ in rigid porphyrin-quinone complexes, shown in Figure 5.11. The all-*trans* isomer exhibited a singlet ET rate approximately two times faster than the cisoid isomer. These examples demonstrate that through-bond coupling of donor and acceptor through saturated bridges plays an important role in determining ET rates, and furthermore, *trans* donor-acceptor configurations result in enhanced ET rates over cisoid configurations.

A discussion of the experimentally determined singlet electronic coupling matrix elements (¹H_{DA}) for the four classes of Ir₂-py⁺ donor-acceptor complexes (*n* = 0, 1, 2,

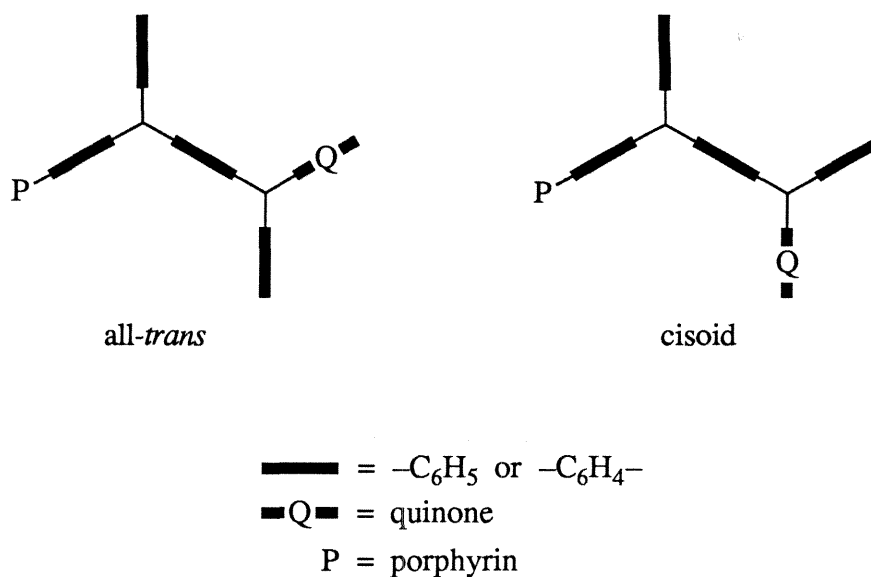


Figure 5.11. Edge-view of porphyrin-quinone complexes.

and 3) will therefore be presented in light of through-bond electron-transfer mechanisms. The discussion that follows hinges on the assumption that in these complexes, photoinduced electron transfer from the singlet excited state of the Ir_2 donor occurs via the *stretched* conformations (stretched and folded conformations are discussed in Chapter 3). In the stretched conformation, gauche interactions between the aromatic rings (phenylene and pyridinium groups) are minimized, implying that it is the lowest energy conformation in solution. Therefore, during the short lifetime of the Ir_2 singlet excited state (~ 100 ps), the most populated structure found in solution would be the stretched conformation.

Through-Bond Electron Transfer Mediated by *One* Methylene Group: The orbital interactions in complexes where π systems are separated by one methylene group can be modelled by the π -orbital overlap in norbornadiene.¹⁸ The π MOs in this complex are known from photoelectron (PE) spectroscopy to interact predominantly through space.¹⁹ Therefore, in the $n = 1$ donor-acceptor complex, $[\text{Ir}_2]\text{-CH}_2\text{-py}^+$, only through-*space* interactions between the phenylene and pyridinium groups are expected to play a role in

coupling $^1\text{Ir}_2^*$ and py^+ . Since it has already been established that solely through-bond interactions couple $^1\text{Ir}_2^*$ and py^+ , the value of $^1\text{H}_{\text{DA}}$ is predicted to be extremely small. The experimentally determined $^1\text{H}_{\text{DA}}$ of 5 cm^{-1} for $[\text{Ir}_2]\text{-CH}_2\text{-py}^+$ is therefore not surprising.

Electron Transfer through Two Methylene Groups: The orbital interactions in complexes where π systems are separated by two methylene groups can be modelled by compound **1** shown in Figure 5.12. From PE spectroscopy, the difference in vertical

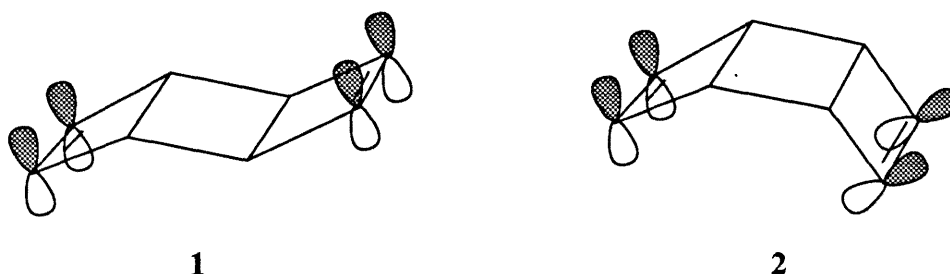


Figure 5.12. Structure of molecules which exhibit strong π through-bond interactions (**1**) and diminished through-bond interactions (**2**)

ionization potential, $\Delta I_{\text{v}}(\pi)$, for the π_- and π_+ MO levels can be calculated.¹⁸ Large values of $\Delta I_{\text{v}}(\pi)$ have been shown to imply efficient through-bond orbital interactions.²⁰ $\Delta I_{\text{v}}(\pi)$ in this molecule was found to be 1.16 eV. This value can be compared to 0.78 eV for the *syn*-isomer, **2**, where the reduced $\Delta I_{\text{v}}(\pi)$ is due to the presence of competing through-space interactions, which are of course absent in the **1**.

The results from this model predict that $^1\text{H}_{\text{DA}}$ for $[\text{Ir}_2]\text{-(CH}_2)_2\text{-py}^+$ ($n = 2$) should be much larger than for $[\text{Ir}_2]\text{-CH}_2\text{-py}^+$ ($n = 1$), due to enhanced through-bond coupling in the former complex. This was experimentally observed: $^1\text{H}_{\text{DA}}(1) = 5\text{ cm}^{-1}$ and $^1\text{H}_{\text{DA}}(2) = 26\text{ cm}^{-1}$.

Electron Transfer through *Three* Methylene Groups: The orbital interactions in complexes where π systems are separated by three methylene groups can be modelled by the compound shown in Figure 5.13. $\Delta I_v(\pi)$ in this compound was found to be only 0.87 eV²¹ as compared to 1.16 eV for compound **1** in Figure 5.12. The diminished through-bond orbital interaction in this compound can be attributed to the trans effect for electron transfer. The relatively small value of $^1H_{DA}$ (7 cm⁻¹) for [Ir₂] $-(CH_2)_3$ -py⁺ is therefore not surprising.

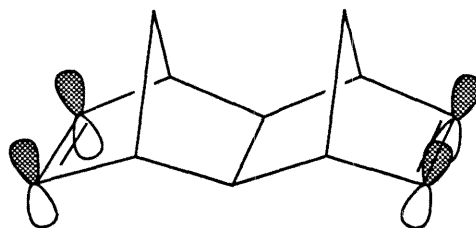


Figure 5.13. Structure of model compound for p orbital interactions through three methylene groups.

The experimental values of $^1H_{DA}$ (given in Table 5.4) for the series of donor-acceptor complexes are adequately explained by invoking through-bond interactions in the stretched conformations of the Ir₂-py⁺ donor-acceptor complexes. The result, which indicates that electronic coupling in the $n = 2$ donor-acceptor complex is the most efficient of the series, can be attributed to the trans effect for electron transfer. The values of $^bH_{DA}$ for the $n = 1$ and 2 complexes are equivalent to the corresponding values of $^1H_{DA}$. A satisfactory explanation for this is not presented; however, this result implies that thermal back electron-transfer in these complexes occurs from a charge-transfer state exhibiting singlet character.

The $n = 0$ complex, [Ir₂]-py⁺, was not modelled in the preceding discussion,

however, its large value of $^1H_{DA}$ (21 cm^{-1}) implies that the p-orbitals at the point of attachment of the pyridinium and phenylene rings interact strongly. This point is discussed in more detail in the next section, where electronic couplings for triplet electron-transfer reactions are considered.

Triplet Electron Transfer:

The results presented in Table 5.4 show that $^3H_{DA}$ values for the $n = 0$ and $n = 1$ donor-acceptor complexes are considerably smaller than for the $n = 2$ and $n = 3$ complexes, and furthermore, the $^3H_{DA}$ for the $n = 2$ complex is larger than for the $n = 3$ complex. These results imply that the through-bond mechanism (which plays an important role in determining values of $^1H_{DA}$) does not play an important role in $^3H_{DA}$. Therefore the $^3H_{DA}$ s will be discussed in terms of through-space (TS) interactions. TS interactions, as the term implies, result from direct spatial overlap of two interacting (basis) orbitals.⁷⁻⁹

Evidence that through-space interactions can lead to such strong couplings of π systems ($^3H_{DA}(2) = 26\text{ cm}^{-1}$) is available in a system comprised of xanthene and related dyes dissolved in the non-polar solvents anthracene, phenanthrene, and 1-chloronaphthalene.²² In this system of interacting aromatic rings a determination of the pure through-space electron-exchange matrix element, H_{DA} , was possible. A value of 35 cm^{-1} for H_{DA} was obtained by fitting the charge-transfer data to the Marcus expression for electron transfer. This system clearly demonstrates that through-space coupling of face-to-face aromatic groups can be considerable. It is, however, not clear what the precise structural requirements are for large through-space interactions to persist, and more precisely, what role, if any, the number of intervening methylene groups play in determining the extent of through-space coupling.

Studies of the charge-transfer quenching of benzophenone phosphorescence (^3ET) by olefins shed some light on these questions.²³ In this system, the benzophenone and olefin were separated by n methylene groups ($n = 1\text{--}21$). It was observed that there was a

sudden increase in $k_{\text{ET}}(n)$ for chains of length $n = 8$ and another significant jump for $n = 9$, as seen in the data presented in Table 5.5. Space-filling models indicated that only chains of at least eight CH_2 groups permit the terminal $-\text{CH}=\text{CH}_2$ group to come within van der Waals contact of the ketone carbonyl. The suggestion was made, from these results, that a close approach between the alkene and the ketone carbonyl group was necessary for quenching of the ketone triplet to occur. The diminished ET rates at large values of n (18 and 21) are most likely due to the decreased probability of the donor and acceptor meeting in a favorable conformation.

Table 5.5. Triplet Electron-Transfer Rates in a series of Benzophenone-Alkene Complexes

n	$k_{\text{ET}} \times 10^{-4} (\text{s}^{-1})$
1	0
2	0
4	1.0
6	1.3
8	23.5
9	54.1
10-15	63.6 ± 10^a
18	36.3
21	30.2

^a Average of rates for $n = 10-15$.

When our results are considered in light of the above observations, a correlation of the number of methylene groups in the bridge to $^3\text{H}_{\text{DA}}$ arises. If through-space coupling is primarily responsible for the observed values of $^3\text{H}_{\text{DA}}$, then the through-space interactions in $[\text{Ir}_2]-(\text{CH}_2)_2\text{-py}^+$ ($n = 2$) are the largest of the series followed by the $n = 3$ complex, and then the $n = 0$ and $n = 1$ complexes which presumably have diminished TS interactions.

In an attempt to quantify the dependence of $^3\text{H}_{\text{DA}}$ on n , the assumption will therefore

be made that the origin of the coupling between the donor and acceptor is specifically the TS interaction between the pyridinium ring and the phenylene ring in the *folded* conformation. Furthermore, since the structures of the folded conformations for the series of complexes (see Figures 3.5-3.10) reveal that the most important interaction between the two aromatic rings is between the C4 atom of the phenylene ring and the N atom of the pyridinium ring, only the TS interaction between the corresponding p-orbitals on C4 and N will be considered. The electron accepting molecular orbital (LUMO) of the pyridinium acceptor has p-character on the N atom,²⁴ warranting consideration of the interactions of the 2p-orbitals on the C4 and N atoms.

Since electron densities usually fall off exponentially as the distance between the electron and the nucleus is increased, the orbital overlap between C4 and N is also expected to fall off exponentially as their separation, r , increases.^{25, 26} If the assumption is made that electron transfer occurs via electronic coupling between the p-orbitals of C4 and N, then the electron-transfer rates would also be expected to fall off exponentially with r . The exponential dependence of electron-transfer rates on r has been demonstrated in many donor-acceptor systems^{11-15, 25, 27-33} and can be expressed by eq 5.1, where A is a

$$k_{\text{ET}} = A \exp(-\beta \cdot r), \quad (5.1)$$

preexponential constant and β is a measure of the steepness of a $\log k_{\text{ET}}$ vs r plot. However, eq 5.1 neglects stereoelectronic details of the p-orbital overlap. The introduction of angular terms into the equation will take into account the asymmetry of the p-orbitals. This is accomplished by considering the angular dependence on the overlap between the 2p-orbitals on C4 and N.

The overlap between two 2p-orbitals, S_{12} , whose axes lie in parallel planes at a distance r is a function of the overlap integral of parallel 2p orbitals, $S_{\pi\pi}$, and the cant angle, γ , which is defined in Figure 5.14a.³⁴ $S_{\pi\pi}$ is a function of the effective nuclear

charge, Z , usually taken to be 3.09, and decays exponentially with r , as described above. Eq 5.2 reflects the dependence of S_{12} on $S_{\pi\pi}$ and γ . When the p-orbitals are also slanted towards one another at the angle θ , as defined in Figure 5.14b, the expression for S_{12} (which is now resolved into σ and π type overlaps) is given by eqs 5.3 and 5.4, where $S_{12}(\sigma)$ and $S_{12}(\pi)$ are the σ and π contributions to the total overlap. The values of $S_{\sigma\sigma}$ and $S_{\pi\pi}$ were obtained from Kopineck's compilation.³⁵ It was established in Chapter 1 that the electron-transfer rates are proportional to the square of the electronic coupling or, in this case the direct orbital overlap (eq 5.5).

$$S_{12} = S_{\pi\pi} \cos\gamma \quad (5.2)$$

$$S_{12} = S_{\sigma\sigma} \cos^2\theta + S_{\pi\pi} \sin^2\theta \cos\gamma \quad (5.3)$$

$$S_{12} = S_{12}(\sigma) + S_{12}(\pi) \quad (5.4)$$

$$k_{\text{ET}} \propto S_{12}^2 \quad (5.5)$$

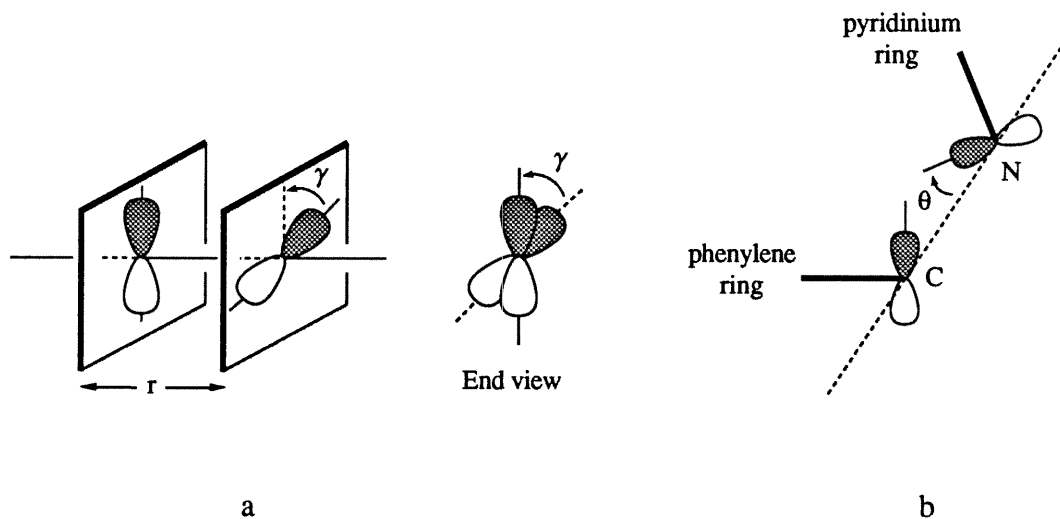


Figure 5.14. (a) Definition of γ and r . (b) Definition of C4, N, and θ .

Before the validity of eq 5.5 is tested, we must consider the statistical distributions in solution of the folded conformations. If we assume that only a finite number of low energy conformations exist in solution and that the energy associated with each possible conformation is approximately the same, then a statistical factor, P , can be introduced into eq 5.5, which is the number of conformations in the folded form divided by the total number of possible conformations. For example, in the $n = 2$ complex there are three possible low energy conformations, shown in Figures 5.15: two folded (a and b) and one

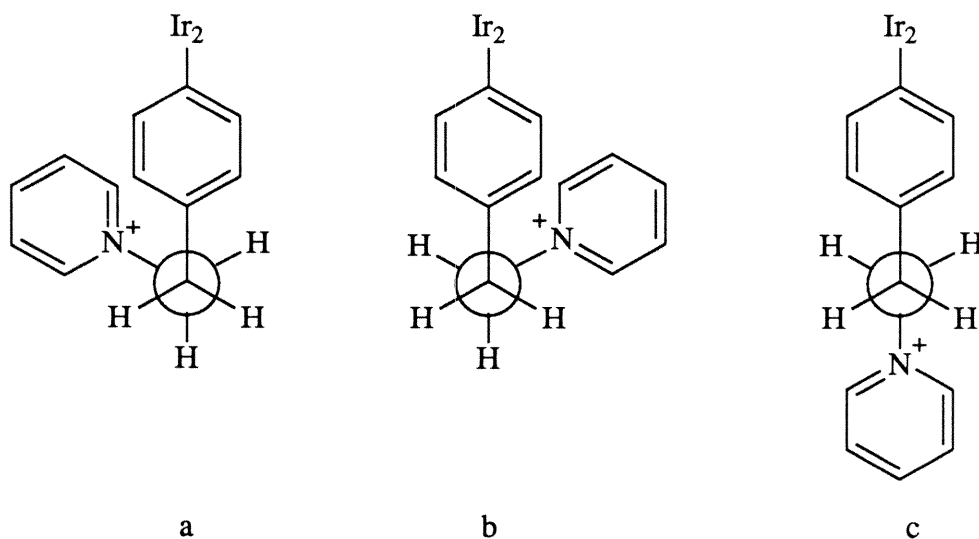


Figure 5.15. Newman projections of the three low energy conformations for $n = 2$ donor-acceptor complex, (a) and (b) represent the folded conformations, and (c) represents the stretched conformation.

stretched (c). Therefore, P in this case is $2/3$. The value of P decreases rapidly as n increases, expressing the fact that at large n the probability of finding the pyridinium ring eclipsed over the phenylene ring is severely diminished (as in bimolecular reactions). P can now be incorporated into eq 5.5 yielding the final expression, eqs 5.7, which relates

electron-transfer rates to the statistical and angular terms of eqs 5.2-5.6.

$$k_{\text{ET}} \propto P S_{12}^2 \quad (5.6)$$

$$k_{\text{ET}} \propto I_{\text{T}}^2 \quad (5.7)$$

The parameters in eqs 5.1, 5.3, and 5.6 (r , γ , θ , P , $S_{\sigma\sigma}$, and $S_{\pi\pi}$) are given in Table 5.6 for the series of donor-acceptor complexes. Included in the table are the parameters for the analogous $n = 4$ complex, which were not prepared in this study, but can lead to predictions concerning future studies.

Table 5.6. Structural and Electronic Parameters for Donor-Acceptor Complexes

Compounds	n	r (Å)	γ	θ	P	$S_{\sigma\sigma}$	$S_{\pi\pi}$
[Ir ₂]-py ⁺	0	1.4	42	90	1	0.32	0.27
[Ir ₂]-CH ₂ -py ⁺	1	2.4	0	55	1	0.17	0.046
[Ir ₂]-CH ₂) ₂ -py ⁺	2	3.1	0	25	.67	0.085	0.015
[Ir ₂]-CH ₂) ₃ -py ⁺	3	3.7	0	20	.11	0.056	0.0074
[Ir ₂]-CH ₂) ₄ -py ⁺	4	4.0	0	8.5	.07	0.038	0.0038

Assuming that $k_{\text{ET}}(n)$ is proportional to the square of the statistically adjusted C4-N p-orbital overlap, $I_{\text{T}}^2(n)$, experimental values of $^3\text{H}_{\text{DA}}^2(n)$ can be compared to the calculated values of $I_{\text{T}}^2(n)$. If the calculated orbital overlaps parallel the experimental results for every n , we would conclude that the p-orbital overlap between C4 and N is responsible for the coupling between the $^3\text{Ir}_2^*$ donor and the py⁺ acceptor. However, if the calculated $I_{\text{T}}^2(n)$ values did not correlate with the experimental values of $^3\text{H}_{\text{DA}}^2(n)$, an alternate analysis would have to be considered. The answers to these questions can be found in Table 5.7. The first column of the table contains the calculated values of I_{T}^2 , the second column is the

Table 5.7. Calculated Orbital Overlaps (I_T^2) and Experimental Matrix Elements (H_{DA}^2)

Compounds	Calculated $I_T^2 \times 10^4$	Normalized I_T^2	Found ${}^3H_{DA}^2$ (cm ⁻²)
[Ir ₂]-py ⁺	400	10,000	0.2
[Ir ₂]-CH ₂ -py ⁺	60	2,000	<0.1
[Ir ₂]-CH ₂) ₂ -py ⁺	30	900	900
[Ir ₂]-CH ₂) ₃ -py ⁺	0.4	10	50
[Ir ₂]-CH ₂) ₄ -py ⁺	0.08	2	—

same data normalized to match ${}^3H_{DA}^2(2)$, and the third column contains the experimental ${}^3H_{DA}^2$ values. The normalized values of $I_T^2(n)$, for all n , do not compare favorably to the experimental ${}^3H_{DA}^2(n)$ values: $I_T^2(1)$ is twice $I_T^2(2)$ which was not observed experimentally (${}^3H_{DA}^2(2) \gg {}^3H_{DA}^2(1)$); the largest orbital overlap is $I_T^2(0)$ which is also not consistent with experiment. Clearly, the C4-N p-orbital overlap is not responsible for the observed coupling in this series of Ir₂-py⁺ donor-acceptor complexes. The calculations must therefore be reanalyzed in a search for the origin of ${}^3H_{DA}(n)$.

It was demonstrated in eq 5.4 that σ and π terms contribute to the total orbital overlap. Table 5.8 summarizes the results of separating I_T^2 into I_σ^2 and I_π^2 components. I_σ^2 and I_π^2 represent σ and π type p-orbital overlaps. These two types of orbital overlaps show dramatically different dependences on n . For example, $I_\pi^2(n)$ values predict (as did $I_T^2(n)$ values) that ${}^3H_{DA}^2(0)$ should be the largest of the series followed by ${}^3H_{DA}^2(1)$ and then ${}^3H_{DA}^2(2)$. However, $I_\sigma^2(n)$ values predict that ${}^3H_{DA}^2(2)$ should be the largest followed by ${}^3H_{DA}^2(1)$. The σ contribution to the total overlap also predicts that ${}^3H_{DA}^2(0)$ should be very small. A comparison of the normalized values of $I_\sigma^2(n)$ with ${}^3H_{DA}^2(n)$ for all n reveals the relatively good agreement of the σ -type p-orbital overlaps with the matrix elements for ³ET: $I_\sigma^2(2) > I_\sigma^2(1) > I_\sigma^2(3) \gg I_\sigma^2(0)$ compared to ${}^3H_{DA}^2(2) > {}^3H_{DA}^2(3) \gg {}^3H_{DA}^2(0) > {}^3H_{DA}^2(1)$.

Table 5.8. Calculated σ and π Orbital Overlaps (I_{σ}^2 and I_{π}^2) and Experimental Matrix Elements (H_{DA}^2)

Compounds	Calculated		Normalized ^a		Found
	$I_{\pi}^2 \times 10^4$	$I_{\sigma}^2 \times 10^4$	I_{π}^2	I_{σ}^2	${}^3H_{DA}^2$
[Ir ₂]-py ⁺	400	0	2×10^7	0	0.2
[Ir ₂]-CH ₂ -py ⁺	6	20	3×10^5	450	<0.1
[Ir ₂]--(CH ₂) ₂ -py ⁺	0.02	40	900	900	900
[Ir ₂]--(CH ₂) ₃ -py ⁺	~0	2	~0	45	50
[Ir ₂]--(CH ₂) ₄ -py ⁺	~0	1	~0	20	20 ^b

$$I_{\sigma}^2 = P S_{12}^2(\sigma)$$

$$I_{\pi}^2 = P S_{12}^2(\pi)$$

^a These values are normalized to ${}^3H_{DA}^2$ for $n = 2$ complex.

^b Predicted value based on normalized I_{σ}^2 value.

The theoretical prediction that through-space coupling is maximized when the number of intervening methylene groups is 2 has also been confirmed in a study of

X-C₆H₄-(CH₂)_n-py⁺-Y complexes, where $n = 1, 2$, or 3 , $X = H, OMe$ and $Y = 3-CN, 4-CN$.³⁶ The intensities of charge-transfer transitions in these complexes, which is a measure of the coupling between the redox sites, were found to strongly depend on the methylene chain length with the $n = 2$ compounds exhibiting by far the most intense CT bands compared to $n = 1$ and 3 compounds.

Although the trend of ${}^3H_{DA}^2(n)$ values is approximately predicted by the $I_{\sigma}^2(n)$ values, there are discrepancies between the magnitudes of these values. Two major disagreements between $I_{\sigma}^2(n)$ and ${}^3H_{DA}^2(n)$ arise when we assume that the value of $I_{\sigma}^2(1)$ accurately describes the through-space interaction between the phenylene and pyridinium rings: (1) the unusually small calculated value for $I_{\sigma}^2(0)$; and (2) the unusually small calculated values of $I_{\sigma}^2(2)$ and $I_{\sigma}^2(3)$.

The small value of $I_{\sigma}^2(0)$ can be adjusted to more closely match its associated ${}^3H_{DA}^2$ by simply invoking a small contribution of π -type orbital overlap in this complex. Since

$I_{\pi}^2(0)$ is much larger than the other $I_{\pi}^2(n)$ values, this would only serve to increase the calculated orbital overlap in the $n = 0$ complex with no appreciable effect on the other complexes.

The unusually small values of $I_{\pi}^2(2)$ and $I_{\pi}^2(3)$ can be attributed to two problems associated with their calculations. First, in considering the conformations that would lead to efficient overlap of the p-orbitals on C4 and N, high energy conformations were neglected, and only low energy staggered configurations were considered. From molecular mechanics calculations (described in Chapter 3) it was apparent that high energy eclipsed conformations exhibited potentially large values of p-orbital overlaps. Consideration of these high energy conformations would almost certainly increase the calculated orbital overlaps. It should be noted that for complexes with $n = 0$ and $n = 1$, such high energy structures need not be considered due to the rigid nature of these bridges. The second possible shortcoming in the calculations is the neglect of the overlap of the remaining p-orbitals of the rings aside from the C4 and N orbitals. If the contribution of all p-orbitals on the phenylene and pyridinium rings are considered in calculating the through-space coupling in these donor-acceptor complexes, a factor of up to 5^2 can be added to the $I_{\sigma}^2(2)$ and $I_{\sigma}^2(3)$ values. Again, this correction would not apply to $n = 0$ and 1 complexes because the large plane angle between the two rings precludes additional p-orbital overlap above that of the C4 and N p-orbitals.

We have demonstrated that there are three factors that contribute to ${}^3H_{DA}$, the electronic coupling between ${}^3Ir_2^*$ and py^+ : (1) the relative orientation and (2) separation between donor and acceptor, and (3) a statistical factor that measures the probability of the donor and acceptor to interact favorably in solution. The conditions for large coupling between the donor and acceptor groups are short distances, relative orientations leading to σ -type p-orbital overlaps (*i.e.*, plane angles between the phenylene and pyridinium rings approaching 0°), and large statistical factors that make contact between donor and acceptor highly probable (*i.e.*, short bridges). When two methylene groups bridge the phenylene

and pyridinium rings, the effect of these three factors appears to be balanced, resulting in the maximum electronic coupling between donor and acceptor. Although the relative orientation in complexes with three methylene groups is more favorable, the distance is longer and statistical factors are unfavorable, thus the result is diminished donor-acceptor coupling. When one methylene group separates donor and acceptor, the beneficial effect of a short through-space separation and a large statistical factor are outweighed by an unfavorable orientation.

Singlet and Triplet Electron Transfer:

The electron transfer results from $[\text{Ir}(\mu\text{-pz}^*)(\text{CO})(\text{Ph}_2\text{P-O-C}_6\text{H}_4\text{-3-(CH}_3)_2\text{-py}^+)]_2$ ($[\text{Ir}_2]\text{-3-(CH}_2)_2\text{-py}^+$), which remain to be discussed, will serve to bridge the two separate discussions of singlet and triplet electron transfer. Recalling the structure of this $n = 2$ donor-acceptor complex reveals the unique nature of its bridge: the phenylene group is 1,3-disubstituted rather than the familiar 1,4-substitution. The ^1ET and ^3ET rates in this complex are compared to those of the similar $n = 2$ complex, $[\text{Ir}_2]\text{-(CH}_2)_2\text{-py}^+$, with the results given in Table 5.9.

Table 5.9. Singlet and Triplet Excited-State Electron-Transfer Rates for Selected Donor-Acceptor Complexes

Compounds	^1ET		^3ET	
	$-\Delta G^\circ(\text{eV})$	$k_{\text{ET}}(\text{s}^{-1})$	$-\Delta G^\circ(\text{eV})$	$k_{\text{ET}}(\text{s}^{-1})$
$[\text{Ir}_2]\text{-(CH}_2)_2\text{-py}^+$	0.67	$1.4 \pm 0.1 \times 10^{10}$	0.17	$1.6 \pm 1.4 \times 10^8$
$[\text{Ir}_2]\text{-3-(CH}_2)_2\text{-py}^+$	0.69	$3.1 \pm 0.2 \times 10^{10}$	0.19	$1.6 \pm 1.3 \times 10^8$

The ^3ET rates in these complexes are identical within experimental error, while the ^1ET rates differ by a factor of more than two. These results are consistent with a through-bond mechanism dominating in the ^1ET reactions and a through-space mechanism dominating in

the ^3ET reactions, in agreement with the discussions of the previous sections.

We have established that in the series of $\text{Ir}_2\text{-py}^+$ donor-acceptor complexes, triplet electron transfer occurs via a folded conformation of the bridge, where through-space interactions between the phenylene and pyridinium rings are maximized. If this is the case, we would expect ^3ET rates in the two complexes to be similar, since the point of attachment of the hydrocarbon chain to the phenylene ring (3- or 4-position) does not affect the distance, orientation, or statistical factor of the folded conformation. The experimental results corroborate this hypothesis.

We have also established that in the series of $\text{Ir}_2\text{-py}^+$ donor-acceptor complexes, singlet electron transfer occurs via a stretched conformation of the bridge, where through-bond interactions between the phenylene and pyridinium rings are maximized. In this case, the point of attachment of the hydrocarbon chain to the phenylene ring does have an effect on the electron-transfer pathway. Namely, the electron-transfer pathway in $[\text{Ir}_2]\text{-3-(CH}_2)_2\text{-py}^+$, across the phenylene group, is shorter than in $[\text{Ir}_2]\text{-(CH}_2)_2\text{-py}^+$, giving rise to a slightly faster ^1ET rate in the former complex.

For the donor-acceptor complex, $[\text{Ir}_2]\text{-3-(CH}_2)_2\text{-py}^+$, the ^1ET rate is consistent with a through-bond mechanism, while ^3ET rate is consistently a through-space mechanism, exclusively.

CONCLUSIONS

The series of iridium donor-acceptor complexes presented in this thesis is the first example of an ET system that exhibits different electronic coupling matrix elements depending on the spin state of the excited donor. The ^1ET and ^3ET rates for the series of $\text{Ir}_2\text{-py}^+$ donor-acceptor complexes have been correlated separately to the number of intervening methylene groups in the bridge. The ^1ET rates in the series, $[\text{Ir}_2]\text{-(CH}_2)_n\text{-py}^+$

($n = 0, 1, 2$, and 3), follow a trend consistent with through-bond mechanisms, where ${}^1H_{DA}(2) \approx {}^1H_{DA}(0) \gg {}^1H_{DA}(3) \approx {}^1H_{DA}(1)$. However, the 3ET rates in the series follow a trend consistent with through-space mechanisms, where ${}^3H_{DA}(2) \gg {}^3H_{DA}(3) \gg {}^3H_{DA}(0) \approx {}^3H_{DA}(1)$. The ET^b rates appeared to parallel the 1ET rates: ${}^1H_{DA}(2,3) = {}^bH_{DA}(2,3)$. Future investigations will be aimed at understanding the back electron-transfer rates in more detail, with the goal of discovering the structural parameters that lead to smaller values of ${}^bH_{DA}$. Theoretical work aimed at elucidating the origin of the observed differences in ${}^3H_{DA}$ and ${}^1H_{DA}$ is currently in progress. Below is a brief summary of our current understanding of this theoretical problem:

This two-electron system can be represented by three orthogonal molecular orbitals, D , D^* , and A , shown in Figure 5.16 (a one-electron treatment of the problem cannot distinguish between singlet and triplet ET). The simplest approximation of the initial and final states (neglecting normalization) for singlet ET is:

$$\begin{aligned}\Psi_I^S &= |\Phi_D \Phi_{D^*}|^S = [\phi_D(1)\phi_{D^*}(2) + \phi_D(2)\phi_{D^*}(1)][\alpha(1)\beta(2) - \alpha(2)\beta(1)] \\ \Psi_F^S &= |\Phi_D \Phi_A|^S = [\phi_D(1)\phi_A(2) + \phi_D(2)\phi_A(1)][\alpha(1)\beta(2) - \alpha(2)\beta(1)],\end{aligned}$$

and similarly for triplet ET,

$$\begin{aligned}\Psi_I^T &= |\Phi_D \Phi_{D^*}|^T = [\phi_D(1)\phi_{D^*}(2) - \phi_D(2)\phi_{D^*}(1)]\alpha(1)\alpha(2) \\ \Psi_F^T &= |\Phi_D \Phi_A|^T = [\phi_D(1)\phi_A(2) - \phi_D(2)\phi_A(1)]\alpha(1)\alpha(2).\end{aligned}$$

For either singlet or triplet ET, the initial and final states must have the same spin wave function for H_{DA} to be nonzero. The Hamiltonian of the system is therefore given by:

$$H = T_1 + T_2 + [(V_{1D} + V_{1A}) + (V_{2D} + V_{2A})] + V_{12},$$

where T is the kinetic energy operator; V_{1D} , V_{1A} , V_{2D} , and V_{2A} are the one-electron interactions between molecular potential wells and the two

electrons, and V_{12} is the electron-electron repulsion. Since the system has been defined in terms of only two states, H_{DA} is equal to $\langle \Psi_I | H | \Psi_F \rangle$. Similarly, $H_{DA}^S = \langle \Psi_I^S | H | \Psi_F^S \rangle$ and $H_{DA}^T = \langle \Psi_I^T | H | \Psi_F^T \rangle$. The only difference between H_{DA}^S and H_{DA}^T is the sign of the two-electron matrix element, $\langle \Psi_I | V_{12} | \Psi_F \rangle$, which enters with a (+) sign for singlets and a (-) sign for triplets because of the different signs in the spatial parts of Ψ^S and Ψ^T . This may account for the smaller value of H_{DA}^T (referred to as ${}^3H_{DA}$ in the main text) in these donor-acceptor complexes. Theoretical work along these lines is in progress.³⁷

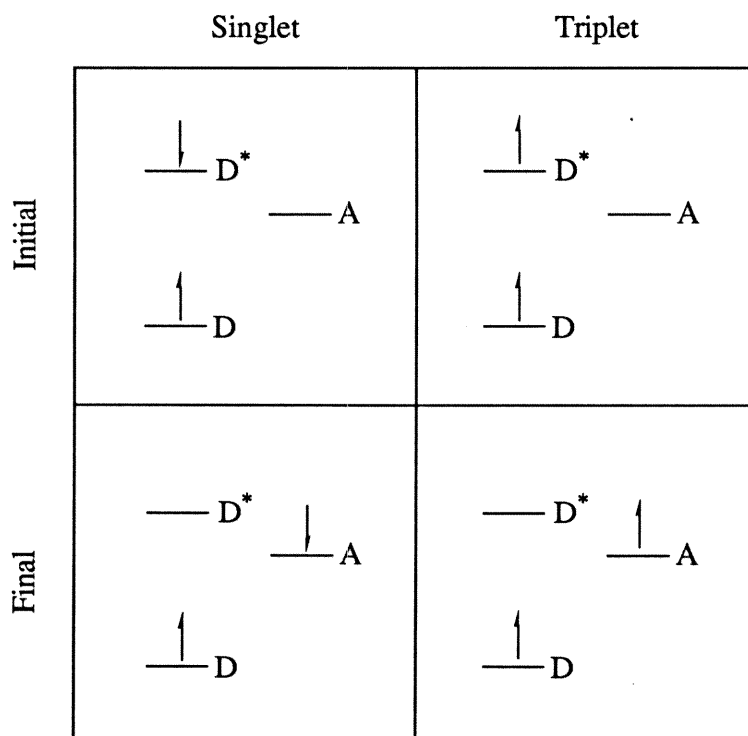


Figure 5.16. Schematic of initial and final states for singlet and triplet electron transfer in a two-electron system, showing the orthogonal molecular orbitals, D , D^* , and A .

REFERENCES

1. Winkler, J. R.; Nocera, D. G.; Netzel, T. L. *J. Am. Chem. Soc.* **1986**, *108*, 4451-4458.
2. Winkler, J. R.; Netzel, T. L.; Creutz, C. *J. Am. Chem. Soc.* **1987**, *109*, 2381-2392.
3. Nocera, D. G.; Winkler, J. R.; Yocom, K. M.; Bordignon, E.; Gray, H. B. *J. Am. Chem. Soc.* **1984**, *106*, 5145-5150.
4. Fox, L. S., Ph.D. Dissertation, California Institute of Technology, Pasadena, CA, 1989.
5. Fox, L. S.; Kozik, M.; Winkler, J. R.; Gray, H. B. *Science* **1990**, *247*, 1069-1071.
6. Marcus, R. A.; Sutin, N. *Biochim. Biophys. Acta* **1985**, *811*, 265-322.
7. Hoffmann, R.; Imamura, A.; Hehre, W. *J. Am. Chem. Soc.* **1968**, *90*, 1499-1509.
8. Hoffmann, R. *Acc. Chem. Res.* **1971**, *4*, 1-9.
9. Paddon-Row, M. N. *Acc. Chem. Res.* **1982**, *15*, 245-251.
10. Pasman, P.; Rob, F.; Verhoeven, J. W. *J. Am. Chem. Soc.* **1982**, *104*, 5127-5133.
11. Heitele, H.; Michel-Beyerle, M. E. *J. Am. Chem. Soc.* **1985**, *107*, 8286-8288.
12. Warman, J. M.; de-Haas, M. P.; Paddon-Row, M. N.; Cotsaris, E.; Hush, N. S.; Oevering, H.; Verhoeven, J. W. *Nature* **1986**, *320*, 615-616.
13. Heitele, H.; Michel-Beyerle, M. E.; Finckh, P. *Chem. Phys. Letters* **1987**, *134*, 273-278.
14. Oevering, H.; Paddon-Row, M. N.; Heppener, M.; Oliver, A. M.; Cotsaris, E.; Verhoeven, J. W.; Hush, N. S. *J. Am. Chem. Soc.* **1987**, *109*, 3258-3269.
15. Penfield, K. W.; Miller, J. R.; Paddon-Row, M. N.; Cotsaris, E.; Oliver, A. M.; Hush, N. S. *J. Am. Chem. Soc.* **1987**, *109*, 5061-5065.

16. Oliver, A. M.; Craig, D. C.; Paddon-Row, M. N.; Kroon, J.; Verhoeven, J. W. *Chem. Phys. Lett.* **1988**, *150*, 366-373.
17. Wasielewski, M. R.; Niemczyk, M. P.; Johnson, D. G.; Svec, W. A.; Minsek, D. W. *Tetrahedron* **1989**, *45*, 4785-4806.
18. Heilbronner, E.; Maier, J. P. In *Electron Spectroscopy: Theory, Techniques and Application*; Brundle, C. R.; Baker, A. D., Ed.; Academic Press: New York, 1977.
19. Heilbronner, E.; Martin, H. D. *Helv. Chim. Acta* **1972**, *55*, 1490.
20. Gleiter, R.; Heilbronner, E.; Hekman, M.; Martin, H. D. *Chem. Ber.* **1973**, *106*, 28.
21. Paddon-Row, M. N.; Patney, H. K.; Brown, R. S.; Houk, K. N. *J. Am. Chem. Soc.* **1981**, *103*, 5575.
22. Kemnitz, K. *Chem. Phys. Letters* **1988**, *152*, 305-310.
23. Mar, A.; Winnik, M. A. *Chem. Phys. Letters* **1981**, *77*, 73-76.
24. Jorgensen, W. L.; Salem, L. *The Organic Chemist's Book of Orbitals*; Academic Press: New York, 1973.
25. Closs, G. L.; Miller, J. R. *Science* **1988**, *240*, 440-447.
26. Marcus, R. A.; Sutin, N. *Biochim. Biophys. Acta* **1985**, *811*, 265-322.
27. Stein, C. A.; Lewis, N. A.; Seitz, G. *J. Am. Chem. Soc.* **1982**, *104*, 2596-2599.
28. Miller, J. R.; Beitz, J. V.; Huddleston, R. K. *J. Am. Chem. Soc.* **1984**, *106*, 5057-5068.
29. Joran, A. D.; Leland, B. A.; Geller, G. G.; Hopfield, J. J.; Dervan, P. B. *J. Am. Chem. Soc.* **1984**, *106*, 6090-6092.
30. Leland, B. A.; Joran, A. D.; Felker, P. M.; Hopfield, J. J.; Zewail, A. H.; Dervan, P. B. *J. Phys. Chem.* **1985**, *89*, 5571-5573.

31. Closs, G. L.; Calcaterra, L. T.; Green, N. J.; Penfield, K. W.; Miller, J. R. *J. Phys. Chem.* **1986**, *90*, 3673-3683.
32. Isied, S. S.; Vassilian, A.; Wishart, J. F. *J. Am. Chem. Soc.* **1988**, *110*, 635-637.
33. Schanze, K. S.; Sauer, K. *J. Am. Chem. Soc.* **1988**, *110*, 1180-1186.
34. Roberts, J. D. *Molecular Orbital Calculations*; W. A. Benjamin, Inc.: New York, 1961.
35. Kopineck, H. J. Z. *Naturforsch* **1950**, *5A*, 420.
36. Verhoeven, J. W.; Dirkx, I. P.; de Boer, T. J. *Tetrahedron* **1966**, *37*, 4399-4404.
37. Beratan, D. N.; Farid, R. S.; Onuchic, J. N.; Gray, H. B. *work in progress*.

Appendix Supplementary material for the X-ray crystal structure determination of
 $[\text{Ir}(\mu\text{-pz}^*)(\text{CO})(\text{Ph}_2\text{P-O-C}_6\text{H}_4\text{-CH}_3)]_2$

Table A.1. Crystal and Intensity Collection Data

Formula: $\text{Ir}_2\text{C}_{50}\text{H}_{48}\text{N}_4\text{O}_4\text{P}_2 \cdot \text{CH}_2\text{Cl}_2$	Formula weight: 1300.28
Crystal color: Orange/red	Habit: Irregular
Space group: $\text{P}2_1/\text{c}$ (#14)	
$a = 18.677(2)\text{\AA}$	
$b = 13.817(1)\text{\AA}$	$\beta = 101.37(1)^\circ$
$c = 20.225(3)\text{\AA}$	
$V = 5116.8(10)\text{\AA}^3$	
$\rho_{\text{calc}} = 1.688 \text{ g cm}^{-3}$	
$\mu = 57.28 \text{ cm}^{-1}$ ($\mu_{\text{Tmax}} = 5.70$)	Transmission coeff. = 0.39 – 0.54
	ω scan
$\lambda = 0.7107\text{\AA}$	Graphite monochromator
2θ range: 3° – 45°	Octants collected: $\pm h, k, \pm l$
$T = 293^\circ\text{K}$	
Number of reflections measured: 14173	
Number of independent reflections: 6662	
Number with $F_o^2 > 0$: 6470	
Number with $F_o^2 > 3\sigma(F_o^2)$: 5547	
Number of reflections used in refinement: 6662	
Goodness of fit for merging data: 1.02	
Final R-index: 0.0316 for 6470 reflections with $F_o^2 > 0$	
Final R-index: 0.0235 for 5547 reflections with $F_o^2 > 3\sigma(F_o^2)$	
Final goodness of fit: 1.46 for 588 parameters and 6662 reflections	

Table A.2. Final Non-Hydrogen Coordinates and Displacement Parameters

x, y, z and $U_{eq}^a \times 10^4$				
Atom	x	y	z	U_{eq}
Ir1	2540(.1)	593(.1)	8324(.1)	370
Ir2	2248(.1)	2833(.2)	8783(.1)	384
P1	2457(1)	−576(1)	9062(1)	438(3)
P2	3275(1)	3689(1)	9024(1)	444(3)
NP1A	2567(2)	1700(3)	7636(2)	408(10)
NP1B	2361(2)	2607(3)	7798(2)	407(11)
NP2A	1458(2)	1024(3)	8281(2)	430(11)
NP2B	1346(2)	1941(3)	8505(2)	444(11)
O1	4071(2)	45(3)	8293(2)	776(13)
O2	1901(3)	3201(3)	10135(2)	835(14)
O3	2176(2)	−1645(3)	8786(2)	576(10)
O4	3235(2)	4862(2)	9105(2)	560(10)
C1	3466(3)	257(4)	8308(3)	553(15)
C2	2050(3)	3056(4)	9611(3)	576(16)
CP1A	2700(3)	1753(4)	7005(3)	526(15)
CP1B	2360(3)	3200(4)	7278(3)	518(15)
CP1C	2577(3)	2681(4)	6771(3)	572(17)
CP1D	2934(4)	880(5)	6668(3)	884(22)
CP1E	2126(4)	4232(4)	7305(3)	733(20)
CP2A	811(3)	579(4)	8120(3)	547(16)

Atom	x	y	z	U_{eq}
CP2B	631(3)	2048(5)	8470(3)	593(17)
CP2C	281(3)	1204(5)	8231(3)	700(20)
CP2D	745(4)	−424(5)	7848(4)	842(21)
CP2E	318(4)	2971(5)	8673(4)	899(22)
CS1A	2366(3)	−2126(4)	8231(3)	506(14)
CS1B	1825(3)	−2647(4)	7831(3)	580(16)
CS1C	1987(3)	−3147(4)	7288(3)	663(18)
CS1D	2668(3)	−3135(4)	7136(3)	607(16)
CS1E	3199(3)	−2608(5)	7550(4)	728(19)
CS1F	3057(3)	−2108(4)	8100(3)	618(17)
CS1G	2830(4)	−3656(5)	6525(4)	895(21)
CS2A	2791(3)	5284(4)	9511(3)	522(15)
CS2B	3087(4)	5539(4)	10151(3)	659(17)
CS2C	2653(5)	5975(5)	10548(4)	863(24)
CS2D	1932(5)	6133(5)	10304(5)	898(25)
CS2E	1649(5)	5887(6)	9652(5)	1078(28)
CS2F	2078(4)	5465(5)	9249(4)	876(22)
CS2G	1439(6)	6555(6)	10748(6)	1621(39)
CA1A	3285(3)	−854(4)	9670(3)	492(14)
CA1B	3455(4)	−1792(4)	9904(3)	654(17)

Atom	x	y	z	U_{eq}
CA1C	4075(4)	−1951(5)	10400(4)	833(22)
CA1D	4508(4)	−1209(7)	10666(4)	882(24)
CA1E	4345(4)	−292(6)	10445(4)	833(22)
CA1F	3739(3)	−111(5)	9947(3)	652(17)
CA2A	3914(3)	3350(4)	9793(3)	475(13)
CA2B	4586(3)	3813(5)	9961(3)	669(17)
CA2C	5068(3)	3585(5)	10544(3)	748(19)
CA2D	4890(4)	2900(6)	10971(3)	807(21)
CA2E	4233(4)	2420(6)	10808(3)	847(22)
CA2F	3758(3)	2641(4)	10213(3)	641(17)
CB2A	3859(3)	3707(4)	8405(2)	470(14)
CB2B	4139(3)	2829(4)	8237(3)	561(15)
CB2C	4623(3)	2792(5)	7798(3)	686(17)
CB2D	4817(4)	3639(6)	7520(3)	791(20)
CB2E	4531(4)	4502(5)	7673(4)	835(21)
CB2F	4055(4)	4555(4)	8117(3)	692(18)
CB1A	1804(3)	−385(4)	9609(3)	443(13)
CB1B	1787(3)	525(4)	9900(3)	599(16)
CB1C	1326(3)	710(5)	10341(3)	660(17)
CB1D	882(3)	−5(6)	10491(3)	704(19)

Atom	x	y	z	U_{eq}
CB1E	891(3)	−890(5)	10210(4)	744(19)
CB1F	1348(3)	−1096(4)	9770(3)	611(16)
Cl1	210(2)	2650(2)	6341(2)	1670(12)
Cl2	491(2)	716(3)	6059(2)	2264(18)
C3	790(5)	1722(7)	6512(5)	1322(35)

$$^a U_{eq} = \frac{1}{3} \sum_i \sum_j [U_{ij}(a_i^* a_j^*)(\vec{a}_i \cdot \vec{a}_j)]$$

Table A.3. Anisotropic Displacement Parameters

Atom	U_{11}	U_{22}	U_{33}	U_{12}	U_{13}	U_{23}
Ir1	353(1)	387(1)	373(1)	13(1)	78(1)	20(1)
Ir2	436(1)	408(1)	322(1)	25(1)	106(1)	–3(1)
P1	432(8)	404(8)	485(8)	–11(7)	111(6)	27(7)
P2	563(9)	405(8)	379(8)	–9(7)	131(7)	–11(6)
NP1A	470(26)	397(25)	393(25)	6(21)	176(20)	–42(20)
NP1B	523(27)	432(26)	260(23)	3(21)	64(19)	17(19)
NP2A	352(25)	467(27)	466(26)	–27(21)	69(20)	42(21)
NP2B	375(26)	507(29)	465(26)	61(21)	116(20)	25(21)
O1	483(26)	901(33)	995(35)	168(24)	269(24)	83(27)
O2	1046(37)	1044(37)	509(27)	–55(29)	379(26)	–147(25)
O3	724(27)	434(21)	616(24)	–95(20)	242(21)	–43(20)
O4	775(27)	380(21)	577(24)	–37(20)	262(21)	–24(18)
C1	595(40)	520(36)	583(38)	15(30)	214(31)	89(28)
C2	543(37)	573(39)	604(40)	–26(29)	90(31)	–48(31)
CP1A	667(39)	559(37)	363(31)	65(30)	126(27)	–63(28)
CP1B	628(38)	541(36)	363(31)	5(29)	41(27)	40(28)
CP1C	804(44)	634(40)	290(30)	31(33)	140(28)	73(29)
CP1D	1361(66)	843(52)	534(41)	250(45)	397(42)	–36(36)
CP1E	1087(55)	523(40)	560(40)	128(36)	94(36)	120(30)
CP2A	388(33)	620(38)	598(37)	–72(31)	10(27)	70(31)
CP2B	395(35)	766(44)	647(39)	138(33)	172(28)	107(34)
CP2C	347(34)	890(50)	855(47)	–81(36)	101(32)	129(40)
CP2D	672(45)	750(49)	1021(55)	–187(37)	–36(39)	47(41)
CP2E	677(47)	963(55)	1116(58)	245(41)	319(42)	16(46)
CS1A	567(38)	462(33)	483(33)	8(29)	87(28)	34(28)
CS1B	480(36)	619(39)	677(40)	–125(30)	200(30)	–59(32)
CS1C	627(43)	641(42)	720(44)	–149(33)	129(33)	–210(34)
CS1D	673(43)	556(39)	631(40)	–107(32)	220(33)	–66(31)
CS1E	571(41)	748(45)	926(51)	–36(35)	297(37)	–123(40)
CS1F	443(36)	612(39)	815(45)	–78(30)	163(31)	–192(35)
CS1G	1069(59)	934(55)	777(48)	–208(45)	411(43)	–222(41)
CS2A	656(41)	369(32)	577(38)	88(28)	212(32)	36(28)
CS2B	877(47)	530(37)	582(41)	16(35)	176(35)	–46(32)
CS2C	1532(78)	485(40)	706(48)	71(47)	547(53)	–7(34)
CS2D	1134(68)	467(42)	1312(75)	130(45)	772(62)	–10(46)
CS2E	871(59)	907(62)	1468(83)	239(47)	261(58)	–239(58)
CS2F	846(55)	779(51)	959(55)	213(43)	74(44)	–166(43)
CS2G	2221(113)	831(62)	2346(116)	137(67)	1753(101)	–174(69)
CA1A	497(34)	491(36)	512(34)	43(28)	161(27)	51(27)
CA1B	809(47)	553(39)	626(40)	111(34)	208(35)	101(32)

Atom	U_{11}	U_{22}	U_{33}	U_{12}	U_{13}	U_{23}
CA1C	886(56)	862(56)	733(49)	403(45)	117(42)	281(42)
CA1D	585(46)	1177(69)	834(53)	196(46)	17(38)	262(51)
CA1E	549(42)	1002(58)	846(51)	−202(39)	−109(36)	177(43)
CA1F	510(38)	647(41)	751(44)	−12(33)	4(32)	111(35)
CA2A	530(35)	464(32)	437(32)	−32(28)	108(26)	−45(27)
CA2B	704(43)	671(43)	581(39)	−138(35)	4(33)	64(33)
CA2C	621(43)	937(52)	649(42)	−156(37)	32(35)	9(38)
CA2D	708(47)	1128(59)	522(39)	−20(44)	−30(34)	103(40)
CA2E	767(49)	1121(60)	603(43)	−78(44)	11(36)	323(40)
CA2F	629(40)	714(43)	571(38)	−145(33)	94(31)	121(33)
CB2A	533(34)	501(35)	384(30)	−55(28)	110(26)	−1(26)
CB2B	606(38)	563(37)	539(35)	−47(31)	171(30)	−10(30)
CB2C	605(40)	831(48)	665(42)	95(36)	233(33)	−24(37)
CB2D	817(51)	960(55)	680(44)	−131(44)	354(38)	−89(41)
CB2E	1067(57)	804(52)	762(48)	−281(44)	493(43)	38(39)
CB2F	931(50)	564(41)	674(42)	−87(35)	387(38)	−7(32)
CB1A	423(31)	492(35)	416(31)	−13(26)	85(24)	23(25)
CB1B	673(40)	595(39)	555(37)	−74(33)	185(31)	−23(31)
CB1C	727(43)	739(45)	561(38)	95(36)	245(33)	−64(33)
CB1D	568(41)	944(54)	663(43)	100(39)	274(33)	92(40)
CB1E	617(42)	777(49)	948(52)	−90(36)	419(39)	65(40)
CB1F	636(40)	503(36)	743(42)	−81(31)	253(33)	37(32)
Cl1	1416(26)	1199(23)	2500(40)	452(19)	645(24)	384(23)
Cl2	2275(44)	1424(31)	2913(55)	305(29)	70(36)	−425(31)
C3	924(68)	1156(77)	1732(99)	−41(59)	−110(62)	392(72)

$U_{i,j}$ values have been multiplied by 10^4

The form of the displacement factor is:

$$\exp -2\pi^2(U_{11}h^2a^{*2} + U_{22}k^2b^{*2} + U_{33}\ell^2c^{*2} + 2U_{12}hka^*b^* + 2U_{13}h\ell a^*c^* + 2U_{23}k\ell b^*c^*)$$

Table A.4. Assigned Hydrogen Parameters

Atom	$x, y \text{ and } z \times 10^4$			B
	x	y	z	
HB1F	1349	-1724	9579	5.8
HB1E	577	-1380	10318	7.0
HB1D	565	120	10796	6.7
HB1C	1318	1332	10538	6.3
HB1B	2095	1025	9795	5.7
HB2F	3865	5161	8223	6.6
HB2E	4661	5078	7469	7.9
HB2D	5151	3623	7222	7.5
HB2C	4818	2190	7690	6.5
HB2B	3996	2246	8425	5.3
HA2F	3312	2293	10094	6.1
HA2E	4107	1940	11101	8.0
HA2D	5219	2755	11380	7.6
HA2C	5527	3903	10651	7.1
HA2B	4713	4295	9669	6.3
HA1F	3634	533	9794	6.2
HA1E	4651	229	10634	7.9
HA1D	4926	-1328	11008	8.4
HA1C	4196	-2591	10554	7.9
HA1B	3150	-2319	9725	6.2
HP2C	-229	1080	8158	6.6
HP1C	2632	2919	6343	5.4
HS1E	3677	-2588	7454	6.9
HS1F	3434	-1756	8384	5.8
HS1B	1346	-2665	7925	5.5
HS1C	1613	-3512	7011	6.3
HS2B	3589	5419	10329	6.2
HS2C	2863	6166	10996	8.2
HS2E	1148	6008	9473	10.2
HS2F	1877	5303	8794	8.3
HP1DA	3388	1016	6546	8.4
HP1DB	2572	745	6279	8.4
HP1DC	2981	356	6976	8.4
HP1EA	2544	4630	7344	6.9
HP1EB	1903	4307	7685	6.9
HP1EC	1787	4371	6901	6.9
HP2DA	871	-860	8215	8.0
HP2DB	1067	-491	7543	8.0
HP2DC	253	-523	7623	8.0

Atom	x	y	z	B
HP2EA	500	3489	8448	8.5
HP2EB	465	3039	9147	8.5
HP2EC	-199	2936	8548	8.5
HS1GA	3335	-3818	6613	8.5
HS1GB	2718	-3234	6150	8.5
HS1GC	2540	-4221	6455	8.5
HS2GA	1682	6500	11203	15.4
HS2GB	996	6201	10669	15.4
HS2GC	1350	7215	10627	15.4
H3A	852	1572	6978	12.5
H3B	1246	1909	6411	12.5

Table A.5. Complete Distances and Angles

Distance(Å)		Distance(Å)	
Ir1 - Ir2	3.307(1)	CS2A - CS2B	1.350(8)
Ir1 - C1	1.797(6)	CS2B - CS2C	1.385(10)
Ir2 - C2	1.810(6)	CS2C - CS2D	1.358(12)
Ir1 - P1	2.224(1)	CS2D - CS2E	1.362(13)
Ir2 - P2	2.224(1)	CS2E - CS2F	1.380(12)
Ir1 - NP1A	2.075(4)	CS2A - CS2F	1.356(9)
Ir2 - NP1B	2.068(4)	CS2D - CS2G	1.524(14)
Ir1 - NP2A	2.091(4)	CA1A - CA1B	1.395(8)
Ir2 - NP2B	2.073(4)	CA1A - CA1F	1.378(8)
C1 - O1	1.174(7)	CA1B - CA1C	1.393(10)
C2 - O2	1.165(7)	CA1C - CA1D	1.351(11)
P1 - O3	1.629(4)	CA1D - CA1E	1.358(11)
P1 - CA1A	1.817(5)	CA1E - CA1F	1.382(9)
P1 - CB1A	1.820(5)	CA2A - CA2B	1.390(8)
O3 - CS1A	1.410(6)	CA2A - CA2F	1.365(8)
P2 - O4	1.633(4)	CA2B - CA2C	1.371(9)
P2 - CA2A	1.826(5)	CA2C - CA2D	1.365(10)
P2 - CB2A	1.815(5)	CA2D - CA2E	1.378(10)
O4 - CS2A	1.404(7)	CA2E - CA2F	1.380(9)
NP1A - NP1B	1.370(6)	CB2A - CB2B	1.389(8)
NP1A - CP1A	1.349(7)	CB2A - CB2F	1.388(8)
NP1B - CP1B	1.334(7)	CB2B - CB2C	1.388(8)
CP1A - CP1C	1.371(8)	CB2C - CB2D	1.377(9)
CP1A - CP1D	1.493(9)	CB2D - CB2E	1.366(10)
CP1B - CP1C	1.377(8)	CB2E - CB2F	1.386(10)
CP1B - CP1E	1.494(8)	CB1A - CB1B	1.392(8)
NP2A - NP2B	1.376(6)	CB1A - CB1F	1.382(8)
NP2A - CP2A	1.337(7)	CB1B - CB1C	1.378(9)
NP2B - CP2B	1.332(7)	CB1C - CB1D	1.362(9)
CP2A - CP2C	1.365(9)	CB1D - CB1E	1.350(10)
CP2A - CP2D	1.488(9)	CB1E - CB1F	1.378(9)
CP2B - CP2C	1.377(9)	C3 - CL1	1.670(10)
CP2B - CP2E	1.493(9)	C3 - CL2	1.697(11)
CS1A - CS1B	1.368(8)	CP1C - HP1C	0.950
CS1B - CS1C	1.380(8)	CP1D - HP1DA	0.947
CS1C - CS1D	1.365(9)	CP1D - HP1DB	0.948
CS1D - CS1E	1.374(9)	CP1D - HP1DC	0.948
CS1E - CS1F	1.379(9)	CP1E - HP1EA	0.946
CS1A - CS1F	1.368(8)	CP1E - HP1EB	0.949
CS1D - CS1G	1.512(9)	CP1E - HP1EC	0.949

Distance(Å)		Distance(Å)	
CP2C - HP2C	0.950	CB2F - HB2F	0.950
CP2D - HP2DA	0.948	C3 - H3A	0.950
CP2D - HP2DB	0.947	C3 - H3B	0.950
CP2D - HP2DC	0.950		
CP2E - HP2EA	0.947		
CP2E - HP2EB	0.948		
CP2E - HP2EC	0.950		
CS1B - HS1B	0.950		
CS1C - HS1C	0.950		
CS1E - HS1E	0.950		
CS1F - HS1F	0.950		
CS1G - HS1GA	0.951		
CS1G - HS1GB	0.947		
CS1G - HS1GC	0.944		
CS2B - HS2B	0.950		
CS2C - HS2C	0.950		
CS2E - HS2E	0.950		
CS2F - HS2F	0.950		
CS2G - HS2GA	0.945		
CS2G - HS2GB	0.948		
CS2G - HS2GC	0.951		
CA1B - HA1B	0.950		
CA1C - HA1C	0.950		
CA1D - HA1D	0.950		
CA1E - HA1E	0.950		
CA1F - HA1F	0.950		
CB1B - HB1B	0.950		
CB1C - HB1C	0.950		
CB1D - HB1D	0.950		
CB1E - HB1E	0.950		
CB1F - HB1F	0.950		
CA2B - HA2B	0.950		
CA2C - HA2C	0.950		
CA2D - HA2D	0.950		
CA2E - HA2E	0.950		
CA2F - HA2F	0.950		
CB2B - HB2B	0.950		
CB2C - HB2C	0.950		
CB2D - HB2D	0.950		
CB2E - HB2E	0.950		

Angle(°)				Angle(°)			
NP1A - Ir1 - NP2A	85.1(2)	Ir2 - P2 - CA2A	116.2(2)				
NP1A - Ir1 - C1	91.6(2)	Ir2 - P2 - CB2A	117.8(2)				
P1 - Ir1 - C1	91.0(2)	CB2A - P2 - CA2A	102.1(2)				
P1 - Ir1 - NP2A	92.3(1)	CA2B - CA2A - P2	119.9(4)				
NP2A - Ir1 - C1	176.3(2)	CA2F - CA2A - P2	122.0(4)				
P1 - Ir1 - NP1A	177.4(1)	CB2B - CB2A - P2	117.5(4)				
NP1B - Ir2 - NP2B	83.1(2)	CB2F - CB2A - P2	123.0(4)				
NP2B - Ir2 - C2	92.9(2)	CA2A - P2 - O4	101.8(2)				
P2 - Ir2 - C2	91.8(2)	CB2A - P2 - O4	95.8(2)				
P2 - Ir2 - NP1B	92.5(1)	CS2A - O4 - P2	121.0(3)				
NP1B - Ir2 - C2	174.1(2)	CS2B - CS2A - O4	119.5(5)				
P2 - Ir2 - NP2B	174.2(1)	CS2F - CS2A - O4	119.6(5)				
Ir1 - NP1A - NP1B	117.9(3)	Ir1 - NP1A - CP1A	135.1(3)				
Ir1 - NP2A - NP2B	117.2(3)	CP1A - NP1A - NP1B	106.8(4)				
Ir2 - NP1B - NP1A	117.1(3)	CP1B - NP1B - NP1A	109.3(4)				
Ir2 - NP2B - NP2A	118.0(3)	Ir2 - NP1B - CP1B	133.0(3)				
NP1A - Ir1 - Ir2	61.7(1)	CP1C - CP1A - NP1A	109.2(5)				
NP2A - Ir1 - Ir2	62.2(1)	CP1D - CP1A - NP1A	120.8(5)				
P1 - Ir1 - Ir2	117.0(1)	CP1D - CP1A - CP1C	130.0(5)				
C1 - Ir1 - Ir2	117.4(2)	CP1C - CP1B - NP1B	108.2(5)				
NP1B - Ir2 - Ir1	62.3(1)	CP1E - CP1B - NP1B	120.8(5)				
NP2B - Ir2 - Ir1	62.5(1)	CP1E - CP1B - CP1C	130.9(5)				
P2 - Ir2 - Ir1	112.1(1)	CP1B - CP1C - CP1A	106.5(5)				
C2 - Ir2 - Ir1	119.6(2)	Ir1 - NP2A - CP2A	134.3(4)				
O1 - C1 - Ir1	179.3(5)	CP2A - NP2A - NP2B	108.4(4)				
O2 - C2 - Ir2	178.0(5)	CP2B - NP2B - NP2A	107.4(4)				
Ir1 - P1 - O3	119.3(1)	Ir2 - NP2B - CP2B	134.5(4)				
Ir1 - P1 - CA1A	116.5(2)	CP2C - CP2A - NP2A	108.6(5)				
Ir1 - P1 - CB1A	116.4(2)	CP2D - CP2A - NP2A	121.6(5)				
CB1A - P1 - CA1A	101.7(2)	CP2D - CP2A - CP2C	129.7(6)				
CA1B - CA1A - P1	122.2(4)	CP2C - CP2B - NP2B	109.1(5)				
CA1F - CA1A - P1	119.4(4)	CP2E - CP2B - NP2B	121.5(5)				
CB1B - CB1A - P1	117.6(4)	CP2E - CP2B - CP2C	129.5(6)				
CB1F - CB1A - P1	124.0(4)	CP2B - CP2C - CP2A	106.5(5)				
CA1A - P1 - O3	102.4(2)	CS1F - CS1A - CS1B	120.7(5)				
CB1A - P1 - O3	97.5(2)	CS1C - CS1B - CS1A	118.7(5)				
CS1A - O3 - P1	125.9(3)	CS1D - CS1C - CS1B	122.3(6)				
CS1B - CS1A - O3	116.5(5)	CS1E - CS1D - CS1C	117.5(6)				
CS1F - CS1A - O3	122.7(5)	CS1G - CS1D - CS1C	121.6(6)				
Ir2 - P2 - O4	119.7(1)	CS1G - CS1D - CS1E	120.9(6)				

Angle(°)			Angle(°)		
CS1F	- CS1E - CS1D	121.8(6)	HP1DB	- CP1D - HP1DA	110.6
CS1E	- CS1F - CS1A	119.0(6)	HP1DC	- CP1D - HP1DA	110.6
CS2F	- CS2A - CS2B	120.8(6)	HP1DC	- CP1D - HP1DB	110.7
CS2C	- CS2B - CS2A	119.6(6)	HP1EA	- CP1E - CP1B	108.4
CS2D	- CS2C - CS2B	120.6(7)	HP1EB	- CP1E - CP1B	108.2
CS2E	- CS2D - CS2C	118.7(8)	HP1EC	- CP1E - CP1B	108.2
CS2G	- CS2D - CS2C	121.2(8)	HP1EB	- CP1E - HP1EA	110.8
CS2G	- CS2D - CS2E	120.1(8)	HP1EC	- CP1E - HP1EA	110.8
CS2F	- CS2E - CS2D	121.2(8)	HP1EC	- CP1E - HP1EB	110.4
CS2E	- CS2F - CS2A	119.1(7)	HS1E	- CS1E - CS1D	119.1
CA1F	- CA1A - CA1B	118.3(5)	HS1E	- CS1E - CS1F	119.1
CA1C	- CA1B - CA1A	119.5(6)	HS1C	- CS1C - CS1B	118.8
CA1D	- CA1C - CA1B	121.0(7)	HS1C	- CS1C - CS1D	118.8
CA1E	- CA1D - CA1C	120.0(7)	HS1B	- CS1B - CS1A	120.7
CA1F	- CA1E - CA1D	120.4(7)	HS1B	- CS1B - CS1C	120.7
CA1E	- CA1F - CA1A	120.8(6)	HP2C	- CP2C - CP2A	126.8
CA2F	- CA2A - CA2B	118.1(5)	HP2C	- CP2C - CP2B	126.8
CA2C	- CA2B - CA2A	120.8(6)	HP2DA	- CP2D - CP2A	108.2
CA2D	- CA2C - CA2B	120.2(6)	HP2DB	- CP2D - CP2A	108.3
CA2E	- CA2D - CA2C	119.9(6)	HP2DC	- CP2D - CP2A	108.3
CA2F	- CA2E - CA2D	119.5(6)	HP2DB	- CP2D - HP2DA	110.8
CA2E	- CA2F - CA2A	121.4(6)	HP2DC	- CP2D - HP2DA	110.6
CB2F	- CB2A - CB2B	119.5(5)	HP2DC	- CP2D - HP2DB	110.7
CB2C	- CB2B - CB2A	120.8(5)	HP2EA	- CP2E - CP2B	108.4
CB2D	- CB2C - CB2B	119.2(6)	HP2EB	- CP2E - CP2B	108.2
CB2E	- CB2D - CB2C	120.2(7)	HP2EC	- CP2E - CP2B	108.4
CB2F	- CB2E - CB2D	121.5(7)	HP2EB	- CP2E - HP2EA	110.6
CB2E	- CB2F - CB2A	118.9(6)	HP2EC	- CP2E - HP2EA	110.7
CB1F	- CB1A - CB1B	118.4(5)	HP2EC	- CP2E - HP2EB	110.5
CB1C	- CB1B - CB1A	120.7(5)	HS1F	- CS1F - CS1A	120.5
CB1D	- CB1C - CB1B	119.7(6)	HS1F	- CS1F - CS1E	120.5
CB1E	- CB1D - CB1C	120.3(6)	HS1GA	- CS1G - CS1D	108.1
CB1F	- CB1E - CB1D	121.3(6)	HS1GB	- CS1G - CS1D	108.1
CB1E	- CB1F - CB1A	119.6(6)	HS1GC	- CS1G - CS1D	108.3
Cl2	- C3 - Cl1	112.8(6)	HS1GB	- CS1G - HS1GA	110.4
HP1C	- CP1C - CP1A	126.7	HS1GC	- CS1G - HS1GA	110.7
HP1C	- CP1C - CP1B	126.7	HS1GC	- CS1G - HS1GB	111.2
HP1DA	- CP1D - CP1A	108.3	HS2B	- CS2B - CS2A	120.2
HP1DB	- CP1D - CP1A	108.3	HS2B	- CS2B - CS2C	120.2
HP1DC	- CP1D - CP1A	108.3	HS2C	- CS2C - CS2B	119.7

Angle(°)			Angle(°)		
HS2C	- CS2C - CS2D	119.7	HB2F	- CB2F - CB2E	120.6
HS2E	- CS2E - CS2D	119.4	HB1B	- CB1B - CB1A	119.6
HS2E	- CS2E - CS2F	119.4	HB1B	- CB1B - CB1C	119.6
HS2F	- CS2F - CS2A	120.5	HB1C	- CB1C - CB1B	120.2
HS2F	- CS2F - CS2E	120.5	HB1C	- CB1C - CB1D	120.2
HS2GA	- CS2G - CS2D	108.3	HB1D	- CB1D - CB1C	119.9
HS2GB	- CS2G - CS2D	108.2	HB1D	- CB1D - CB1E	119.9
HS2GC	- CS2G - CS2D	108.1	HB1E	- CB1E - CB1D	119.3
HS2GB	- CS2G - HS2GA	111.1	HB1E	- CB1E - CB1F	119.3
HS2GC	- CS2G - HS2GA	110.7	HB1F	- CB1F - CB1A	120.2
HS2GC	- CS2G - HS2GB	110.4	HB1F	- CB1F - CB1E	120.2
HA1B	- CA1B - CA1A	120.3	H3A	- C3 - Cl1	108.6
HA1B	- CA1B - CA1C	120.3	H3B	- C3 - Cl1	108.6
HA1C	- CA1C - CA1B	119.5	H3A	- C3 - Cl2	108.7
HA1C	- CA1C - CA1D	119.5	H3B	- C3 - Cl2	108.7
HA1D	- CA1D - CA1C	120.0	H3B	- C3 - H3A	109.4
HA1D	- CA1D - CA1E	120.0			
HA1E	- CA1E - CA1D	119.8			
HA1E	- CA1E - CA1F	119.8			
HA1F	- CA1F - CA1A	119.6			
HA1F	- CA1F - CA1E	119.6			
HA2B	- CA2B - CA2A	119.6			
HA2B	- CA2B - CA2C	119.6			
HA2C	- CA2C - CA2B	119.9			
HA2C	- CA2C - CA2D	119.9			
HA2D	- CA2D - CA2C	120.1			
HA2D	- CA2D - CA2E	120.1			
HA2E	- CA2E - CA2D	120.3			
HA2E	- CA2E - CA2F	120.3			
HA2F	- CA2F - CA2A	119.3			
HA2F	- CA2F - CA2E	119.3			
HB2B	- CB2B - CB2A	119.6			
HB2B	- CB2B - CB2C	119.6			
HB2C	- CB2C - CB2B	120.4			
HB2C	- CB2C - CB2D	120.4			
HB2D	- CB2D - CB2C	119.9			
HB2D	- CB2D - CB2E	119.9			
HB2E	- CB2E - CB2D	119.3			
HB2E	- CB2E - CB2F	119.3			
HB2F	- CB2F - CB2A	120.6			

Table A.6. Observed and Calculated Structure Factors

The columns contain, in order, ℓ , $10F_{obs}$, $10F_{calc}$ and $10\left(\frac{F_{obs}^2 - F_{calc}^2}{\sigma F_{obs}^2}\right)$. A minus sign preceding F_{obs} indicates that F_{obs}^2 is negative.

-20 0 1				-12 0 1				-6 0 1				0 0 1			
4	651	597	26	2	958	925	23	2	186	53	38	2	552	432	143
6	730	721	5	4	224	234	-3	4	2275	2258	8	4	2877	2935	-23
-19 0 1				6	314	272	15	6	344	354	-7	6	2873	2871	0
2	251	227	7	8	2012	2063	-25	8	844	899	-48	8	1017	1033	-13
4	985	996	-6	10	1281	1300	-11	10	505	443	35	10	349	337	6
6	985	963	13	12	2291	2320	-12	12	926	932	-3	12	517	530	-8
8	379	405	-9	14	2016	2058	-21	14	2513	2529	-6	14	1750	1749	0
10	1610	1616	-3	16	904	878	17	16	213	174	8	16	273	115	30
-18 0 1				18	1339	1334	2	18	2102	2099	1	18	1543	1530	7
2	602	614	-6	-11 0 1				20	842	810	19	20	1347	1289	35
4	624	608	9	2	1429	1398	19	-5 0 1				1 0 1			
6	1024	1016	5	4	868	864	3	2	2295	2302	-3	2	5518	5551	-6
8	1585	1614	-17	6	1076	1069	4	4	1149	1099	39	4	3601	3742	-45
10	122	98	3	8	544	584	-25	6	1871	1846	14	6	1963	2040	-44
12	1578	1565	7	10	2007	2026	-9	8	1101	1076	18	8	1756	1719	21
-17 0 1				12	1551	1597	-26	10	575	625	-40	10	263	276	-5
2	112	70	5	14	2223	2244	-9	12	1808	1836	-15	12	201	215	-5
4	846	832	9	16	1803	1833	-17	14	223	240	-4	14	315	273	13
6	1208	1200	4	18	224	177	10	16	2494	2499	-2	16	1473	1460	7
8	128	149	-3	20	1132	1091	25	18	764	752	8	18	804	801	1
10	1943	1955	-6	-10 0 1				20	1783	1767	8	20	665	644	11
12	423	450	-11	2	966	976	-7	-4 0 1				2 0 1			
14	1058	1071	-8	4	643	645	-1	2	1317	1319	-1	0	5869	5876	-1
-16 0 1				6	803	788	11	4	4288	4379	-24	2	1589	1423	107
2	341	334	3	8	1662	1657	2	6	1295	1313	-13	4	2652	2653	0
4	819	826	-5	10	1048	1070	-15	8	1312	1355	-32	6	2367	2393	-11
6	435	399	18	12	2516	2544	-11	10	1134	1162	-20	8	748	751	-2
8	1566	1602	-22	14	1784	1827	-22	12	140	124	4	10	652	663	-8
10	518	459	31	16	756	778	-15	14	2197	2240	-19	12	412	385	13
12	1714	1736	-12	18	1718	1747	-16	16	418	426	-3	14	570	550	10
14	1202	1183	12	20	202	236	-7	18	2297	2298	0	16	245	158	19
16	956	923	20	-9 0 1				20	899	851	30	18	1071	1052	13
-15 0 1				2	1554	1514	24	-3 0 1				20	1362	1325	22
2	106	51	4	4	407	397	5	2	4115	4226	-30	3 0 1			
4	194	208	-3	6	1403	1457	-36	4	545	488	53	0	1041	1010	28
6	1353	1345	4	8	681	688	-5	6	1494	1549	-38	2	5216	5183	6
8	344	330	4	10	1661	1709	-28	8	320	274	26	4	1884	1836	27
10	1843	1891	-26	12	1696	1731	-19	10	471	469	0	6	3215	3268	-19
12	956	937	12	14	1702	1732	-16	12	1951	2017	-34	8	1703	1729	-15
14	1554	1569	-8	16	2099	2105	-3	14	342	348	-2	10	203	72	28
16	1304	1309	-3	18	236	143	22	16	2295	2308	-5	12	616	621	-2
-14 0 1				20	1533	1515	11	18	622	592	17	14	193	111	27
2	223	170	13	-8 0 1				20	1357	1338	11	16	810	781	20
4	561	570	-5	2	854	823	26	-2 0 1				18	902	873	19
6	126	90	4	4	989	1014	-21	2	1388	1383	4	20	345	287	17
8	1967	1986	-9	6	261	274	-6	4	2460	2519	-27	4 0 1			
10	1038	1071	-19	8	1874	1854	11	6	1180	1211	-25	0	5254	5357	-20
12	2122	2122	0	10	1235	1267	-21	8	1027	1045	-15	2	4579	4554	6
14	1605	1635	-18	12	1506	1541	-21	10	919	885	27	4	3323	3230	31
16	999	993	4	14	2306	2356	-22	12	180	120	14	6	1734	1705	17
18	1074	1045	18	16	312	240	18	14	2376	2362	6	8	470	465	2
-13 0 1				18	1838	1825	7	16	356	331	10	10	1716	1705	6
2	816	812	3	20	524	544	-9	18	1806	1821	-8	12	251	41	37
4	227	155	19	-7 0 1				20	1255	1211	27	14	127	73	6
6	1517	1485	18	2	2499	2492	3	-1 0 1				16	527	535	-4
8	829	778	30	4	964	980	-13	2	5728	5710	3	18	648	652	-2
10	2400	2419	-8	6	452	458	-4	4	407	359	42	20	1268	1246	13
12	1501	1499	0	8	1073	1077	-2	6	2942	3035	-36	5 0 1			
14	1759	1739	11	10	1966	1992	-13	8	494	380	72	0	1970	1846	66
16	1645	1638	4	12	1977	2042	-33	10	133	67	14	2	3211	3179	11
18	493	473	9	14	885	894	-5	12	1924	1975	-27	4	3604	3552	16
				16	2216	2204	5	14	209	52	27	6	1239	1228	8
				18	540	512	15	16	1987	1986	0	8	2555	2647	-39
				20	1618	1603	9	18	921	891	21	10	296	49	48
								20	1102	1080	14	12	998	983	9
												14	164	29	13

16	406	368	17	0	1561	1565	-2	7	641	631	5	1	207	175	7
18	949	924	16	2	2519	2469	20	8	928	919	5	2	380	379	0
				4	750	721	17	9	330	365	-11	3	1321	1305	10
	6	0	1	6	2075	2019	26	10	132	220	-16	4	401	415	-5
				8	681	698	-8					5	827	833	-3
0	3929	3983	-15	10	1317	1289	18	-18	1	1		6	1021	1009	7
2	4227	4207	5	12	986	988	-1					7	136	64	7
4	2830	2814	6	14	273	206	19	1	494	488	2	8	826	838	-7
6	3308	3283	8					2	555	529	13	9	1406	1416	-5
8	541	412	64	13	0	1		3	889	867	14	10	1006	1025	-10
10	1746	1771	-13					4	346	331	5	11	647	679	-20
12	319	137	40	0	831	814	10	5	600	611	-6	12	1113	1113	0
14	378	404	-8	2	1033	1035	0	6	997	974	15	13	171	116	9
16	283	255	9	4	1779	1744	18	7	125	60	7	14	836	830	4
18	407	420	-5	6	298	282	4	8	102	87	1	15	613	614	0
				8	1751	1724	15	9	674	658	9	16	750	737	8
	7	0	1	10	862	835	18	10	942	922	12	17	668	668	0
				12	685	657	16	11	701	667	19	18	649	638	5
								12	111	131	-2				
0	1949	1923	14	14	0	1		13	-36	34	-1	-13	1	1	
2	3278	3206	24												
4	3308	3321	-4	0	944	937	4	-17	1	1		1	1589	1580	5
6	2218	2213	2	2	1082	1062	12	1	1162	1164	-1	2	616	617	0
8	3248	3371	-43	4	159	84	19	2	-135	72	-14	3	487	494	-3
10	328	243	23	6	1590	1609	-11	3	174	148	5	4	560	544	8
12	1138	1090	28	8	284	264	6	4	724	690	22	5	868	862	4
14	461	384	36	10	1066	1035	20	5	403	385	8	6	687	705	-10
16	150	132	3	12	1039	1011	18	6	202	126	16	7	1647	1631	8
18	700	679	12					7	818	847	-19	8	1082	1067	9
	8	0	1	15	0	1		8	1002	984	12	9	216	178	9
				0	102	28	6	9	355	361	-2	10	1064	1091	-17
0	2419	2413	2	2	658	665	-3	10	78	43	2	11	821	829	-4
2	3595	3512	25	4	1211	1182	19	11	398	411	-5	12	1247	1246	0
4	2533	2480	23	6	79	97	-2	12	1025	1031	-3	13	920	937	-12
6	3587	3562	8	8	1251	1228	15	13	672	679	-3	14	984	1004	-13
8	754	716	25	10	773	781	-4	14	469	445	10	15	480	457	11
10	2126	2198	-35									16	464	444	9
12	554	536	7	16	0	1		-16	1	1		17	325	337	-4
14	471	419	25	0	373	383	-4	1	351	322	12	18	843	816	17
16	144	116	4	2	455	423	15	2	676	650	17	-12	1	1	
	9	0	1	4	152	33	15	3	774	764	7				
				6	1144	1105	25	4	97	92	0	1	557	523	19
0	1467	1461	3	8	603	556	25	5	752	767	-11	2	152	154	0
2	2338	2318	9					6	1036	1054	-12	3	1617	1662	-26
4	3043	2948	34	17	0	1		7	127	9	11	4	701	697	2
6	1413	1385	18	0	258	304	-16	8	141	206	-15	5	1287	1286	0
8	3072	2979	32	2	226	152	19	9	786	778	4	6	910	887	16
10	285	310	-8	4	993	975	12	10	1096	1114	-12	7	524	521	2
12	1232	1215	11	6	362	317	15	11	633	628	2	8	993	1002	-6
14	704	726	-14					12	322	338	-5	9	1446	1457	-6
16	186	35	20	18	0	1		13	172	114	10	10	1084	1058	16
	10	0	1	0	301	318	-5	14	792	810	-11	11	619	630	-5
				2	585	542	22	15	467	410	24	12	1380	1404	-14
2	3013	2999	5	4	218	105	20	16	528	539	-5	13	131	132	0
4	1421	1447	-16					-15	1	1		14	763	763	0
6	2984	2991	-2	19	0	1						15	781	809	-19
8	-77	7	-4	0	110	47	6	1	1139	1092	28	16	846	858	-8
10	1566	1554	7	2	245	205	10	2	255	249	1	17	632	638	-3
12	690	672	12					3	356	318	12	18	581	542	21
14	398	444	-19	-20	1	1		4	895	913	-10	19	26	59	-1
16	372	332	13					5	443	420	9	-11	1	1	
	11	0	1	3	812	796	9	6	268	214	14				
				4	352	298	17	7	1187	1189	-1	1	2361	2361	0
0	1681	1614	38	5	313	291	6	8	1046	996	28	2	881	888	-5
2	1585	1542	25					9	219	193	7	3	492	495	-2
4	3267	3228	13	-19	1	1		10	592	585	4	4	215	19	37
6	661	628	18					11	604	610	-3	5	1584	1565	11
8	2086	2041	21	1	894	871	14	12	1203	1228	-16	6	1304	1293	7
10	677	709	-23	2	233	250	-4	13	750	717	21	7	1373	1423	-33
12	736	749	-9	3	79	119	-4	14	736	743	-4	8	936	950	-9
14	716	747	-20	4	772	749	13	15	380	400	-8	9	51	52	0
	12	0	1	5	571	571	0	16	709	693	9	10	1108	1113	-3
				6	315	283	9	17	170	186	-3	11	868	891	-15
								-14	1	1		12	1160	1156	2
												13	1032	1005	16

14	1312	1332	-11	-7	1	1	5	609	577	29	11	1602	1639	-22	
15	193	150	10				6	1212	1241	-24	12	608	634	-17	
16	469	474	-2	1	2628	2660	-13	7	138	9	26	13	1810	1842	-17
17	433	448	-7	2	453	448	4	8	1258	1258	0	14	1029	1018	7
18	1033	1042	-6	3	600	573	24	9	1745	1802	-34	15	352	338	4
19	691	672	11	4	183	116	21	10	1244	1258	-9	16	812	837	-13
20	284	270	4	5	2004	1989	7	11	1460	1488	-18	17	754	749	3
	-10	1	1	6	861	905	-38	12	871	873	-1	18	981	986	-3
1	578	565	9	7	1184	1232	-36	13	1205	1243	-26	19	675	671	2
2	699	699	0	8	190	268	-32	14	585	607	-11	20	1006	993	8
3	2090	2107	-8	9	1150	1164	-10	15	1240	1264	-15	21	203	123	15
4	1339	1379	-27	10	1207	1234	-18	16	1509	1489	11		0	1	1
5	1252	1269	-12	11	1677	1708	-18	17	134	152	-3	1	1118	1136	-18
6	561	545	10	12	223	189	10	18	773	743	20	2	3358	3317	12
7	901	871	21	13	1330	1345	-9	19	133	4	12	3	2546	2540	2
8	1329	1386	-38	14	1742	1761	-10	20	1201	1185	10	4	1002	990	11
9	1424	1464	-25	15	101	85	2	21	407	379	11	5	3088	3121	-12
10	843	890	-33	16	178	152	4		-3	1	1	6	2012	2030	-9
11	870	898	-18	17	893	858	25	1	1299	1225	58	7	957	972	-14
12	1292	1323	-19	18	1249	1259	-6	2	917	861	56	8	456	458	-1
13	367	381	-5	19	419	428	-4	3	408	390	16	9	2489	2526	-16
14	474	500	-10	20	572	537	17	4	1524	1537	-9	10	1206	1216	-6
15	1021	1048	-15	21	418	366	20	5	314	171	77	11	934	959	-18
16	1128	1165	-27		-6	1	1	6	866	882	-15	12	-35	3	-1
17	551	541	6	1	1423	1413	6	7	2786	2827	-16	13	922	912	6
18	296	357	-22	2	1295	1303	-6	8	1446	1462	-11	14	721	735	-8
19	130	36	8	3	1817	1771	26	9	304	322	-10	15	1567	1562	2
20	969	987	-11	4	1231	1227	3	10	1015	1020	-4	16	969	957	7
	-9	1	1	5	1505	1487	12	11	1666	1718	-31	17	440	434	3
1	1988	1964	12	6	490	505	-12	12	1182	1188	-4	18	838	816	14
2	573	571	1	7	154	88	16	13	1661	1669	-4	19	335	300	12
3	301	273	14	8	611	639	-23	14	1471	1499	-16	20	628	624	2
4	265	239	10	9	1486	1502	-10	15	312	311	0	21	586	530	27
5	1532	1546	-8	10	922	898	18	16	847	833	8		1	1	1
6	930	921	7	11	1380	1423	-28	17	664	651	6	0	3965	3918	12
7	1627	1623	2	12	1444	1486	-26	18	1406	1412	-4	1	2529	2521	3
8	568	530	24	13	915	938	-15	19	502	450	26	2	1016	1064	-49
9	271	239	12	14	231	258	-8	20	873	837	23	3	286	286	0
10	1014	1054	-28	15	1417	1447	-18	21	252	206	11	4	3380	3330	16
11	993	996	-2	16	1535	1557	-11		-2	1	1	5	1431	1432	0
12	565	571	-3	17	236	256	-6	1	1656	1584	47	6	1488	1482	4
13	1461	1483	-13	18	506	496	5	2	3543	3407	37	7	2468	2521	-24
14	1613	1647	-18	19	142	95	8	3	2425	2383	19	8	1800	1762	21
15	168	181	-3	20	1303	1282	12	4	1358	1350	6	9	171	127	21
16	333	351	-7	21	351	342	3	5	1511	1520	-6	10	206	169	12
17	666	652	9		-5	1	1	6	3208	3286	-27	11	1335	1381	-31
18	1160	1155	3	1	2113	2071	21	7	549	542	6	12	691	693	0
19	595	589	3	2	197	108	35	8	978	992	-12	13	1760	1778	-9
20	154	82	9	3	223	180	22	9	1921	2004	-46	14	440	440	0
	-8	1	1	4	1401	1384	12	10	1793	1828	-19	15	153	26	22
1	498	504	-4	5	1814	1848	-20	11	1084	1116	-24	16	762	738	13
2	763	724	33	6	341	261	41	12	744	749	-4	17	877	858	13
3	2366	2379	-5	7	1499	1525	-17	13	1297	1314	-11	18	657	628	18
4	161	123	11	8	1544	1571	-17	14	890	916	-16	19	678	638	24
5	826	861	-30	9	1330	1338	-5	15	1404	1424	-11	20	984	975	6
6	667	665	2	10	977	993	-12	16	1378	1385	-3	21	239	114	24
7	1057	1094	-28	11	1605	1623	-10	17	441	397	23		2	1	1
8	1290	1291	0	12	230	251	-7	18	684	675	5	0	734	687	57
9	1144	1173	-20	13	1339	1380	-26	19	188	121	13	1	186	93	60
10	476	467	5	14	1662	1691	-16	20	822	807	9	2	3219	3144	26
11	1636	1647	-6	15	221	211	2	21	421	409	5	3	3080	3087	-2
12	1444	1469	-15	16	364	385	-7		-1	1	1	4	693	658	36
13	560	606	-26	17	969	961	5	1	1959	1852	61	5	1386	1361	18
14	188	202	-3	18	1399	1390	6	2	1095	1055	39	6	2309	2277	15
15	1310	1326	-9	19	265	232	10	3	242	170	57	7	1284	1280	2
16	1262	1233	17	20	797	763	21	4	3033	3056	-8	8	706	672	28
17	476	489	-7	21	408	350	21	5	3352	3386	-11	9	1115	1123	-5
18	120	52	7		-4	1	1	6	696	664	31	10	877	925	-39
19	125	53	9	1	1409	1397	9	7	3156	3191	-12	11	985	1019	-24
20	1079	1060	12	2	1403	1374	21	8	1903	1985	-46	12	526	480	25
21	445	446	0	3	2369	2362	2	9	327	324	1	13	900	888	8
				4	712	714	-2	10	180	146	10	14	797	789	4

15	1555	1564	-4	6	1	1	10	1543	1583	-23	10	904	879	16	
16	313	251	20				11	1227	1236	-5	11	641	625	9	
17	444	436	4	0	2499	2474	11	12	290	213	26	12	482	519	-18
18	825	799	17	1	2010	2001	4	13	1042	1034	5	13	552	540	5
19	539	511	14	2	2577	2546	13	14	742	758	-10				
20	419	365	20	3	2335	2291	20	15	128	85	5	14	1	1	
				4	2163	2141	10	16	127	161	-5				
3	1	1		5	311	188	60	17	853	819	20	0	712	655	32
				6	476	484	-5					1	1084	1080	2
0	1765	1655	67	7	175	166	3	10	1	1		2	132	142	-1
1	2066	2003	34	8	2174	2187	-6					3	969	932	22
2	1246	1184	50	9	1235	1268	-23	0	1712	1699	7	4	892	834	32
3	468	478	-11	10	913	907	4	1	1959	1917	21	5	200	102	21
4	874	839	34	11	983	995	-7	2	772	728	32	6	345	354	-3
5	1369	1388	-14	12	1169	1154	8	3	1314	1252	40	7	669	653	10
6	863	855	7	13	723	728	-3	4	2487	2456	13	8	1081	1039	28
7	1863	1853	5	14	574	573	0	5	320	339	-8	9	558	569	-6
8	1178	1196	-13	15	1342	1327	9	6	647	605	25	10	508	509	0
9	107	22	9	16	300	266	11	7	478	429	23	11	166	176	-1
10	905	928	-17	17	260	259	0	8	1487	1466	12	12	795	749	27
11	1292	1257	23	18	713	661	29	9	1312	1288	14				
12	980	983	-1	19	669	596	39	10	-47	78	-7	15	1	1	
13	1479	1492	-7					11	785	815	-22				
14	139	115	3	7	1	1		12	1248	1249	-1	0	407	424	-6
15	100	108	0					13	555	567	-6	1	775	747	15
16	894	899	-3	0	1722	1690	19	14	84	117	-4	2	382	360	9
17	1097	1088	6	1	1643	1596	29	15	1007	977	19	3	771	779	-5
18	215	183	8	2	2370	2300	32	16	299	342	-14	4	450	410	20
19	479	474	2	3	716	717	-1					5	815	808	4
20	983	957	16	4	801	785	13	11	1	1		6	1093	1047	31
				5	878	821	45					7	310	273	13
4	1	1		6	2221	2200	10	0	204	193	3	8	447	417	13
				7	445	422	14	1	1080	1092	-8	9	387	357	11
0	1257	1205	39	8	621	615	4	2	2156	2109	22	10	828	775	32
1	1655	1635	13	9	377	353	12	3	411	488	-40				
2	1775	1725	30	10	1742	1726	8	4	131	205	-16	16	1	1	
3	3300	3328	-9	11	1229	1240	-6	5	987	963	16				
4	354	265	58	12	528	496	14	6	1767	1720	25	0	225	142	20
5	554	560	-5	13	1328	1309	10	7	853	810	26	1	1086	1052	23
6	872	895	-21	14	767	736	20	8	321	340	-6	2	461	476	-7
7	591	575	14	15	260	205	16	9	-104	76	-8	3	998	986	8
8	1476	1507	-20	16	484	449	17	10	1286	1251	24	4	618	607	6
9	1312	1337	-17	17	899	853	29	11	973	948	17	5	271	191	21
10	1545	1540	3	18	164	161	0	12	219	227	-2	6	175	175	0
11	1134	1129	3					13	842	843	0	7	657	656	0
12	663	685	-13	8	1	1		14	652	644	5	8	829	797	19
13	734	747	-8					15	134	61	8	9	372	381	-3
14	721	713	4	0	1348	1372	-17								
15	1551	1534	9	1	2323	2313	4	12	1	1		17	1	1	
16	273	181	26	2	1100	1083	13								
17	365	331	14	3	1489	1504	-9	0	1346	1334	7	0	377	399	-9
18	928	918	6	4	2096	2089	3	1	1524	1481	25	1	829	834	-2
19	583	571	5	5	307	312	-2	2	204	88	21	2	328	270	18
20	253	21	34	6	1144	1156	-9	3	1243	1264	-13	3	577	589	-6
				7	522	496	16	4	1542	1525	9	4	331	323	2
5	1	1		8	1882	1925	-23	5	311	314	-1	5	945	923	13
				9	920	948	-19	6	181	4	19	6	741	684	33
0	3887	3804	24	10	435	436	0	7	559	556	1	7	225	234	-2
1	1919	1888	17					8	1434	1412	12				
2	2871	2796	29	11	968	995	-17	9	834	842	-5	18	1	1	
3	668	664	4	12	1373	1410	-22	10	372	368	2				
4	1369	1318	37	13	859	849	7	11	443	422	10	0	-73	23	-3
5	2167	2200	-16	14	282	206	24	12	760	735	15	1	950	899	32
6	1305	1349	-32	15	1254	1192	40	13	467	434	16	2	481	467	6
7	656	665	-7	16	369	336	12	14	352	351	0	3	1002	980	14
8	1034	1045	-8	17	223	212	2					4	468	423	18
9	682	707	-18					13	1	1		5	164	111	7
10	1168	1162	3	9	1	1									
11	1054	1047	4					0	-94	45	-7	19	1	1	
12	771	781	-5	0	1725	1695	17	1	912	900	7				
13	1595	1599	-2	1	1500	1472	17	2	1370	1329	24	0	458	456	1
14	633	639	-3	2	2555	2557	0	3	591	594	-1	1	752	756	-2
15	133	56	11	3	1196	1127	48	4	198	88	19	2	248	189	13
16	907	901	3	4	840	830	7	5	1025	977	28				
17	976	960	11	5	1112	1082	21	6	1223	1198	14	-19	2	1	
18	117	9	8	6	1929	1931	0	7	442	434	4				
19	437	419	6	7	704	710	-4	8	332	313	8	1	125	198	-11
				8	750	739	7	9	236	158	21	2	1020	992	18
				9	513	487	13								

3	809	788	12							12	672	659	7						
4	741	707	20	-14	2	1				13	169	200	-8	-7	2	1			
5	187	167	4							14	-65	65	-4						
6	464	434	13	1	1113	1061	31			15	344	349	-2	1	710	701	7		
7	327	259	20	2	1382	1385	-1			16	198	222	-6	2	987	955	26		
8	316	299	5	3	691	714	-12			17	538	507	16	3	1330	1337	-5		
9	267	310	-12	4	1125	1143	-10			18	713	703	6	4	3302	3252	17		
10	198	42	20	5	994	992	1			19	262	290	-8	5	1653	1629	14		
				6	1387	1355	18							6	1208	1200	4		
-18	2	1		7	995	943	31			-10	2	1		7	490	517	-19		
				8	176	66	15							8	2577	2595	-7		
1	963	953	6	9	138	131	0			1	2048	2040	4	9	1673	1681	-4		
2	663	631	18	10	550	540	5			2	2284	2257	12	10	1963	2006	-22		
3	207	134	17	11	499	500	0			3	865	883	-14	11	405	352	26		
4	742	710	20	12	138	14	12			4	420	449	-15	12	1068	1055	9		
5	653	655	-1	13	145	128	2			5	2132	2171	-19	13	888	887	0		
6	677	657	12	14	-141	12	-12			6	2075	2129	-27	14	706	741	-21		
7	366	391	-10	15	428	406	10			7	1590	1594	-2	15	596	606	-5		
8	204	248	-11	16	561	561	0			8	736	727	6	16	285	288	-1		
9	-78	62	-5	17	328	284	13			9	455	496	-22	17	460	463	-2		
10	158	56	15	18	-136	29	-9			10	1672	1714	-24	18	81	151	-11		
11	180	53	16							11	904	904	0	19	97	49	4		
12	96	104	-1	-13	2	1				12	417	450	-14	20	514	487	13		
				1	474	473	0			13	166	13	21	21	78	43	2		
-17	2	1		2	1741	1714	14			14	363	370	-2						
				3	1296	1279	10			15	360	329	14	-6	2	1			
1	121	151	-4	4	2000	2027	-13			16	145	116	5						
2	1202	1207	-3	5	1043	1067	-15			17	-75	14	-3	1	2100	2078	11		
3	831	816	9	6	532	493	19			18	362	359	1	2	2823	2755	26		
4	841	821	13	7	939	934	3			19	466	439	12	3	842	829	12		
5	438	449	-5	8	1580	1605	-14			20	750	739	6	4	128	94	9		
6	620	603	9	9	912	909	1												

4 1539 1530 5	10 3565 3650 -27	14 509 517 -3	6 2 1
5 410 385 21	11 513 556 -27	15 218 199 4	0 815 788 23
6 2499 2489 4	12 -128 47 -10	16 1664 1653 6	1 118 76 10
7 2786 2803 -6	13 1738 1745 -3	17 746 770 -16	2 887 881 6
8 1954 1980 -14	14 2417 2438 -9	18 442 397 19	3 336 354 -12
9 435 456 -14	15 714 740 -14	19 420 412 3	4 184 152 11
10 1897 1915 -10	16 174 143 4	20 525 535 -4	5 232 92 46
11 1779 1800 -11	17 365 349 7	3 2 1	6 461 433 20
12 2530 2584 -23	18 799 777 15	0 1370 1361 6	7 593 604 -8
13 928 935 -4	19 199 198 0	1 1330 1318 8	8 1795 1807 -6
14 673 688 -9	20 159 46 14	2 179 125 23	9 233 274 -16
15 734 743 -5	21 240 163 20	3 644 660 -17	10 382 370 5
16 1023 1002 13	0 2 1	4 440 416 22	11 582 633 -31
17 246 223 8	0 1180 1182 -1	5 1590 1618 -19	12 1793 1809 -8
18 130 151 -4	1 887 844 48	6 1811 1837 -15	13 1344 1304 24
19 -82 72 -7	2 863 872 -10	7 -88 45 -10	14 1111 1115 -2
20 90 177 -13	3 1316 1357 -33	8 865 899 -29	15 -59 166 -18
21 212 148 14	4 1716 1722 -3	9 1230 1252 -16	16 1140 1126 9
-3 2 1	5 1809 1792 10	10 2917 2960 -16	17 851 874 -14
1 185 168 10	6 1735 1711 15	11 672 710 -27	18 925 899 16
2 540 507 37	7 2815 2856 -16	12 257 260 0	7 2 1
3 529 518 12	8 3422 3476 -17	13 759 759 0	0 1933 1906 15
4 2169 2099 35	9 614 625 -8	14 1953 1951 1	1 1941 1859 44
5 2456 2455 0	10 818 831 -9	15 1370 1384 -7	2 634 629 3
6 1456 1455 1	11 2158 2163 -2	16 696 695 0	3 685 676 7
7 424 402 17	12 2908 2954 -17	17 299 306 -2	4 213 216 -1
8 2099 2139 -21	13 812 835 -14	18 1111 1115 -2	5 199 107 29
9 2267 2303 -17	14 497 526 -12	19 466 492 -12	6 678 692 -12
10 2341 2431 -42	15 360 367 -2	20 491 476 6	7 277 261 7
11 617 611 4	16 1400 1437 -21	4 2 1	8 464 435 17
12 763 736 18	17 628 649 -14	0 1306 1284 17	9 654 672 -13
13 1478 1501 -14	18 314 315 0	1 900 890 10	10 1568 1631 -38
14 1947 1979 -16	19 390 337 22	2 1323 1303 14	11 745 754 -5
15 632 694 -35	20 564 545 9	3 270 274 -2	12 971 984 -8
16 -153 77 -17	21 114 144 -4	4 170 125 18	13 471 495 -10
17 212 143 18	1 2 1	5 726 699 26	14 1426 1453 -17
18 649 632 11	0 470 428 56	6 243 173 33	15 1143 1127 10
19 137 45 11	1 2030 1973 31	7 1510 1566 -37	16 1001 1004 -2
20 223 257 -10	2 548 509 47	8 2314 2339 -11	17 217 169 10
21 116 50 6	3 103 41 16	9 460 498 -25	18 694 648 24
-2 2 1	4 201 41 58	10 43 24 0	8 2 1
1 488 443 52	5 2274 2256 8	11 910 901 6	0 407 370 22
2 1149 1107 37	6 1669 1653 10	12 2375 2376 0	1 407 349 37
3 2766 2701 26	7 192 184 3	13 1317 1311 4	2 1411 1419 -5
4 350 308 36	8 913 910 2	14 965 949 9	3 267 258 4
5 1864 1828 20	9 2448 2440 3	15 86 114 -5	4 358 330 16
6 2562 2508 23	10 2954 3003 -18	16 1480 1484 -2	5 401 364 22
7 2429 2444 -6	11 517 522 -2	17 1048 1070 -15	6 124 60 16
8 2611 2626 -6	12 166 220 -12	18 616 630 -7	7 415 453 -23
9 415 437 -15	13 722 680 27	19 374 334 14	8 835 853 -13
10 1478 1463 9	14 2205 2172 15	5 2 1	9 594 620 -17
11 2301 2343 -19	15 1082 1108 -16	0 2562 2503 25	10 675 667 4
12 2860 2896 -13	16 519 514 2	1 947 951 -2	11 769 760 5
13 764 810 -29	17 247 269 -7	2 516 506 8	12 1508 1509 0
14 -97 112 -12	18 1015 974 28	3 177 206 -14	13 920 927 -5
15 868 873 -3	19 306 299 2	4 350 349 0	14 1114 1125 -7
16 1471 1446 14	20 163 151 2	5 206 173 15	15 175 47 17
17 303 325 -8	2 2 1	6 1191 1198 -5	16 887 849 23
18 245 102 35	0 307 280 26	7 241 236 2	17 883 857 15
19 217 195 5	1 1707 1738 -20	8 175 147 9	9 2 1
20 478 454 11	2 2017 2006 5	9 1122 1124 -1	0 2050 2045 2
21 151 55 10	3 2850 2845 2	10 2317 2317 0	1 2021 2007 7
-1 2 1	4 281 211 49	11 841 835 3	2 1198 1193 3
1 337 350 -15	5 574 606 -36	12 920 893 16	3 597 573 17
2 549 536 16	6 961 957 3	13 449 448 0	4 570 581 -7
3 1030 1025 4	7 1833 1857 -14	14 1804 1756 24	5 391 361 16
4 2521 2486 15	8 2433 2433 0	15 1330 1337 -4	6 159 61 19
5 1540 1537 1	9 541 512 20	16 887 873 9	7 -70 4 -4
6 3017 3027 -4	10 593 616 -15	17 180 149 5	8 299 267 11
7 131 2 24	11 1355 1387 -21	18 851 833 11	9 977 1011 -22
8 1955 1996 -22	12 2768 2789 -8	19 608 559 25	10 1145 1160 -9
9 2646 2716 -29	13 1201 1188 8		

11 742 730 6	12 683 654 17	5 114 78 3	2 1473 1458 8
12 1007 1015 -6	13 141 141 0	6 834 826 4	3 274 191 22
13 419 377 20		7 680 692 -6	4 1939 1921 9
14 987 992 -3	14 2 1	8 151 99 6	5 301 321 -6
15 988 1001 -9		9 498 504 -2	6 421 404 6
16 1243 1203 24	0 1580 1583 -1		7 537 470 31
	1 225 203 7	-18 3 1	8 1594 1625 -17
10 2 1	2 994 982 6		9 301 259 12
	3 442 396 17	1 -95 102 -10	10 189 127 14
0 1455 1431 15	4 1498 1457 22	2 862 846 10	11 1150 1155 -3
1 293 287 2	5 498 512 -7	3 -37 67 -3	12 283 266 7
2 1530 1518 7	6 132 77 7	4 1208 1164 27	13 128 93 5
3 367 330 18	7 -78 62 -6	5 587 585 0	14 100 17 5
4 1019 1029 -7	8 234 218 4	6 316 271 14	15 741 744 -2
5 272 292 -7	9 291 272 6	7 366 335 11	16 483 501 -8
6 210 173 10	10 253 201 13	8 725 717 5	17 276 201 19
7 684 684 0	11 223 200 7	9 641 668 -15	
8 248 242 1	12 404 370 13	10 122 140 -3	-13 3 1
9 264 207 18		11 583 578 2	
10 721 709 7	15 2 1	12 327 371 -15	1 239 194 14
11 718 712 4			2 1894 1900 -3
12 1068 1073 -4	0 922 923 0	-17 3 1	3 297 250 14
13 884 905 -15	1 891 879 6		4 747 752 -3
14 1111 1136 -17	2 1526 1551 -15	1 -138 35 -11	5 287 270 5
15 57 26 1	3 841 821 14	2 1307 1321 -8	6 2091 2059 15
16 625 622 1	4 415 418 -1	3 310 291 7	7 464 466 -1
	5 322 281 14	4 593 588 3	8 157 89 10
11 2 1	6 734 735 0	5 315 280 11	9 962 969 -3
	7 456 448 3	6 1084 1060 16	10 977 957 11
0 2054 2031 11	8 152 158 -1	7 521 555 -18	11 -127 134 -16
1 1544 1503 24	9 186 199 -3	8 172 107 11	12 420 436 -8
2 1416 1380 22	10 -100 38 -6	9 706 715 -5	13 1086 1091 -3
3 633 575 35		10 234 219 3	14 190 103 17
4 352 373 -8	16 2 1	11 410 421 -4	15 130 124 1
5 374 357 6		12 218 217 0	16 523 520 1
6 391 321 28	0 1424 1409 10	13 575 556 9	17 774 795 -12
7 396 376 8	1 610 617 -4	14 613 609 2	18 298 279 5
8 339 312 11	2 682 655 16		
9 592 608 -8	3 691 661 18	-16 3 1	-12 3 1
10 590 564 17	4 1352 1376 -15		
11 539 543 -2	5 627 624 2	1 151 149 0	1 792 784 5
12 754 809 -38	6 88 143 -7	2 1067 1067 0	2 1410 1379 19
13 365 353 5	7 -167 32 -20	3 337 306 12	3 331 323 3
14 720 697 14	8 448 386 26	4 1444 1444 0	4 2307 2328 -9
15 602 628 -14	9 384 373 4	5 505 502 1	5 297 244 17
		6 390 377 5	6 210 163 12
12 2 1	17 2 1	7 427 435 -3	7 775 773 1
		8 870 850 13	8 1878 1878 0
0 1744 1735 5	0 626 617 5	9 334 359 -9	9 426 374 20
1 188 217 -8	1 1045 1030 10	10 88 79 1	10 445 418 11
2 1225 1231 -3	2 1416 1409 4	11 748 745 1	11 1315 1332 -10
3 514 530 -8	3 812 808 2	12 114 172 -9	12 439 394 17
4 1339 1342 -1	4 -57 6 -1	13 178 86 16	13 160 7 19
5 407 386 8	5 180 121 10	14 391 372 7	14 325 334 -3
6 161 65 13	6 794 804 -5	15 690 689 0	15 1162 1143 13
7 471 462 4	7 550 569 -9		16 412 381 13
8 74 2 4		-15 3 1	17 316 337 -7
9 171 146 5	18 2 1		18 894 883 7
10 423 417 3		1 203 110 15	19 631 627 1
11 482 449 17	0 1276 1258 11	2 1488 1456 17	
12 451 460 -4	1 564 525 19	3 130 46 8	-11 3 1
13 497 512 -8	2 197 196 0	4 883 869 8	
14 859 843 10	3 425 413 4	5 457 452 2	1 234 213 6
	4 1145 1137 5	6 1594 1596 0	2 2326 2347 -9
13 2 1	5 750 718 18	7 505 499 3	3 618 609 6
		8 217 284 -22	4 976 960 11
0 1286 1269 10	19 2 1	9 790 811 -14	5 599 589 6
1 1175 1174 0		10 443 419 12	6 2455 2478 -9
2 1933 1936 -1	0 311 256 15	11 166 44 16	7 410 378 14
3 715 695 11	1 684 661 12	12 181 26 22	8 743 714 19
4 472 418 22	2 1170 1159 6	13 817 810 4	9 1398 1396 1
5 76 107 -2		14 201 214 -3	10 1562 1604 -24
6 777 766 6	-19 3 1	15 -69 28 -3	11 47 111 -5
7 362 358 1		16 689 666 13	12 598 585 6
8 -65 22 -3	1 -55 0 -1		13 1154 1170 -9
9 406 395 5	2 678 696 -10	-14 3 1	14 146 31 17
10 168 182 -3	3 370 382 -4		15 236 235 0
11 125 200 -15	4 618 620 -1	1 347 364 -5	16 299 283 6

17	874	893	-13	4	196	139	18	10	2179	2218	-18	16	1208	1205	1
18	20	16	0	5	713	701	9	11	395	386	4	17	447	472	-13
19	448	394	22	6	3961	3924	10	12	730	730	0	18	656	642	8
-10	3	1		7	-12	40	-1	13	960	964	-2	19	981	963	12
1	657	668	-8	8	1213	1236	-16	14	1095	1103	-5	20	180	236	-13
2	905	863	31	9	738	706	23	15	526	533	-3	21	209	231	-5
3	103	65	5	10	2183	2213	-14	16	349	293	18	0	3	1	
4	3198	3190	2	11	438	425	8	17	684	692	-5	1	2747	2722	10
5	495	480	8	12	1349	1364	-9	18	256	225	10	2	400	392	8
6	409	429	-11	13	1259	1294	-22	19	329	292	13	3	1093	1082	9
7	1068	1059	6	14	408	430	-10	20	144	97	6	4	2838	2847	-3
8	2697	2666	12	15	360	360	0	21	810	769	24	5	432	430	1
9	-52	57	-3	16	211	238	-8	-3	3	1		6	1820	1841	-12
10	1297	1348	-32	17	592	578	8	1	502	437	64	7	1253	1238	11
11	1365	1367	-1	18	232	157	19	2	3235	3224	3	8	2275	2258	8
12	956	950	3	19	857	857	0	3	421	396	22	9	4	78	-7
13	327	313	4	20	605	573	17	4	866	843	22	10	3398	3410	-4
14	453	497	-18	21	148	93	7	5	1508	1492	9	11	391	352	21
15	962	975	-9	-6	3	1		6	3269	3216	18	12	215	226	-3
16	307	294	4	1	2072	2038	17	7	558	527	26	13	696	718	-14
17	378	342	14	2	134	43	22	8	2297	2314	-8	14	2189	2181	3
18	744	745	0	3	859	832	23	9	81	64	2	15	373	337	13
19	493	478	7	4	3273	3204	23	10	1912	1925	-7	16	540	541	0
20	267	226	12	5	228	172	24	11	410	401	5	17	659	678	-12
-9	3	1		6	1820	1824	-2	12	2335	2353	-8	18	441	425	7
1	343	330	6	7	359	331	16	13	534	549	-9	19	195	145	10
2	2114	2076	18	8	3754	3746	2	14	121	157	-6	20	410	370	16
3	1067	1063	3	9	81	102	-4	15	874	865	5	1	3	1	
4	253	192	21	10	2138	2154	-8	16	1003	1007	-2	0	447	444	3
5	328	300	13	11	1006	1007	0	17	581	595	-9	1	2155	2087	34
6	3181	3189	-2	12	1084	1087	-2	18	367	304	25	2	1946	1940	3
7	77	101	-3	13	658	683	-16	19	859	837	15	3	1138	1125	11
8	1202	1198	2	14	655	694	-22	20	125	36	8	4	1561	1613	-36
9	879	870	6	15	690	707	-10	21	-157	107	-23	5	1965	1947	9
10	1982	1993	-5	16	-144	60	-12	-2	3	1		6	1989	1988	0
11	314	280	12	17	620	624	-2	1	814	817	-2	7	703	689	12
12	1106	1114	-5	18	161	141	4	2	371	393	-22	8	2822	2845	-9
13	1178	1173	2	19	307	278	9	3	2018	2012	3	9	720	709	8
14	165	96	19	20	271	260	3	4	3314	3273	14	10	559	601	-28
15	357	368	-2	21	860	839	13	5	497	479	17	11	121	38	14
16	160	2	18	-5	3	1		6	1818	1819	0	12	2885	2920	-13
17	641	666	-15	1	653	657	-4	7	521	513	7	13	118	96	3
18	-43	61	-3	2	2405	2342	28	8	2930	2918	4	14	400	387	4
19	526	524	0	3	909	878	28	9	112	61	8	15	318	295	7
20	881	845	21	4	779	769	9	10	3043	3100	-21	16	1142	1161	-14
-8	3	1		5	1538	1516	15	11	825	809	11	17	323	311	4
1	1283	1267	11	6	3860	3832	8	12	458	416	23	18	673	661	7
2	961	917	34	7	1193	1174	14	13	1147	1154	-4	19	688	681	4
3	638	629	7	8	1343	1344	0	14	1750	1777	-14	20	224	255	-8
4	3445	3435	3	9	288	279	4	15	605	593	6	2	3	1	
5	359	347	7	10	1813	1856	-24	16	487	486	0	0	1201	1157	36
6	487	494	-4	11	335	335	0	17	825	814	8	1	1635	1651	-10
7	671	665	4	12	1723	1727	-2	18	416	448	-15	2	212	217	-3
8	2744	2788	-18	13	576	590	-8	19	-131	100	-16	3	935	920	14
9	344	318	11	14	206	152	13	20	406	355	20	4	1639	1672	-21
10	1580	1602	-13	15	557	544	6	21	871	856	9	5	1026	1058	-29
11	1214	1200	8	16	402	389	5	-1	3	1		6	1663	1722	-38
12	1187	1211	-15	17	319	355	-15	1	2321	2330	-4	7	1988	1975	6
13	357	335	8	18	41	41	0	2	3929	3952	-6	8	1331	1323	5
14	575	561	7	19	1027	991	24	3	388	363	24	9	123	83	8
15	969	934	21	20	265	208	15	4	215	92	52	10	2766	2777	-4
16	326	321	2	21	168	146	3	5	1550	1534	11	11	192	216	-7
17	590	595	-3	-4	3	1		6	2852	2813	15	12	212	114	22
18	473	469	2	1	1584	1515	45	7	74	18	6	13	79	141	-8
19	374	363	4	2	382	366	14	8	2284	2286	0	14	1958	1980	-11
20	296	294	1	3	865	856	8	9	228	196	12	15	216	72	23
-7	3	1		4	4027	3938	25	10	1188	1205	-12	16	712	720	-5
1	249	206	20	5	687	689	-2	11	635	656	-15	17	363	370	-2
2	2920	2857	24	6	810	805	4	12	2907	2903	1	18	591	596	-3
3	920	913	5	7	932	877	47	13	552	602	-31	19	58	57	0
				8	3001	3002	0	14	506	523	-8	20	454	444	4
				9	306	326	-10	15	849	840	5				

3	3	1				6	1082	1092	-7			7	628	655	-17		
0	106	16	17			7	1328	1318	7	0	1710	1685	14	8	119	159	-8
1	2704	2748	-18			8	936	981	-35	1	371	341	15	9	705	726	-13
2	200	130	33			9	1005	1006	-1	2	1316	1307	5	10	240	263	-7
3	1513	1487	17			10	1996	2042	-23	3	1521	1518	2	11	-102	2	-7
4	971	984	-12			11	352	360	-3	4	75	52	2				
5	1629	1623	3			12	402	415	-5	5	413	413	0	15	3	1	
6	1727	1739	-7			13	161	214	-11	6	168	81	16				
7	112	11	13			14	1347	1337	6	7	1034	1063	-19	0	1530	1556	-16
8	2068	2085	-8			15	272	256	5	8	361	288	32	1	375	393	-8
9	844	840	2			16	1078	1093	-10	9	625	646	-11	2	423	374	23
10	464	488	-14			17	295	295	0	10	1072	1087	-9	3	125	78	7
11	89	214	-26			18	423	385	15	11	248	232	5	4	1126	1138	-7
12	2530	2535	-1							12	513	482	18	5	500	485	7
13	333	282	18			7	3	1		13	361	386	-11	6	187	136	12
14	473	498	-10			0	428	380	33	14	624	632	-4	7	688	691	-1
15	205	156	10			1	2321	2278	20	15	108	101	0	8	93	140	-6
16	1319	1304	9			2	1358	1405	-34					9	127	116	1
17	-97	68	-8			3	170	78	25	11	3	1		10	149	146	0
18	768	756	7			4	389	371	11	0	1501	1490	7	16	3	1	
19	505	523	-9			5	1684	1736	-31	1	773	775	-1				
20	203	162	10			6	790	777	11	2	1040	1035	3	0	895	897	-1
						7	913	891	16	3	432	385	23	1	53	59	0
						8	1713	1743	-17	4	973	994	-14	2	1381	1384	-1
						9	599	625	-17	5	1495	1482	8	3	215	158	13
						10	389	396	-2	6	454	438	7	4	124	68	7
						11	561	595	-19	7	541	564	-11	5	454	458	-1
						12	1165	1166	0	8	131	56	16	6	525	537	-5
						13	74	115	-6	9	256	232	8	7	239	235	0
						14	962	967	-3	10	267	310	-17	8	310	339	-9
						15	166	85	13	11	621	627	-4				
						16	861	856	3	12	762	769	-4	17	3	1	
						17	83	136	-6	13	198	8	27				
						18	1046	1008	23	14	795	801	-3	0	1158	1199	-27
										12	3	1		1	118	3	9
						8	3	1		0	1239	1239	0	2	263	265	0
						0	1792	1791	0	1	125	55	8	3	336	367	-11
						1	44	34	0	2	1759	1744	8	4	1033	1012	13
						2	1063	1061	2	3	1253	1242	7	5	142	171	-4
						3	1402	1390	7	4	-40	72	-4	6	431	398	13
						4	465	483	-12	5	251	204	12	18	3	1	
						5	120	57	9	6	518	493	11	0	548	554	-3
						6	92	137	-8	7	596	587	4	1	191	133	10
						7	1264	1296	-22	8	-66	14	-3	2	1308	1307	0
						8	778	784	-4	9	961	978	-12	3	194	141	9
						9	626	638	-7	10	662	654	5	4	180	249	-15
						10	1505	1528	-14	11	207	173	10				
						11	345	298	17	12	493	478	7	19	3	1	
						12	600	607	-3	13	410	439	-12	0	1117	1097	12
						13	412	418	-3					1	133	35	8
						14	1048	1065	-12	13	3	1		-19	4	1	
						15	269	237	11					1	234	256	-7
						16	1124	1125	0					2	141	177	-7
						17	-170	107	-21					3	426	429	-1
														4	227	17	30
						9	3	1						5	1113	1141	-18
						0	1063	1035	20					6	517	508	3
						1	1128	1144	-12					7	275	266	2
						2	991	980	8					-18	4	1	
						3	264	223	16					1	401	406	-2
						4	751	743	6					2	319	295	8
						5	1644	1662	-10					3	901	913	-7
						6	674	690	-11					4	299	276	7
						7	576	580	-2					5	198	193	1
						8	808	817	-5					6	-101	37	-6
						9	642	616	15					7	1217	1219	0
						10	102	37	5					8	576	586	-4
						11	694	721	-15					9	825	822	1
						12	1205	1231	-18					10	156	37	14
						13	340	317	10					11	805	800	3
						14	920	925	-3								
						15	91	105	-1								
						16	582	562	10								
						10	3	1									
						0	1252	1260	-4								
						1	131	98	4								
						2	1468	1479	-6								
						3	615	616	0								
						4	187	130	12								
						5	487	518	-17								
						6	435	449	-6								

				4	181	209	-6	19	1286	1249	22	6	629	667	-32
-17	4	1		5	1163	1176	-8					7	510	501	7
				6	742	761	-11	-9	4	1		8	211	224	-4
1	221	223	0	7	346	282	20					9	512	522	-7
2	363	366	-1	8	571	559	6	1	1361	1319	27	10	1176	1187	-7
3	456	445	5	9	1190	1190	0	2	215	201	6	11	208	172	13
4	257	218	11	10	595	633	-18	3	923	923	0	12	-85	82	-10
5	1216	1231	-10	11	1857	1883	-14	4	1483	1472	7	13	1544	1520	14
6	461	446	7	12	734	738	-2	5	432	435	-2	14	1169	1184	-9
7	477	492	-7	13	217	155	13	6	56	49	0	15	1104	1134	-18
8	-99	13	-5	14	441	463	-10	7	347	337	4	16	152	43	15
9	1131	1131	0	15	1354	1351	1	8	1314	1336	-14	17	1190	1191	0
10	620	638	-9	16	364	359	2	9	1019	1046	-19	18	805	843	-25
11	1174	1190	-9	17	679	669	5	10	229	185	12	19	1725	1707	9
12	126	136	-1					11	1777	1756	11	20	254	170	19
13	202	202	0	-12	4	1		12	716	712	2				
				1	457	416	19	13	770	749	11	-5	4	1	
-16	4	1		2	654	630	14	14	-86	75	-6				
				3	470	454	8	15	1648	1644	2	1	2175	2124	25
1	233	155	19	4	72	13	4	16	818	786	22	2	1248	1249	0
2	494	432	32	5	116	108	1	17	1107	1081	17	3	1790	1742	28
3	783	802	-13	6	538	556	-9	18	262	295	-10	4	1222	1235	-9
4	481	500	-10	7	1258	1290	-20	19	776	793	-10	5	392	389	1
5	176	7	21	8	889	857	20	20	631	634	-1	6	687	693	-5
6	233	223	3	9	1084	1091	-4					7	-87	150	-29
7	1082	1096	-10	10	414	416	0	-8	4	1		8	1038	1047	-6
8	481	486	-2	11	585	554	14					9	553	573	-15
9	1141	1138	1	12	542	541	0	1	930	939	-7	10	556	572	-11
10	302	333	-10	13	2048	2073	-12	2	1369	1370	0	11	1026	997	20
11	760	777	-10	14	662	671	-6	3	667	652	11	12	910	928	-13
12	804	818	-8	15	364	314	22	4	911	896	12	13	987	962	16
13	1145	1125	12	16	341	341	0	5	355	379	-14	14	160	155	1
14	88	32	3	17	1148	1136	8	6	729	724	4	15	1060	1042	11
				18	612	583	14	7	735	737	-1	16	757	775	-12
-15	4	1						8	337	326	5	17	1495	1472	14
				-11	4	1		9	824	836	-9	18	136	112	3
1	197	176	5					10	1483	1495	-7	19	578	591	-7
2	598	613	-9					11	395	336	24	20	620	626	-3
3	258	259	0	1	816	854	-27	12	138	4	20				
4	354	351	0	2	238	155	25	13	1717	1745	-15	-4	4	1	
5	1106	1107	0	3	937	940	-2	14	809	823	-7				
6	737	752	-10	4	698	686	7	15	949	950	0	1	1757	1744	8
7	351	343	3	5	743	758	-10	16	-142	37	-13	2	1028	1007	18
8	591	571	11	6	116	102	2	17	1266	1296	-19	3	1328	1300	21
9	887	922	-24	7	571	566	2	18	935	935	0	4	1811	1812	-1
10	692	708	-10	8	669	674	-2	19	1515	1496	11	5	2379	2344	16
11	1444	1470	-16	9	1267	1266	1	20	116	62	5	6	628	627	0
12	264	266	0	10	376	367	3					7	428	451	-18
13	204	145	11	11	1927	1946	-9	-7	4	1		8	557	577	-17
14	503	484	9	12	526	508	8					9	-97	23	-12
15	1043	1046	-2	13	317	312	1	1	1972	1947	13	10	1210	1201	6
16	95	144	-5	14	286	262	8	2	903	884	16	11	170	47	22
				15	1518	1551	-20	3	1548	1530	11	12	511	518	-4
-14	4	1		16	677	677	0	4	727	730	-2	13	1042	1030	8
				17	987	999	-7	5	93	4	9	14	801	807	-3
1	427	435	-3	18	202	162	8	6	930	895	27	15	1134	1141	-4
2	256	247	2	19	947	926	12	7	155	118	10	16	108	50	6
3	406	401	2					8	990	964	19	17	948	957	-6
4	672	673	0	-10	4	1		9	906	867	29	18	603	600	1
5	131	152	-4					10	121	31	10	19	1628	1620	4
6	431	424	2	1	877	862	11	11	1504	1476	17	20	416	446	-12
7	1121	1082	22	2	492	508	-10	12	1134	1133	1				
8	930	948	-10	3	267	249	6	13	805	846	-25	-3	4	1	
9	933	948	-11	4	78	76	0	14	128	232	-19				
10	437	447	-4	5	186	190	-1	15	1597	1609	-6	1	2608	2582	11
11	719	688	20	6	749	759	-7	16	857	855	1	2	2329	2308	9
12	612	593	11	7	939	937	1	17	1429	1434	-3	3	2924	2884	15
13	1488	1533	-28	8	151	80	12	18	71	111	-4	4	1715	1694	13
14	227	255	-7	9	1226	1181	29	19	663	641	12	5	429	386	34
15	296	254	12	10	624	640	-9	20	620	631	-6	6	416	403	10
16	395	384	4	11	331	274	24					7	1105	1099	4
17	942	967	-15	12	200	156	11	-6	4	1		8	249	250	0
				13	1946	1940	3					9	485	479	4
-13	4	1		14	748	740	5	1	1064	1070	-4	10	678	660	13
				15	636	670	-21	2	928	927	0	11	556	562	-4
1	515	506	4	16	410	384	11	3	956	926	25	12	707	712	-3
2	448	452	-2	17	1323	1329	-3	4	700	707	-6	13	720	726	-3
3	647	663	-9	18	833	824	5	5	1219	1242	-18	14	556	525	17

15	878	913	-21					6	644	635	7	17	229	258	-8			
16	316	309	2	0	186	40	48	7	1658	1656	0							
17	1624	1624	0	1	3114	3032	29	8	1227	1236	-6		8	4	1			
18	282	285	-1	2	2319	2309	4	9	1808	1796	6							
19	467	457	4	3	3869	3858	3	10	431	452	-11		0	461	477	-11		
20	422	425	-1	4	1108	1122	-11	11	1011	1020	-6		1	2452	2437	6		
				5	1064	1071	-5	12	884	891	-4		2	905	930	-20		
-2	4	1		6	1234	1222	9	13	-99	24	-6		3	1097	1092	3		
				7	2598	2569	11	14	42	81	-3		4	485	512	-17		
1	2670	2681	-4	8	337	344	-4	15	587	602	-9		5	2830	2867	-14		
2	377	376	0	9	709	692	13	16	526	523	1		6	1030	1027	2		
3	1283	1269	11	10	804	805	0	17	106	113	0		7	1756	1802	-25		
4	253	119	62	11	243	172	24	18	-97	1	-5		8	447	479	-16		
5	3093	3016	27	12	411	391	10	19	974	956	11		9	1420	1419	1		
6	376	400	-18	13	440	430	4						10	538	488	25		
7	1094	1061	26	14	713	717	-2		5	4	1		11	1298	1312	-8		
8	397	396	0	15	229	233	-1						12	115	104	2		
9	243	253	-4	16	140	185	-10		0	2012	2004	3	13	66	41	2		
10	1144	1115	21	17	1248	1267	-13		1	497	484	11	14	323	349	-11		
11	414	355	33	18	711	715	-2		2	1576	1558	11	15	192	193	0		
12	483	503	-12	19	-114	47	-8		3	4231	4268	-10	16	236	221	5		
13	1042	1060	-12	20	366	366	0		4	1145	1139	4						
14	398	399	0						5	942	969	-22		9	4	1		
15	1349	1374	-15		2	4	1		6	671	679	-6						
16	925	920	2						7	2279	2321	-19		0	1118	1119	0	
17	900	897	2		0	1506	1426	54	8	674	660	10		1	206	168	12	
18	347	356	-3		1	3023	2946	28	9	1802	1814	-6		2	391	316	38	
19	1781	1775	3		2	609	563	45	10	897	877	14		3	2455	2496	-18	
20	582	575	3		3	999	983	14	11	667	659	4		4	723	730	-5	
					4	1590	1575	10	12	334	321	4		5	1186	1212	-17	
-1	4	1			5	3546	3573	-8	13	290	278	3		6	304	307	-1	
					6	431	392	27	14	465	474	-5		7	1724	1740	-9	
1	3685	3654	9		7	1151	1177	-19	15	136	147	-2		8	502	542	-21	
2	2212	2200	5		8	1072	1132	-48	16	171	114	10		9	1676	1695	-10	
3	2199	2142	28		9	1052	1072	-15	17	585	592	-4		10	94	18	4	
4	115	82	9		10	543	552	-6	18	415	412	1		11	493	486	3	
5	1021	1026	-4		11	748	749	0						12	692	696	-2	
6	423	441	-14		12	870	873	-2		6	4	1		13	815	822	-4	
7	1658	1636	14		13	303	225	24						14	114	170	-10	
8	797	765	27		14	175	200	-6		0	1617	1613	2	15	150	151	0	
9	686	712	-21		15	818	840	-13		1	3153	3139	5	16	449	433	7	
10	1123	1112	8		16	762	741	15		2	846	863	-15					
11	591	573	12		17	228	199	8		3	414	409	3		10	4	1	
12	315	268	19		18	342	311	11		4	926	952	-22					
13	679	684	-2		19	1240	1219	12		5	2780	2812	-13		0	141	120	4
14	968	990	-14		20	641	617	13		6	867	861	4		1	1827	1837	-5
15	826	826	0							7	1941	1940	0		2	900	894	4
16	466	425	22			3	4	1		8	386	404	-9		3	547	562	-8
17	1643	1623	11							9	1436	1456	-12		4	114	78	4
18	555	575	-10		0	263	166	52		10	606	590	10		5	2167	2224	-27
19	-107	144	-16		1	2785	2824	-15		11	1122	1166	-29		6	868	884	-10
20	144	201	-10		2	1502	1479	16		12	498	502	-2		7	1658	1662	-2
					3	3779	3722	17		13	206	169	8		8	71	48	1
0	4	1			4	593	575	16		14	63	110	-5		9	921	941	-11
					5	356	309	27		15	157	189	-7		10	673	726	-38
0	2283	2236	19		6	1127	1165	-31		16	429	432	-1		11	1362	1393	-20
1	3305	3258	16		7	2242	2257	-7		17	97	2	7		12	94	1	6
2	997	977	18		8	445	460	-9		18	213	154	13		13	191	28	24
3	1985	1997	-6		9	886	918	-24							14	515	488	14
4	1599	1596	2		10	1294	1297	-2		7	4	1			15	309	280	9
5	3962	3955	2		11	556	539	10										
6	145	39	21		12	409	357	23		0	1125	1092	25		11	4	1	
7	977	997	-16		13	61	149	-11		1	614	609	3					
8	913	937	-21		14	711	704	4		2	962	998	-30		0	820	831	-7
9	579	540	30		15	208	75	29		3	3250	3294	-15		1	387	405	-8
10	289	234	24		16	290	265	9		4	986	985	0		2	223	149	19
11	387	395	-4		17	895	887	5		5	977	978	0		3	1891	1901	-5
12	1026	1043	-11		18	564	550	8		6	570	609	-27		4	1115	1128	-9
13	689	702	-8		19	37	61	-1		7	2087	2126	-19		5	1258	1274	-10
14	265	196	20							8	657	681	-17		6	81	71	0
15	1286	1268	10			4	4	1		9	1977	1982	-2		7	1710	1713	-1
16	763	759	2							10	400	416	-7		8	834	855	-12
17	374	337	15		0	1450	1454	-3		11	821	815	3		9	1680	1718	-23
18	245	299	-17		1	4012	4055	-12		12	337	345	-3		10	-193	33	-25
19	1727	1689	20		2	1055	1061	-5		13	498	502	-2		11	203	170	9
20	712	719	-4		3	671	681	-8		14	325	302	9		12	494	493	0
					4	1644	1656	-8		15	90	146	-9		13	881	918	-25
1	4	1			5	3647	3694	-14		16	275	229	14		14	-37	123	-10

10	380	379	0	19	381	440	-24	5	1077	1093	-13	13	568	586	-10
11	1047	1039	5	20	1041	1023	11	6	675	676	0	14	420	371	20
12	815	843	-17					7	991	1063	-60	15	447	439	4
13	1042	1014	17		-3	5	1	8	1640	1701	-38	16	162	145	3
14	1737	1719	9					9	923	922	0	17	312	304	3
15	951	968	-13	1	789	785	3	10	483	434	30	18	916	887	19
16	192	163	6	2	486	463	19	11	353	368	-6	19	681	686	-3
17	733	702	20	3	2117	2106	5	12	127	127	0				
18	1324	1332	-5	4	1650	1604	28	13	1010	1029	-12	4	5	1	
19	784	792	-5	5	962	971	-7	14	122	73	5	0	910	901	8
20	483	475	3	6	1571	1560	7	15	182	155	5	1	774	765	8
				7	1134	1106	21	16	971	946	17	2	1834	1857	-13
				8	57	30	2	17	769	757	8	3	1884	1885	0
				9	130	120	3	18	825	804	13	4	1702	1717	-9
				10	185	112	17	19	345	337	2	5	509	498	8
				11	532	527	3	20	886	884	1	6	876	911	-29
				12	755	744	7					7	1675	1669	3
				13	230	189	11	1	5	1		8	1912	1980	-37
				14	984	986	-1					9	112	43	8
				15	752	762	-5	0	2965	2943	8	10	111	35	7
				16	79	9	5	1	2559	2518	18	11	993	1022	-20
				17	483	479	2	2	1142	1123	15	12	384	374	3
				18	1383	1366	11	3	1655	1653	0	13	219	190	7
				19	892	900	-5	4	2543	2532	4	14	224	240	-5
				20	812	791	12	5	611	594	14	15	476	487	-6
								6	2705	2699	2	16	585	574	7
								7	304	333	-16	17	415	421	-2
								8	19	69	-3	18	401	382	7
								9	895	888	5				
								10	725	774	-37	5	5	1	
								11	876	854	16	0	2929	2957	-10
								12	293	277	7	1	2401	2429	-12
								13	588	584	2	2	1685	1689	-2
								14	712	682	17	3	479	517	-29
								15	904	871	24	4	1857	1868	-6
								16	242	235	2	5	1873	1905	-18
								17	209	223	-3	6	2372	2388	-7
								18	1028	1018	6	7	158	117	11
								19	878	873	3	8	211	172	13
												9	1371	1378	-4
												10	1219	1215	2
												11	-72	60	-5
												12	424	435	-5
												13	783	745	22
												14	174	166	2
												15	148	140	1
												16	94	48	4
												17	328	355	-10
												18	665	645	11
												6	5	1	
												0	703	716	-11
												1	264	234	13
												2	2370	2418	-22
												3	2039	2113	-39
												4	2450	2471	-9
												5	121	127	-1
												6	649	682	-25
												7	1933	1937	-2
												8	2140	2173	-16
												9	277	207	28
												10	300	338	-13
												11	827	847	-12
												12	495	503	-3
												13	149	157	-1
												14	268	266	0
												15	565	578	-7
												16	410	396	6
												17	72	110	-5
												7	5	1	
												0	2047	2044	1
												1	1585	1638	-33
												2	1716	1724	-4

3	105	23	17	3	547	511	19	6	13	19	0	2	213	136	21
4	1045	1081	-28	4	481	521	-19	7	362	280	26	3	657	658	0
5	1551	1583	-19	5	926	916	6					4	184	141	9
6	2382	2418	-16	6	1868	1903	-17	17	5	1		5	1587	1581	3
7	481	467	8	7	862	869	-4					6	419	415	2
8	481	430	26	8	581	553	18	0	379	307	27	7	757	752	3
9	1079	1076	2	9	638	638	0	1	186	135	9	8	780	768	8
10	1168	1193	-16	10	1256	1272	-11	2	227	208	5	9	649	649	0
11	370	405	-13	11	688	702	-9	3	413	395	7	10	92	59	3
12	726	712	10	12	973	981	-5	4	263	223	10	11	243	273	-9
13	601	622	-14	13	391	328	24	5	230	182	10	12	515	522	-4
14	114	45	8									13	-64	57	-4
15	-110	48	-10	12	5	1		18	5	1		14	477	462	7
16	-40	97	-8									15	519	494	11
17	306	301	1	0	118	21	11	0	139	199	-14				
				1	530	555	-13	1	294	201	24	-13	6	1	
8	5	1		2	903	898	2	2	329	334	-1				
				3	866	872	-3					1	400	418	-7
0	345	312	16	4	1441	1466	-14	-18	6	1		2	466	418	20
1	181	89	30	5	674	672	0					3	1798	1777	10
2	1471	1519	-32	6	22	5	0	1	988	992	-2	4	562	525	17
3	1403	1445	-27	7	849	859	-7	2	357	342	5	5	763	778	-8
4	1543	1588	-28	8	1573	1615	-26	3	106	102	0	6	490	489	0
5	283	260	9	9	779	787	-5	4	158	160	0	7	1237	1237	0
6	263	248	5	10	740	763	-15	5	874	867	4	8	-69	148	-20
7	1358	1369	-6	11	333	323	3	6	428	427	0	9	585	581	2
8	1492	1543	-31	12	825	807	11	7	228	147	15	10	757	746	7
9	615	632	-9					-17	6	1		11	416	402	7
10	721	715	3	13	5	1						12	390	384	2
11	673	686	-9	0	499	453	21	1	-5	58	-1	13	43	77	-2
12	876	894	-13	1	668	611	31	2	132	142	-1	14	483	487	-1
13	361	390	-14	2	780	789	-5	3	1349	1342	4	15	191	104	15
14	397	416	-8	3	710	708	0	4	419	440	-9	16	632	609	12
15	322	343	-8	4	492	480	6	5	356	279	26				
16	325	276	16	5	738	737	0	6	583	588	-2	-12	6	1	
				6	1575	1606	-19	7	870	855	9	1	1960	1967	-3
9	5	1		7	795	835	-27	8	227	174	11	2	202	171	6
0	1814	1793	11	8	441	417	11	9	49	99	-5	3	993	998	-3
1	1639	1673	-20	9	483	449	16	10	806	825	-11	4	168	65	18
2	1074	1091	-12	10	1080	1075	3	11	245	293	-13	5	1803	1803	0
3	608	600	5	11	767	785	-11					6	486	480	2
4	710	701	6					-16	6	1		7	1079	1062	10
5	1613	1676	-37	14	5	1						8	687	690	-1
6	1931	1967	-19	0	130	14	12	1	1709	1716	-4	9	718	699	10
7	677	668	5	1	688	697	-6	2	235	255	-6	10	202	189	3
8	411	376	15	2	428	355	36	3	295	295	0	11	552	537	9
9	756	761	-2	3	492	438	29	4	212	199	3	12	662	649	8
10	1466	1517	-34	4	1117	1121	-2	5	1490	1510	-12	13	166	206	-9
11	743	731	9	5	831	834	-1	6	388	382	2	14	640	614	16
12	632	647	-9	6	201	91	25	7	537	537	0	15	166	98	10
13	454	443	5	7	537	517	10	8	765	775	-6	16	365	371	-2
14	160	102	10	8	1202	1186	10	9	625	582	24	17	458	439	8
15	179	281	-29	9	759	762	-1	10	190	164	6				
				10	591	605	-7	11	143	83	9	-11	6	1	
10	5	1						12	642	636	3				
0	518	503	9	15	5	1		13	183	132	8	1	582	583	0
1	747	748	0					-15	6	1		2	784	779	3
2	1078	1085	-5	0	139	152	-2					3	1949	1974	-12
3	1404	1422	-11	1	195	140	12	1	205	158	12	4	626	612	8
4	1737	1734	1	2	505	512	-3	2	250	265	-5	5	1563	1578	-8
5	643	665	-13	3	823	819	3	3	1796	1806	-5	6	474	467	3
6	148	82	9	4	274	339	-22	4	381	399	-7	7	962	988	-16
7	852	833	11	5	453	419	16	5	684	662	13	8	365	314	17
8	1780	1790	-5	6	1038	1051	-8	6	420	434	-6	9	1280	1281	0
9	1032	1075	-32	7	654	679	-14	7	1042	1053	-7	10	769	761	4
10	655	694	-26	8	368	358	3	8	178	127	10	11	357	404	-22
11	607	610	-1	9	217	235	-4	9	527	515	6	12	621	633	-7
12	905	885	14					10	781	812	-20	13	332	357	-10
13	401	404	0	16	5	1		11	200	160	10	14	579	575	2
14	652	684	-19					12	280	226	15	15	229	270	-13
				0	85	41	3	13	201	240	-9	16	741	745	-2
11	5	1		1	485	468	9	14	473	467	2	17	270	194	22
0	963	962	0	2	417	425	-3					-10	6	1	
1	958	958	0	3	159	83	11	-14	6	1					
2	949	946	1	4	716	714	1	1	1689	1707	-11	1	1820	1813	4
				5	586	571	8					2	298	292	2

3	1428	1433	-2	17	-73	71	-6	7	328	296	15	18	581	566	8
4	158	125	8	18	217	11	33	8	436	459	-14	19	334	285	15
5	1812	1817	-2	19	478	477	0	9	2530	2561	-13				
6	645	688	-26					10	666	663	1		1	6	1
7	2202	2211	-3		-6	6	1	11	721	720	1				
8	649	658	-5					12	451	471	-9	0	817	815	1
9	576	556	10	1	1736	1749	-7	13	1509	1515	-3	1	361	341	15
10	300	252	16	2	278	281	-1	14	585	566	9	2	1602	1618	-10
11	1077	1102	-15	3	1516	1533	-11	15	669	660	6	3	162	124	12
12	758	745	8	4	955	944	8	16	384	378	2	4	1474	1477	-2
13	156	158	0	5	1454	1441	8	17	119	63	7	5	1723	1745	-13
14	856	834	15	6	389	371	10	18	172	125	8	6	136	36	19
15	206	213	-1	7	3585	3616	-9	19	135	156	-4	7	274	258	6
16	451	399	24	8	729	720	6					8	583	568	11
17	556	562	-3	9	673	677	-2	-2	6	1		9	2232	2260	-13
18	785	778	4	10	418	407	4					10	174	96	17
				11	2170	2170	0	1	827	841	-13	11	1529	1523	3
				12	899	895	2	2	148	77	22	12	-38	9	-1
				13	245	185	15	3	1974	1965	5	13	1724	1743	-9
				14	693	686	3	4	909	922	-11	14	154	104	7
				15	494	536	-25	5	797	781	13	15	1470	1480	-6
				16	193	211	-4	6	1406	1369	25	16	499	504	-2
				17	137	21	12	7	2886	2889	-1	17	438	458	-9
				18	737	720	11	8	523	488	23	18	225	186	9
				19	119	89	3	9	586	584	1	19	642	602	21
								10	612	595	11				
								11	2207	2181	12		2	6	1
								12	773	777	-2				
								13	924	914	6	0	1608	1594	8
								14	482	477	2	1	450	454	-3
								15	716	698	12	2	1054	1066	-9
								16	62	38	1	3	931	909	19
								17	643	627	10	4	883	906	-20
								18	882	888	-4	5	808	780	23
								19	-55	3	-2	6	1077	1103	-20
												7	2131	2163	-15
												8	389	346	23
												9	1191	1186	3
												10	503	504	0
												11	1828	1859	-16
												12	343	318	10
												13	1355	1357	-1
												14	698	701	-2
												15	845	857	-8
												16	135	138	0
												17	1132	1107	16
												18	446	463	-7
													3	6	1
												0	254	225	15
												1	132	43	18
												2	1843	1864	-12
												3	454	443	8
												4	986	972	11
												5	1739	1769	-18
												6	532	534	-1
												7	882	899	-13
												8	614	591	16
												9	1996	2061	-34
												10	164	94	13
												11	1393	1398	-2
												12	206	165	9
												13	1008	1015	-5
												14	551	579	-17
												15	1678	1688	-5
												16	303	318	-5
												17	285	280	1
												18	193	180	2
													4	6	1
												0	2037	2050	-7
												1	1643	1605	23
												2	923	971	-42
												3	596	587	8
												4	1753	1765	-6
												5	590	579	8

6 1358 1382 -17	0 1117 1126 -6	5 364 335 13	7 281 256 7
7 1447 1491 -29	1 395 413 -10	6 981 954 20	8 -128 89 -18
8 173 140 10	2 629 646 -12	7 114 83 4	-16 7 1
9 1124 1144 -13	3 385 395 -5	8 137 173 -8	1 301 365 -22
10 544 533 6	4 1092 1083 6	9 312 272 14	2 443 471 -14
11 1237 1267 -19	5 180 165 4	10 473 480 -3	3 1701 1701 0
12 556 565 -4	6 1115 1119 -2	11 152 119 5	4 371 392 -8
13 1683 1720 -22	7 582 567 8	12 488 495 -3	5 399 380 7
14 278 299 -7	8 254 243 3	13 6 1	6 141 100 5
15 612 630 -10	9 720 734 -8	0 300 303 -1	7 768 759 5
16 86 82 0	10 676 684 -6	1 1629 1632 -1	8 295 290 2
17 1022 1016 3	11 408 380 14	2 461 495 -19	9 424 396 11
18 416 444 -11	12 547 542 2	3 497 511 -8	10 293 289 1
5 6 1	13 1132 1137 -3	4 522 507 8	11 141 22 10
0 231 244 -5	14 179 115 11	5 420 424 -1	-15 7 1
1 788 781 6	15 -136 85 -14	6 102 2 6	1 1877 1870 3
2 1193 1209 -12	9 6 1	7 148 102 7	2 497 504 -3
3 728 712 13	0 380 395 -7	8 703 702 0	3 111 118 -1
4 1609 1584 15	1 1650 1650 0	9 141 6 12	4 125 50 8
5 785 810 -20	2 884 889 -3	10 291 306 -5	5 1445 1437 5
6 744 772 -21	3 186 19 24	11 551 545 2	6 358 347 4
7 648 671 -17	4 777 769 5	14 6 1	7 690 685 3
8 765 788 -16	5 153 128 7	0 551 538 7	8 204 161 10
9 1757 1768 -6	6 277 267 3	1 245 209 11	9 471 440 15
10 258 263 -2	7 230 166 16	2 396 420 -11	10 280 262 5
11 1408 1426 -10	8 805 798 4	3 1075 1099 -17	11 77 140 -8
12 216 206 3	9 498 517 -12	4 306 285 7	12 344 286 19
13 843 863 -14	10 496 508 -7	5 402 426 -11	13 207 160 10
14 519 517 0	11 823 817 4	6 660 654 4	-14 7 1
15 1438 1436 1	12 310 316 -2	7 308 281 9	1 380 388 -3
16 265 281 -5	13 71 4 3	8 146 160 -2	2 368 356 5
17 147 127 3	14 485 504 -9	9 -50 25 -1	3 1780 1807 -15
6 6 1	15 1084 1089 -3	15 6 1	4 743 748 -3
0 1259 1263 -2	10 6 1	0 62 117 -5	5 460 449 5
1 1404 1410 -3	0 1089 1105 -11	1 1609 1631 -13	6 365 332 13
2 282 267 6	1 281 204 25	2 357 350 2	7 1287 1286 0
3 197 192 1	2 130 208 -16	3 486 520 -17	8 410 388 9
4 1301 1314 -8	3 1116 1112 2	4 475 492 -8	9 707 735 -18
5 267 176 33	4 766 785 -12	5 532 547 -7	10 273 270 0
6 996 999 -2	5 374 355 7	6 157 81 12	11 144 63 10
7 1291 1318 -18	6 846 870 -15	7 341 388 -18	12 -121 98 -14
8 164 21 19	7 133 155 -4	8 538 510 13	13 203 45 28
9 834 863 -20	8 368 374 -2	16 6 1	14 -107 41 -7
10 312 259 17	9 319 266 21	0 415 397 7	-13 7 1
11 998 1004 -3	10 668 691 -15	1 351 391 -16	1 1813 1838 -14
12 762 767 -3	11 262 275 -4	2 126 192 -12	2 691 678 8
13 1334 1362 -18	12 459 469 -5	3 879 869 6	3 172 2 23
14 43 84 -4	13 1005 1026 -14	4 377 346 11	4 249 262 -4
15 -59 52 -4	14 99 39 5	5 558 607 -25	5 1311 1318 -4
16 -8 110 -7	11 6 1	6 546 518 13	6 646 671 -16
17 1081 1069 7	0 146 157 -2	17 6 1	7 736 699 25
7 6 1	1 1751 1773 -12	0 190 84 16	8 121 115 1
0 129 45 13	2 981 962 12	1 1081 1082 -1	9 538 572 -20
1 711 723 -9	3 465 448 7	2 391 361 10	10 202 149 12
2 1287 1299 -7	4 642 640 1	3 637 666 -16	11 616 596 13
3 235 219 6	5 509 471 18	18 6 1	12 456 457 0
4 943 971 -21	6 212 67 22	0 290 329 -11	13 -162 95 -20
5 757 771 -11	7 179 144 8	-17 7 1	14 335 347 -4
6 803 835 -24	8 936 968 -24	1 1395 1417 -13	15 175 175 0
7 534 512 13	9 196 242 -13	2 332 297 11	1 391 359 11
8 581 618 -22	10 277 317 -14	3 -98 91 -10	2 466 443 9
9 965 949 10	11 790 802 -7	4 175 151 4	3 1850 1890 -20
10 479 477 1	12 264 297 -10	5 976 994 -12	4 769 775 -3
11 1127 1145 -13	13 -65 100 -7	6 298 300 0	5 722 739 -9
12 458 438 11	12 6 1	8 527 531 -2	6 168 167 0
13 151 148 0	0 676 677 0	7 1016 1032 -11	7 1016 1032 -11
14 330 357 -10	1 292 227 21	8 527 531 -2	8 527 531 -2
15 1317 1348 -20	2 442 418 10		
16 283 257 8	3 1178 1183 -2		
8 6 1	4 486 458 12		

9	947	965	-13	7	1158	1153	3	12	627	626	0
10	438	428	5	8	1187	1180	4	13	1620	1625	-2
11	-61	43	-4	9	2548	2568	-8	14	306	284	8
12	192	114	16	10	190	193	0	15	1037	1031	4
13	437	461	-11	11	108	116	0	16	-166	72	-20
14	92	30	4	12	264	109	33	17	1025	992	22
15	97	113	-2	13	1220	1254	-23	18	162	143	4
16	359	374	-5	14	412	406	3	19	339	346	-2
				15	254	229	7				
				16	238	206	9				
				17	158	75	12				
				18	234	200	8				
-11	7	1							0	7	1
1	2020	2025	-2					10	1026	1032	-4
2	814	829	-9					11	717	704	7
3	631	650	-10					12	120	88	4
4	131	69	10					13	1349	1356	-3
5	1643	1606	20					14	468	435	18
6	956	957	0					15	739	712	19
7	1486	1498	-7					16	481	431	26
8	159	93	15					17	171	146	6
9	567	562	3					18	-157	92	-22
10	420	445	-13					19	-54	82	-6
11	797	835	-28								
12	431	445	-7								
13	138	103	5								
14	317	329	-4								
15	202	225	-5								
16	286	311	-8								
17	348	355	-2								
-10	7	1									
1	485	506	-10								
2	455	479	-11								
3	2199	2203	-1								
4	941	956	-9								
5	1559	1547	6								
6	106	43	7								
7	1082	1063	12								
8	780	796	-9								
9	2008	1992	7								
10	200	217	-3								
11	191	222	-8								
12	-118	3	-9								
13	813	804	6								
14	245	225	6								
15	201	122	16								
16	350	311	14								
17	-185	16	-19								
-9	7	1									
1	1833	1830	1								
2	785	781	2								
3	1277	1249	18								
4	262	254	2								
5	1557	1558	0								
6	643	636	3								
7	2046	2024	10								
8	193	162	6								
9	376	384	-3								
10	637	654	-8								
11	1851	1817	17								
12	253	237	5								
13	213	189	7								
14	357	354	1								
15	492	513	-11								
16	155	107	8								
17	363	360	1								
18	114	205	-17								
-8	7	1									
1	641	617	15								
2	513	525	-6								
3	1890	1889	0								
4	811	805	4								
5	2037	2036	0								
6	161	27	16								
					</						

2	99	44	9	7	7	1	3	1460	1456	1	2	441	464	-10	
3	145	123	5				4	605	581	12	3	238	27	32	
4	212	179	12	0	750	737	5	399	369	15	4	-76	68	-5	
5	472	431	26	1	466	449	6	354	385	-15	5	581	575	3	
6	716	695	16	2	28	21	7	256	280	-8	6	508	529	-10	
7	2159	2182	-11	3	307	287	8	310	346	-17	7	368	381	-5	
8	277	290	-5	4	223	219	9	511	500	6	8	802	799	1	
9	1547	1547	0	5	205	192	10	362	318	17	9	663	654	5	
10	419	411	3	6	568	580	-7	11	193	115	17				
11	1672	1641	16	7	648	628	12	12	376	369	2	-15	8	1	
12	749	758	-4	8	327	355	-10								
13	2049	2050	0	9	997	998	0	12	7	1	1	-95	30	-6	
14	297	265	11	10	-64	30	-3				2	418	405	5	
15	722	704	11	11	768	773	-3	0	340	310	3	609	605	2	
16	115	200	-15	12	523	494	17	1	1769	1742	4	566	563	1	
17	1062	1053	5	13	1432	1433	0	2	661	661	0	5	142	80	8
				14	193	219	-6	3	469	471	0	6	471	494	-11
	4	7	1	15	20	26	0	4	318	337	-9	7	731	731	0
								5	655	654	0	8	363	366	-1
0	241	236	2	8	7	1		6	110	71	4	9	324	292	10
1	1232	1227	3					7	102	36	5	10	1012	1008	2
2	531	548	-12	0	317	318	0	8	472	441	15	11	688	681	4
3	506	498	5	1	1386	1403	-10	9	-93	122	-17				
4	681	689	-6	2	617	609	5	10	443	466	-11	-14	8	1	
5	1262	1274	-8	3	286	280	2	11	755	740	9				
6	52	20	2	4	451	456	-2					1	656	646	6
7	803	798	3	5	162	106	11	13	7	1		2	400	366	15
8	729	726	2	6	143	30	16					3	168	55	16
9	1829	1851	-11	7	502	495	3	0	597	617	-13	4	-78	0	-4
10	513	519	-2	8	358	360	0	1	385	384	0	5	474	471	1
11	1922	1923	0	9	633	639	-4	2	139	33	14	6	714	710	2
12	-88	18	-5	10	605	617	-8	3	1178	1206	-20	7	154	126	4
13	1020	1012	5	11	1087	1113	-18	4	357	328	13	8	843	843	0
14	521	531	-5	12	152	103	8	5	281	244	12	9	869	869	0
15	1456	1471	-9	13	107	104	0	6	442	442	0	10	156	27	14
16	504	507	-1	14	225	237	-4	7	388	367	9	11	190	218	-6
17	110	94	1	15	1259	1256	1	8	83	161	-11	12	837	843	-3
								9	364	309	21	13	789	789	0
								10	249	197	13				
												-13	8	1	
5	7	1		9	7	1		14	7	1		1	-101	112	-18
0	506	497	5	0	502	497	2					2	561	579	-11
1	992	976	12	1	-59	10	-2	0	407	391	7	3	551	521	17
2	391	428	-23	2	189	136	12	1	1654	1680	-15	4	737	734	1
3	469	439	19	3	1012	1031	-12	2	421	451	-14	5	93	37	5
4	378	352	14	4	414	374	17	3	438	469	-15	6	493	489	2
5	384	403	-10	5	186	200	-3	4	379	345	14	7	900	906	-4
6	581	585	-3	6	223	207	4	5	768	774	-4	8	609	633	-15
7	1315	1325	-6	7	-55	62	-4	6	277	277	0	9	218	149	16
8	340	369	-12	8	426	432	-3	7	189	147	10	10	862	862	0
9	1197	1229	-21	9	577	580	-1	8	327	325	0	11	876	875	0
10	388	377	4	10	314	281	12					12	459	447	5
11	1365	1368	-1	11	145	246	-25	15	7	1		13	192	59	19
12	652	660	-5	12	367	382	-6	0	586	601	-8	14	546	522	11
13	1755	1805	-29	13	1297	1297	0	1	416	428	-5				
14	256	285	-9	14	124	110	1	2	163	60	14	-12	8	1	
15	260	227	9					3	1178	1180	-1				
16	176	173	0	10	7	1		4	405	382	9	1	753	765	-9
								5	586	637	-27	2	675	682	-4
								6	311	352	-14	3	209	188	6
												4	266	200	21
6	7	1		0	500	486	6	16	7	1		5	610	612	-1
0	465	470	-2	1	1952	1941	5					6	1038	1050	-8
1	1276	1271	3	2	527	534	-3	0	231	195	10	7	186	125	12
2	653	667	-10	3	466	457	4	1	1370	1398	-17	8	823	815	5
3	238	178	21	4	216	193	6	2	433	400	13	9	914	922	-6
4	361	366	-2	5	656	655	0	3	781	793	-7	10	-58	3	-2
5	480	475	3	6	166	123	10	4	321	330	-3	11	-125	87	-17
6	281	257	8	7	155	84	13					12	918	915	1
7	556	570	-8	8	555	538	11	17	7	1		13	971	997	-16
8	557	564	-3	9	135	136	0					14	736	760	-14
9	1067	1057	6	10	546	524	13	0	381	386	-1	15	309	298	3
10	670	672	-1	11	978	993	-10	1	599	621	-11				
11	1452	1459	-4	12	182	59	19					-11	8	1	
12	164	226	-17	13	97	17	5								
13	577	546	18									1	420	411	3
14	338	353	-6	11	7	1						2	697	705	-4
15	1483	1494	-6	0	651	688	-21	-16	8	1					
16	446	423	10	1	453	456	-1	1	658	657	0	1	420	411	3
				2	251	250	0					2	697	705	-4

3	655	622	18	3	69	103	-7				12	836	798	22	
4	958	963	-2	4	735	743	-5	-3	8	1	13	608	609	0	
5	302	260	16	5	1198	1177	14				14	544	545	0	
6	309	240	26	6	137	45	11	1	1450	1443	4	15	1064	1064	0
7	633	617	11	7	500	508	-4	2	1670	1686	-9	16	262	286	-7
8	559	544	9	8	326	318	2	3	783	783	0	17	259	266	-1
9	465	472	-4	9	901	874	16	4	742	747	-3				
10	958	914	31	10	1325	1306	11	5	948	896	38	1	8	1	
11	1031	1032	0	11	433	442	-3	6	159	121	10				
12	559	571	-6	12	604	609	-2	7	261	220	14	0	650	630	15
13	333	264	23	13	761	737	16	8	1136	1105	21	1	1014	1000	11
14	568	592	-13	14	886	894	-5	9	976	969	4	2	1713	1698	8
15	856	847	5	15	798	830	-21	10	1400	1405	-2	3	1475	1478	-2
16	871	859	7	16	909	937	-18	11	111	23	9	4	1285	1278	4
				17	743	717	15	12	279	257	6	5	626	620	4
-10	8	1						13	845	825	14	6	374	375	0
				-6	8	1		14	949	948	0	7	1356	1350	3
1	585	601	-8					15	-157	19	-15	8	1557	1561	-1
2	903	861	26	1	427	400	14	16	792	779	8	9	539	501	21
3	619	629	-5	2	1080	1061	12	17	1027	1026	0	10	1136	1121	9
4	682	709	-15	3	1435	1437	-1	18	135	92	6	11	788	779	5
5	463	499	-17	4	654	661	-5					12	348	326	10
6	745	724	12	5	458	451	3	-2	8	1		13	895	885	7
7	444	472	-12	6	753	759	-4					14	662	635	17
8	646	624	11	7	963	989	-18	1	1165	1156	6	15	291	289	0
9	668	694	-18	8	654	656	-1	2	364	348	8	16	748	736	8
10	243	210	11	9	597	545	29	3	865	881	-13	17	737	737	0
11	551	567	-10	10	127	171	-7	4	479	508	-19				
12	867	837	20	11	707	751	-25	5	227	170	18	2	8	1	
13	1041	1021	13	12	1470	1475	-3	6	1205	1198	4				
14	922	924	-1	13	686	647	25	7	814	806	6	0	2457	2463	-2
15	447	464	-7	14	1023	1028	-3	8	660	656	3	1	1803	1803	0
16	96	132	-4	15	995	985	6	9	-50	77	-6	2	1090	1100	-7
				16	335	278	19	10	601	588	7	3	825	840	-11
-9	8	1		17	580	558	11	11	851	846	2	4	793	828	-26
				18	608	623	-8	12	1209	1175	20	5	1485	1514	-18
1	1112	1106	3					13	171	106	13	6	1622	1660	-22
2	1251	1248	1	-5	8	1		14	533	565	-19	7	528	542	-8
3	592	603	-6					15	1179	1181	-1	8	432	410	9
4	1135	1142	-4	1	1722	1754	-18	16	318	267	16	9	1196	1187	5
5	795	783	7	2	1566	1561	3	17	216	88	22	10	420	394	10
6	330	244	28	3	101	72	3	18	540	519	10	11	714	727	-7
7	728	695	19	4	1057	1031	18					12	988	968	15
8	526	515	5	5	1352	1340	7	-1	8	1		13	513	511	1
9	866	872	-3	6	425	395	16					14	507	474	18
10	789	773	11	7	509	487	12	1	1200	1241	-29	15	629	606	14
11	801	771	21	8	529	543	-7	2	1571	1575	-2	16	228	185	10
12	417	441	-11	9	1159	1140	12	3	1009	1043	-26	17	433	445	-5
13	425	417	3	10	1416	1388	16	4	934	953	-15				
14	825	835	-6	11	322	284	15	5	1035	1041	-4	3	8	1	
15	808	801	4	12	455	441	5	6	207	146	22				
16	883	886	-2	13	785	786	0	7	518	548	-18	0	508	474	22
17	481	475	2	14	1023	1014	6	8	1361	1366	-3	1	781	798	-12
				15	465	437	13	9	984	982	1	2	1863	1857	3
-8	8	1		16	969	993	-16	10	1251	1241	6	3	1762	1811	-28
				17	940	921	12	11	271	283	-4	4	1399	1410	-7
1	414	428	-6	18	109	93	2	12	81	39	2	5	475	461	7
2	774	770	2					13	849	840	6	6	760	727	23
3	1061	1065	-3	-4	8	1		14	570	569	0	7	1443	1450	-4
4	834	839	-3					15	209	203	1	8	1463	1485	-13
5	342	291	19	1	1014	1019	-4	16	689	693	-2	9	412	361	21
6	815	804	7	2	669	630	28	17	1076	1068	5	10	1014	1032	-11
7	944	952	-5	3	1800	1792	4	18	259	189	16	11	1039	1040	0
8	641	632	4	4	421	409	6					12	419	346	37
9	667	646	11	5	223	169	16	0	8	1		13	526	523	1
10	83	51	2	6	774	760	9					14	657	632	15
11	700	707	-4	7	896	883	9	0	2207	2201	2	15	397	415	-8
12	1111	1110	0	8	1003	981	15	1	1468	1467	0	16	965	929	23
13	859	836	15	9	124	121	0	2	944	932	9	17	545	531	7
14	989	992	-2	10	244	188	15	3	963	956	5				
15	744	721	14	11	920	915	3	4	641	646	-4	4	8	1	
16	386	408	-8	12	1521	1514	3	5	1189	1198	-6				
17	693	703	-5	13	-52	51	-3	6	1577	1566	7	0	2173	2210	-18
				14	708	711	-2	7	588	551	23	1	1955	1966	-5
-7	8	1		15	1103	1088	10	8	417	426	-4	2	1112	1089	16
				16	377	392	-6	9	812	796	10	3	150	126	5
1	1324	1343	-12	17	201	207	-1	10	462	473	-5	4	1632	1635	-1
2	1580	1570	6	18	618	654	-20	11	785	759	16	5	1638	1656	-10

6	1288	1288	0	7	465	444	9	5	873	887	-9	5	356	347	3
7	115	27	11	8	512	500	7	6	282	247	10	6	153	160	-1
8	235	178	16	9	767	756	8	7	534	489	22	7	1050	1055	-3
9	1321	1314	4	10	428	397	15	8	689	709	-11	8	162	84	12
10	302	251	15	11	299	354	-21					9	518	513	2
11	399	394	2	12	832	821	7	14	8	1		10	245	237	2
12	892	862	22	13	676	671	3					11	1568	1567	0
13	634	605	18	14	228	156	16	0	743	746	-2	12	89	109	-2
14	542	543	0					1	262	235	8	13	161	58	11
15	341	353	-4	9	8	1		2	311	269	13				
16	468	477	-4					3	884	898	-9	-11	9	1	
				0	309	352	-16	4	683	652	18				
	5	8	1	1	675	688	-7	5	372	371	0	1	457	441	9
				2	1393	1403	-5	6	751	726	15	2	162	193	-8
0	109	43	7	3	1037	1038	0	7	661	659	1	3	345	367	-10
1	103	102	0	4	728	722	3					4	106	103	0
2	2255	2259	-1	5	586	594	-4	15	8	1		5	703	696	5
3	1664	1673	-5	6	333	375	-20					6	-88	153	-21
4	856	877	-15	7	600	593	4	0	157	237	-18	7	564	592	-17
5	167	176	-2	8	869	880	-8	1	777	764	8	8	130	25	11
6	861	881	-14	9	537	518	11	2	798	830	-20	9	1408	1419	-8
7	1491	1472	11	10	817	824	-4	3	163	218	-14	10	-100	40	-7
8	1004	1006	-1	11	845	837	5	4	686	650	20	11	218	211	1
9	171	193	-5	12	146	154	-1	5	788	801	-7	12	-125	106	-14
10	1037	1049	-8	13	315	297	6					13	1685	1679	3
11	683	679	3					16	8	1		14	381	355	9
12	125	130	0	10	8	1									
13	227	213	4	0	1432	1414	10	0	714	736	-13	-10	9	1	
14	696	695	0	1	962	950	7	1	105	32	5				
15	512	486	13	2	480	421	25	2	243	266	-6	1	1104	1111	-4
16	721	679	24	3	767	796	-16					2	202	172	6
				4	933	947	-11	-15	9	1		3	156	160	0
	6	8	1	5	623	626	-1					4	319	316	1
0	2277	2295	-8	6	1058	1071	-9	1	169	188	-4	5	61	73	-1
1	1674	1692	-10	7	776	803	-19	2	173	11	19	6	209	165	12
2	931	932	0	8	301	273	11	3	240	276	-11	7	963	966	-2
3	200	214	-4	9	683	704	-14	4	357	357	0	8	161	203	-10
4	1576	1603	-15	10	604	599	3	5	343	285	19	9	234	243	-2
5	1510	1541	-18	11	463	458	2	6	61	56	0	10	52	142	-10
6	846	879	-22	12	834	833	0	7	740	724	9	11	1564	1550	8
7	148	122	5					8	295	260	9	12	292	321	-9
8	384	417	-13	11	8	1		9	1034	1028	3	13	56	111	-4
9	798	830	-19									14	128	69	6
10	443	458	-8	0	247	234	3	-14	9	1		15	1300	1303	-1
11	160	121	7	1	769	757	6								
12	687	697	-6	2	1292	1301	-6	1	416	370	20	-9	9	1	
13	672	668	2	3	754	778	-17	2	67	171	-14				
14	442	435	3	4	878	883	-3	3	-150	87	-18	1	430	366	26
15	257	232	7	5	776	786	-7	4	-117	75	-11	2	143	2	12
				6	144	135	1	5	543	520	12	3	775	756	11
	7	8	1	7	594	620	-16	6	347	365	-7	4	371	392	-8
0	105	93	1	8	944	943	0	7	764	751	8	5	-99	39	-6
1	159	140	6	9	629	638	-5	8	-47	33	-1	6	400	401	0
2	1738	1729	4	10	720	731	-7	9	620	631	-5	7	125	21	13
3	1340	1362	-13	11	525	503	10	10	316	317	0	8	131	25	13
4	985	990	-3					11	1363	1342	12	9	1317	1320	-1
5	477	478	0	12	8	1						10	243	252	-2
6	509	483	13	0	999	1009	-7	-13	9	1		11	210	255	-13
7	1085	1095	-6	1	590	585	3					12	-26	149	-16
8	791	741	30	2	227	195	9	1	372	369	1	13	1512	1509	2
9	258	225	11	3	759	785	-18	2	147	103	7	14	449	453	-1
10	844	861	-12	4	418	468	-25	3	139	164	-5	15	581	575	2
11	761	795	-24	5	657	619	23	4	164	198	-8				
12	206	199	1	6	1069	1061	5	5	477	490	-6	-8	9	1	
13	-119	78	-12	7	776	792	-10	6	-78	177	-24	1	1547	1531	9
14	783	791	-5	8	161	165	0	7	684	696	-7	2	578	571	4
				9	469	450	8	8	100	145	-6	3	562	540	12
	8	8	1	10	499	453	21	9	1161	1156	2	4	37	150	-13
0	1524	1521	2					10	-76	134	-12	5	389	376	5
1	1555	1586	-18	13	8	1		11	425	436	-4	6	123	115	1
2	570	570	0					12	251	335	-23	7	384	388	-1
3	600	608	-4	0	271	284	-4					8	98	105	-1
4	1130	1147	-10	1	623	652	-19	-12	9	1		9	234	224	3
5	1022	1036	-8	2	788	804	-11					10	123	107	2
6	638	574	35	3	417	385	15	1	643	676	-23	11	1412	1407	3
				4	727	762	-23	2	144	53	14	12	575	580	-3
								3	76	48	2	13	222	206	4
								4	-125	16	-10				

14	140	73	10	14	108	7	7	12	244	236	2	10	246	234	4
15	1350	1347	1	15	1115	1087	18	13	307	316	-3	11	429	432	-1
16	461	462	0	16	302	265	11	14	384	380	1	12	165	134	8
	-7	9	1	17	1213	1187	16	15	673	670	1	13	362	350	5
								16	197	157	8	14	288	252	11
					-3	9	1					15	248	198	13
1	674	647	16					1	9	1					
2	55	79	-2	1	1721	1736	-8					5	9	1	
3	975	968	4	2	585	548	23	0	662	682	-13				
4	371	359	6	3	1367	1369	-1	1	2585	2599	-5	0	812	809	1
5	595	551	25	4	370	306	26	2	634	622	7	1	2669	2709	-16
6	136	108	6	5	1658	1653	3	3	1365	1368	-1	2	383	400	-7
7	51	85	-2	6	180	134	11	4	341	315	11	3	407	391	6
8	176	175	0	7	382	363	8	5	1917	1963	-24	4	838	837	0
9	1107	1089	10	8	152	173	-4	6	550	566	-9	5	2274	2269	2
10	432	419	7	9	115	130	-2	7	353	318	14	6	492	466	12
11	175	103	16	10	255	219	11	8	325	295	11	7	801	827	-16
12	261	259	0	11	560	547	8	9	584	580	2	8	331	305	8
13	1472	1438	21	12	122	122	0	10	495	487	3	9	935	973	-29
14	499	524	-13	13	1228	1226	1	11	71	21	3	10	301	276	9
15	921	900	13	14	198	196	0	12	259	234	8	11	717	730	-9
16	-134	10	-9	15	989	961	18	13	341	325	6	12	174	199	-6
	-6	9	1	16	65	52	0	14	220	126	22	13	15	36	0
				17	638	603	18	15	578	527	28	14	113	50	7
								16	222	268	-13	15	134	168	-6
1	1762	1754	4		-2	9	1								
2	520	515	2					2	9	1		6	9	1	
3	1035	1022	8	1	2450	2454	-1								
4	274	258	5	2	340	354	-6	0	879	885	-4	0	280	250	9
5	642	626	10	3	2172	2203	-15	1	1866	1861	2	1	533	552	-10
6	-180	70	-23	4	248	223	8	2	535	555	-12	2	745	741	2
7	98	175	-13	5	924	913	7	3	2725	2719	2	3	2665	2691	-10
8	301	272	9	6	265	230	13	4	482	470	6	4	152	124	4
9	165	138	5	7	858	851	4	5	443	439	1	5	652	656	-2
10	305	305	0	8	248	228	6	6	329	305	9	6	490	491	0
11	1166	1145	14	9	304	292	5	7	1344	1344	0	7	1605	1597	4
12	640	639	1	10	116	44	7	8	410	380	12	8	444	459	-9
13	562	559	1	11	343	359	-8	9	282	252	9	9	941	941	0
14	153	183	-6	12	59	39	1	10	243	196	15	10	194	157	8
15	1288	1286	1	13	627	597	18	11	491	494	-1	11	518	531	-7
16	336	390	-19	14	175	160	3	12	-60	52	-4	12	-85	14	-4
17	1122	1090	19	15	945	966	-14	13	47	76	-2	13	475	457	9
	-5	9	1	16	-82	116	-11	14	399	346	23	14	137	82	7
				17	1190	1185	3	15	376	373	1				
								16	371	367	1	7	9	1	
1	1541	1526	8		-1	9	1								
2	587	582	3					3	9	1		0	525	453	37
3	1165	1159	4	1	2669	2689	-8					1	2283	2319	-16
4	360	350	4	2	250	222	9	0	734	714	13	2	227	188	9
5	1125	1101	15	3	1335	1351	-10	1	2719	2756	-15	3	364	367	-1
6	298	287	3	4	595	608	-8	2	568	570	-1	4	517	545	-13
7	94	160	-10	5	1987	2001	-7	3	690	686	2	5	2046	2062	-7
8	17	25	0	6	151	181	-7	4	469	449	10	6	256	266	3
9	491	488	1	7	239	261	-7	5	2089	2091	-1	7	885	901	-11
10	366	269	32	8	312	325	-4	6	472	498	-12	8	19	141	-13
11	537	530	4	9	225	199	7	7	512	495	9	9	909	927	-13
12	294	259	14	10	418	376	17	8	363	366	-1	10	296	213	27
13	1294	1303	-5	11	370	334	18	9	1008	1011	-2	11	906	877	20
14	353	383	-12	12	170	186	-4	10	190	181	2	12	-44	93	-7
15	982	947	22	13	724	743	-13	11	390	319	34	13	150	101	9
16	-143	23	-11	14	-25	45	-2	12	143	177	-10				
17	796	791	2	15	854	834	13	13	184	184	0				
	-4	9	1	16	242	229	3	14	117	177	-13	8	9	1	
				17	393	428	-14	15	299	304	-1	0	-100	33	-6
								16	160	195	-7	1	242	190	13
1	1941	1953	-6		0	9	1					2	510	507	1
2	446	452	-3					4	9	1		3	2232	2257	-11
3	1516	1497	11	1	1931	1956	-13					4	276	224	13
4	315	264	18	2	482	473	5	0	503	502	0	5	517	536	-12
5	659	668	-5	3	2329	2335	-2	1	1531	1556	-15	6	278	310	-12
6	180	149	12	4	221	229	-2	2	1085	1075	6	7	1332	1360	-19
7	412	394	8	5	685	694	-6	3	2470	2495	-10	8	424	426	0
8	62	59	0	6	325	323	0	4	275	249	8	9	1000	1022	-15
9	273	251	6	7	944	965	-14	5	192	185	1	10	118	99	2
10	154	219	-14	8	464	464	0	6	520	504	8	11	517	529	-6
11	712	726	-9	9	332	305	9	7	1574	1581	-4	12	193	222	-6
12	314	305	3	10	269	258	3	8	407	403	1				
13	677	686	-6	11	128	29	12	9	492	498	-3	9	9	1	

0	261	263	0	1	579	575	2	5	127	7	12	12	287	226	19
1	1963	1967	-2	2	110	161	-7	6	333	313	8	13	506	489	8
2	135	124	2	-14	10	1		7	568	569	0	14	759	745	8
3	313	370	-24					8	769	755	9	15	607	609	0
4	236	224	3	1	154	150	0	9	100	40	5	-4	10	1	
5	1833	1837	-2	2	750	735	9	10	843	833	6				
6	621	617	2	3	-36	73	-3	11	720	682	24	1	844	845	0
7	947	945	1	4	365	337	9	12	267	242	7	2	913	916	-1
8	-40	15	-1	5	165	131	7	13	-69	156	-15	3	703	696	4
9	907	896	7	6	839	833	3	14	469	466	1	4	69	48	1
10	232	248	-4	7	406	433	-11	-8	10	1		5	870	877	-4
11	949	960	-6	8	204	189	3	1	-218	48	-25	6	1348	1346	1
12	98	96	0	-13	10	1		2	840	808	19	7	355	352	1
10	9	1		3	196	240	-10	3	419	442	-9	8	926	904	13
0	139	33	14	4	293	314	-8	4	293	314	-8	9	205	192	4
1	270	260	3	5	148	54	14	5	148	54	14	10	460	462	0
2	123	108	2	6	1140	1129	7	6	1140	1129	7	11	682	650	21
3	1766	1790	-13	7	66	171	-16	7	66	171	-16	12	1182	1182	0
4	511	496	8	8	857	833	16	8	857	833	16	13	495	513	-9
5	855	863	-5	9	670	654	10	9	670	654	10	14	161	114	7
6	159	150	2	10	654	654	0	10	654	654	0	15	799	780	11
7	1373	1385	-7	11	-93	2	-6	11	-93	2	-6	16	418	400	6
8	506	504	1	12	748	761	-8	12	748	761	-8	-3	10	1	
9	1008	1033	-17	13	672	692	-12	13	672	692	-12	1	1001	1007	-3
10	289	259	9	14	38	43	0	14	38	43	0	2	700	688	7
11	263	272	-2	15	622	576	24	15	622	576	24	3	1339	1314	15
11	9	1		-7	10	1		-7	10	1		4	1233	1216	10
0	-61	31	-3	1	197	251	-15	1	894	881	7	5	583	584	0
1	1324	1340	-11	2	988	1013	-16	2	822	802	12	6	585	598	-7
2	313	318	-1	3	297	285	3	3	304	242	20	7	844	842	1
3	354	358	-1	4	283	286	0	4	1223	1217	3	8	1040	1008	19
4	135	34	11	5	278	271	2	5	98	47	5	9	706	717	-8
5	1452	1477	-15	6	861	863	0	6	395	390	2	10	1245	1227	12
6	581	586	-2	7	368	337	12	7	96	71	3	11	198	140	13
7	968	967	0	8	464	487	-10	8	1055	1064	-6	12	105	200	-17
8	72	163	-14	9	839	864	-15	9	110	59	5	13	484	447	18
9	542	555	-6	10	286	280	2	10	928	928	0	14	953	926	17
12	9	1		11	125	179	-8	11	486	486	0	15	464	459	2
0	172	163	2	-11	10	1		12	214	212	0	16	372	373	0
1	294	227	22	1	589	563	15	13	386	355	12	-2	10	1	
2	36	103	-5	2	582	599	-9	14	537	543	-3	1	1362	1365	-1
3	1285	1314	-19	3	349	340	3	15	780	777	1	2	817	812	3
4	500	486	7	4	1206	1217	-8	-6	10	1		3	680	713	-20
5	663	701	-23	5	104	76	3	1	794	799	-2	4	-77	7	-3
6	148	75	11	6	374	337	15	2	1124	1086	23	5	1200	1193	4
7	925	929	-2	7	753	752	0	3	440	469	-12	6	1300	1266	20
8	437	460	-9	8	644	666	-14	4	129	112	2	7	199	312	-33
13	9	1		9	307	270	12	5	323	399	-28	8	1084	1032	32
0	300	340	-15	10	612	592	11	6	1452	1421	17	9	227	226	0
1	968	962	4	11	782	805	-14	7	110	123	-1	10	370	337	14
2	350	314	13	12	-60	54	-3	8	905	902	2	11	606	617	-6
3	368	400	-13	-10	10	1		9	306	276	11	12	1383	1387	-2
4	141	37	11	1	162	122	8	10	483	474	5	13	424	452	-13
5	953	946	4	2	1156	1171	-10	11	303	302	0	14	226	186	10
6	445	418	11	3	334	331	1	12	1034	1030	2	15	766	771	-3
7	853	892	-25	4	265	236	9	13	641	665	-14	16	525	543	-8
14	9	1		5	405	381	11	14	-126	31	-9	-1	10	1	
0	176	80	16	6	840	831	6	15	798	760	23	1	1246	1252	-4
1	-151	25	-13	7	127	167	-8	-5	10	1		2	526	525	0
2	-129	67	-11	8	740	729	7	1	860	842	11	3	1266	1258	5
3	968	950	12	9	859	853	3	2	555	580	-13	4	846	858	-8
4	323	301	7	10	506	512	-3	3	555	517	20	5	661	622	23
5	583	601	-9	11	36	1	0	4	1148	1126	13	6	786	772	8
15	9	1		12	557	567	-5	5	218	194	6	7	801	797	2
0	115	40	9	13	909	903	3	6	773	714	34	8	569	565	1
				-9	10	1		7	285	288	0	9	568	545	15
				1	755	767	-8	8	966	962	2	10	1308	1294	9
				2	601	615	-9	9	499	503	-2	11	-156	32	-20
				3	392	423	-16	10	1196	1168	19	12	159	70	12
				4	1046	1045	0	11	233	234	0	13	437	439	0
												14	977	958	12

9	299	210	31	3	196	231	-8	11	901	892	6	8	539	536	1
10	864	862	1	4	1310	1312	-1	12	194	37	23	9	690	672	11
11	804	770	22	5	1289	1281	4	13	426	377	19	10	87	49	2
12	759	764	-3	6	847	851	-3								
13	254	242	3	7	177	81	18	3	11	1		8	11	1	
	-6	11	1	8	1135	1149	-9	0	217	276	-21	0	963	954	6
				9	1583	1543	24	1	115	83	4	1	585	555	19
1	234	224	3	10	1315	1301	8	2	532	576	-23	2	239	261	-7
2	280	262	6	11	708	691	9	3	117	81	8	3	124	90	4
3	887	896	-6	12	407	433	-11	4	187	232	-10	4	-43	17	-1
4	1618	1637	-11	13	778	763	9	5	121	35	10	5	151	107	7
5	992	997	-3	14	874	882	-4	6	913	933	-15	6	244	232	3
6	578	543	20		-1	11	1	7	821	829	-5	7	484	503	-10
7	340	352	-4					8	968	980	-8	8	-55	108	-8
8	1099	1087	7	1	339	333	2	9	555	583	-16	9	209	158	13
9	1010	984	18	2	754	780	-16	10	326	323	1				
10	988	975	8	3	701	705	-2	11	638	635	2	9	11	1	
11	252	263	-3	4	834	819	9	12	1034	1071	-24				
12	502	493	4	5	152	46	13	13	853	823	18	0	560	549	5
13	653	643	6	6	1375	1370	3					1	304	301	1
14	568	562	3	7	1196	1204	-5	4	11	1		2	445	443	0
				8	1213	1228	-10					3	509	512	-2
	-5	11	1	9	463	407	26	0	440	430	4	4	181	45	22
				10	813	802	7	1	574	560	7	5	-55	0	-1
1	528	502	12	11	1000	997	2	2	337	283	18	6	67	137	-9
2	1481	1462	10	12	1069	1052	11	3	136	176	-10	7	57	1	2
3	1092	1098	-4	13	627	608	10	4	413	458	-26	8	343	333	4
4	203	170	8	14	94	67	2	5	280	330	-21				
5	489	511	-12					6	531	523	5	10	11	1	
6	1286	1266	13	0	11	1		7	191	137	15	0	989	974	10
7	1056	1056	0					8	563	585	-13	1	902	927	-17
8	1066	1078	-8	1	397	409	-4	9	919	930	-7	2	454	453	0
9	178	190	-3	2	510	512	-1	10	1107	1127	-13	3	-51	39	-2
10	942	943	0	3	162	75	13	11	1001	992	6	4	-47	37	-2
11	937	916	14	4	970	984	-8	12	139	108	4	5	254	283	-9
12	961	973	-7	5	815	824	-4					6	127	33	11
13	449	459	-4	6	970	962	5	5	11	1		7	228	211	4
14	61	107	-5	7	158	96	12								
				8	905	896	6	0	579	543	18	11	11	1	
	-4	11	1	9	1414	1402	7	1	77	58	1				
				10	1221	1194	18	2	56	3	2	0	606	602	2
1	298	245	17	11	737	765	-17	3	495	479	10	1	132	91	5
2	-108	33	-6	12	187	163	4	4	69	22	4	2	380	361	7
3	515	506	4	13	583	559	12	5	109	40	9	3	657	646	6
4	1639	1606	18	14	842	836	3	6	440	426	7	4	265	327	-20
5	1200	1207	-4					7	499	485	7	5	-107	161	-21
6	799	793	4	1	11	1		8	833	869	-25				
7	238	255	-5					9	650	675	-15	12	11	1	
8	1225	1192	22	0	173	168	2	10	166	154	2	0	758	779	-12
9	1371	1367	2	1	162	76	15	11	443	425	7	1	827	820	4
10	1172	1166	4	2	367	364	1	12	1018	994	14	2	503	586	-41
11	569	594	-13	3	663	633	18					3	208	191	4
12	497	530	-15	4	660	668	-4	6	11	1		4	158	27	14
13	795	749	28	5	324	304	7	0	656	666	-7	13	11	1	
14	835	828	4	6	876	894	-13	1	530	532	-1	0	637	657	-10
				7	1065	1051	10	2	433	413	11	1	-175	105	-21
	-3	11	1	8	1095	1114	-13	3	-119	137	-23				
				9	422	438	-7	4	222	177	13	-11	12	1	
1	264	316	-17	10	437	423	6	5	166	148	5	0	175	195	-3
2	1121	1111	5	11	757	750	4	6	367	376	-3	2	159	122	5
3	1212	1200	7	12	1007	1000	4	7	461	473	-6	3	1042	1055	-8
4	501	460	18	13	730	705	15	8	427	393	16	4	575	560	7
5	453	422	12	14	219	212	1	9	428	449	-10	5	883	880	1
6	1306	1323	-11					10	792	783	5	6	46	70	-1
7	1202	1176	18	2	11	1		11	962	947	10	7	547	506	19
8	1269	1266	2												
9	329	362	-12	0	200	191	2	7	11	1		-10	12	1	
10	967	978	-8	1	149	172	-4	0	703	720	-12	1	905	918	-8
11	1268	1243	15	2	-149	29	-13	1	236	210	8	2	569	545	12
12	1211	1197	9	3	176	74	16	2	267	260	2	3	725	736	-6
13	682	663	11	4	776	741	21	3	339	361	-10	4	-103	111	-12
14	-59	117	-9	5	606	627	-15	4	202	114	21				
				6	680	703	-16	5	282	299	-6				
	-2	11	1	7	270	283	-4	6	329	312	6				
				8	836	821	10	7	81	109	-3				
1	151	154	0	9	1165	1151	10								
2	53	9	1	10	1123	1099	15								

5	835	826	5	1	673	691	-12	2	1277	1305	-19	6	767	761	4
6	496	505	-4	2	389	417	-13	3	323	318	2	7	605	619	-8
7	946	940	3	3	786	789	-2	4	190	190	0	8	209	224	-4
8	266	255	3	4	605	603	1	5	1073	1059	10	9	225	300	-21
-9	12	1		5	758	771	-8	6	574	578	-2	7	12	1	
1	337	293	15	6	112	107	0	7	184	116	13	0	590	583	3
2	250	202	12	7	1560	1529	18	8	146	87	9	1	448	479	-16
3	1117	1104	8	8	375	399	-10	9	1063	1070	-4	2	499	481	9
4	481	473	4	9	126	11	9	10	259	254	1	3	432	433	0
5	922	910	7	10	492	477	7	11	609	592	9	4	797	822	-17
6	100	1	5	11	1147	1137	6	12	54	163	-15	5	199	210	-2
7	721	710	6	12	229	230	0	2	12	1		6	380	349	12
8	400	386	5	-3	12	1		0	940	931	7	7	106	83	2
9	1012	1015	-1	1	362	364	0	1	205	226	-7	8	563	585	-12
10	379	334	16	2	722	724	-1	2	-144	22	-15	8	12	1	
-8	12	1		3	937	923	10	3	347	352	-2	0	271	244	10
1	900	899	0	4	120	107	1	4	1127	1163	-26	1	89	76	1
2	432	465	-15	5	1280	1264	10	5	336	293	17	2	700	711	-7
3	698	695	1	6	645	612	20	6	261	232	11	3	384	354	12
4	301	322	-6	7	449	466	-8	7	1100	1106	-4	4	496	488	4
5	937	909	18	8	311	297	5	8	254	263	-3	5	217	258	-11
6	429	437	-3	9	1414	1407	4	9	196	191	1	6	683	668	8
7	1172	1140	21	10	357	312	16	10	99	161	-9	7	526	494	16
8	226	168	13	11	554	537	8	11	962	963	0	9	12	1	
9	358	357	0	12	516	524	-3	3	12	1		0	631	614	9
10	478	511	-15	-2	12	1		0	345	342	1	1	717	734	-10
11	764	787	-10	1	443	470	-15	1	276	218	20	2	378	358	7
-7	12	1		2	392	391	0	2	1016	1011	3	3	282	278	1
1	257	247	3	3	729	696	22	3	608	608	0	4	685	711	-16
2	454	472	-9	4	918	908	7	4	197	179	4	5	167	1	16
3	1041	1029	8	5	636	613	14	5	793	818	-17	6	309	274	11
4	494	504	-5	6	93	58	4	6	543	541	1	10	12	1	
5	1097	1107	-6	7	1476	1475	0	7	-90	14	-5	0	255	216	10
6	122	66	7	8	537	579	-23	8	330	371	-16	1	196	143	10
7	711	706	3	9	57	42	0	9	1015	1024	-6	2	667	662	3
8	242	261	-5	10	470	492	-10	10	270	254	5	3	519	530	-5
9	1246	1225	13	11	1155	1128	17	11	630	621	5	4	264	255	2
10	-87	106	-10	12	338	334	1	4	12	1		11	12	1	
11	217	218	0	-1	12	1		0	885	881	3	0	599	574	13
-6	12	1		1	55	44	0	1	143	141	0	1	775	791	-9
1	937	915	15	2	1257	1279	-15	2	210	119	26	2	191	163	6
2	448	439	4	3	500	529	-17	3	-53	101	-9	-9	13	1	
3	704	697	4	4	-57	69	-5	4	672	669	1	0	235	151	23
4	483	487	-2	5	1333	1339	-4	5	481	471	5	1	242	208	9
5	1017	994	15	6	757	772	-10	6	512	521	-5	3	340	321	6
6	339	322	6	7	215	234	-5	7	894	903	-5	4	118	75	4
7	1271	1277	-4	8	134	138	0	8	327	325	0	5	170	158	2
8	-51	89	-6	9	1300	1286	8	9	301	306	-1	-8	13	1	
9	-111	136	-20	10	261	296	-11	10	281	275	1	1	270	295	-8
10	390	403	-5	11	609	583	14	5	12	1		2	581	552	16
11	921	921	0	12	389	372	7	6	268	326	-20	3	286	261	8
12	-101	92	-10	0	12	1		7	-52	73	-4	4	208	207	0
-5	12	1		0	1216	1229	-7	8	431	399	14	5	247	241	1
1	367	357	4	1	144	85	12	9	965	977	-8	6	126	51	8
2	714	706	5	2	98	52	4	10	149	148	0	7	156	196	-8
3	1141	1141	0	3	525	511	8	6	12	1		-7	13	1	
4	247	248	0	4	1119	1128	-6	7	433	426	3	1	242	221	6
5	1243	1247	-2	5	385	341	19	8	503	477	15	2	150	104	7
6	390	392	-1	6	189	186	1	9	807	818	-8	3	404	374	13
7	585	584	0	7	1285	1271	9	10	466	512	-26	4	492	502	-4
8	128	209	-15	8	358	387	-12	11	656	649	4	5	243	201	11
9	1426	1406	12	9	162	178	-3	12	384	417	-15	6	349	327	8
10	285	271	4	10	195	154	10	0	268	326	-20				
11	433	426	3	11	944	941	2	1	-52	73	-4				
12	585	572	6	12	344	297	15	2	431	399	14				
-4	12	1		1	12	1		3	140	51	11				
0	-158	16	-18	0	1216	1229	-7	4	556	552	1				
1	-129	48	-13	1	144	85	12	5	431	440	-4				

7 342 339 1	9 145 141 0	6 1284 1304 -13	5 529 533 -2
8 438 413 10	10 261 157 26	7 91 160 -11	6 67 28 2
-6 13 1	0 13 1	6 13 1	7 505 453 24
1 277 242 11	1 68 155 -11	0 460 458 1	-1 14 1
2 972 965 5	2 1595 1612 -10	1 208 153 12	1 431 469 -17
3 119 185 -11	3 161 177 -3	2 970 972 -1	2 1069 1083 -9
4 305 286 6	4 739 754 -10	3 219 127 19	3 633 643 -5
5 377 353 9	5 228 224 1	4 1380 1380 0	4 195 180 3
6 279 294 -4	6 749 739 6	5 -154 68 -17	5 286 252 9
7 192 174 4	7 85 37 3	6 374 356 6	6 722 701 12
8 101 116 -2	8 642 654 -6	7 13 1	7 490 486 1
9 411 425 -6	9 321 384 -24	0 786 800 -8	0 14 1
-5 13 1	10 80 124 -5	1 122 91 3	0 1060 1040 9
1 142 161 -3	1 13 1	2 843 831 8	1 645 628 9
2 -42 47 -3	0 1639 1640 -1	3 125 97 3	2 161 162 0
3 168 197 -6	1 204 238 -9	4 756 750 3	3 -68 18 -2
4 804 813 -6	2 391 345 19	5 183 150 5	4 1156 1145 7
5 52 70 -1	3 -123 70 -12	8 13 1	5 740 725 9
6 391 414 -10	4 1192 1171 14	0 496 520 -12	6 266 206 16
7 410 404 2	5 183 79 21	1 191 176 3	7 547 530 8
8 127 121 1	6 844 881 -26	2 765 754 6	1 14 1
9 269 185 22	7 234 216 4	3 129 27 8	0 111 33 6
-4 13 1	8 402 324 31	4 1144 1156 -7	1 171 237 -15
1 152 167 -2	9 260 253 2	9 13 1	2 1159 1168 -5
2 1229 1227 1	10 326 375 -18	0 660 650 5	3 684 665 11
3 113 98 1	2 13 1	1 175 137 6	4 382 354 10
4 505 482 12	0 202 158 10	2 739 741 -1	5 463 462 0
5 335 332 1	1 146 101 7	-6 14 1	6 711 721 -6
6 520 501 10	2 1430 1458 -17	1 474 492 -8	2 14 1
7 181 156 5	3 222 274 -16	2 376 357 9	0 965 950 9
8 266 273 -2	4 759 775 -10	3 146 109 6	1 657 673 -10
9 442 472 -14	5 270 189 22	4 506 495 5	2 143 179 -6
10 117 98 2	6 630 633 -1	-5 14 -1	3 247 193 13
-3 13 1	7 -171 35 -21	1 323 324 0	4 978 985 -4
1 142 101 7	8 895 877 12	2 896 883 8	5 772 781 -5
2 75 145 -11	9 230 260 -8	3 645 660 -8	6 476 509 -15
3 315 363 -19	3 13 1	4 199 145 11	3 14 1
4 1045 1058 -9	0 1261 1264 -2	5 302 307 -1	0 141 179 -7
5 -138 37 -12	1 271 281 -3	-4 14 1	1 260 224 10
6 488 471 9	2 457 441 8	1 624 648 -13	2 957 955 1
7 396 415 -8	3 57 11 1	2 180 191 -2	3 853 854 0
8 100 127 -3	4 1023 1041 -11	3 91 52 3	4 516 487 13
9 141 22 12	5 300 187 32	4 758 736 13	5 295 326 -9
10 115 60 6	6 1016 988 18	5 476 457 8	4 14 1
-2 13 1	7 151 213 -13	6 109 15 6	0 939 912 18
1 272 327 -19	8 322 279 13	-3 14 1	1 722 707 8
2 1339 1332 4	9 184 161 4	1 424 392 13	2 413 442 -11
3 126 34 9	4 13 1	2 1067 1055 7	3 -158 67 -15
4 508 502 3	0 309 314 -1	3 687 667 12	4 801 804 -1
5 283 279 1	1 -35 116 -8	4 -176 0 -16	5 14 1
6 731 716 9	2 1126 1148 -15	5 266 213 14	0 363 322 14
7 150 199 -10	3 274 259 4	6 472 482 -4	1 255 204 15
8 439 434 2	4 1051 1073 -14	7 231 215 3	2 768 792 -14
9 547 561 -7	5 59 129 -8	-2 14 1	3 852 855 -2
10 -111 70 -9	6 573 550 11	1 567 567 0	6 14 1
-1 13 1	7 102 91 1	2 98 56 3	0 721 706 8
1 213 117 20	8 1043 1047 -2	3 -140 107 -17	1 660 685 -14
2 181 192 -2	5 13 1	4 1014 1014 0	2 559 569 -5
3 341 303 14	0 1162 1155 4		
4 1111 1123 -8	1 263 217 13		
5 124 88 4	2 850 864 -9		
6 642 625 10	3 -195 53 -22		
7 303 289 4	4 919 917 1		
8 308 332 -8	5 227 210 4		